AUTHOR QUERY FORM

ELSEVIER	**Journal:** MSR **Article Number:** 100525	**Please e-mail your responses and any corrections to:** **E-mail:**

Dear Author,

Please check your proof carefully and mark all corrections at the appropriate place in the proof (e.g., by using on-screen annotation in the PDF file) or compile them in a separate list. Note: if you opt to annotate the file with software other than Adobe Reader then please also highlight the appropriate place in the PDF file. To ensure fast publication of your paper please return your corrections within 48 hours.

For correction or revision of any artwork, please consult http://www.elsevier.com/artworkinstructions.

Any queries or remarks that have arisen during the processing of your manuscript are listed below and highlighted by flags in the proof. Click on the 'Q' link to go to the location in the proof.

Location in article	Query / Remark: click on the Q link to go Please insert your reply or correction at the corresponding line in the proof
Q1	Figs. 12,13,15,20,21,30,54,55,57,58,75,76,84,86,88 and 90 will appear in black and white in print and in color on the web. Based on this, the respective figure captions have been updated. Please check, and correct if necessary.
Q2	Your article is registered as a regular item and is being processed for inclusion in a regular issue of the journal. If this is NOT correct and your article belongs to a Special Issue/Collection please contact m.radhakrishnan@elsevier.com immediately prior to returning your corrections.
Q3	The author names have been tagged as given names and surnames (surnames are highlighted in teal color). Please confirm if they have been identified correctly.
Q4	Correctly acknowledging the primary funders and grant IDs of your research is important to ensure compliance with funder policies. We could not find any acknowledgement of funding sources in your text. Is this correct?
Q5	Out of four authors biography for one only one author was supplied in resupply stage, therefore biography for rest of the authors have not been included in the article. Kindly check.
	Please check this box or indicate your approval if you have no corrections to make to the PDF file ☐

Thank you for your assistance.

Materials Science and Engineering R xxx (2019) xxx–xxx

Contents lists available at ScienceDirect

Materials Science and Engineering R

journal homepage: www.elsevier.com/locate/mser

Towards a predictive thermodynamic description of Fsorption processes in polymers: The synergy between theoretical EoS models and vibrational spectroscopy

Giuseppe Mensitieri[a,*], Giuseppe Scherillo[a], Costas Panayiotou[b], Pellegrino Musto[c]

[a] Dept. of Chemical, Materials and Production Engineering, University of Naples Federico II, 80125 Naples, Italy
[b] Dept. of Chemical Engineering, Aristotle University of Thessaloniki, Thessaloniki, 54024, Greece
[c] Institute on Polymers, Composites and Biomaterials, National Research Council of Italy, via Campi Flegrei, 34, Pozzuoli, Naples, 80078, Italy

ARTICLE INFO

Article history:
Received 29 May 2019
Received in revised form 3 October 2019
Accepted 2 December 2019
Available online xxx

Keywords:
Rubbery polymers
Glassy polymers
Sorption thermodynamics in polymers
Vibrational spectroscopy
Equations of State models
NRHB
SAFT

ABSTRACT

Understanding and predicting sorption thermodynamics of low molecular weight compounds in rubbery and glassy polymers is of great relevance to elucidate important phenomena in areas at the interface of various scientific branches, such as the colloid and interface science, membrane science, polymer foaming, tissue engineering, scaffolding, microcellular materials, aerogels, and for the implementation of technological applications. The development of thermodynamic models for polymer-based mixtures, applicable over a wide range of conditions, remains an active and fascinating research area. Recent advances in statistical thermodynamics and a better understanding of intra- and inter-molecular interactions, thanks to accurate experimental measurements and molecular simulations using realistic force fields, have contributed significantly to this end. In fact, sorption thermodynamics in polymers plays a relevant role in describing phase equilibria of polymer mixtures, (hydro)gel swelling, intramolecular association, hydrogen-bonding cooperativity and polymer degradation and stability, in assessing durability of polymers exposed to aggressive environments, in predicting penetrant induced crystallization and plasticization phenomena in polymers, in designing polymer-based separation processes, in tailoring polymer foaming processes, in improving gas and vapor barrier properties of polymer packaging, in modelling devolatilization of polymer solutions and migration phenomena of additives, in designing drug delivery systems, to mention a few.

In the last decades, models have been introduced rooted on Equation of State theories, some of them based on compressible lattice frameworks. Notably, these models have been structured to specifically account for non-random distribution of molecular species and for dealing with several kinds of self-interactions that establish between polymer molecules and between penetrant molecules as well as cross-interactions that establish between moieties present on polymer backbone and penetrants. These models have been built to describe the behaviour of both rubbery polymers and out-of-equilibrium glassy polymers. Towards the further development of these approaches to gain an increased predictive capability of this thermodynamic description, recently have been also introduced approaches aimed at the estimation of relevant parameters based on molecular descriptors for calculations of properties of pure-components bulk phases and solutions.

Such a quantitative description of the sorption process by use of advanced thermodynamic theories invariably relies on a molecular-level characterization of the system under scrutiny to validate and support the theoretical framework. Information is required on the molecular aggregates formed in the system, their structure, stoichiometry and, whenever possible, their population. In this respect, vibrational spectroscopy (FTIR, Raman) has demonstrated to be among the most powerful techniques, due to its sensitivity towards H-bonding detection and to its sampling flexibility, which allows the development of in-situ, time-resolved measurements. In the last ten years, significant advancements have occurred in terms of both experimental approaches and data analysis techniques, which considerably contributed to deepening the interpretation of the molecular interactions scenario. In particular, Two-dimensional correlation spectroscopy (2D-COS), Difference spectroscopy (DS) and first-

* Corresponding author.
E-mail address: mensitie@unina.it (G. Mensitieri).

http://dx.doi.org/10.1016/j.mser.2019.100525

Please cite this article in press as: G. Mensitieri, G. Scherillo, C. Panayiotou et al. Towards a predictive thermodynamic description of Fsorption processes in polymers: The synergy between theoretical EoS models and vibrational spectroscopy. Mater. Sci. Eng. R (2020), https://doi.org/10.1016/j.mser.2019.100525

principles quantum chemistry calculations have made a strong impact on the amount and quality of the acquired information.

In view of the progress in this rapidly advancing and technologically relevant subject, this review article summarizes the state of the art on sorption thermodynamics modelling and on synergic combination with the wealth of information recently made available thanks to advanced vibrational spectroscopy techniques.

Contents

1. Introduction

1.1. General survey on the issues related to polymer solution thermodynamics

The systems of fluids of practical interest to chemists, materials scientists, and chemical engineers are as a rule complex, departing significantly from ideal-solution behaviour. The systems at interfaces are, in addition, inhomogeneous exhibiting density gradients and, when multicomponent, they also exhibit composition gradients or peculiar composition profiles across the interfaces. Thus, development of thermodynamic models for complex fluids and polymer systems applicable over a wide range of external conditions remains an active and fascinating research area.

Recent advances in statistical thermodynamics and better understanding of intra- and intermolecular interactions thanks to accurate experimental measurements and molecular simulations using realistic force fields have contributed significantly to this end. Many of the recent thermodynamic models based on statistical mechanics are rooted to the pioneering work of Guggenheim [1] and Flory [2] on lattice models for complex fluids, including polymers. The Lattice Fluid (LF) theory of Sanchez and Lacombe (SL) [3–5] is probably one of the most widely used and successful lattice models for polymer solutions.

Significant improvement in the performance of these models is obtained by accounting explicitly for the nonrandom distribution of molecular species and free volume, and for highly specific forces between neighboring molecules resulting in hydrogen bonding [6–9].

Please cite this article in press as: G. Mensitieri, G. Scherillo, C. Panayiotou et al. Towards a predictive thermodynamic description of Fsorption processes in polymers: The synergy between theoretical EoS models and vibrational spectroscopy. Mater. Sci. Eng. R (2020), https://doi.org/10.1016/j.mser.2019.100525

Nonrandomness is essentially omnipresent in fluids as the molecular species are, as a rule, distributed nonrandomly in their mixtures. In other words, the local composition in the immediate neighbourhood of a molecule is, in general, different from the overall or bulk composition of the mixture. Even in pure fluids, there is a degree of nonrandomness in the distribution of their functional groups. In fact, modern experimental techniques, such as positron annihilation spectroscopy, reveal significant nonrandomness in the distribution of free volume throughout the volume of the pure fluid, even in nonpolar systems [10,11]. One of the principal causes of nonrandomness is of course hydrogen bonding.

Hydrogen bonding is by itself a subject of remarkable diversity as it is present in and dictates the behaviour of an enormous type of systems including aqueous solutions, systems of biological/biomedical interest, pharmaceuticals, colloids and surfactants, physical networks and gels, adhesives and pastes, extractives and binders, and polymer alloys and blends. There are many reviews of the subject in the open literature [12–27] each addressing, usually, one aspect or type of application of hydrogen bonding. Because of its many-facets character, unified approaches of treatment of hydrogen bonding are particularly useful, especially in areas at the interface of various scientific branches, such as the colloid and interface science.

For the treatment of hydrogen bonding in associated fluids and mixtures, a variety of different approaches is popular. We could divide the overwhelming majority of these approaches into two groups: the association models [6,19,28–32] and the combinatorial models [27,33]. Association models invoke the existence of multimers or association complexes and seek expressions for their population. Combinatorial models do not invoke the existence of association complexes but, instead, they focus on the donor–acceptor contacts and seek combinatorial expressions for the number of ways of forming hydrogen bonds in systems of given proton–donor and proton–acceptor groups. Both types of models imply that the molecules tend to be distributed in the system nonrandomly for more efficient hydrogen-bonding interaction.

Earlier [27], we had compared the two approaches of hydrogen bonding and applied to the description of phase equilibria and mixture properties of systems of fluids. The key conclusion was that in the systems where both approaches apply, they prove to be, essentially, equivalent. However, the combinatorial approach has a much broader field of applications as it can be applied even to systems forming three-dimensional hydrogen-bonding networks. Subsequently [37], we had presented an updated review on the thermodynamic aspects of hydrogen bonding in pure fluids and their mixtures by focusing on the combinatorial hydrogen-bonding formalism. A variety of examples were given in applications ranging from phase equilibria of simple aqueous mixtures to (hydro)gel swelling, to intramolecular association, and to hydrogen-bonding cooperativity. More recently [38], besides hydrogen bonding for the study of bulk phases as well as interfaces, emphasis was also given to the progress in accounting for non-randomness in solution thermodynamics.

The present review is, in a sense, a continuation of the aforementioned reviews. The thermodynamic aspects of hydrogen bonding (combinatorial approach) in pure fluids and their mixtures will be presented in a way that can be combined with any thermodynamic model. Here, it should become clear at the outset that, in general, hydrogen bonding makes a *contribution* only and is not sufficient for the complete evaluation of the various thermodynamic properties of fluids and their mixtures. Thus, hydrogen bonding formalisms are usually combined with thermodynamic models, which account for all other contributions collectively called physical contributions. For the purposes of this review, we will use two kinds of thermodynamic frameworks: Equation of State theories (EoS) and predictive activity coefficient models.

The former (EoS approach), is applicable to fluids over an extended range of external conditions encompassing liquids, vapors, gases, supercritical fluids, amorphous and glassy polymers, homogeneous as well as inhomogeneous systems, complex aqueous systems, associated polymer mixtures, rubbers, and gels. Thus, the hydrogen bonding formalism will be combined with two equation of state models, the Quasi-Chemical-Hydrogen-Bonding theory (QCHB) [8] and its recent development the Non-Random-Hydrogen-Bonding model (NRHB) [9,39]. Both models take into account the non-random distribution of free volume in the system by using Guggenheim's *quasi-chemical* approach [1].

The latter (predictive approach) is based on the partial solvation parameters [40–44] and focuses on the prediction of thermodynamic properties of complex systems where almost no experimental data is available.

In what follows, we will review first, in section 2, the foundations of the modern equation-of-state approach to polymer solutions. After an exposition of the essentials of the combinatorial hydrogen bonding formalism, we will present the equation of state approach and characteristic applications to mixtures of hydrogen bonding fluids. Then, we present EoS approaches rooted on perturbation theories, used to describe sorption thermodynamics endowed with hydrogen bonding and other types of interactions, focusing our attention on models of the Statistical Associating Fluid Theory (SAFT) family [45–49].

The EoS theories briefly described above, are well suited to deal with systems at equilibrium. When dealing with sorption of low molecular weight compounds in glassy polymers one has to cope with the non-equilibrium nature of these systems. Sub-section 2.2 is, in fact, devoted to approaches proposed a few decades ago to extend equilibrium thermodynamics EoS theories to the case of sorption in non-equilibrium glassy polymers [50–52].

In the sub-section 2.3, a few pages are also devoted to the description of molecular simulation approaches, addressing the current predictive capability of Molecular Dynamics (MD) and Monte-Carlo (MC) methods in the context of sorption thermodynamics in polymers.

Models developed for interpreting sorption thermodynamics in rubbery and glassy polymers require proper validation and estimates of parameters, To this end, several experimental strategies have been proposed to gather information on relevant model parameters and to verify the suitability of the theoretical approach to provide a correct interpretation of thermodynamics. This is the issue addressed in section 3 of this review, with a special focus on methods rooted on vibrational spectroscopy measurements and their interpretation and elaboration. In fact, techniques based on vibrational spectroscopy provide a wealth of qualitative and quantitative information that is of great importance, particularly for systems endowed with specific Lewis acid/base or hydrogen-bonding interactions. The combination of gravimetric determination of sorption isotherms, vibrational spectroscopy measurements, detailed analysis of spectra, quantum chemistry calculations and macroscopic modelling by EoS theories is presented as a powerful approach to provide an interpretation of polymer mixture thermodynamics grounded on a molecular perspective.

Predictive methods to determine relevant parameters are also discussed in thesub-section 3.8.3, presenting the essentials of the Partial Solvation Parameter (PSP) approach [40–44,53–55].

Finally, in section 4 are presented case studies and applications, illustrating the use of EoS approaches to interpret sorption thermodynamics in rubbery and glassy polymers, possibly endowed with specific interactions. Several relevant examples of the synergic integration of vibrational spectroscopy investigation

Please cite this article in press as: G. Mensitieri, G. Scherillo, C. Panayiotou et al. Towards a predictive thermodynamic description of Fsorption processes in polymers: The synergy between theoretical EoS models and vibrational spectroscopy. Mater. Sci. Eng. R (2020), https://doi.org/10.1016/j.mser.2019.100525

with EoS based theoretical modelling are discussed. In the subsections 4.2, 4.3 and 4.4 some physical phenomena, for systems of practical interest in engineering and technological applications, like retrograde vitrification, bubble nucleation and growth in polymer foaming and gel swelling and collapse, are interpreted using the discussed EoS approaches.

2. Theoretical approaches

2.1. The equation of state approaches to polymer solution equilibrium thermodynamics

2.1.1. Foundations and early developments of lattice fluid theories

2.1.1.1. The Flory-Huggins theory of polymer solutions. Most of the developments in polymer solution thermodynamics, in one way or another, refer to the Flory – Huggins (FH) theory of polymer solutions [2,56,57]. This theory offered two cornerstones for the subsequent developments: a most simple combinatorial expression for the mixing entropy and an even simpler expression for the mixing enthalpy. For the purposes of this review, we will confine ourselves to the key equations of the theory.

Let us consider a system of N_1 solvent molecules and N_2 linear polymer molecules each consisting of r segments. In the FH approach, the system of molecules is assumed to be arranged on a quasi-lattice of coordination number z and N_T total number of sites. The distinguishable number of arrangements on the quasi-lattice or the number of iso-energetic microstates is given by Eq. (1):

$$\Omega_p = \frac{N_T!}{N_2!N_1!}\left[\frac{z-1}{N_T}\right]^{N_2(r-1)} \tag{1}$$

Applying Boltzmann's law, one obtains from Eq. (1) the following equation for the entropy of the mixture:

$$\frac{S^M}{k} = -N_1 ln\left(\frac{N_1}{N_1+rN_2}\right) - N_2 ln\left(\frac{rN_2}{N_1+rN_2}\right) + N_2\left\{(r-1)ln\frac{(z-1)}{e} + ln\, r\right\} \tag{2}$$

From this equation for the mixture, we obtain the corresponding equations for the entropy of pure polymer and solvent by setting $N_1 = 0$ and $N_2 = 0$, respectively, in Eq. (2), or $S_1 = 0$, and

$$S_2 = N_2\left\{(r-1)ln\frac{(z-1)}{e} + ln\, r\right\} \tag{3}$$

Thus, in the FH approach, the mixing entropy is given by Eq. (4):

$$\Delta S^M = S^M - S_1 - S_2 = -k(N_1 ln\phi_1 + N_2 ln\phi_2) \tag{4}$$

where, the segment or volume fractions, ϕ_i, are defined as follows:

$$\phi_1 = \frac{N_1}{N_1+rN_2} = \frac{N_1}{N_1+\frac{V_2}{V_1}N_2} = \frac{N_1V_1}{N_1V_1+N_2V_2}$$

$$\phi_2 = \frac{rN_2}{N_1+rN_2} = \frac{N_2V_2}{N_1V_1+N_2V_2} \tag{5}$$

V_i being the molecular size (volume) of component *i*.

The above division of the polymer chain into *r* segments was done on the basis of the solvent volume. If the solvent changes, the number of polymer segments changes and this would cause some confusion if one would like to extent the FH approach to multicomponent polymer solutions with more than one solvent. Obviously, it would be more convenient if the number of polymer segments were constant regardless of the solvent used. A simple way to do this is by using a reference volume, V_0, for obtaining the number of segments of all molecules, or:

$$V_1 = r_1V_0;\ V_2 = r_2V_0$$

and

$$V = n_1V_1 + n_2V_2 = (n_1r_1 + n_2r_2)V_0 = nrV_0 \tag{6}$$

n being, now, the total number of moles in the system ($n = n_1 + n_2$). Replacing expressions (6) in Eqs. (4) and (5), we obtain for the mixing entropy the following alternative form:

$$\frac{\Delta S^M}{R} = -\frac{V}{V_0}\left(\frac{\phi_1}{r_1}ln\,\phi_1 + \frac{\phi_2}{r_2}ln\,\phi_2\right) = -rn\left(\frac{\phi_1}{r_1}ln\,\phi_1 + \frac{\phi_2}{r_2}ln\,\phi_2\right) \tag{7}$$

It should be pointed out that the expressions for the entropy of mixing are consistent with the assumption that both the volume and the enthalpy of mixing were zero. In the framework of the regular-solution behavior, which is the one assumed by the FH theory, one may still consider Eqs. (4) and (7) valid even when the enthalpy of mixing is non-zero. Thus, the next step in the FH approach is the estimation of the mixing enthalpy in the polymer-solvent mixture.

The formation of the mixture implies intermolecular contact or bond breaking and new bond formation. By breaking one 1-1 bond and one 2-2 bond for the formation of two 1–2 bonds we may visualize an exchange interaction or interchange energy given by the following equation:

$$\Delta\varepsilon_{12} = \varepsilon_{11} + \varepsilon_{22} - 2\varepsilon_{12} \tag{8}$$

The number of external contacts per polymer chain is (Flory approximation):

$$q_2z = (r_2-2)(z-2) + 2(z-1) = r_2(z-2) + 2 \cong r_2z \tag{9}$$

The number N_{12} of 1–2 intermolecular bonds in the mixture may, then, be obtained by multiplying the number of external contact sites of type 2 (polymer segment) with the probability to have as first neighbor a site of type 1 (solvent segment). For a perfect random distribution, this probability is simply equal to the volume fraction of component 1. Thus:

$$\Delta H^M = \frac{N_2zr_2\phi_1\Delta\varepsilon_{12}}{2} = \frac{N_1zr_1\phi_2\Delta\varepsilon_{12}}{2} = N_1r_1\phi_2kT\chi_{12} \tag{10}$$

The dimensionless Flory-Huggins interaction parameter, χ_{12}

$$\chi_{12} = \frac{z\Delta\varepsilon_{12}}{2kT} \tag{11}$$

is a most useful parameter in polymer solution thermodynamics. Combining Eqs. (7) and (10), we obtain for the free energy of mixing (in molar terms) Eq. (12):

$$\Delta G^M = \Delta H^M - T\Delta S^M = rnRT\left[\frac{\phi_1}{r_1}\ln\phi_1 + \frac{\phi_2}{r_2}\ln\phi_2 + \phi_1\phi_2\chi_{12}\right] \tag{12}$$

From Eq. (12) one may obtain the equation for the activity of the solvent, or

$$\frac{\mu_1-\mu_1^0}{RT} = \ln a_1 = ln(\gamma_1x_1) = \left[\ln(1-\phi_2) + \left(1-\frac{r_1}{r_2}\right)\phi_2 + r_1\phi_2^2\chi_{12}\right] \tag{13}$$

Doubtless, Eq. (12) was a cornerstone in the development of polymer solution thermodynamics. However, there are significant limitations in the FH approach, the most important being recalled in the following. A first important issue is that in the mathematical formulation of the theoretical model some relevant approximations were adopted in translating the scheme of lattice fluid framework

Please cite this article in press as: G. Mensitieri, G. Scherillo, C. Panayiotou et al. Towards a predictive thermodynamic description of Fsorption processes in polymers: The synergy between theoretical EoS models and vibrational spectroscopy. Mater. Sci. Eng. R (2020), https://doi.org/10.1016/j.mser.2019.100525

[58]. In fact, the probability of occurrence of 1–2 pairs on neighbouring lattice sites is simply calculated as the product $\phi_1\phi_2$. As a consequence, in the enthalpy expression given by Eq. (10) any correlation effect in the occupancy of lattice sites is neglected. This kind of mean-field approximation determines a critical behaviour that is reported for phase transitions by the Landau theory [59], that deviates from the correct one expected in accordance to the "universal" regime close to the critical point [60,61]. Actually, this last feature is common also to the other theories discussed in this review (see later sub-sections on Sanchez-Lacombe, SAFT and NRHB approaches) that all perform rather well if one restricts to regions far away from critical points. As further remark, in Eq. (11) the use of z determines an overestimation in the calculation of the number of monomers belonging to other molecules that interact with a considered monomer, thus determining an overestimation of χ_{12}. A third comment regards the relevant approximation that is implicit in the expression of the entropy of mixing (Eq. (7)), where the constraint that macromolecular chains must be mutually avoiding is largely neglected. In addition, when comparing FH model with experimental results, some inconsistencies and limitations emerge. In fact, the value of χ_{12} parameter retrieved from experimental data is not a constant but it is found to vary with composition, temperature and pressure. Moreover, the FH approach cannot account for the Lower Critical Solution Temperature (LCST) behavior occurring in polymer solutions and polymer mixtures [4]. Finally, the theory does not apply to gaseous systems and, thus, it cannot handle vapor – liquid equilibria or supercritical systems. Actually, it is not clear if this disagreement with experimental outcomes results from the adopted lattice fluid scheme or is due to the approximations adopted in the statistical mechanics treatment.

In order to remove the above first two limitations (i.e. that χ_{12} is not a constant and that the LCST behavior is not predicted), the Flory-Patterson-Prigogine (FPP) cell theory [62–64] was proposed, which had a significant impact in the development of the equation-of-state approach to polymer solutions. Volume changes and pressure / temperature effects on density were accounted for by allowing a change in volume of each cell of the lattice and were obtained via the following equation of state:

$$\frac{\frac{\sim P \sim V}{\sim T} = \sim V^{1/3}}{\sim V^{1/3} - 1 - \frac{1}{\sim V \sim T}} \tag{14}$$

Three reduced quantities for temperature, pressure, and volume were obtained by the following defining equations:

$$\sim T = \frac{T}{T^*};\ \sim P = \frac{P}{P^*};\ \sim V = \frac{V}{V^*} \tag{15}$$

The star quantities, T^*, P^*, and V^* being the characteristic equation-of-state or scaling constants for temperature, pressure, and volume, respectively of the fluid.

At nearly the same time another important development was made by Simha and Somcynsky [65,66]. Their model allows also for empty sites throughout the system volume but otherwise it is also a cell model (allowing for variable volume of each cell in the lattice) as the FPP one and, as a consequence, both of them do not apply to the gaseous state. However, soon after, the LF theory of Sanchez-Lacombe [3–5], discussed in the next sub-section, was developed which was responding to all above three limitations.

2.1.1.2. The lattice-fluid theory of Sanchez-Lacombe. The first key difference of the SL model from the FH one was the allowance for empty sites in the quasi-lattice. Otherwise, the empty sites and the molecular sites (lattice sites occupied by molecular segments) were considered to be randomly distributed throughout the quasi-lattice in pretty much the same way as in FH approach. There is a number of variations in the SL formalism [3–5] but in the present review we will focus on the rather most prevailing one.

In the case of description of the behavior of a pure component i, the SL approach considers each molecule of type i as being characterized by a number of segments, r_i, having each a characteristic hard-core volume, v_i^*, and an average intersegmental interaction energy, $\varepsilon_i^* = (z/2)\varepsilon_{ii}$, ε_{ii} being the i-i contact interaction energy. These characteristic equation-of-state constants for component i may be used to express the equivalent scaling constants, T^*, P^*, and ρ^* for temperature, pressure and density, respectively, with the following equations:

$$\varepsilon_i^* = kT_i^* = P_i^* v_i^*;\ r_i v_i^* = \frac{M_{W_i}}{\rho_i^*} = M_{W_i} v_{sp,i}^* \tag{16}$$

M_{W_i} being the molecular weight of compound i. Similarly, to the FPP model, the reduced quantities are, then, defined as follows:

$$\sim T_i = \frac{T}{T_i^*};$$

$$\sim P_i = \frac{P}{P_i^*};$$

$$\sim v_i = \frac{1}{\sim \rho_i} = \frac{\rho_i^*}{\rho_i} = \frac{M_i v_{sp,i}}{r_i v_i^*} = \frac{V_i}{V_i^*} \tag{17}$$

V_i being the molar volume of compound i.

In the LF approach, the contacts with empty sites are attributed a zero interaction energy and the number of empty sites at equilibrium are obtained by minimizing the free-energy of the system. This minimization condition, with respect to the number of empty sites or to the density of the system, resulted in the following simple form of the SL equation of state for a pure component:

$$\frac{PV}{nRT} = r\frac{\sim P \sim v}{\sim T} = 1 - r\left[1 + \frac{\ln(1 - \sim \rho)}{\sim \rho} + \frac{\sim \rho}{\sim T}\right] \tag{18}$$

It is easy to show that this equation leads to the ideal-gas limit at zero densities (or very high temperatures). The form of Eq. (18) is also valid for multicomponent mixtures.

The chemical potential of pure component i is given by the following equation:

$$\frac{\mu_i^0}{RT} = r_i(\sim v_i - 1)\ln(1 - \sim \rho_i) + \ln\frac{\sim \rho_i}{\omega_i} - r_i\frac{\sim \rho_i}{\sim T_i} + r_i\frac{\sim P_i \sim v_i}{\sim T_i} \tag{19}$$

Here ω_i is an internal parameter accounting for symmetry and flexibility of molecule i (more on this later), which cancels out in phase equilibrium calculations.

In the case of mixtures, the following mixing and combining rules are adopted in the LF approach:

$$v^* = \sum\nolimits_i (\phi_i v_i^*) \tag{20}$$

$$\varepsilon^* = \sum_I (\phi_i \varepsilon_i^*) - RT\sum\nolimits_i \sum\nolimits_{j>i} \left(\phi_i \phi_j X_{ij}\right) \tag{21}$$

where

$$X_{ij} = \frac{\varepsilon_i^* + \varepsilon_j^* - 2\varepsilon_{ij}^*}{R{\cdot}T} \tag{22}$$

and

$$\varepsilon_{ij}^* = \xi_{ij}\sqrt{\varepsilon_i^* \varepsilon_j^*} \tag{23}$$

Please cite this article in press as: G. Mensitieri, G. Scherillo, C. Panayiotou et al. Towards a predictive thermodynamic description of Fsorption processes in polymers: The synergy between theoretical EoS models and vibrational spectroscopy. Mater. Sci. Eng. R (2020), https://doi.org/10.1016/j.mser.2019.100525

ξ_{ij} being a binary adjustable parameter near unity. Quadratic mixing and combining rules have been adopted also [67] in place of Eq. (20). The average number of segments per molecule in the mixture is given by:

$$rn = \sum_i r_i n_i \tag{24}$$

With the above rules, the total volume of the mixture is given by the following equation:

$$V = rn \sim v \sum_i (\phi_i v_i^*) = rn \sim v v^* \tag{25}$$

and the total potential energy by the equation:

$$-E = rn \sim \rho \varepsilon^* \tag{26}$$

where $\sim\rho = \frac{1}{\sim v}$. Thus, for a binary mixture,

$$-E = rn \sim \rho \left(\phi_1 \varepsilon_1^* + \phi_2 \varepsilon_2^* - \phi_1 \phi_2 RTX_{12}\right) \tag{27}$$

The corresponding expression for the total Gibbs free energy of a binary mixture is:

$$G = E + PV - TS =$$

$$P{\cdot}V - rn\{\sim \rho(\phi_1 \varepsilon_1^* + \phi_2 \varepsilon_2^* - \phi_1 \phi_2 RTX_{12}) - RT[(\sim v - 1)\ln(1 - \sim \rho) + \frac{\ln \sim \rho}{r} + \frac{\phi_1}{r_1}\ln\frac{\phi_1}{\omega_1} + \frac{\phi_2}{r_2}\ln\frac{\phi_2}{\omega_2}]\} \tag{28}$$

This equation may be used for obtaining various thermodynamic quantities for the mixture. The equation for the chemical potential of component '1' is:

$$\frac{\mu_1}{RT} = \ln\phi_1 + \left(1 - \frac{r_1}{r_2}\right)\phi_2 + r_1 \sim \rho X_{12}\phi_2^2 + r_1(\sim v - 1)\ln(1 - \sim \rho) + \ln\frac{\sim \rho}{\delta_1} - r_1\frac{\sim \rho}{\sim T_1} + r_1\frac{\sim P_1 \sim v}{\sim T_1} \tag{29}$$

There are several issues resulting from the assumptions and simplifications endowed with SL theory.

The first relevant issue is related to the adoption of the mean-field approximation. It is computationally advantageous since it brings back many-body problems to one-body problems, considering only averaged interactions acting on a single particle. However, this approach is appropriate if fluctuations are not important and correlations occur on a very short range distance. This makes questionable the application of the SL theory near second-order phase transitions (e.g. the critical point).

A second issue that has to be considered is that the theory is substantially based on a configurational partition function with uncomplete account for molecular internal degrees of freedom. In fact, rotational, vibrational, and other internal degrees of freedom are not considered in the SL framework since do not play a role in the interpretation of sorption thermodynamics. Hence SL theory is not expected to provide reliable predictions of thermodynamic quantities related to these degrees of freedom, as is the case, for example, of heat capacities.

Both these two issues are also shared by the other lattice fluid theories illustrated in this review.

Also, at coexistence, the SL EOS is often solved analytically, requiring rather severe approximations which can corrupt the agreement with experiment [68].

Beside those reported above, an extremely relevant issue is that of thermodynamic inconsistency of the SL theory for mixtures. In fact, the thermodynamic consistency of the expressions of chemical potentials provided by the SL theory for mixtures has been questioned by Neau [69], whatever are the mixing rules considered. It is demonstrated that, except for the special case that the mixture characteristic parameter v^* (that corresponds to the hole volume, v_0) is a constant independent of composition, in SL theory the reference term for the chemical potential of a compound, μ_{ref}, is a function of both temperature and molar fractions and thus does not cancel out when imposing phase equilibrium. Moreover, this circumstance implies also that the expressions of chemical potentials do not converge to the corresponding ones in the ideal gas state. To circumvent this problem, Neau proposed the use of fugacity coefficients obtained from the SL-EoS to perform thermodynamically consistent phase equilibrium calculations, based on the assumption that the 'configurational' pressure, obtained starting from the configurational expression of the Helmholtz energy provided by the SL theory, is coincident with the absolute pressure.

This procedure, proposed by Neau to correct for thermodynamic inconsistencies, has recently received a well-argued criticism by Thompson et al. [68,70,71]. In fact, these authors beside providing further evidence of the inconsistency of the SL theory that arises from the mixing rules, at the same time demonstrated that the calculation procedure of phase equilibria based on fugacity coefficients proposed by Neau is incorrect and, thus, is not a viable mean to remove the inconsistency. In particular, Neau failed to account for the fact that, in a lattice hole theory, as the SL theory is, the number of holes in the lattice depends upon the total volume. Thompson et al., based on an off-lattice formalism, were able to re-obtain the SL EOS showing that the reported inconsistency does not originate from the lattice framework. These authors proposed a variant of the SL-EOS that makes use of a constant, composition-independent, hole volume of the mixture, that is a different for each mixture ('constant hole-SL' (ch-SL) model [70]). Their version of SL EOS theory for mixtures is 'near' consistent for solubility calculations. The 'near' consistency is related to the fact that if v_0 is constant for a mixture, it cannot limit correctly to the hole volume values of the pure components. Moreover, some inconsistency is also related to the fact that, when dealing with phase equilibria, the chemical potentials in the different phases use different hole volumes. As a consequence, the difference between the constant hole volume for the mixture and that for the pure component phase, implies that the chemical potentials in the two phases at equilibrium are based on different zeros of energies. However, this variant of SL theory can still be considered feasible to provide a reasonable quantitative agreement with experimental data for solubilities, when the value of hole volume of the mixture, as determined by fitting experimental sorption isotherms, is found to be rather close to the values for the pure components. As final assessment, abandoning the use of mixing rules for hole volume of a mixture to adopt a constant hole volume not only does simplify the theory, but provides, at the same time, a better performance as compared to SL theory in predicting sorption of low molecular weight compounds in rubbery polymers [68]. Notably, in the view of the authors, the holes are interpreted, at least in part, as an empirical correction for the fact that in a mean field theory correlations are missing.

A viable alternative to recover a full consistency of lattice based models is that adopted in the Panayiotou-Vera (PV) [72,73] and NRHB theory [39] models that will be discussed later. In these models the characteristic volume, v^*, is assumed to take the universal value of 9.75 cm^3/mol, both for pure compounds and for their mixtures, thus implying a constant value of hole volume for the mixture that trivially complies to the pure components limits.

2.1.2. Amendments to the LF approach

The SL approach has found numerous applications. Even today, it remains one of the most commonly used equations in polymer solution thermodynamics. Yet, the SL calculations are, in general, in qualitative agreement with experimental data and there is a noticeable failure in the case of systems interacting with strong specific forces. In a first attempt for the improvement of the SL approach, molecular shape characteristics have been

Please cite this article in press as: G. Mensitieri, G. Scherillo, C. Panayiotou et al. Towards a predictive thermodynamic description of Fsorption processes in polymers: The synergy between theoretical EoS models and vibrational spectroscopy. Mater. Sci. Eng. R (2020), https://doi.org/10.1016/j.mser.2019.100525

introduced through the surface-to-volume ratios, s_i [67] as well as quadratic mixing rule for v^* (with the discussed consistency issues). Surface area fractions are needed in this case, which are defined as follows:

$$\theta_i = \frac{\phi_i s_i}{\sum_{k=1}^{t}(\phi_k s_k)} = \frac{\phi_i s_i}{s} \tag{30}$$

The average intersegmental interaction energy in a binary mixture is given by

$$\varepsilon^* = \phi_1 \varepsilon_1^* + \phi_2 \varepsilon_2^* - \phi_1 \theta_2 RTX_{12} \tag{31}$$

and

$$X_{12} = \frac{\varepsilon_1^* + \frac{s_1}{s_2}\varepsilon_2^* - \left(2\sqrt{\frac{s_1}{s_2}}\right)\varepsilon_{12}^*}{RT} \tag{32}$$

The quadratic mixing rule reads:

$$v^* = \phi_1^2 v_1^* + \phi_2^2 v_2^* + 2\phi_1\phi_2 v_{12}^* \tag{33}$$

where

$$v_{12}^* = \zeta_{12}\left(\frac{v_1^{*1/3} + v_2^{*1/3}}{2}\right)^3 \tag{34}$$

The equation of state remains identical in form to Eq. (18) above. For a binary mixture, the equation for the chemical potential becomes:

$$\begin{aligned}\frac{\mu_1}{RT} &= \ln\phi_1 + \left(1 - \frac{r_1}{r_2}\right)\phi_2 + r_1 \sim \rho X_{12}\theta_2^2 \\ &+ r_1(\sim v - 1)\ln(1 - \sim \rho) + \ln\frac{\sim \rho}{\omega_1} - r_1\frac{\sim \rho}{\sim T_1} \\ &+ r_1\frac{\sim P_1 \sim v}{\sim T_1}\left(\frac{2\phi_1 v_1^* + 2\phi_2 v_{12}^* - v^*}{v_1^*}\right)\end{aligned} \tag{35}$$

These amendments introduced in the SL formalism have led to an improved performance of the LF model as regards to calculations of phase equilibria and related properties [67]. However, still the model could not handle adequately systems interacting with strong specific forces. In fact, such strong interactions affect drastically the distribution of molecular species and the Flory-Huggins random distribution, which is also adopted in the LF model, is likely inadequate for these systems. To circumvent such a drawback, a rather drastic change had to be introduced in the LF formalism.

A first attempt to introduce non-randomness in the LF model was proposed in the early eighties [72,73]. Guggenheim's Quasi-Chemical (QC) approach was used for this purpose. Non-randomness factors were introduced reflecting the departure of the real system from the fictitious system of perfect randomness, as follows [74]: if N_{ij} is the number of first-neighbor intermolecular contacts of molecular species i and j in the real system, and N_{ij}^0 is the corresponding number of contacts i-j if the molecular species were distributed at random, then, non randomness factors for the contact pairs i-j in the system, Γ_{ij}, can be defined as follows:

$$N_{ij} = \Gamma_{ij} N_{ij}^0 \tag{36}$$

A system is considered to attain a perfectly random distribution when the interchange energies (cf. Eqs. (8), (11), (22)) are zero. In a binary mixture of N_1 and N_2 molecules of species 1 and 2, respectively, the QC approach envisions the formation of two interactions 1–2, being generated by breaking one interaction 1-1 and one 2-2, as a quasi-chemical reaction of the form:

$$(1-1) + (2-2) \rightarrow (1-2) + (2-1) \tag{37}$$

Applying mass-action law to the reaction expressed by Eq. (37) at equilibrium, we obtain:

$$\begin{aligned}\frac{\left(\frac{N_{12}}{2}\right)^2}{N_{11}N_{22}} &= \frac{N_{12}^2}{4N_{11}N_{22}} = \frac{\left(N_{12}^0\Gamma_{12}\right)^2}{4\left(N_{11}^0\Gamma_{11}\right)\left(N_{22}^0\Gamma_{22}\right)} \\ &= \frac{\left(N_{12}^0\right)^2}{4N_{11}^0N_{22}^0}\frac{\Gamma_{12}^2}{\Gamma_{11}\Gamma_{22}} = \frac{\Gamma_{12}^2}{\Gamma_{11}\Gamma_{22}} = K_{12}\end{aligned} \tag{38a}$$

This is the "quasi-chemical condition" for the intermolecular contact pair 1–2. Species specific non-randomness factors, which will be useful below, may be introduced through the equation:

$$\Gamma_{ij} = \Gamma_i\Gamma_j \exp\left(\frac{-\Delta\varepsilon_{ij}}{kT}\right) = \Gamma_i\Gamma_j\tau_{ij} \tag{39}$$

Replacing in Eq. (38a), we obtain the following alternative expression for the quasi-chemical condition:

$$\frac{\Gamma_{ij}^2}{\Gamma_{ii}\Gamma_{jj}} = \frac{\tau_{ij}^2}{\tau_{ii}\tau_{jj}} = K_{ij} \tag{38b}$$

In the LF approach, a binary mixture is handled as a quasi-ternary mixture, the third species being the empty lattice sites. Three QC conditions apply in this case for the contact pairs 1–2, 1–0, and 2–0, 0 indicating the empty site. The full formalism and the method for obtaining $\Gamma_{\iota\xi}$'s was reported by Panayiotou and Vera [72]. A simplified formalism was adopted in a later work [73] where the same authors have considered that only the molecular species are distributed non-randomly. As anticipated, they have also considered that the hard-core segment volume, v_i^*, is the same for all compounds and equal to 9.75 cm^3/mol. This universal value was obtained as the average characteristic volume of a large number of studied pure compounds. In addition, it was considered that the interaction energy is rather an interaction free-energy and depends linearly on temperature, or

$$\varepsilon_i^* = \varepsilon_{h,i}^* + (T - 298.15)\varepsilon_{s,i}^* \tag{40}$$

With these assumptions, a non-random LF equation-of-state model (Panayiotou-Vera, PV, model) was developed, which constituted a rather significant improvement of the SL model. Similar models have followed the PV model [67,75–77] and applied to a variety of mixtures showing all significant improvement over the original SL model.

In parallel, hydrogen bonding interactions were introduced explicitly in the LF model by splitting the intermolecular interaction forces into physical (dispersion, weak to moderate polar) and chemical (strong specific Lewis acid/base or hydrogen-bonding) interactions. This division led to a factorization of the partition function of the system into a physical and a chemical factor. Initially [6,31,32], the hydrogen bonding interactions were accounted for by invoking the formation of complexes or cluster associates in the system and the model was known as the LFAS (Lattice-Fluid Associated-Solutions) model. This was a rather successful equation-of-state model handling properly the strong specific interactions. Its main drawback was its difficulty to handle three-dimensional hydrogen-bonding networks, such as those occurring in polymer mixtures or in aqueous polymer solutions.

In early 90's, however, the LF model was enhanced with a powerful hydrogen-bonding approach, which had the versatility and strength of LFAS model but could also handle three-dimensional hydrogen-bonding networks [36]. The Veytsman statistics [35] was adapted to the equation of state approach and the resulting model is known as the Lattice-Fluid with Hydrogen-Bonding (LFHB) model [27]. The LFHB approach has been proved efficient in handling complex phase equilibrium calculations,

Please cite this article in press as: G. Mensitieri, G. Scherillo, C. Panayiotou et al. Towards a predictive thermodynamic description of Fsorption processes in polymers: The synergy between theoretical EoS models and vibrational spectroscopy. Mater. Sci. Eng. R (2020), https://doi.org/10.1016/j.mser.2019.100525

cooperativity, intramolecular association, rubber swelling, gel collapse, just to name a few of its numerous applications [27,78–80]. Since then, LFHB underwent a series of improvements, mainly, by incorporating non-randomness in the distribution of free-volume and molecular species in the system [8,9,39]. In what follows, then, we will review the essentials of this incorporation of hydrogen-bonding and non-randomness in the LF equation of state approach.

2.1.3. Non-randomness in the equation-of-state approach

The central objective in this sub-section is the presentation of a coherent formalism interconnecting the above LF formalism and the latest developments in the NRHB approach. For this purpose, our first task will be the formulation of the configurational partition function of a multicomponent system of N_1, N_2, . . . , N_t molecules of components 1,2, . . . ,*t*, respectively and N_o empty cells, at temperature, *T*, total volume *V*, and external pressure, *P*.

In particular the canonical partition function of such system is given by:

$$Q(T,N_0,N_1,N_2,\ldots,N_t) = \sum_{N_{ij},N_{\substack{H\\ \alpha\beta}}} Q\left(T,N_0,N_1,N_2,\ldots,N_t,N\ ij,\ N\ \alpha\beta^H\right) \tag{41}$$

Here and in the following, $N\ \alpha\beta^H$ represents an array of variables, whose generic $N^H_{\alpha\beta}$ term represents the total number of hydrogen bonding interactions between proton donors of type α and proton acceptors of type β present in the system under consideration. Furthermore, here and in the following, $N\ ij$ represents an array of variables, whose generic N_{ij} term stands for the number of lattice fluid contacts between a segment of a molecule of type *i* and a segment of a molecule of type *j*, with *i* ranging from 0 to *t* and $j > i$.

In Eq. (41) the summation spans over all the admissible values of the set of internal variables of the model, $N\ ij$ and $N\ \alpha\beta^H$. Note that the same symbol *Q* has been used in order to express both the generic term of sum in the calculation of canonical partition function and the canonical partition function itself. No ambiguity is generated by such notation since the corresponding different set of independent variables for the two cases has been explicitly indicated. It is worth observing that the N_{ij} variables are not all independent of each other, since they must satisfy the following *t* +1 material balance equations:

$$2N_{ii} + \sum_{j\,(j\neq i)}^{t} N_{ij} = N_i z q_i \ \forall\, i\ (i = 0,\ldots t) \tag{42}$$

In Eq. (42) zq_i represents the number of external lattice contacts per molecule for component *i*. As a consequence, only an independent subset of the N_{ij} variables is to be considered in the $N\ ij$ array. In particular, based on Eq. (42), it is trivial to express any of the *t*+1 N_{ii} variables as a function of the remaining N_{ij} variables with *i* ranging from 0 to *t* and for $j > i$. A key assumption is the factorization of the partition function $Q(T,N_0,N_1,N_2,\ldots,N_t)$ into a random, or *athermal*, and an energetic, or *thermal*, part, as follows [1,9,36,72–74,81–90]:

$$\begin{aligned} Q(N_1,N_2,\ldots,N_t,T,N_0) &= \sum\nolimits_i \left(\Omega_i e^{-\beta E_i}\right) \cong Q_{Athermal} Q_{Thermal} \\ &= Q_R Q_E \end{aligned} \tag{43}$$

The summation in the above equation spans all microstates *i* in the phase space of our system characterized by a corresponding energy level E_i, while Ω_i is the degeneration or multiplicity factor for all microstates corresponding to the energy level E_i and β is the thermal energy factor equal to *1/kT*. The random term Q_R represents the limiting value of the partition function when all intermolecular interaction energies are identical, and the molecules are distributed randomly throughout the volume of the system. The energetic part, Q_E, is then a correction term for the non-random distribution of molecular species, which should become equal to one in the limiting case of zero interchange energies (cf. Eq. (38)). In highly non-ideal systems of molecules interacting with strong specific forces, the energetic part may be further factorized, for convenience, into a non-randomness term, Q_{NR}, and a chemical or hydrogen bonding term, Q_H, that explicitly accounts for establishment of strong specific interactions. Thus, the configurational partition function can be written alternatively as:

$$\begin{aligned} Q(N_1,N_2,\ldots,N_t,T,N_0) &= Q_R Q_E = Q_R\{Q_{NR} Q_H\} = \{Q_R Q_{NR}\} Q_H \\ &= Q_{Ph} Q_H \end{aligned} \tag{44}$$

In this way, the partition function can be then factorized into a "physical", Q_{Ph}, and a "chemical" or hydrogen-bonding term, Q_H:

$$Q = Q_{Ph}(T,N_0,N_1,N_2,\ldots,N_t) Q_H(T,N_0,N_1,N_2,\ldots,N_t) \tag{45}$$

The subscript '*Ph*' indicates 'physical' and the subscript '*H*' indicates 'hydrogen bonding'. Consistently with this framework, in the statistical models associated to LFHB theories, the physical contribution to the canonical partition function can be generally expressed as:

$$Q_{Ph}(T,N_0,N_1,N_2,\ldots,N_t) = \sum_{N_{ij}} Q_{Ph}(T,N_0,N_1,N_2,\ldots,N_t,N\ ij) \tag{46}$$

and the hydrogen bonding contribution as:

$$Q_H(T,N_0,N_1,N_2,\ldots,N_t) = \sum_{N_{\substack{H\\ \alpha\beta}}} Q_H\left(T,N_0,N_1,N_2,\ldots,N_t,N\ \alpha\beta^H\right) \tag{47}$$

Finally, the Gibbs partition function, Ψ, in the isobaric-isothermal (N, P, T) ensemble can be obtained from *Q* according to classical statistical thermodynamics as follows:

$$\Psi(T,P,N_1,N_2,\ldots,N_t) =$$

$$\sum_{N_0=0}^{\infty}\left[Q_{Ph}(T,N_0,N_1,N_2,\ldots,N_t) Q_H(T,N_0,N_1,N_2,\ldots,N_t) exp\left(-\frac{PV}{kT}\right)\right] \tag{48}$$

Here *P* and *V* represent, respectively, the pressure and the volume of the mixture. In turn, the volume can be expressed as:

$$V = V_{Ph} + V_H = rN\sim vv^* + \sum_{\alpha=1}^{m}\sum_{\beta=1}^{n} N^H_{\alpha\beta} V^0_{\alpha\beta} \tag{49}$$

where $V^0_{\alpha\beta}$ is the molecular volume change associated to the formation of an α-β hydrogen bond, while V_{Ph} is the contribution of the physical term, which is described by a LF framework. Based on this relationship the total volume *V* is a function of $T,N_0,N_1,N_2,\ldots,N_t,N\ ij,\ N\ \alpha\beta^H$.

An explicit expression for this function will be given in sub-section 2.1.5 where the NRHB model is discussed in detail. Any LF model endowed with HB interactions described in this review, allows the expression of N_0 as a function of *V*, i.e. $N_0 = f\left(T,V,N_1,N_2,\ldots,N_t,N\ ij,\ N\ \alpha\beta^H\right)$. Consequently, N_0 can take the role of an internal state variable of the system in place of V. More on this in section 2.1.5.

From Eq. (48) the Gibbs energy can be then obtained as:

$$G = -kTln[\Psi(T,P,N_1,N_2,\ldots,N_t)] \tag{50}$$

According to a standard procedure used when applying mean-field statistics, the summation in Eq. (48), can be approximated by its maximum term. In the classical maximum term approximation

[3–5,32] this is mathematically equivalent to first equating G to the logarithm of the generic term of the Gibbs partition function i.e.:

$$G(T,P,N_0,N_1,N_2,\ldots,N_t,N^H_{\alpha\beta},N\,ij) = -kT\ln[Q_{Ph}(T,N_0,N_1,N_2,\ldots,N_t,N\,ij)Q_H\left(T,N_0,N_1,N_2,\ldots,N_t,N\,\alpha\beta^H\right)exp\left(-\frac{PV}{kT}\right)] \quad (51a)$$

and then finding its minimum with respect to the three sets of internal variables given respectively by $N\,ij$, $N\,\alpha\beta^H$ and N_0 or V. It is worth noting that, in place of N_0 or V, one could also consider the variable $\sim v$.

As a direct consequence of the above factorization and of Eq. (49), one can write:

$$G(T,P,N_0,N_1,N_2,\ldots,N_t,N^H_{\alpha\beta},N\,ij) = -kT\ln\left[Q_{Ph}(T,N_0,N_1,N_2,\ldots,N_t,N\,ij)exp\left(-\frac{PV_{Ph}}{kT}\right)\right]$$

$$-kT\ln\left[Q_H\left(T,N_0,N_1,N_2,\ldots,N_t,N\,\alpha\beta^H\right)exp\left(-\frac{PV_H}{kT}\right)\right] = G_{Ph}+G_H \quad (51b)$$

Gibbs energy, G, can be considered as the sum of a *physical* term and a *chemical* or *hydrogen bonding* term.

$N\,\alpha\beta^H$, $N\,ij$ and the total volume of the mixture, V, are, in fact, internal state variables and, at equilibrium, the Gibbs energy is at a minimum with respect to them, at fixed P, T and composition. The role of these variables is of fundamental importance in the development of non-equilibrium extension of NRHB to glassy polymers, as discussed in the sub-section 2.2.2. Actually, it can be demonstrated that, for the purpose of calculation of equilibrium properties, the variable V can be replaced by $\sim v$, thus, the following simultaneous minimization conditions apply for G:

$$\left(\frac{\partial G}{\partial N_{ij}}\right)_{P,T,N,\sim v,N_{rs\neq ij},N\,\alpha\beta^H} = \left(\frac{\partial G_{Ph}}{\partial N_{ij}}\right)_{P,T,N,\sim v,N_{rs\neq ij}} = 0 \text{ for each } i,j = 0,1,\ldots t \text{ and } j > 1 \quad (52a)$$

$$\left(\frac{\partial G}{\partial N^H_{\alpha\beta}}\right)_{P,T,N,\sim v,\,N\,ij,N^H_{\gamma\delta\neq\alpha\beta}} = \left(\frac{\partial G_H}{\partial N^H_{\alpha\beta}}\right)_{P,T,N,\sim v,N^H_{\gamma\delta\neq\alpha\beta}} = 0 \text{ for each } \alpha,\beta \quad (52b)$$

$$\left(\frac{\partial G}{\partial\sim v}\right)_{P,T,N,\,N\,ij,N\,\alpha\beta^H} = \left(\frac{\partial G_{Ph}}{\partial\sim v}\right)_{P,T,N,\,N\,ij} + \left(\frac{\partial G_H}{\partial\sim v}\right)_{P,T,N,N\,\alpha\beta^H} = 0 \quad (52c)$$

In Eqs. (52a,b,c) $\underline{N}$ indicates the composition variables set $(N_1,N_2,\ldots,N_t)$. The third condition (Eq. (52c)) leads to the expression of the equation of state, *EoS*. The set of all equations (52) allows for the calculation of the equilibrium values of V, $N\,\alpha\beta^H$ and $N\,ij$.

At equilibrium, the chemical potential of component k is obtained by coupling the set of Eqs. (52a,b,c) with the following general expression:

$$\mu_k = \left(\frac{\partial G}{\partial N_k}\right)_{P,T,N_{j\neq k},\sim v,N\,ij,N\,\alpha\beta^H} = \left(\frac{\partial G_{Ph}}{\partial N_k}\right)_{P,T,N_{j\neq k},\sim v,N\,ij} + \left(\frac{\partial G_H}{\partial N_k}\right)_{P,T,N_{j\neq k},\sim v,N\,\alpha\beta^H} = \mu_{k,Ph}+\mu_{k,H} \quad (53)$$

More details on this procedure will be given in the sub-section 2.2.2 dealing with NRHB model.

In the next section, we will present the Veytsman statistics [35] or the combinatorial formalism for hydrogen bonding, which is used for estimating the hydrogen-bonding contribution, Q_H, to the partition function. This approach can be combined with any other appropriate thermodynamic model able to describe the non-hydrogen bonding contributions to the thermodynamic properties of the studied systems. In this review, the *physical* term, Q_{Ph}, of the partition function will be estimated using the NRHB [39] and QCHB [8] equation of state approaches, presented in the sub-section 2.1.5, and the PSP formalism [40–44,53–55], presented in the sub-section 3.8.1, for the prediction of thermodynamic properties of complex systems.

2.1.4. Accounting for strong specific interactions in the equation-of-state approaches

Let us focus now on the hydrogen bonding or chemical term of the partition function, Q_H. Let us assume that there are m different kinds of hydrogen-bonding donors and n kinds of hydrogen-bonding acceptors in the system. Let d^k_α be the number of hydrogen bonding donors of type α (α = 1,m) in each molecule of type k (k = 1, t) and a^k_β the number of hydrogen-bonding acceptors of type β (β = 1,n) in each molecule of type k. The total number N^α_d of hydrogen-bonding donors α in the system is:

$$N^\alpha_d = \sum_{k=1}^{t} d^k_\alpha N_k \quad (54)$$

and the total number N^β_a of hydrogen-bonding acceptors β in the system is:

$$N^\beta_a = \sum_{k=1}^{t} a^k_\beta N_k \quad (55)$$

The potential energy of the system due to hydrogen bonding is *in excess* of that due to physical interactions. The total energy E_H of the system due to hydrogen bonding is given by:

$$E_H = \sum_{\alpha=1}^{m}\sum_{\beta=1}^{n} N^H_{\alpha\beta}E^0_{\alpha\beta} \quad (56)$$

where $N^H_{\alpha\beta}$ is the number of hydrogen bonds between donors of type α and acceptors of type β, and $E^0_{\alpha\beta}$ the corresponding molecular energy of formation of an α-β hydrogen bonding.

The total number of hydrogen bonds, N_H, in the system is:

$$N_H = \sum_{\alpha=1}^{m}\sum_{\beta=1}^{n} N^H_{\alpha\beta} \quad (57)$$

What is now required is the number of ways, Ω_H, of distributing the $N^H_{\alpha\beta}$ bonds between the functional groups of the system. In order to find the different number of isoenergetic configurations of our system (number of different ways of forming or distributing the hydrogen bonds in the system) we have to find the number of distinguishable ways for:

a) Selecting the associated donor sites out of the donor population.
b) Selecting the associated acceptor sites out of the acceptor population.

Please cite this article in press as: G. Mensitieri, G. Scherillo, C. Panayiotou et al. Towards a predictive thermodynamic description of Fsorption processes in polymers: The synergy between theoretical EoS models and vibrational spectroscopy. Mater. Sci. Eng. R (2020), https://doi.org/10.1016/j.mser.2019.100525

c) Making hydrogen bonds between the selected donor and acceptor sites.

Having the number of distinguishable ways, Ω_H, of distributing the $N^H_{\alpha\beta}$ bonds among the functional groups of the system, we may write:

$$Q_H\left(T, N_0, N_1, N_2, \ldots, N_t, N\,\alpha\beta^H\right) = \Omega_H\left[\prod_{\alpha=1}^{m}\prod_{\beta=1}^{n} P_{\alpha\beta}^{N^H_{\alpha\beta}} \exp\left(\frac{-N^H_{\alpha\beta}E^0_{\alpha\beta}}{kT}\right)\right] \quad (58)$$

where $P_{\alpha\beta}$ is the probability of formation of a donor α acceptor β pair. There are several factors contributing to this probability. First, one has to consider the mean field probability P that a specific acceptor β will be in the proximity of a given donor α. This term is proportional to the volume of the acceptor group divided by the total system volume that is, $P \sim 1/V$. However, even spatial proximity does not guarantee that a bond actually forms. In fact, bond formation requires that donor and acceptor adopt a unique spatial orientation with respect to one another which is accompanied by a loss of rotational degrees of freedom (associated to an entropy decrease). Steric considerations will also come into play in bond formation. In general, for a donor α acceptor β pair, this probability is given by [27,36]:

$$P_{\alpha\beta} = e^{S^0_{\alpha\beta}/k}\left(\frac{\sim\rho}{rN}\right) \quad (59)$$

where $S^0_{\alpha\beta}$ is the molecular entropy loss (intrinsically negative) associated with hydrogen bond formation of an (α,β) pair. The term $\frac{\sim\rho}{r\cdot N}$ in Eq. (59) is derived from the expression for the volume V by the model (physical term) based upon a LF framework. We remind that rN represents the total number of cells occupied by the molecules in the system.

In the following sections (2.1.4.1, 2.1.4.2. and 2.1.4.3) will be presented three different cases for which the specialized expression for Ω in Eq. (58) is provided.

2.1.4.1. Association complexes and three - dimensional hydrogen-bonding networks. In this sub-section we briefly summarize the rationale for the enumeration process and apply it, first, to the simple case of a system of molecules with *one proton donor* and *one acceptor group*, such as systems with hydroxyl groups, which self-associate. At this stage we will assume that no cyclic *r*-mers are formed.

Let us consider a system with N molecules, each having one donor and one acceptor site (1) with $N^H{}_{11}$ hydrogen bonds among them. The number of ways of selecting the $N^H{}_{11}$ associated donors out of the donor population N is just the binomial coefficient $N!/(N\text{-}N^H{}_{11})!\,N^H{}_{11}!$. Similarly, the number of ways of selecting the $N^H{}_{11}$ associated acceptors out of the acceptor population N is again the binomial coefficient $N!/(N\text{-}N^H{}_{11})!\,N^H{}_{11}!$. The free donor groups in the system are $N - N^H{}_{11} = N^H{}_{10}$. This is also the number of free acceptor groups, $N^H{}_{01}$, in this particular system. Now, a specific donor can hydrogen bond with any of the $N^H{}_{11}$ acceptors, a second donor can hydrogen bond with any of the remaining $N^H{}_{11}$ -1 acceptors, and so on. The number of ways that $N^H{}_{11}$ bonds can be formed between $N^H{}_{11}$ donors and $N^H{}_{11}$ acceptors is just $N^H{}_{11}!$. Thus, the total number of ways that $N^H{}_{11}$ bonds can form between N donors and N acceptors is the product of the above three terms, or

$$\Omega = \frac{N!}{\left(N-N^H{}_{11}\right)!N^H{}_{11}!}\frac{N!}{\left(N-N^H{}_{11}\right)!N^H{}_{11}!}N^H{}_{11}! = \frac{N!}{N^H{}_{10}!}\frac{N!}{N^H{}_{10}!N^H{}_{11}!} \quad (60)$$

These arguments, when extended to the general case of multigroup molecules, lead to the following equation [26,27,34–36] (Veytsman statistics):

$$\Omega = \prod_{\alpha=1}^{m}\left(\frac{N^\alpha_d!}{N^H_{\alpha0}!N^H_{\alpha1}!\ldots N^H_{\alpha n}!}\right)\prod_{\beta=1}^{n}\left(\frac{N^\beta_a!}{N^H_{0\beta}!N^H_{1\beta}!\ldots N^H_{m\beta}!}\right)\prod_{\alpha=1}^{m}\prod_{\beta=1}^{n}N^H_{\alpha\beta}! = \prod_{\alpha=1}^{m}\frac{N^\alpha_d!}{N^H_{\alpha0}!}\prod_{\beta=1}^{n}\frac{N^\beta_a!}{N^H_{0\beta}!}\prod_{\alpha=1}^{m}\prod_{\beta=1}^{n}\frac{1}{N^H_{\alpha\beta}!} \quad (61)$$

Inserting Eqs. (61) and (59) in Eq. (58), one obtains for Q_H:

$$Q_H\left(T, N_0, N_1, N_2, \ldots, N_t, N\,\alpha\beta^H\right) = \left(\frac{\sim\rho}{rN}\right)^{N_H}\prod_{\alpha=1}^{m}\frac{N^\alpha_d!}{N^H_{\alpha0}!}\prod_{\beta=1}^{n}\frac{N^\beta_a!}{N^H_{0\beta}!}\prod_{\alpha=1}^{m}\prod_{\beta=1}^{n}\frac{\exp\left(-\frac{N^H_{\alpha\beta}F^0_{\alpha\beta}}{kT}\right)}{N^H_{\alpha\beta}!} \quad (62)$$

where $F^0_{\alpha\beta} = E^0_{\alpha\beta} - TS^0_{\alpha\beta}$, with $F^0_{\alpha\beta}$ the Helmholtz energy of formation of the α-β hydrogen bonding, $N^H_{\alpha0}$ the number of free (non-hydrogen bonded) donor groups of type α and $N^H_{0\beta}$ the respective number of free acceptor groups of type β:

$$N^H_{\alpha0} = \sum_{i=1}^{t}N_i d^i_\alpha - \sum_{\beta=1}^{n}N^H_{\alpha\beta} \quad (63a)$$

$$N^H_{0\beta} = \sum_{i=1}^{t}N_i a^i_\beta - \sum_{\alpha=1}^{m}N^H_{\alpha\beta} \quad (63b)$$

Here d^i_α represents the number of proton donor of kind α on a molecule of kind i and a^i_β is the number of proton acceptor of kind β on a molecule of kind i.

From Eq. (52b), for a system with n proton donors and m proton acceptors, one obtains the following equations:

$$\frac{\nu_{\alpha\beta}}{\nu_{\alpha0}\nu_{0\beta}} = \sim\rho\exp\left(\frac{-G^0_{\alpha\beta}}{kT}\right)\text{ for each }\alpha,\ \beta \quad (64a)$$

or:

$$\nu_{\alpha\beta} = \left[\nu^\alpha_d - \sum_{k=1}^{n}\nu_{\alpha k}\right]\left[\nu^\beta_a - \sum_{k=1}^{m}\nu_{k\beta}\right] \sim \rho\exp\left(\frac{-G^0_{\alpha\beta}}{kT}\right) \quad (64b)$$

where

$\nu_{\alpha\beta} = \frac{N^H_{\alpha\beta}}{rN}$; $\nu_{\alpha0} = \frac{N^H_{\alpha0}}{rN}$; $\nu_{0\beta} = \frac{N^H_{0\beta}}{rN}$; $\nu^\alpha_d = \frac{N^\alpha_d}{rN}$; $\nu^\beta_a = \frac{N^\beta_a}{rN}$and
$G^0_{\alpha\beta} = F^0_{\alpha\beta} + PV^0_{\alpha\beta} = E^0_{\alpha\beta} - TS^0_{\alpha\beta} + PV^0_{\alpha\beta}$

This is a system of $(m \times n)$ quadratic equations for ν_{ij}. This system must be solved in combination with the equation of state Eq. (52c) and, in the general case of non-random LF model, with Eq. (52a). On the basis of Eq. (62) we can calculate the expression of the G_H:

$$\frac{G_H}{k\cdot T} = rN\left\{\sum_{\alpha=1}^{m}\sum_{\beta=1}^{n}\nu_{\alpha\beta}\left[1 + \frac{G^0_{\alpha\beta}}{kT} + \ln\left(\frac{\sim\nu\nu_{\alpha\beta}}{\nu_{\alpha0}\nu_{0\beta}}\right)\right] + \sum_{\alpha=1}^{m}\nu^\alpha_d\ln\left(\frac{\nu_{\alpha0}}{\nu^\alpha_d}\right) + \sum_{\beta=1}^{n}\nu^\beta_a\ln\left(\frac{\nu_{0\beta}}{\nu^\beta_a}\right)\right\} \quad (65)$$

As a consequence, according to Eq. (53) we can find the general expression of the HB contribution to the molecular chemical potential of species k:

$$\frac{\mu_{i,H}}{kT} = \left(\frac{\partial\left(\frac{G_H}{kT}\right)}{\partial N_i}\right)_{P,T,N_{j\neq i},\sim\nu,N\,\alpha\beta^H} = r_i\nu_H - \sum_{\alpha=1}^{m}\left[d^i_\alpha\ln\left(\frac{\nu^\alpha_d}{\nu_{\alpha0}}\right)\right] - \sum_{\beta=1}^{n}\left[a^i_\beta\ln\left(\frac{\nu^\beta_a}{\nu_{0\beta}}\right)\right] \quad (66)$$

Please cite this article in press as: G. Mensitieri, G. Scherillo, C. Panayiotou et al. Towards a predictive thermodynamic description of Fsorption processes in polymers: The synergy between theoretical EoS models and vibrational spectroscopy. Mater. Sci. Eng. R (2020), https://doi.org/10.1016/j.mser.2019.100525

where r_k represents the number of cells occupied (on the lattice model adopted to describe the physical contribution) by a molecule of species k and $\nu_H = \frac{N_H}{r \cdot N}$ represents the average number of hydrogen bonds (intermolecular) per segment. The Eq. (66), coupled with Eqs (52a,b,c) provides the HB contribution to the equilibrium molar chemical potential of species k.

2.1.4.2. The dimerization of acids. The lower aliphatic organic acids are associated rather peculiarly and, thus, a second case that will be investigated here is their dimerization [91]. In such systems, dimers are the overwhelming majority of the association species. For simplicity, then, we will consider dimerization only, in order to describe this hydrogen bonding behavior.

Let N_{dm} be the number of dimers in the system. Then, the number of ways of selecting these dimerized molecules out of the N acid molecules is:

$$\frac{N!}{(2N_{dm})!(N-2N_{dm})!} \tag{67}$$

The number of ways of selecting the N_{dm} dimers is:

$$\begin{aligned}\Omega &= \frac{N!}{(2N_{dm})!(N-2N_{dm})!}(2N_{dm}-1)(2N_{dm}-3)\ldots 1 \\ &= \frac{N!}{(N-2N_{dm})!N_{dm}!2^{N_{dm}}}\end{aligned} \tag{68}$$

The free energy change upon formation of one dimer is:

$$G_{dm} = E_{dm} + PV_{dm} - TS_{dm} \tag{69}$$

Consequently, the hydrogen-bonding factor in the partition function becomes:

$$Q_H = \frac{N!}{(N-2N_{dm})!N_{dm}!2^{N_{dm}}}\left(\frac{\sim \rho}{rN}\right)^{N_{dm}} \exp\left(-\frac{N_{dm}G_{dm}}{RT}\right) \tag{70}$$

The equilibrium number of dimers per mol of acid segments, ν_{dm}, is obtained from the above equation through the usual free energy minimization condition, or

$$\nu_{dm} = \frac{2 + \frac{1}{K_{dm}} - \sqrt{\frac{1}{K_{dm}^2} + \frac{4}{K_{dm}}}}{4r} \tag{71}$$

where

$$K_{dm} = \frac{\sim \rho}{r}\exp\left(\frac{-G_{dm}}{RT}\right) \tag{72}$$

In this case of dimerization, the hydrogen-bonding contribution to the chemical potential is:

$$\frac{\mu_H}{RT} = r\nu_{dm} - \ln\frac{1}{1-2r\nu_{dm}} \tag{73}$$

2.1.4.3. Intra-molecular hydrogen bonding. Both aforementioned cases referred to inter-molecular hydrogen bonding. However, the rationale is easily extended to systems with both inter- and intra-molecular hydrogen bonds [78,79,92,93]. In the general case of alkoxy alkanols, as an example, if x is the number of ether oxygen acceptor sites, the number of proton donors and acceptors of type 1 (−OH) is N_1, and of proton acceptors of type 2 (-O-) is xN_1. As was done previously [92,93], x is assumed to be equal to 2. As a consequence, the total number of free proton donors is:

$$N_{10} = N_1 - N_{11} - N_{22} - B \tag{74}$$

where B the number of intramolecular bonds OH—O- in the system.

In order to find the number of ways Ω of distributing the various hydrogen bonds in the system, we have first to select the N_{11}, N_{12}, B, and N_{10} donors out of the N_1 donor population. This can be done in $N_1!/[B!N_{11}!N_{12}!N_{10}!]$ ways. Secondly, we have to select the hydrogen bonded N_{11} acceptors of type 1 out of the N_1 acceptor population, which can be done in $N_1!/[N_{11}!\,(N_1\text{-}N_{11})!]$ ways. Next, we have to select the B acceptors of type 2 out of the xN_1 acceptor population. However, once we have selected the B proton donors that participate in intramolecular bonds, we have also selected the molecules with the acceptor sites of type 2 that participate in the B intramolecular bonds. We assume for simplicity that all x acceptor sites are equivalent for the intramolecular bonds. In each of these B molecules, we must now select the acceptor site of type 2 for the intra- molecular bond out of the x acceptors of type 2 that exist in such a molecule. For each molecule, this can be done in $x!\,/\,[1!\,(x\text{-}1)!]$ ways and, consequently, for the B molecules it can be done in $\{x!\,/\,[1!\,(x\text{-}1)!]\}^B = x^B$ ways. Having selected the B acceptor sites of type 2, we must now select, out of the remaining $(xN_1\text{-}B)$ acceptor type 2 population, the N_{12}, which will participate in the intermolecular bonds. This can be done in $(xN_1\text{-}B)!\,/\,[(xN_1 - B - N_{12})!N_{12}!]$ ways. The N_{11} and N_{12} bonds can be done in $N_{11}!\cdot N_{12}!$ ways, while the B bonds in only one way after having selected, both, the donor and the acceptor sites in each molecule. Thus, the number of configurations in the hydrogen bonded system is:

$$\Omega = \frac{N_1!}{B!N_{11}!N_{12}!N_{10}!}\frac{N_1!}{N_{11}!(N_1-N_{11})!}\left(\frac{x!}{(x-1)!}\right)^B \frac{(xN_1-B)!}{(xN_1-B-N_{12})!N_{12}!}N_{11}!N_{12}! =$$

$$= \frac{(xN_1-B)!(N_1!)^2x^B}{B!N_{11}!N_{12}!N_{10}!(N_1-N_{11})!(xN_1-B-N_{12})!} \tag{75}$$

The number of the three types of hydrogen bonds can be obtained from the following coupled minimization equations:

$$\frac{B(xN_1-B)}{(xN_1-B-N_{12})N_{10}x} = c\exp\left(-\frac{G_B^0}{kT}\right) = K_B \tag{76}$$

$$\frac{N_{11}}{(N_1-N_{11})N_{10}} = \frac{\sim \rho}{rN}\exp\left(-\frac{G_{11}^0}{kT}\right) = \frac{K_{11}}{N} \tag{77}$$

$$\frac{N_{12}}{(xN_1-B-N_{12})N_{10}} = \frac{\sim \rho}{rN}\exp\left(-\frac{G_{12}^0}{kT}\right) = \frac{K_{12}}{N} \tag{78}$$

where G_{11}° and G_{12}° are the free energy changes upon formation of the intermolecular hydrogen bonds of type 1–1, and 1–2, respectively, and G_B° is the corresponding free energy change upon formation of the intramolecular hydrogen bonds. The free energy change for the i-j bond is given by $G_{ij}^\circ = E_{ij}^\circ + PV_{ij}^\circ - TS_{ij}^\circ$, E_{ij}°, V_{ij}°, S_{ij}° being the energy, volume, and entropy change, respectively, upon formation of the same hydrogen bond.

After some algebra, the above three equations lead to the following expressions:

$$N_{12} = \frac{K_{12}}{K_BNx}B(xN_1-B) \tag{79}$$

$$N_{11} = \frac{K_{11}}{K_BNx + B(K_{11}-K_{12})}BN_1 \tag{80}$$

$$B = \frac{(NxK_B - K_{12}.B)}{N}\left[N_1 - B - B\frac{K_{12}}{xK_B}\frac{(xN_1-B)}{N} - N_1\frac{K_{11}B}{xNK_B + B(K_{11}-K_{12})}\right] \tag{81}$$

The last equation contains only the unknown B and it can be solved numerically by successive substitutions. The solution for B can then be replaced in Eqs. (79) and (80) in order to obtain N_{12} and

Please cite this article in press as: G. Mensitieri, G. Scherillo, C. Panayiotou et al. Towards a predictive thermodynamic description of Fsorption processes in polymers: The synergy between theoretical EoS models and vibrational spectroscopy. Mater. Sci. Eng. R (2020), https://doi.org/10.1016/j.mser.2019.100525

N_{11}, respectively. Having obtained the numbers of hydrogen bonds in the system, the average number of hydrogen bonds (intermolecular) per segment, ν_H, can be calculated by:

$$\nu_H \frac{N_H}{rN} = \frac{N_{11} + N_{12}}{rN} \tag{82}$$

and the hydrogen bonding contribution to the chemical potential of alkoxyalkanol is given by [78]:

$$\frac{N_1 \mu_{1H}}{RT} = N_H + N_1 \ln(1 - \frac{N_H + B}{N_1}) + N_1 \ln(1 - \frac{N_{11}}{N_1}) + xN_1 \ln(1 - \frac{N_{12}}{xN_1 - B}) \tag{83}$$

The corresponding contribution for the inert compound of the mixture is given by:

$$\frac{\mu_{2H}}{RT} = r\nu_H \tag{84}$$

The above examples give a good picture of the versatility of the Veytsman statistics [35,36] to cope with complex hydrogen bonding cases.

2.1.5. The NRHB equation-of-state model

2.1.5.1. Description of the NRHB model. There are numerous expressions for the physical contribution to the partition function (see Eq. (44)) depending on the adopted framework. The hydrogen bonding contribution discussed above can, then, be implemented in several equation of state or activity coefficient model frameworks. In this section, we will illustrate the NRHB equation of state approach [9,39] of the broader LF framework, which does account for the non-random distribution of empty sites and molecular segments and also for hydrogen bonding (and other association interactions) by including the contribution to the partition function discussed in the previous section.

Let our molecular system consist of $N_1, N_2, \ldots, N_t$ molecules of components *1,2, . . . ,t*, respectively. As previously with the LF framework, each component of type *i* consists of r_i segments, each of segmental volume v_i^*. The molecules are assumed to be arranged on a quasi- lattice of coordination number *z* and made of N_r sites, N_0 of which are empty. The total number N_r of lattice sites is given by the expression:

$$N_r = N_1 r_1 + N_2 r_2 + \ldots + N_t r_t + N_0 = rN + N_0 = N(x_1 r_1 + x_2 r_2 + \ldots + x_t r_t) + N_0 \tag{85}$$

where $N = N_1 + N_2 + \ldots + N_t$ is the total number of molecules in the system and x_i is the mole fraction of component *i*. The average intersegmental interaction energy per segment of molecule *i* is given by:

$$\varepsilon_i^* = \left(\frac{z}{2}\right)\varepsilon_{ii} \tag{86}$$

where ε_{ii} is the interaction energy per *i* - *i* contact. If zq_i is the number of external contacts per molecule *i*, a geometric characteristic of molecule *i* is its "surface-to-volume" ratio, $s_i = q_i/r_i$. This ratio can be estimated for a very large number of different compounds by using the widely used UNIFAC group contribution model [87,88]. In this way, s_i is not a fitted parameter but is calculated based on well-established theories.

In a mixture, parameters *r* and *q* are calculated through the following simple mixing rules:

$$r = \sum_{i=1}^{t} x_i r_i \tag{87}$$

$$q = \sum_{i=1}^{t} x_i q_i \tag{88}$$

and so:

$$s = q/r \tag{89}$$

Furthermore, segment fractions ϕ_i and surface (contact) fractions θ_i are defined as:

$$\phi_i = \frac{r_i N_i}{rN} = \frac{x_i r_i}{r} \text{ with } i = 1.2, \ldots, t \tag{90}$$

and

$$\theta_i = \frac{q_i N_i}{\sum_{k=1}^{t}(q_k N_k)} = \frac{q_i N_i}{qN} = \frac{\phi_i s_i}{\sum_{k=1}^{t}(\phi_k s_k)} = \frac{\phi_i s_i}{s} \text{ with } i = 1.2, \ldots, t \tag{91}$$

The total number of external contact sites in the system is:

$$zN_q = zqN + zN_0 \tag{92}$$

while V_{Ph} is given by the expression:

$$V_{Ph} = rNv^* + N_0 v^* = N_r v^* = V^* + N_0 v^* \tag{93}$$

where the same average segmental volume v^* is assigned to an empty site as to an occupied site. Furthermore, it is assumed that two neighboring empty sites on the quasi-lattice remain discrete and do not coalesce. In what follows we will adopt the above mentioned "universal" value of 9.75 $cm^3\ mol^{-1}$ [39,73] for v^* for all fluids.

The structure of the NRHB model includes a G_H term that is given by Eq. (65), while the G_{Ph} term is given by Eq. (51b), once proper expressions are provided for Ω_R and Ω_{NR}:

$$Q_{Ph}(T, N_0, N_1, N_2, \ldots, N_t, N\ ij) exp\left(-\frac{PV_{Ph}}{kT}\right) = \Omega_R \Omega_{NR} \cdot \exp\left(-\frac{E_{Ph} + PV_{Ph}}{kT}\right) \tag{94}$$

Here E_{Ph} represents the total energy of the system associated to physical "mean field" interactions and it will be specified in the following (see Eq. (110)). Ω_R is the combinatorial term for a hypothetical system with a random distribution of the empty sites and molecular species and Ω_{NR} is a correction term for the actual non-random distribution. As already mentioned, for the random combinatorial term, the Flory expression [2] was used first, resulting in the Sanchez-Lacombe lattice fluid theory [3,4] or the Guggenheim expression [1] resulting in the PV model [73] and the QCHB model [8]. The PV model formed the basis for the development of many other lattice models in recent years. In NRHB [9,39], the generalized Guggenheim-Staverman expression [86] is adopted:

$$\Omega_R = \left(\prod_{i=1}^{t} \omega_i^{N_i}\right)\left[\frac{N_r! \prod_{i=1}^{t} N_r^{l_i \cdot N_i}}{N_0! \prod_{i=1}^{t} N_i!}\left(\frac{N_q!}{N_r!}\right)^{\frac{z}{2}}\right] \tag{95}$$

where, again, ω_i is a characteristic quantity for fluid *i* that accounts for the flexibility and symmetry of the molecule. In phase equilibrium calculations, this quantity cancels out. The Staverman parameter l_i is given by:

$$l_i = \frac{z}{2}(r_i - q_i) - (r_i - 1) \tag{96}$$

For the non-random correction, the quasi chemical theory of Guggenheim is used [72] in the NRHB model:

$$\Omega_{NR} = \frac{\prod_{i=0}^{t} N_{ii}^0! \prod_{i=0}^{t} \prod_{j>i}^{t} \left[\left(\frac{N_{ij}^0}{2}\right)!\right]^2}{\prod_{i=0}^{t} N_{ii}! \prod_{i=0}^{t} \prod_{j>i}^{t} \left[\left(\frac{N_{ij}}{2}\right)!\right]^2} \tag{97}$$

where, N_{ij} is the number of external *i-j* contacts. In this equation, *i* runs from zero (empty site) to the number of components, *t*, while

Please cite this article in press as: G. Mensitieri, G. Scherillo, C. Panayiotou et al. Towards a predictive thermodynamic description of Fsorption processes in polymers: The synergy between theoretical EoS models and vibrational spectroscopy. Mater. Sci. Eng. R (2020), https://doi.org/10.1016/j.mser.2019.100525

the superscript '0' refers to the case of random distribution of empty sites and molecular species.

Actually, two alternative ways of calculating Ω_{NR} have been proposed in the literature, resulting in two different versions of the model. Initially, Panayiotou et al. [9] adopted a 'simplified' version of NRHB model that considers only the non-randomicity in the distribution of empty sites around a central empty site and the non-randomicity in the distribution of an occupied (molecular) site around a central molecular site. Consequently, Ω_{NR} takes the following simplified form:

$$\Omega_{NR} = \frac{N_{rr}^0! N_{00}^0! \left[\left(\frac{N_{r0}^0}{2}\right)!\right]^2}{N_{rr}! N_{00}! \left[\left(\frac{N_{r0}}{2}\right)!\right]^2} \tag{98}$$

where N_{rr} is the number of external contacts between segments belonging to molecules and N_{00} is the number of contacts between empty sites. In the second case [39], the full Eq. (97) is used and the non-randomness of every *i-j* contact ($i = 0$ to t and $j \geq i$) is accounted for. In the present contribution, by NRHB we refer to this second approach [39,94–100].

In the random case, the number of external contacts between segments belonging to molecules, N_{rr}^0, takes the form:

$$N_{rr}^0 = \frac{1}{2} zqN \frac{qN}{N_0 + qN} = \frac{z}{2} qN\theta_r \tag{99}$$

where,

$$\theta_r = 1 - \theta_0 = \frac{q/r}{q/r + \sim v - 1} \tag{100}$$

and, as before, the reduced volume, $\sim v$, is defined as:

$$\sim v = \frac{V_{Ph}}{V^*} = \frac{1}{\sim \rho} = \frac{1}{\sum_i f_i} \tag{101}$$

and

$$\sim \rho = \frac{V^*}{V_{Ph}} = \frac{rN}{N_r} \tag{102}$$

The site fractions f_0 and f_i, for the empty sites and molecular segments of component *i*, respectively, are defined as follows:

$$f_0 = \frac{N_0}{N_r} = \frac{N_r - \sum_i (r_i N_i)}{N_r} = 1 - \sum_i f_i \tag{103}$$

In the random case, the number of contacts between empty sites, N_{00}^0, is given by the equation:

$$N_{00}^0 = \frac{1}{2} N_0 z \frac{N_0}{N_q} = \frac{z}{2} N_0 \theta_0 \tag{104}$$

while the number of contacts between a segment and an empty site, N_{r0}^0, is given by:

$$N_{r0}^0 = zqN \frac{N_0}{N_q} = zN_0 \frac{qN}{N_q} = zqN\theta_0 = zN_0\theta_r \tag{105}$$

The total number of inter-segmental contacts is calculated as the sum of contributions between like molecules and between unlike molecules:

$$N_{rr}^0 = \sum_{i=1}^{t} N_{ii}^0 + \sum_{i=1}^{t} \sum_{j>i}^{t} N_{ij}^0 \tag{106}$$

where:

$$N_{ii}^0 = \frac{z}{2} q_i N_i \frac{q_i N_i}{N_q} = \frac{z}{2} q_i N_i \theta_i \theta_r \tag{107a}$$

$$N_{ij}^0 = zq_i N_i \frac{q_j N_j}{N_q} = zq_i N_i \theta_j \theta_r = zq_j N_j \theta_i \theta_r \text{ with } i \neq j \tag{107b}$$

We may then express the number of intermolecular contacts in the non-random case by using the non-randomness factors, Γ, mentioned above. This leads to the following $2t + t(t-1)/2 + 1$ expressions:

$$N_{ii} = N_{ii}^0 \Gamma_{ii} \text{ with } i = 1, \ldots, t$$

$$N_{ij} = N_{ij}^0 \Gamma_{ij} \text{ with } t \geq j > i \geq 1$$

$$N_{00} = N_{00}^0 \Gamma_{00}$$

$$N_{i0} = N_{i0}^0 \Gamma_{i0} \text{ with } i = 1, \ldots, t \tag{108}$$

Trivially, in the case of random distribution, all non-random factors, Γs, are equal to one, while in all the other cases they should obey the following material (contact) balance expressions, which results from Eq. (42):

$$\sum_{i=0}^{t} \Theta_i \Gamma_{ij} = 1 \text{ with } j = 0, 1, \ldots, t \tag{109}$$

where $\Theta_0 = \theta_0$ and $\Theta_i = \theta_i \theta_r$.

It is recalled that in the LF approach only first-neighbor molecular segment – segment interactions contribute to the potential energy *E* of the system. Consequently, for a mixture, the potential energy E_{Ph} is given by:

$$-E_{Ph} = \sum_{i=1}^{t} N_{ii}\varepsilon_{ii} + \sum_{i=1}^{t} \sum_{j>i}^{t} N_{ij}\varepsilon_{ij} \tag{110}$$

and

$$\varepsilon_{ij} = \sqrt{\varepsilon_{ii}\varepsilon_{jj}}(1 - k_{ij}) = \xi_{ij}\sqrt{\varepsilon_{ii}\varepsilon_{jj}} \tag{111}$$

where k_{ij} (or ξ_{ij}) is a binary adjustable interaction parameter for the pair *i, j*.

By substituting Eqs. (95), (96) and (97) in the Eq. (51), and using Eq. (103), the expression for G_{Ph} can be obtained. In particular, the following relationship holds:

$$\frac{G_{Ph}}{kT} =$$

$$-rN\left\{\sum_{i=1}^{t} \frac{i}{r_i} \ln \delta_i + \frac{l}{r} - \sum_{i=1}^{t} \frac{i}{r_i} \ln \frac{i}{r_i} - \ln \frac{\sim \rho}{r} - (\sim v - 1)\right.$$

$$\left. \ln\left(1 - \sim \rho\right) + \frac{z}{2}\left(\sim v - 1 + \frac{q}{r}\right) \ln\left(1 - \sim \rho + \frac{q}{r} \sim \rho\right)\right\}$$

$$+rN\left\{\sum_{i=0}^{t} \frac{zq}{2r} \vartheta_i \ln\left[\Gamma_{ii} \exp\left(-\frac{\varepsilon_{ii}}{kT}\right)\right] + \sum_{i=0}^{t} \sum_{j>i}^{t} \frac{N_{ij}}{2rN} \ln\left[\frac{\Gamma_{ij}^2}{\Gamma_{ii}\Gamma_{jj}} \exp\left(\frac{\Delta\varepsilon_{ij}}{kT}\right)\right]\right.$$

$$\left. + \frac{\sim P \sim v}{\sim T}\right\} \tag{112}$$

Finally, summing Eq. (112) and Eq. (65) we obtain the expression for the generic term of Gibbs energy, *G*, for the NRHB model (referred to as G_{NRHB}):

$$\frac{G_{NRHB}}{kT} = -rN\left\{\sum_{i=1}^{t} \frac{i}{r_i} \ln \delta_i + \frac{l}{r} - \sum_{i=1}^{t} \frac{i}{r_i} \ln \frac{i}{r_i} - \ln \frac{\sim \rho}{r} - (\sim v - 1)\right.$$

$$\left. \ln(1 - \sim \rho) + \frac{z}{2}\left(\sim v - 1 + \frac{q}{r}\right) \ln\left(1 - \sim \rho + \frac{q}{r} \sim \rho\right)\right\}$$

$$+rN\left\{\sum_{i=0}^{t} \frac{zq}{2r} \vartheta_i \ln\left[\Gamma_{ii} \exp\left(-\frac{\varepsilon_{ii}}{kT}\right)\right] + \sum_{i=0}^{t} \sum_{j>i}^{t} \frac{N_{ij}}{2rN} \ln\left[\frac{\Gamma_{ij}^2}{\Gamma_{ii}\Gamma_{jj}} \exp\left(\frac{\Delta\varepsilon_{ij}}{kT}\right)\right] + \sim P \frac{\sim v}{\sim T}\right\}$$

$$+rN\left\{\sum_{\alpha=1}^{m}\sum_{\beta=1}^{n}\nu_{\alpha\beta}\left[1+\frac{G^{0}_{\alpha\beta}}{kT}+\ln\left(\frac{\sim v\,\nu_{\alpha\beta}}{\nu_{\alpha 0}\nu_{0\beta}}\right)\right]+\sum_{\alpha=1}^{m}\nu_{d}^{\alpha}\ln\left(\frac{\nu_{\alpha 0}}{\nu_{d}^{\alpha}}\right)+\sum_{\beta=1}^{n}\nu_{a}^{\beta}\ln\left(\frac{\nu_{0\beta}}{\nu_{a}^{\beta}}\right)\right\} \tag{113}$$

It is worth reminding that the reported expressions of G_{Ph}, G_H, and G_{NRHB} represent the generic term contributions to the calculation of the equilibrium Gibbs energy of the system and that, according to the maximum term approximation, their expressions must be minimized with respect to the sets of internal state variables (see Eqs (52a,b,c)) in order to obtain the equilibrium expression of Gibbs energy, from which all the main equilibrium thermodynamic quantities may be obtained. A similar procedure also applies to the case of the 'simplified' version of NRHB mode. Details on this procedure are provided in the following with reference to both versions of NRHB.

As discussed, the Gibbs energy can be split in two contributions:

$$G_{NRHB}\left(T,P,N_1,N_2,\ldots,N_t,\sim v,N\,ij,N\,\alpha\beta^{H}\right)=$$

$$G_{Ph}(T,P,N_1,N_2,\ldots,N_t,\sim v,N\,ij)+G_H\left(T,P,N_1,N_2,\ldots,N_t,\sim v,N\,\alpha\beta^{H}\right) \tag{114}$$

According to macroscopic thermodynamics endowed with internal state variables, the equilibrium expression of G_{NRHB} is obtained by specializing the minimization Eqs. (52). In the case of NRHB, this minimization procedure provides the following set of equations:

The value of G_{NRHB} for the mixture at equilibrium, at assigned T, P and composition (N) of the system, i.e. G^{EQ}_{NRHB}, is then obtained by substituting in its expression, Eq. (113), the equilibrium values of $\sim v$ and of the set of variables $N\,ij$ and $N\,\alpha\beta^{H}$ that are obtained by solving the set of Eqs. (115a,b,c):

$$G^{EQ}_{NRHB}(T,P,N_1,N_2,\ldots,N_t)=$$

$$G_{NRHB}\left(T,P,N_1,N_2,\ldots,N_t,\sim v^{EQ}(T,P,N_1,N_2,\ldots,N_t),N\,ij^{EQ}(T,P,N_1,N_2,\ldots,N_t),N\,\alpha\beta^{H,\,EQ}(T,P,N_1,N_2,\ldots,N_t)\right) \tag{122}$$

No closed form is, however, available, since this whole set of equations can only be solved numerically. Once the expression of G^{EQ}_{NRHB} is available, the equilibrium molecular chemical potential of species i, can be calculated as:

$$\mu^{EQ}_{i,NRHB}(T,P,N_1,N_2,\ldots,N_t)\equiv\left(\frac{\partial\left(G^{EQ}_{NRHB}\right)}{\partial N_i}\right)_{P,T,N_{j\neq i},} \tag{123}$$

and it could be obtained by performing the numerical derivation of the Eq. (122) at selected values of T, P and $\underline{N}$, satisfying the constraints imposed by Eqs. (115a,b,c). Alternatively, it is possible to carry out the following procedure based upon the chain-rules of derivative operation. The various steps involved are briefly described.

$$\begin{cases}\dfrac{\Gamma_{ij}^{\,2}}{\Gamma_{ii}\Gamma_{jj}}=\exp\left(-\dfrac{\Delta\varepsilon_{ij}}{kT}\right)\ for\ each\ i,j=0,1,\ldots,t\ and\ j>i\\ \dfrac{\nu_{\alpha\beta}}{\nu_{\alpha 0}\nu_{0\beta}}=\sim\rho\exp\left(\dfrac{-G^{0}_{\alpha\beta}}{k\cdot T}\right)\ for\ each\ \alpha,\beta\ \dfrac{rN}{\sim T}\left\{\sim P+\sim T\left[\ln\left(1-\sim\rho\right)-\sim\rho\left(\sum_{i=1}^{t}{}_{i}\frac{l_i}{r_i}-\nu_H\right)-\frac{z}{2}\ln\left(1-\sim\rho+\frac{q}{r}\sim\rho\right)+\frac{z}{2}\ln\Gamma_{00}\right]\right\}=0\end{cases} \tag{115a, b, c}$$

where

$$\Delta\varepsilon_{ij}=\varepsilon_{ii}+\varepsilon_{jj}-2(1-k_{ij})\sqrt{\varepsilon_{ii}\varepsilon_{jj}} \tag{116}$$

and $\varepsilon_{00}=0$.

Moreover,

$$\sim T=\frac{T}{T^*}=\frac{kT}{\varepsilon^*} \tag{117}$$

$$\sim P=\frac{P}{P^*}=\frac{Pv^*}{kT^*} \tag{118}$$

The following mixing rule is adopted:

$$\varepsilon^*=\sum_{i=1}^{t}\sum_{j=1}^{t}\theta_i\theta_j\varepsilon^*_{ij} \tag{119}$$

with

$$\varepsilon^*_{ij}=\xi_{ij}\sqrt{\varepsilon^*_i\varepsilon^*_j}\ \text{or}\ \varepsilon^*_{ij}=\sqrt{\varepsilon^*_i\varepsilon^*_j}(1-k_{ij}) \tag{120}$$

The EoS of NRHB model, directly obtained from Eq (115c), is:

$$\sim P+\sim T\left[\ln\left(1-\sim\rho\right)-\sim\rho\left(\sum_{i=1}^{t}{}_{i}\frac{l_i}{r_i}-\nu_H\right)-\frac{z}{2}\ln\left(1-\sim\rho+\frac{q}{r}\sim\rho\right)+\frac{z}{2}\ln\Gamma_{00}\right]=0 \tag{121}$$

The LF contribution to the EoS is obtained by setting $\nu_H=0$ in Eq. (121). Since the whole procedure presented here is valid for a general multicomponent system, Eqs. (115a,b,c) and (121) hold also for the case of a pure component system, if one sets $\phi_i=1$ and $\theta_i=1$.

a) we first proceed by expliciting the generic expressions of the chemical potential in the case of NRHB model:

$$\frac{\mu_{i,Ph}}{kT}=\left(\frac{\partial\left(\frac{G_{Ph}}{kT}\right)}{\partial N_i}\right)_{P,T,N_{j\neq i},\,\sim v,N\,ij}$$

$$=\ln\frac{i}{\delta_i r_i}-r_i\sum_{j=1}^{t}\frac{{}_{j}l_j}{r_j}+\ln\sim\rho+r_i(\sim v-1)\cdot\ln(1-\sim\rho)$$

$$-\frac{z}{2}r_i\left(\sim v-1+\frac{q_i}{r_i}\right)\ln\left(1-\sim\rho+\frac{q}{r}\sim\rho\right)$$

$$+q_i\frac{z}{2}\left[\ln\Gamma_{ii}+\frac{r_i}{q_i}\left(\sim v-1\right)\ln\Gamma_{00}\right]$$

$$+r_i\sim P\,\frac{\sim v}{\sim T-\frac{q_i}{\sim T_i}} \tag{124a}$$

$$\frac{\mu_{i,H}}{kT}=\left(\frac{\partial\left(\frac{G_H}{kT}\right)}{\partial N_i}\right)_{P,T,N_{j\neq i},\,\sim v,N\,\alpha s^H}=r_i\nu_H-\sum_{\alpha=1}^{m}d^i_\alpha\ln\left(\frac{\nu_d^\alpha}{\nu_{\alpha 0}}\right)-\sum_{\beta=1}^{n}a^i_\beta\ln\left(\frac{\nu_a^\beta}{\nu_{0\beta}}\right) \tag{124b}$$

Please cite this article in press as: G. Mensitieri, G. Scherillo, C. Panayiotou et al. Towards a predictive thermodynamic description of Fsorption processes in polymers: The synergy between theoretical EoS models and vibrational spectroscopy. Mater. Sci. Eng. R (2020), https://doi.org/10.1016/j.mser.2019.100525

And, finally, we can write:

$$\frac{\mu_{i,NRHB}}{kT} = \frac{\mu_{i,LF}}{kT} + \frac{\mu_{i,H}}{kT}$$
$$= \ln\frac{i}{\delta_i r_i} - r_i \sum_{j=1}^{t} \frac{j l_j}{r_j} + \ln\sim\rho + r_i(\sim\nu - 1)\cdot\ln(1 - \sim\rho)$$

$$-\frac{z}{2} r_i \left(\sim\nu - 1 + \frac{q_i}{r_i}\right) \ln\left(1 - \sim\rho + \frac{q}{r}\sim\rho\right)$$
$$+ q_i \frac{z}{2}\left[\ln\Gamma_{ii} + \frac{r_i}{q_i}(\sim\nu - 1)\ln\Gamma_{00}\right] + r_i \frac{\sim P \sim \nu}{\sim T} - \frac{q_i}{\sim T_i}$$

$$+ r_i \nu_H - \sum_{\alpha=1}^{m} d_\alpha^i \ln\left(\frac{\nu_d^\alpha}{\nu_{\alpha 0}}\right) - \sum_{\beta=1}^{n} a_\beta^i \ln\left(\frac{\nu_a^\beta}{\nu_{0\beta}}\right) \quad (125)$$

With the same procedure, the corresponding expression for the chemical potential of pure component, μ_i^o/kT, can be obtained by setting $\varphi_i = \theta_i = 1$ in Eq. (124a).

b) by using chain derivative rules, we can then calculate:

$$\frac{\mu_{i,NRHB}^{EQ}}{kT} = \left(\frac{\partial\left(\frac{G_{NRHB}^{EQ}}{kT}\right)}{\partial N_i}\right)_{P,T,N_{j\neq i}}$$
$$= \left(\frac{\partial\left(\frac{G_{NRHB}}{kT}\right)}{\partial N_i}\right)_{P,T,N_{j\neq i},\sim\nu,N_{ij},N\alpha\beta^H,}$$
$$+ \sum_{i\neq 0}^{t}\sum_{j>i}^{t} \left(\frac{\partial\left(\frac{G_p}{kT}\right)}{\partial N_{ij}}\right)_{P,T,N,\sim\nu,N_{rs\neq ij}} \left(\frac{\partial N_{ij}}{\partial N_i}\right)_{P,T,N_{j\neq i}}$$
$$+ \sum_{\alpha=1}^{m}\sum_{\beta=1}^{n} \left(\frac{\partial\left(\frac{G_H}{kT}\right)}{\partial N_{\alpha\beta}^H}\right)_{P,T,N,\sim\nu,N_{\gamma\delta\neq\alpha\beta}^H} \left(\frac{\partial N_{\alpha\beta}^H}{\partial N_i}\right)_{P,T,N_{j\neq i}}$$
$$+ \left(\frac{\partial\left(\frac{G_{NRHB}}{kT}\right)}{\partial\sim\nu}\right)_{P,T,N,N\,ij,N\,\alpha\beta^H} \left(\frac{\partial\sim\nu}{\partial N_i}\right)_{P,T,N_{j\neq i}} \quad (126)$$

where all Gibbs energy derivatives are intended to be evaluated at equilibrium. In view of the minimization Eqs. (52a,b,c), that hold at equilibrium, it follows that:

$$\frac{\mu_{i,NRHB}^{EQ}}{kT} = \left(\frac{\partial\left(\frac{G_{NRHB}}{kT}\right)}{\partial N_i}\right)_{P,T,N_{j\neq i},\sim\nu^{EQ}} , N_{ij}^{EQ}, N\alpha\beta^{H,EQ} \quad (127)$$

where the superscript '*EQ*' remarks that the corresponding quantities are evaluated at equilibrium, i.e. they are provided by solving the set of minimizations equations.

We just recall here that, the QCHB model [8] is obtained in a similar manner, the main difference from NRHB being that, in place of Eq. (95) (the Guggenheim-Staverman approximation), the plain Guggenheim combinatorial term [1] is used to calculate Ω_R:

$$\Omega_R = \left(\frac{1}{f_0}\right)^{N_0} \prod_{i=1}^{t} \left(\frac{\delta_i}{f_i}\right)^{N_i} \quad (128)$$

where the symbols have the usual meaning. The expression for Ω_{NR} is the 'simplified' form provided by Eq. (98). In the case of QCHB, the equation of state takes the following form:

$$\sim P + \sim T\left[\ln(1 - \sim\rho) + \sim\rho\left(1 - \frac{1}{r} + \nu_H\right) + \frac{s}{2}\ln\Gamma_{00}\right] = 0 \quad (129)$$

The generic expressions of the 'physical' contribution to the general molecular chemical potential in a binary mixture becomes for the QCHB model:

$$\frac{\mu_{1,Ph}}{kT} = \ln\phi_1 + \left(1 - \frac{r_1}{r_2}\right)\phi_2 + r_1\sim\rho X_{12}\theta_2^2\Gamma_{rr}$$
$$+ r_1(\sim\nu - 1)\cdot\ln(1 - \sim\rho) + ln\frac{\sim\rho}{\omega_1} - \frac{r_1\sim\rho}{\sim T_1}\Gamma_{rr}$$
$$+ r_1\frac{\sim P\sim\nu}{\sim T}\frac{v_1^*}{v^*} + \frac{r_1 s_1}{2}\left[ln\Gamma_{rr} + (\sim\nu - 1)ln\Gamma_{00}\right]$$
$$- r_1\frac{\theta_1}{\phi_1}\frac{1 - \sim\rho\Gamma_{rr}}{\sim T} \quad (130)$$

while the $\mu_{i,H}/kT$contribution is still given by Eq. (66).

Again, the equilibrium chemical potential for each species is obtained by coupling the generic expression of the chemical potential with the minimization conditions. Full details of QCHB model are provided in ref [8].

Once the expressions for the equilibrium chemical potential of the components of the rubbery polymer mixture are available it is possible to model sorption equilibrium of low molecular weight penetrants in polymers. Sorption equilibrium between a condensed polymer phase and external fluid phase is ruled by the equivalence of the values of temperature, pressure and chemical potentials of all the species in the two phases. We will assume here that no polymer is present in the external fluid phase. As a consequence, equality of chemical potentials in the two phases has to be imposed only for the low molecular weight penetrants. In the cases in which such an assumption is not legitimate, also the equality condition of the chemical potential of polymer species in the two phases has to be fulfilled. Numerical problem could arise in this latter case if the concentration of polymer in the external phase is expected to be extremely low.

The set of equations to be solved to model, using the NRHB theory, the equilibrium sorption isotherms of an infinite volume mixture of *t*-1 low molecular weight (penetrant) of assigned composition, in the polymer-penetrant mixture of t components is made of:

1) the equations expressing the equality of the equilibrium penetrant chemical potentials in the external fluid phase and in the polymer-penetrant phase for any penetrant species.
2) Minimization conditions for $N\alpha\beta^H$ and $\underline{N_{ij}}$ for the polymer-penetrant phase and for the external fluid phase.
3) NRHB equation of state for the two co-existing phases.

This approach can be easily extended to the cases in which more than one polymer species is present.

2.1.5.2. Pure fluid parameters and mixing rules of NRHB model. As mentioned in the previous sub-section the parameters for pure component *i* in the NRHB model [39], are, the number of segments, r_i, the surface-to-volume-ratio factor, s_i, and the mean interaction energy per molecular segment, ε_i^*. This is treated as free-energy and is split into two scaling parameters, $\varepsilon_{i,h}^*$ and $\varepsilon_{i,s}^*$, according to the following relation:

$$\varepsilon_i^* = \varepsilon_{i,h}^* + (T - 298.15)\varepsilon_{i,s}^* \quad (131)$$

Subscripts *h* and *s* in Eq. (131) indicate an "enthalpic" and an "entropic" contribution to the interaction (free) energy parameter.

Instead of r_i, a third scaling constant,$v_{i,sp,0}^*$, is equivalently used for the calculation of the close packed density, $\rho_i^* = 1/v_{i,sp}^*$ given by the following relation:

$$v_{i,sp}^* = v_{i,sp,0}^* + (T - 298.15)v_{sp,1}^* \quad (132)$$

As already mentioned, the hard-core volume per segment, v^*, is considered to be a universal constant equal to 9.75 $cm^3\,mol^{-1}$ for all fluids and their mixtures. The parameter $v_{sp,1}^*$in Eq. (132) is

Table 1
NRHB parameters for some representative fluids.

Fluid	ε_h^*(Jmol^{-1})	ε_s^*(Jmol^{-1}K^{-1})	$v_{sp,0}^*$(cm^{3}g^{-1})	s	Reference
n-hexane	3957.1	1.6580	1.27753	0.857	[94]
n-heptane	4042.0	1.7596	1.25328	0.850	[94]
n-Octane	4105.3	1.8889	1.23687	0.844	[94]
Benzene	5148.5	−0.2889	1.06697	0.753	[94]
Methanol	4202.3	1.52690	1.15899	0.941	[94]
Ethanol	4378.5	0.75100	1.15867	0.903	[94]
1-Propanol	4425.6	0.87240	1.13923	0.881	[94]
1-Butanol	4463.1	1.19110	1.13403	0.867	[94]
2-Butanol	4125.1	1.45711	1.11477	0.867	[99]
1-Hexanol	4522.7	1.64571	1.11545	0.850	[100]
1-Heptanol	4521.2	1.76223	1.12464	0.844	[100]
1-Octanol	4532.1	1.86863	1.12094	0.839	[97]
1-Nonanol	4576.7	1.87264	1.10261	0.836	[97]
Water	5336.5	−6.5057	0.97034	0.861	[94]
Carbon dioxide	3468.4	−4.5855	0.79641	0.909	[98]
Acetone	4909.0	−1.15000	1.14300	0.908	[94]
Acetic acid	6198.8	−2.0598	0.92434	0.941	[94]
Dichloromethane	5163.3	−1.3305	0.688	0.881	[94]
Benzoic acid	7228.5	−3.3473	0.8552	0.774	[98]
Acetanilide	7243.2	1.9411	0.8955	0.780	[97]
Phenacetin	6246.3	−0.5539	0.9333	0.827	[97]
[C_4mim]Tf_2N	5465.37	2.11139	0.66240	0.824	[100]
[C_6mim+][Tf_2N-]	5389.10	2.63354	0.69229		[100]
1,2 Propylene glycol (PG)	5088.9	1.05260	0.9084	0.903	[99]
Poly(ethylene glycol) 200 < M_W<100000 g mol^{-1}	6273.0	0.71110	0.86620 - M_W7.98·10^{-8}	0.829	[99]
Poly(vinyl acetate)	5970.4	2.59194	0.80924	0.825	[99]
Linear Polyethylene	7434.9	−7.94296	1.20994	0.800	[99]

treated as a constant for a given homologous series [94–100] and it is set equal to - 0.412·10^{-3} cm^3 g^{-1} K^{-1} for non aromatic hydrocarbons, - 0.310·10^{-3} cm^3 g^{-1} K^{-1} for alcohols, - 0.240·10^{-3} cm^3 g^{-1} K^{-1} for acetates, - 0.300·10^{-3} cm^3 g^{-1} K^{-1} for water and 0.150·10^{-3} cm^3 g^{-1} K^{-1} for all the other fluids [99,100].

The following relation holds: $r_i = M_{wi}v_{i,sp}^*/v^*$, where M_{wi} is the molecular weight of component i. It is recalled here that the shape factor is defined as the ratio of molecular surface to molecular volume, $s_i = q_i/r_i$, and is calculated through the UNIFAC group contribution method [87,88].

For hydrogen-bonded compounds, the knowledge of two additional parameters that characterize the specific association, namely, the association energy, $E^0_{\alpha\beta}$, and the association entropy, $S^0_{\alpha\beta}$ (for simplification purposes, the association volume, $V^0_{\alpha\beta}$, is usually set equal to zero) is also required. Pure fluid parameters for representative fluids are shown in Table 1. Table 2 reports the number of the hydrogen bonding sites assumed on every functional group, while Table 3 presents the association energy and entropy for the strong specific (i.e. hydrogen bonding, Lewis acid - base) interactions between two functional groups.

Once the scaling parameters for the fluids of interest are available, the model can predict all thermodynamic properties of pure fluids and mixtures. In case of mixtures the mixing and combining rules expressed by Eqs. (87–89) and Eqs. (119–120) are adopted.

Furthermore, combining rules are also used for estimating the cross- hydrogen bonding parameters in cases where no experimental data exists. The following combining rules are used for the cross interaction between two self-associating groups:

$$E^0_{\alpha\beta} = \frac{E^0_{\alpha\alpha} + E^0_{\beta\beta}}{2} \tag{133a}$$

$$S^0_{\alpha\beta} = \left(\frac{S^0_{\alpha\alpha}1/3 + S^0_{\beta\beta}1/3}{2}\right)^3 \tag{133b}$$

while, for the cross interaction between one self-associating α and one non self-associating group β the combining rules are:

$$E^0_{\alpha\beta} = \frac{E^0_{\alpha\alpha}}{2} \tag{134a}$$

$$S^0_{\alpha\beta} = \frac{S^0_{\alpha\alpha}}{2} \tag{134b}$$

One of the main reasons for the PSP developments is the prediction of hydrogen bonding interaction energies. At this stage, the PSPs do not distinguish between the various hydrogen bonding sites in a molecule and give an average acidity or basicity molecular descriptor. Thus, the original differentiation of hydrogen bonding sites by NRHB remains useful in practice. In contrast, the development of the Conductor-like Screening Model - Non-Randomness Factors (COSMO-NRF) [101] does make this differentiation through the cosmo-files of the compounds and may be used in a predictive manner.

Table 2
Hydrogen bonding (HB) sites in each functional group.

Group	HB sites	
	Positive (Proton donors)	Negative (Proton acceptors)
−OH	1	1
Benzene	0	1
HOH	2	2
Benzoic Acid	1	1
>NH	1	1
>C=O (in pharmaceuticals)	0	1
−O−	0	2
−O−C=O	0	1
ILs	5	5

Please cite this article in press as: G. Mensitieri, G. Scherillo, C. Panayiotou et al. Towards a predictive thermodynamic description of Fsorption processes in polymers: The synergy between theoretical EoS models and vibrational spectroscopy. Mater. Sci. Eng. R (2020), https://doi.org/10.1016/j.mser.2019.100525

Table 3
Parameters for hydrogen bonding (HB) interactions.

HB groups	E^{hb} (J mol^{-1})	S^{hb} (J mol^{-1} K^{-1})	Reference
—OH···OH— (Methanol)	−25,100	−26.5	[94]
—OH···OH— (Alkanols)	−24,000	−27.50	[94]
—OH···OH— (Polymers)	−22,500	−27.5	[99]
HOH···HOH	−16,100	−14.70	[94]
Acetic Acid	−14,682	−6.9	[94]
Benzoic Acid	−16,380	−20.34	[98]
>NH···NH<	−8500	−10.25	[97]
>NH···O=C<	−9176	−6.94	[97]
>NH···—O—	−10,900	−6.90	[97]
>NH···OH—	−18,100	−16.00	[97]
—OH···O=C<	−16,868	−13.25	[97]
—OH···—O—	−10,943	−13.75	[97]
—OH···—O— (polymers)	−14,900	−27.8	[99]
HOH···HOH	−16,100	−14.70	[94]
HOH···benzene	combining rule (Eq. 88)	combining rule (Eq. 88)	[96]
—OH···O=C—O—	−22,100	−27.30	[99]
HOH···—O—	−17,000	−27.0	[99]
HOH···OH—	combining rule (Eq. 87)	combining rule (Eq. 87)	[98]
IL—IL	−19,800	−26.5	[100]
IL—water	−16,100	−20.0	[100]

2.1.6. Extension of COSMO-RS to the COSMO-NRF equation-of-state model

In a series of papers [101–104], an approximate, yet coherent and consistent equation-of-state model was developed by combining the quantum-mechanics based 'COSMO for Real Solvents' (COSMO-RS) model [105–111] with NRHB approach. This combination turned out to be a most natural one since the statistical thermodynamic basis of COSMO-RS is very similar to that of NRHB. In essence, what has really occurred as regards the statistical-thermodynamic aspect of COSMO-RS, is the rediscovery of the widely used Quasi-Chemical theory of mixtures [1] in a brilliant way by Klamt [105,106,112]. The significant feature of Klamt's version of Quasi-Chemical theory is the very efficient numerical algorithm for its solution in the case of complex multicomponent/multigroup systems. The combination, then, of COSMO-RS with NRHB could be done by recasting both formalisms in terms of Non-Randomness Factors and the resulting equation-of-state model is termed COSMO-NRF [101]. The COSMO-RS formalism is, in essence, based on a rigid-lattice, while that of COSMO-NRF is based on a lattice-fluid type allowing for free-volume or empty space throughout the system. In what follows, the key features of the COSMO-NRF model will be presented.

COSMO-RS accounts for three types of contributions to the intermolecular interaction energy associated to London – dispersion, electrostatic and strong-specific or hydrogen-bonding forces. The electrostatic interactions, collectively referred to as polar interactions, include the Keesom (dipole + dipole) and the Debye (dipole + induced-dipole) interactions. The electrostatic interaction energy in COSMO-RS is assumed proportional to the following quadratic term [105–111]:

$$(\sigma_m + \sigma_n)^2 \tag{135}$$

where, σ_i is the surface charge density of the interacting segment i. Empty sites are attributed a zero surface charge density, or $\sigma_0 = 0$. Adoption of this approach in the calculation of the electrostatic interaction energy would, then, imply that an encounter of a molecular segment with an empty site is characterized by a non-zero electrostatic energy. At the end, as explained in [101,97], this would lead to an equation of state which would not meet the ideal-gas limit. Two alternatives could be considered. First, one could replace the above misfit term with the product, $2\sigma_m\sigma_n$. This would lead to a fully predictive and consistent up to the ideal-gas limit equation of state but one would have to re-parameterize COSMO-RS from the beginning. Second, one could adopt for the van der Waals and non-specific electrostatic interactions of segments m and n an interaction energy ε_{mn} of the lattice-fluid type [5,9,39,73,113] and use COSMO-RS formalism for the strong specific (hydrogen-bonding) interactions since this part is compatible with the ideal gas limit. This second alternative is the basis of the COSMO-NRF equation of state model. Although the formalism for the first alternative is also available, we will confine ourselves here to the second alternative.

The direct consequence of the above division of intermolecular interactions is the factorization of the system partition function, in analogy with NRHB model, into a hydrogen-bonding, Q_{HB}, and a physical or van der Waals factor, Q_{Ph}, or

$$Q = Q_{Ph}Q_{HB} = (Q_R Q_{NR,Ph})Q_{HB} \tag{136}$$

Again, the physical factor is further divided into a combinatorial term, Q_R, accounting for the random repartition of segments and a correction term, $Q_{NR,Ph}$, accounting for the non-random distribution of the species interacting with these van der Waals forces. Common to, both, COSMO-RS and NRHB is the Guggenheim-Staverman (GS) [86] equation for the combinatorial term, Q_R. Guggenheim's Quasi-Chemical theory [1] is used here for the correction factor for non-randomness, $Q_{NR,Ph}$, and the hydrogen-bonding factor, as done in COSMO-RS.

Panayiotou and Vera [73,113] had introduced the non-randomness factors, Γ_{ij}, as the ratio of n_{ij} contacts in the real system over the corresponding number of contacts, n_{ij}^0, in a fictitious system of perfect randomness, or:

$$\Gamma_{ij} = \frac{n_{ij}}{n_{ij}^0};$$

$$\Gamma_{ii} = \frac{n_{ii}}{n_{ii}^0};$$

$$\tau_{ij} = \exp\left(-\frac{\varepsilon_{ij}}{kT}\right);$$

$$\frac{\Gamma_{ij}^2}{\Gamma_{ii}\Gamma_{jj}} = \frac{\tau_{ij}^2}{\tau_{ii}\tau_{jj}} \tag{137}$$

The Quasi-Chemical condition expressed in terms of the non-randomness factors is the last expression in Eqs. (137). On the basis of this condition, one may split the binary non-randomness factors, Γ_{mn}, into the segment-specific non-randomness factors, Γ_i, through the defining equation:

$$\Gamma_{mn} = \Gamma_m \Gamma_n \exp\left[\frac{-\varepsilon_{pair}(\sigma_m, \sigma_n)}{kT}\right] = \Gamma_m \Gamma_n \tau_{mn} \tag{138}$$

In terms of NRFs, the main equation for the activity coefficient of component i in the mixture takes the following form [101,108,109]:

$$\begin{aligned} \ln\gamma_i &= (\ln\gamma_i)^0 + \sum_k \left[\nu_{ki} z Q_k \left(\ln\Gamma_k - \ln\Gamma_k^{(0)}\right)\right] \\ &= (\ln\gamma_i)^0 + \frac{A_i}{\alpha_{eff}} \sum_k p_i(\sigma_k)\left[\ln\Gamma_k - \ln\Gamma_k^{(0)}\right] \end{aligned} \tag{139}$$

The equivalence of the two alternative expressions in Eq. (139) is established through the equations:

$$p_i(\sigma_m) = \frac{A_i(\sigma_m)}{A_i} = \Theta_m^i = \frac{z\nu_{mi}Q_m}{zq_i} \tag{140}$$

A_i is the surface area of molecule i and α_{eff} is the standard surface area per segment. According to Eq. (140), the probability, $p_i(\sigma_m)$, to find segment m in molecule i is equal to the surface area fraction, $\Theta_m{}^i$, which is the product of the ν_m segments m in the molecule, each having $z{\cdot}Q_m$ contact sites, divided by the total number of external contact sites, $z{\cdot}q_i$, of molecule i.

With the above definitions, assumptions, Guggenheim-Staverman and NRHB nomenclature, the equation of state in terms of the segment non-randomness factors (NRF), Γ, is [101,103,104]:

$$\frac{PV}{NRT} = \frac{\sim P \sim v}{\sim T} = \left[\frac{l}{r} - \sim v \ln(1 - \sim \rho) + \frac{z}{2} \sim v \cdot \ln\left(1 - \sim \rho + \frac{q}{r} \sim \rho\right) - z \sim v \ln\Gamma_0\right] \text{(COSMO – NRF)} \tag{141}$$

while the chemical potential is

$$\frac{\mu_i}{RT} =$$

$$\ln\frac{\phi_i}{\omega_i r_i} + ln \sim \rho - r_i \ln(1 - \sim \rho) + \frac{z}{2}[r_i - q_i]\ln\left[1 - \sim \rho + \frac{q}{r} \sim \rho\right] - z r_i \ln\Gamma_0 + z q_i \left[\sum_m \left(\Theta_m^i \ln\Gamma_m\right)\right] \text{(COSMO – NRF)} \tag{142}$$

where ω_i is a characteristic quantity for each fluid that takes into account the flexibility, conformational changes, and the symmetry of the molecule. The corresponding equation for pure components is:

$$\frac{\mu_i^0}{RT} = ln \sim \rho_i - r_i \ln(1 - \sim \rho_i) + \frac{z}{2}[r_i - q_i]\ln\left[1 - \sim \rho_i + \frac{q_i}{r_i} \sim \rho_i\right] - z r_i \ln\Gamma_0 + z q_i \left[\sum_m \left(\Theta_m^i \ln\Gamma_m\right)\right] \text{(COSMO – NRF)} \tag{143}$$

It is important to point out that alternative equation of state formalisms may be used for the above non-hydrogen-bonding part.

Thus, COSMO-NRF is a coherent and consistent equation of state model, which requires two pure component scaling constants, ρ^* and ε^*, as in NRHB or in LFHB. In contrast, however, to NRHB and LFHB, the COSMO-NRF model does not need any hydrogen bonding parameters since this is obtained directly from the COSMO-RS *cosmo-files*. Extensive tables with these scaling constants are reported in [101]. These scaling constants seem to correlate very well with the corresponding comoments of COSMO-RS model [105–111]. In Fig. 1 it is shown the linear correlation of hard-core molar volume, $V^* = M/\rho^*$, with the COSMO volume [114]. On the other hand, ε^* seems to correlate also, rather satisfactorily, with Linear Solvation Energy Relationships – PSPs (LSER-PSPs) (cf. subsection 3.8.1). An exploration of this capacity would lead to an entirely predictive equation-of-state model of highly complex multicomponent systems. Nevertheless, having the scaling constants, ρ^* and ε^*, of pure compounds, one may use the present model to predict the phase behavior and related properties of mixtures.

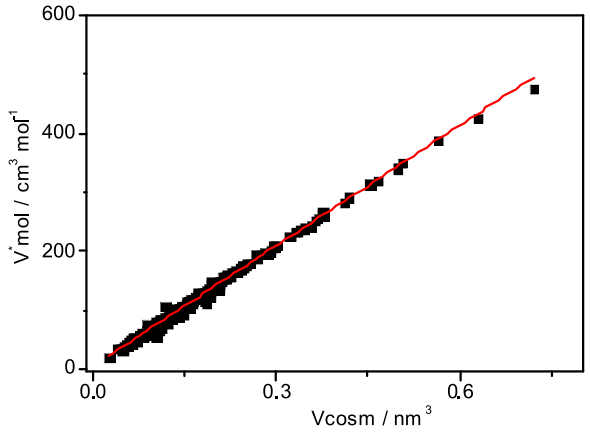

Fig. 1. The correlation of the hard-core molar volume with the COSMO volume. The equation for the straight line is $V^* = 6.0876 + 678.97\ V_{cosm}$, ($R^2 = 0.9954$).

2.1.7. Perturbation theories

2.1.7.1. Statistical associating fluid theory (SAFT). Equations of state rooted on perturbation theories can be effectively used to simulate and even predict phase equilibria involving polymeric systems. In fact, in this approach, a suitable reference system accounting for repulsive interactions is perturbed by accounting for Van der Waals or hydrogen bonding attractive forces. These theories are suited for dealing with polymers since they account explicitly for the chain structure of macromolecules. [115].

In perturbation theories, the residual Helmholtz free energy of the system, A^{res} (i.e. the difference between the Helmholtz free energy, A, and the Helmholtz free energy of the ideal gas state, A^{id}), is assumed to be expressed as the sum of several contributions that is a reference term, A^{ref}, and a series of perturbation terms, collectively reported as A^{pert}:

$$A = A^{id} + A^{res} = A^{id} + A^{ref} + A^{pert} \tag{144}$$

The reference term provides the main contribution to thermodynamic properties. A suitable reference term is the hard sphere, *hs*, system, where the molecules are considered as being purely repulsive spheres of a specified diameter. However other kinds of reference terms have also been introduced. Real systems generally deviate from the reference one, due both to the presence of dispersive and specific (or associative) attractive interactions and to the non-spherical shape of the molecules, including the chain-like form of polymer macromolecules of specific interest in the present context. These effects are accounted for by the introduction of different perturbation terms which are assumed to be mutually independent. Several models have been proposed in the framework of this approach, differing for the kind of reference and of perturbation accounted for and/or for the expression adopted for these terms.

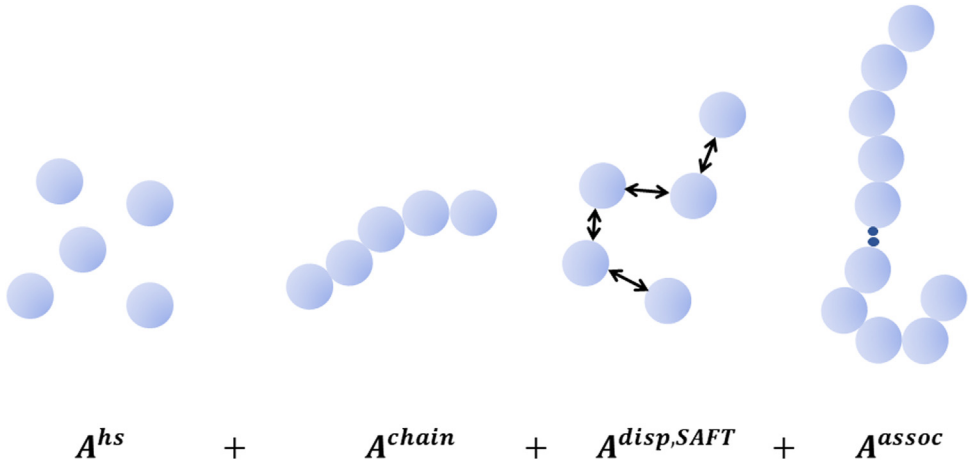

Fig. 2. Schematic of construction of the Helmholtz free energy according to SAFT.

The papers where the Statistical Associating Fluid Theory was first proposed are those by Chapman et al. [45–48], referred to as 'original SAFT', and by Huang and Radosz [49], referred to as 'CK-SAFT', that has been also extended to the case of mixtures [116].

SAFT assumes that the fluid is made of molecules that consist in chains with association sites. A fluid is 'constructed' starting from a system of hard-spheres to which are then associated attractive forces (dispersive potential, e.g. 'square-well' or 'LJ' potential). Subsequently, are added chain sites to obtain a chain structure. In the end, the system is endowed with association sites (e.g. Hydrogen Bonding) that allow the formation of complexes [117]. In this approach the reference contribution is formed by a number m of hard sphere molecules, mA^{hs}. The perturbation terms include a term accounting for the formation of chains made of m hard spheres, A^{chain}, a term accounting for dispersive attractive interactions, mA^{disp}, and a term accounting for the attractive interactions involving association sites, A^{assoc}:

$$A^{res} = mA^{hs} + A^{chain} + mA^{disp,\,SAFT} + A^{assoc} \tag{145}$$

The expressions of A^{chain} and A^{assoc} terms are based on the Wertheim's pioneering work based on graphs theory [118–122] and are essentially the same in the different versions of SAFT, that are instead characterized by a variety of expressions for the *attractive* contribution. In Fig. 2 is reported schematically the construction of the Helmholtz free energy according to SAFT.

Several modifications of SAFT were later proposed by several groups with different expressions for the perturbation terms appearing in Eq. (145) [123–128]. In general, the various expressions proposed for EoS of the SAFT type are characterized by very similar chain and association terms and differ mainly for the adopted expressions of the dispersion and repulsion terms. The different SAFT variants proposed in the literature can be classified as follows [117]: Original SAFT [47,48], Chen Kreglewski-SAFT (CK-SAFT) [49,116], Simplified SAFT [129], Lennard-Jones SAFT (LJ-SAFT) [130,131], Variable Range – SAFT (SAFT-VR) [125,132], Soft SAFT [133], Perturbed Chain SAFT (PC-SAFT) [134], Simplified PC-SAFT [135,136].

Other modifications of the SAFT were introduced. Simplified structures have been proposed by using a cubic EoS to substitute the chain and dispersion terms ('Cubic-Plus-Association' EoS, *CPA EoS*) [137–139] or by simplifying the association term [140–144]. To allow the application of SAFT approach when experimental data to be used for the evaluation of pure compounds parameters are lacking, were developed Group Contribution (GC) variants of SAFT to be used to estimate the values of these parameters [145–153].

One of the especially attractive features of SAFT-type approaches, which stems from their theoretical origin, is that no mixing rules are needed in the chain and association terms. These terms are thus rigorously extended to mixtures. Mixing rules are needed, however, in the dispersion term of the equation for all SAFT variants. Moreover, combining rules are needed for the segment energy and volume (or diameter) parameters and the Lorentz–Berthelot rules are typically used. As with cubic EoS, a correction–interaction parameter k_{ij} is often used in the combining rule for the cross-energy parameter.

In the present context, the PC-SAFT model, proposed by Gross and Sadowski [134,154,155], is of particular interest. This model has been specifically developed to deal with chain-like molecules. The relevant aspect is that the refence system is now a chain of hard spheres (i.e. *hard chain*, *hc*). In fact, the dispersion term refers to attraction between the chains instead of segments, so that the expression of residual Helmholtz energy is constructed by first forming chains of hard spheres and then adding dispersion term for the whole chain (thus implying that, instead of an intersegment, an interchain radial distribution function comes into play). The expression for A^{res} is then [115]:

$$A^{res} = A^{hc} + A^{disp,\,PC-SAFT} + A^{assoc} \tag{146}$$

where $A^{disp,\,PC-SAFT}$ is now a function of the length m of the chain molecules. In Fig. 3 is reported schematically the construction of the Helmholtz free energy according to PC-SAFT

The PC-SAFT EoS for pure compounds, in the case of non-associating molecules, needs three parameters. The 'geometrical' parameters, m and σ, account, respectively, for the non-spherical shape of molecules and for the diameter of each segment. The energy related parameter, ε, accounts for the dispersive interaction between two segments. If the system is endowed with self-association or cross-association (in mixtures), as is the case of hydrogen bonding, there are two further parameters for each kind of association couple, *AB*, which characterize the volume (κ^{AB}) and energy (ε^{AB}) of association. In fact, in the framework of PC-SAFT it is assumed that the association is characterized by a very strong, short-range potential. Modified PC-SAFT expressions have also been introduced to account for long-range forces related to electrostatic effects due to dipole and quadrupole (and induced) moments or to the presence of charges. PC-SAFT was in fact improved by adding polar and quadrupolar contributions and

Please cite this article in press as: G. Mensitieri, G. Scherillo, C. Panayiotou et al. Towards a predictive thermodynamic description of Fsorption processes in polymers: The synergy between theoretical EoS models and vibrational spectroscopy. Mater. Sci. Eng. R (2020), https://doi.org/10.1016/j.mser.2019.100525

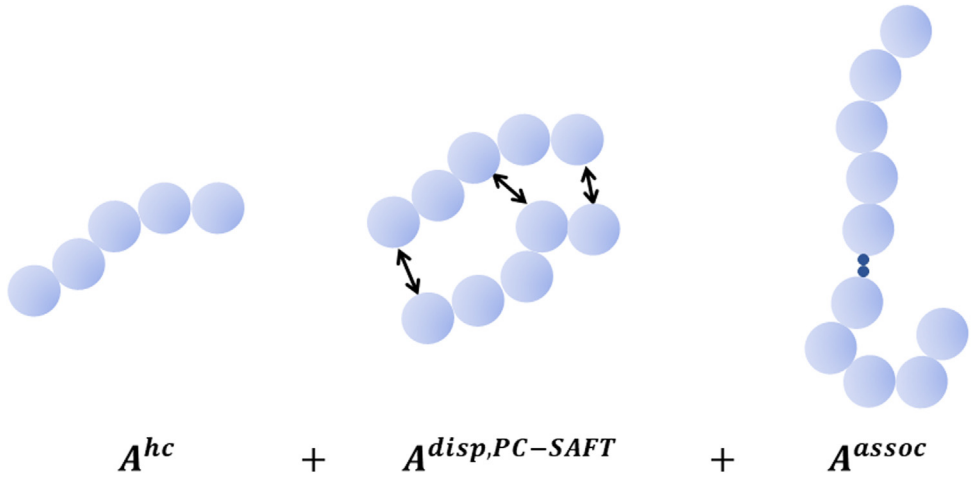

Fig. 3. Schematic of construction of the Helmholtz free energy according to PC-SAFT.

extending PC-SAFT to electrolytes [156–166], with the obvious introduction of additional parameters.

In view of the theoretical structure of SAFT models, in the case of binary mixtures no mixing rules are required for the chain and association terms. However, one needs to know the parameters ruling the cross-associations. To avoid the introduction of additional parameters, combining rules for the cross-association parameters based on self-association parameters have been proposed (see Chap. 8, p. 240 in [117]). It is evident that this is a viable option only in the case both compounds are self-associating. Conversely, mixing rules are needed for the dispersion term. In this term, the parameter related to the interaction energy between segments of different molecules generally deviates from the geometric mean of the energy related parameters of each of the two compounds and one needs to introduce an additional binary interaction parameter, k_{ij}, to account for these deviations. In addition, combining rules, which are in general the Lorentz–Berthelot ones, are also used for the evaluation of segment energy and volume (or diameter) parameters.

The structure of the various contributions present in Eq. (146) is discussed in [115]. Once the expression of Helmholtz free energy is available, one can readily calculate, by standard thermodynamic relationships, all the thermodynamic properties that are required to perform phase-equilibria calculations.

PC-SAFT has been used not only to deal with homopolymers, but has also been extended to describe the thermodynamic behaviour of copolymers [167]. In this case different kinds of monomers and, in turn, different model parameters, are considered for the macromolecules. Consistently, the different terms contributing to the expression of Helmholtz free energy are properly modified. The pure copolymer parameters for the different monomers are taken from the corresponding values for pure homopolymers. Also the number of binary interaction parameters is increased. In fact, in the simple case of a copolymer made of two different kinds of monomers, to describe a copolymer/solvent system one needs to know two binary interaction parameters between each type of copolymer segment and solvent segments, which can be obtained from the two corresponding homopolymer/solvent systems, and a third binary parameter related to the interaction energy between the unlike monomer units in the copolymer.

Although the molecular weight distribution of the polymer (polydispersity) does not determine any significant effect on vapor-liquid phase equilibria in polymer/solvent systems, it can have relevant effects on liquid-liquid equilibria. PC-SAFT has been successfully used to deal with polydispersity of the polymer component in binary mixtures by introducing multiple pseudo-components, used to represent the experimental molecular weight distribution of the polymer (see the case of poly(ethylene co acrylic acid) copolymers with different acrylic acid contents in ethene in [115]).

A simplified version of PC-SAFT has been introduced, i.e. the simplified PC-SAFT [135]. The two models share the same type and number of parameters for pure compounds, however in the latter simpler mixing rules are introduced. In fact, the equations for hard sphere and association terms are simplified. Limited differences are also introduced in the chain term in view of the different expression adopted for the radial distribution function.

2.2. Extension of equilibrium thermodynamics EoS approaches to non-equilibrium glassy polymers

2.2.1. The NETGP approach

The first successful attempt to provide a physically sound interpretation of sorption of low molecular weight compounds in glassy polymers dates back to about 60 years ago and is the so called *Dual Sorption* model [168,169]. This is an empirical model envisaging sorbed penetrant molecules as consisting of two *populations*. One is contributed by penetrant molecularly dispersed within the bulk of polymer matrix, that is assumed to have a state analogous to penetrant molecules absorbed in equilibrium rubbery polymers. The other is assumed to be contributed by penetrant molecules adsorbed onto the surfaces of the micro-voids frozen within the glassy polymer that collectively form the excess free volume associated to non-equilibrium glassy state. Rooted on this physical picture, the Dual Sorption model consists in the sum of two contributions: the first contribution takes the form provided by a mean field equilibrium approach, such as Flory–Huggins theory [2] that, in the limit of small penetrant concentration, approaches the limit of Henry's law, while the second contribution takes the form of a Langmuir-type adsorption term. These two populations are assumed to be in a reciprocal instantaneous equilibrium. This model, although is currently still used in many cases since it provides a rather successful framework to interpret sorption thermodynamics in glassy polymers, is not predictive and it is only suitable for correlation purposes.

With the aim of developing a consistent theoretical sorption thermodynamics approach with a predictive capability, efforts have been devoted to build models grounded on rational non-equilibrium thermodynamics. These approaches were based on thermodynamics endowed with internal state variables, which consist in order parameters that quantify the departure of glassy

Please cite this article in press as: G. Mensitieri, G. Scherillo, C. Panayiotou et al. Towards a predictive thermodynamic description of Fsorption processes in polymers: The synergy between theoretical EoS models and vibrational spectroscopy. Mater. Sci. Eng. R (2020), https://doi.org/10.1016/j.mser.2019.100525

systems from the equilibrium conditions. The procedure consists in extending the equilibrium mixture theories developed for rubbery polymers to the non-equilibrium glassy polymer–penetrant mixtures. The concept of order parameter has been often used to deal with thermodynamics of non equilibrium systems. This approach, rooted on the description of non-equilibrium states introduced by De Donder [170], that made use of additional structural order parameters, was further developed, in the specific field of thermodynamics of glassy polymers, with the contributions provided by Staverman [171], Gibbs and Di Marzio [172], Astarita et al. [173], Wissinger and Paulaitis [174] and Doghieri and Sarti [50]. In brief, for the case of a non-equilibrium glassy polymer – penetrant mixture, the state is described, in addition to the standard external state variables adopted at equilibrium, such as pressure, temperature and composition, also by a set of order parameters. In particular, Wissinger and Paulaitis [174] (WP) used, as additional structural order parameter, the fractional free volume of the polymer at the glass transition temperature, T_g. They also assumed that the free volume remains at the same value it takes at T_g, also at lower values of temperature (*frozen in* free volume). Although this approach allowed a reasonable interpretation of CO_2 sorption isotherms in polymethyl methacrylate and polystyrene, it is unable to reproduce hysteresis phenomena during desorption runs, as well as swelling-enhanced sorption capacity of the polymer matrix. Later, Conforti et al. [175], in an attempt to overcoming these drawbacks, introduced, as order parameter, the number of holes per polymer mass in the mixture, in the framework of a lattice fluid model of the polymer system. However, this model allows the proper interpretation of typical sorption–desorption hysteresis of glassy systems only resorting to two adjustable parameters to estimate the value of the order parameter [176]. The fact that these parameters have to be retrieved from experimental analyses of the volumetric behaviour of the polymer–penetrant system during sorption and desorption process represents a major drawback for the effective use of such a model in a predictive fashion.

More recently, Doghieri and Sarti [50–52] introduced, as order parameter and internal state variable, the density of the polymer in the mixture, developing a procedure based on rational thermodynamic to extend equilibrium EoS theories to the case of non equilibrium glassy systems. The state is then described, beside the usual set of state variables, i.e. temperature, pressure and composition, also by the nonequilibrium density of the glassy polymer. This general approach, referred to in the following as Non-Equilibrium Thermodynamics for Glassy Polymers (NETGP) theory [51], applies to homogeneous, isotropic, and amorphous phases. In principle, one should specify the evolution kinetics of the internal state variable. This information is often not available and, to simplify the matter, in the analysis of sorption thermodynamics the NETGP approach has often been applied considering the system as being in a Pseudo-Equilibrium (PE) state, in the sense that the two-phase equilibrium is attained with the polymer phase in a kinetically locked non-equilibrium state. This procedure has been applied to many binary and ternary polymer–penetrant glassy systems with a good agreement with experimental data, extending several statistical thermodynamics equilibrium models, ranging from lattice fluid models [50] to perturbation theories [177], resulting to be a powerful tool to predict the solubility of low molecular weight compounds in polymers where specific interactions are not present.

In the following, we discuss the fundamental aspects of the NETGP theory with reference to binary polymer-penetrant systems (the subscripts '1' and '2' refer, respectively, to the penetrant and the polymer) and then we address the specific case of extension of the equilibrium Sanchez – Lacombe lattice fluid theory.

The starting point is the expression of the Gibbs energy for a uniform polymer-penetrant mixture in the non-equilibrium glassy state, considering a fixed number of moles of polymer, n_2. The Gibbs energy is taken as being a function of the set of state variables T, P, n_1 and ρ_2 [52]:

$$G = g(T, P, n_1, \rho_2) \tag{147}$$

Here n_1 is the number of moles of penetrant. The polymer density, ρ_2, is the additional *order parameter* representing the internal state variable of the polymer-penetrant mixture. As anticipated, it quantifies the departure of the system from the equilibrium state. As dictated by thermodynamics endowed with internal state variables [178], in non-equilibrium conditions the rate of variation of ρ_2, is itself a function of the state of the system, i.e:

$$\frac{d\rho_2}{dt} = f(T, P, n_1, \rho_2) \tag{148}$$

The qualitative and quantitative definition of the functional form of this evolution kinetics is a rather challenging task. However, when the temperature is much lower than the glass transition temperature of the polymer and the penetrant concentration is sufficiently small, the system relaxation rate is correspondingly small and, consequently, the value of f can be considered to be negligible, although not exactly zero, even when the system is far away from true equilibrium. From this it follows that, in such conditions, ρ_2 can be assumed to take a constant value, referred to with the symbol $\rho_{2,\infty}$, and the polymer-penetrant mixture, when exposed to a pure penetrant, attains an apparent time invariant composition which corresponds to a *PE* state. Conversely, if the time to achieve this PE state is of the same order of magnitude of the characteristic time of evolution of the order parameter, a thermodynamically consistent expression for evolution kinetics of ρ_2 is required [52].

Obviously, the value of $\rho_{2,\infty}$ $\rho_{2,\infty}$cannot be retrieved from an EoS expression but is dictated by the intrinsic evolution rate of the polymer as determined by the thermo-mechanical and penetrant concentration history. A suitable choice for $\rho_{2,\infty}$ $\rho_{2,\infty}$is the value of density of the pure starting polymer, ρ_2^0, in the cases where the penetrant induced swelling is negligible. Conversely, if a penetrant induces a non negligible swelling, it can be often still possible to assume a quasi-constant value for ρ_2 at each pressure, but its value is different from that of the density of the starting pure polymer. In this event, one needs either to retrieve experimentally the value of the specific volume of the polymer-penetrant system at each absorbed penetrant concentration at PE with the external pure fluid phase, or, alternatively, to assume a dependence of the polymer density on the partial pressure of the swelling penetrant. In particular, at low penetrant activities in the pure fluid phase in contact with the polymer (as is the case of several light gases [179–181]), a simple linear form is appropriate for this dependence and the value of $\rho_{2,\infty}$, can be in fact expressed as:

$$\rho_{2,\infty}(P) = \rho_2^0(1 - k_{sw}P) \tag{149a}$$

where it has been introduced a *swelling coefficient*, k_{sw} [182]. If experimental data on specific volume are not available, k_{sw} can be used as a further fitting parameter of sorption isotherms. In the case of a number 'k' of penetrants, Eq. (149a) takes the following form:

$$\rho_{2,\infty}(P) = \rho_2^0\left(1 + \sum_{i=1}^{k} k_{sw,i}P_i\right)^{-1} \tag{149b}$$

where P_i is the partial pressure in the external phase of penetrant 'i' and $k_{sw,i}$ is the associated swelling coefficient.

Please cite this article in press as: G. Mensitieri, G. Scherillo, C. Panayiotou et al. Towards a predictive thermodynamic description of Fsorption processes in polymers: The synergy between theoretical EoS models and vibrational spectroscopy. Mater. Sci. Eng. R (2020), https://doi.org/10.1016/j.mser.2019.100525

In brief, when the conditions are met, the glassy mixture is assumed to be in a kinetically hindered state resulting in a time invariant value of ρ_2. Accordingly, we have that [50]:

$$\frac{d\rho_2}{dt} \cong 0 \tag{150a}$$

and

$$\rho_2 = \rho_{2,\infty} \neq \rho_2^{EQ}(T, P, n_1) \tag{150b}$$

We consider now the specific case of a phase PE between a pure penetrant and a polymer-penetrant mixture which is in a kinetically hindered state. It is explicitly noted here that we consider the simplified case of a polymer that is insoluble in the external penetrant phase. On the basis of the first and second laws of thermodynamics and if the assumption formalized by Eqs. (150) holds true, it can be proven [52] that the thermodynamic condition for phase PE is still dictated by the equivalence of penetrant chemical potentials in the two phases in contact. Moreover, on the same basis, it can also be demonstrated that the chemical potentials of the penetrant and of the polymer in the polymer-penetrant are not dependent on P. The pseudo phase equilibrium is then expressed as:

$$\mu_{1,\,pol}\left(T,\, n_1^{PE},\, \rho_{2,\infty}\right) = \mu_{1,\,ext}(T,\, P) \tag{151}$$

The superscript 'PE' emphasizes the fact that Eq. (151) refers to a pseudo-equilibrium condition. The value of penetrant chemical potential in the polymer-penetrant mixture is calculated, consistently with previous procedure, according to the following expression:

$$\mu_{1,\,pol} = \left.\frac{\partial G}{\partial n_1}\right|_{T,\,P,\,\rho_{2,\infty}} \tag{152}$$

where, in view of PE condition, the derivative on the r.h.s. side of Eq. (152) is evaluated at $\rho_2 = \rho_{2,\infty}$ and $n_1 = n_1^{PE}$.

To proceed with the calculation of the chemical potential, an explicit expression for non-equilibrium G is needed. This expression for G can be obtained as the logarithm of the generic term of the Gibbs partition function where the density of the polymer takes a specific value of $\rho_{2,\infty}$. Actually, there is another, straightforward, way to obtain the expression of nonequilibrium chemical potentials. The procedure is based on the relevant result of the NET-GP approach that the nonequilibrium Helmholtz energy of the system is independent of pressure and, consequently, it is found that its value is the same as the corresponding equilibrium value provided by an EoS of choice at the same temperature, polymer density and composition (although at a different pressure):

$$a^{NE}(T,\, P, n_1,\, \rho_2) = a^{EQ}(T,\, n_1,\, \rho_2) \tag{153}$$

From Eq. (153) it follows that, under the non-equilibrium glassy state conditions, the chemical potential of the penetrant can be calculated as:

$$\mu_1^{NE} = \left(\frac{\partial a^{NE}}{\partial \rho_1}\right)_{T,\,\rho_2} \tag{154}$$

One can then evaluate the non-equilibrium chemical potential by simply equating it to the corresponding equilibrium value calculated at the same temperature, composition and polymer density:

$$\mu_1^{NE}(T,\, P, n_1,\, \rho_2) = \mu_1^{EQ}(T,\, n_1,\, \rho_2) \tag{155}$$

This approach is straightforward when the selected EoS theory provides the expression of equilibrium chemical potential in a closed analytical form. More attention should be applied in cases where the theory just provides a general expression of chemical potential that has to be coupled with minimization conditions to obtain the expression of equilibrium chemical potential. This is the case, for example, of the NRHB theory.

In implementing this procedure, Sarti et al. started from several equilibrium statistical thermodynamics EoS theories, ranging from lattice fluid theories [50] to perturbation theories [177]. In particular, if one considers the extension to the out-of-equilibrium conditions, of the Sanchez-Lacombe theory, the following expression is obtained [50]:

$$\frac{\mu_{1,pol}}{RT} = ln(\sim \rho\phi_1) - \left[r_1^0 + (r_1 - r_1^0)/\sim \rho\right] ln(1 - \sim \rho) - r_1$$

$$-\sim \rho\left[r_1^0 v_1^*\left(P_1^* + P^* - \phi_2^2 \Delta p^*\right)\right]/(RT) \tag{156}$$

where

$$\Delta p^* = \left[P_1^* + P_2^* - 2(1 - k_{12})\sqrt{P_1^* P_2^*}\right] \tag{157}$$

It is worth noting that:

$$\sim \rho = \frac{\rho_{2,\infty}}{\omega_2 \rho^*} \tag{158}$$

where ω_2 is the mass fraction of the polymer and ρ^* the *closed packed* density of the mixture.

Eq. (156) is the relevant expression of the so-called Non-Equilibrium Lattice Fluid (NELF) model [50], that is a specialized version of the general NETGP theory.

2.2.2. Extension of equilibrium NRHB model to glassy polymers: the NETGP-NRHB model

In the previous sub-section, it has been illustrated a procedure, rooted on thermodynamics endowed with internal state variables, developed to extend equilibrium theories to describe phase PE for glassy polymer-penetrant systems exposed to a fluid phase. This approach has been later generalized [183] to systems consisting in a polymer and more than one penetrant. To deal with glassy polymer-penetrants systems exhibiting specific interactions, such as hydrogen-bonding or formation of Lewis acid/Lewis base complexes, our group, still exploiting the NETGP framework, have proposed an extension of the NRHB model to the case of non-equilibrium glassy polymers [184], developing the so called NETGP-NRHB model. As in the original development of NETGP model proposed by Sarti and Doghieri [52], also in this case the model addresses the situation in which no spatial gradients of any variable is present.

The procedure to extend NRHB model is significantly more complex than in the cases presented in the previous sub-section in view of the higher number of internal variables involved. In fact, beside the polymer mass density in the mixture, ρ_p, i.e. the mass of polymer per unit volume of the mixture, the other internal state variables, to be accounted for the description of the glassy state, are also the set of variables $N\,\alpha\beta^H$ and $N\,ij$, that have been already introduced in the sub-section devoted to the NRHB model. As extensively discussed there, the values of these variables at equilibrium is dictated by the minimization conditions of Gibbs energy to be imposed (Eq. (52)) as a function of P, T, $\underline{N}$. Conversely, in nonequilibrium conditions, the values of these variables are determined by the system of ordinary differential equations expressing their evolution kinetics. These kinetics expressions can be complex functions of the non-equilibrium state of the system, that is expressed in terms of the whole non-equilibrium set of the internal state variables.

Please cite this article in press as: G. Mensitieri, G. Scherillo, C. Panayiotou et al. Towards a predictive thermodynamic description of Fsorption processes in polymers: The synergy between theoretical EoS models and vibrational spectroscopy. Mater. Sci. Eng. R (2020), https://doi.org/10.1016/j.mser.2019.100525

Again, it is assumed that the polymer is insoluble in the external fluid phase in contact with it, thus determining that the number of polymer molecules, N_p, is constant in the polymer phase. As already discussed in the description of the NRHB model, when describing the thermodynamics of the polymer-penetrants mixture, we deal with more than one internal variable. For the first one the choice made here is the polymer mass density in the mixture, ρ_P. It is worth noting that, since N_p in the mixture is assumed to be constant, it would be possible to use, equivalently, as internal state variable also the total volume of the mixture, V, as has been reported in the development of NRHB equilibrium model. Since we are following here the NETGP approach, it is preferred the use of ρ_P. In addition, there are also two sets of other extensive internal variables, i.e. $N\,\alpha\beta^H$ and $N\,ij$, as it emerged from the discussion on NRHB theory. Beside these internal variables, the state of the system is also defined by external state variables. These are the temperature, T, the pressure, P, and the set of variables representing the number of molecules of each component present in the mixture, i.e. $\underline{N} = (N_1, N_2, \ldots N_{t-1}, N_p)$. The external fluid phase, assumed to be without polymer macromolecules, is considered as being in an equilibrium state, that is represented only by the external variables P, T and number of molecules of each penetrant.

Consistently with these premises, one can find the expression for Gibbs energy for the polymer-penetrant mixture in a non-equilibrium condition, generically represented as:

$$G = g(T, P, N_1, N_2, \ldots, N_{t-1}, N_p, \rho_p, N\,ij, N\,\alpha\beta^H) \tag{159}$$

This expression can be obtained by taking the logarithm of the generic term of the Gibbs partition function provided by the NRHB theory, at a specific non-equilibrium values of $\rho_p, N\,ij$ and $N\,\alpha\beta^H$. Eq. (159) has to be coupled with the systems of constitutive equations describing the evolution kinetics of all the internal variables of the polymer-penetrants mixture, in non-equilibrium conditions:

$$\frac{\partial \rho_P}{\partial t} = r_p\left(T, P, N_1, N_2, \ldots, N_{t-1}, N_p, \rho_P, N\,ij, N\,\alpha\beta^H\right) \tag{160a}$$

$$\frac{\partial N\,ij}{\partial t} = r\,N\,ij\left(T, P, N_1, N_2, \ldots, N_{t-1}, N_p, \rho_P, N\,ij, N\,\alpha\beta^H\right) \tag{160b}$$

$$\frac{\partial N\,\alpha\beta^H}{\partial t} = r\,N\,\alpha\beta^H\left(T, P, N_1, N_2, \ldots, N_{t-1}, N_p, \rho_P, N\,ij, N\,\alpha\beta^H\right) \tag{160c}$$

It is difficult to identify proper expressions for the rates of evolution of these variables toward their equilibrium values. There are two ways of avoiding this issue, that is either assume that these rates are infinitely fast (the variables thus being always at their equilibrium values) or assume that these rates are infinitely slow (the variables thus staying indefinitely at whatever value they may have). To this end, in the development of NETGP-NRHB model illustrated in this sub-section, an *instantaneous* evolution kinetics has been assumed for the two sets of internal state variables $N\,ij$ and $N\,\alpha\beta^H$ while, similarly to what has been proposed by Sarti and Doghieri in the original NETGP development, the polymer density in the glassy mixture, ρ_P, is considered to be in a kinetically hindered state resulting in a time invariant non-equilibrium value, $\rho_{P,\infty}$, as will be discussed later.

The physical grounds on which is founded the assumption of instantaneous evolution of the state variables $N\,ij$ and $N\,\alpha\beta^H$ stands in the presumption that the dynamics of such variables do involve prevalently local rearrangement of the system, which take place on a time scale much smaller than the long time scale of the relaxation processes associated with the volumetric *ageing* of the mixture toward a true equilibrium state. In other words, it is assumed that the values of $N\,ij$ and $N\,\alpha\beta^H$ are the ones that the system would exhibit if it was at equilibrium at the current values of polymer density, pressure, temperature and concentration. That is, the values of these variables are provided by minimization conditions of G toward $N\,ij$ and $N\,\alpha\beta^H$:

$$\left(\frac{\partial G}{\partial N_{ij}}\right)_{P,T,N,\,\rho_P,N_{rs\neq ij}} = 0 \text{ for each } i,j = 0, 1, \ldots t \text{ and } j > i \tag{161a}$$

$$\left(\frac{\partial G}{\partial N^H_{\alpha\beta}}\right)_{P,T,N,\,\rho_P,N^H_{\gamma\delta\neq\alpha\beta}} = 0 \text{ for each } \alpha,\ \beta \tag{161b}$$

Evidently, these values do not correspond to the equilibrium ones, in view of the fact that the value of ρ_P is not the one dictated by the equilibrium condition, that is minimization condition of G toward ρ_P (as we will see later, in the simple case of infinitely slow evolution kinetics of polymer density, its value is 'frozen'). This assumption, in view of the previous arguments, is indicated as *instantaneous equilibrium* (IE) hypothesis for the state variables $N\,ij$ and $N\,\alpha\beta^H$. Consequently, a non-equilibrium value of G corresponds, in the proposed framework for the NETGP-NRHB model, to a value calculated under the illustrated IE hypothesis, G^{IE}:

$$G^{IE} = g\left(T, P, N_1, \ldots, N_{t-1}, N_p, \rho_P, N\,ij^{IE}(T, P, N_1, \ldots, N_{t-1}, N_p, \rho_P), N\,\alpha\beta^{IE,H}(T, P, N_1, \ldots, N_{t-1}, N_p, \rho_P)\right) = g^{IE}(T, P, N_1, \ldots, N_{t-1}, N_p, \rho_P) \tag{162}$$

The value of the internal state variable, ρ_P, is provided by its evolution equation:

$$\frac{\partial \rho_P}{\partial t} = r_p\left(T, P, N_1, \ldots, N_{t-1}, N_p, \rho_P, N\,ij^{IE}(T, P, N_1, \ldots, N_{t-1}, N_p, \rho_P), N\,\alpha\beta^{IE,H}(T, P, N_1, \ldots, N_{t-1}, N_p, \rho_P)\right) = r^{IE}_p(T, P, N_1, \ldots, N_{t-1}, N_p, \rho_P) \tag{163}$$

Based on the previous discussion, it follows that:

$$\left(\frac{\partial G}{\partial \rho_P}\right)_{P,T,N,N_{ij},N^H_{\alpha\beta}} \neq 0 \tag{161c}$$

From Eqs. (162) and (163) it is evident that, due to the IE assumption, the constitutive class of the polymer-penetrant system is $\{T, P, N_1, \ldots, N_{t-1}, N_p, \rho_P\}$, that is perfectly equivalent to the constitutive class of the original version of multicomponent NETGP formulation, where ρ_P represents the sole internal state variable. It is then possible, from this point on, to replicate the same procedure of NETGP approach, observing that now G^{IE} plays the role of G in the original NETGP model. Introducing here the simplifying assumption that the value of ρ_P takes a time invariant value, $\rho_{P,\infty}$ (infinitely slow evolution kinetics), as is frequently done when applying the original NETGP procedure, we have that:

$$\frac{\partial \rho_P}{\partial t} = r^{IE}_P(T, P, N_1 \ldots, N_{t-1}, N_p, \rho_{P,\infty}) \cong 0 \tag{164}$$

As reported for the original NETGP procedure, in the case of infinitely slow evolution kinetics of polymer density, phase equilibrium is still dictated by the equivalence of chemical potentials for the different penetrants. To highlight that this

phase equilibrium involves a polymer mixture in a PE state, we introduce the superscript 'PE' and we can write the equivalence of chemical potentials for the generic penetrant k in the two phases in contact as:

$$\mu^{IE}_{k,pol}\left(T,P,N_1^{PE},\ldots,N_{t-1}^{PE},N_P,\rho_{P,\infty}\right) = \mu^{EQ}_{k,ext}(T,P,N_{1,ext},\ldots,N_{t-1,ext}) \text{ for } k=1,\ldots t-1 \quad (165)$$

Here $\mu^{IE}_{k,pol}$ represents the non-equilibrium molecular chemical potential of component k within the polymer-penetrant mixture, given by:

$$\mu^{IE}_{k,pol} = \left(\frac{\partial G^{IE}}{\partial N_k}\right)_{P,T,N_{j\neq k},\rho_{p,\infty}} \quad (166)$$

Conversely, $\mu^{EQ}_{k,ext}$ represents the molecular chemical potential of penetrant k present in the external fluid phase. Its expression is directly provided by the equilibrium NRHB theory.

The previous description reports, in a synthetic way, the formalism of the procedure used in the NETGP-NRHB approach. In the next paragraphs we provide a detailed discussion of the equations that are operatively used in interpreting phase equilibria.

We start from the expression of the generic term of the Gibbs energy provided by the NRHB model (G_{NRHB}), see Eq. (113). It is important to note that, for the purposes of the NETGP-NRHB development, in expression (113) $\sim\rho$ and $\sim v$ ($\sim v = 1/\sim\rho$) are replaced by ρ_P, using the following relationship:

$$\rho_P = \frac{m_P}{V} = \frac{m_P}{rn\sim v v^* + \sum_{\alpha=1}^{m}\sum_{\beta=1}^{n}\left(N^H_{\alpha\beta}V^0_{\alpha\beta}\right)} \quad (167)$$

Once this substitution is performed, we obtain the general expression of Gibbs energy, G, i.e. $g(T,P,N_1,N_2,\ldots,N_{t-1},N_p,\rho_{P,\infty},N\,ij,N\,\alpha\beta^H)$. Actually, in view of the Instantaneous Equilibrium assumption, the sets of variables $N\,ij$ and $N\,\alpha\beta^H$ are a function of the other variables (i.e. $T,P,N_1,N_2,\ldots,N_{t-1},N_p,\rho_{P,\infty}$) through the minimization conditions for G. $\mu^{IE}_{k,pol}$ can then be calculated as:

$$\mu^{IE}_{k,pol} = \left(\frac{\partial G}{\partial N_k}\right)_{P,T,N_{j\neq k},\rho_{P,\infty},N\,ij,N\,\alpha\beta^H} + \sum_{i=0}^{t}\sum_{j>i}^{t}\left[\left(\frac{\partial G}{\partial N_{ij}}\right)_{P,T,N,\rho_{P,\infty},N_{rs\neq ij}}\left(\frac{\partial N_{ij}}{\partial N_k}\right)_{P,T,\rho_{P,\infty},N_{j\neq k}}\right] + \sum_{\alpha=1}^{m}\left[\sum_{\beta=1}^{n}\left(\frac{\partial G}{\partial N^H_{\alpha\beta}}\right)_{P,T,N,\rho_{P,\infty},N\,ij,N^H_{\gamma\delta\neq\alpha\beta}}\left(\frac{\partial N^H_{\alpha\beta}}{\partial N_k}\right)_{P,T,\rho_{P,\infty},N_{j\neq k}}\right] \quad (168a)$$

Since, in view of IE assumption, we have that:

$$\left(\frac{\partial G}{\partial N_{ij}}\right)_{P,T,N,\rho_{P,\infty},N_{rs\neq ij},N^H_{\alpha\beta}} = 0 \text{ for } i=0,\ldots,t \text{ and } j=i+1,\ldots,t \quad (169a)$$

$$\left(\frac{\partial G}{\partial N^H_{\alpha\beta}}\right)_{P,T,N,\rho_{P,\infty},N_{rs\neq ij},N^H_{\alpha\beta}} = 0 \text{ for each } \alpha,\ \beta \quad (169b)$$

It follows that:

$$\mu^{IE}_{k,pol} = \left(\frac{\partial G}{\partial N_k}\right)_{P,T,N_{j\neq k},\rho_{P,\infty},N\,ij,N\,\alpha\beta^H} \quad (168b)$$

In summary, according to this approach, $\mu^{IE}_{k,pol}$ is calculated by performing the derivative, with respect to N_k, of the general expression of the Gibbs energy, G, i.e. $g(T,P,N_1,N_2,\ldots,N_{t-1},N_p,\rho_{P,\infty},N\,ij,N\,\alpha\beta^H)$, at fixed values of $N\,ij$ and $N\,\alpha\beta^H$, dictated by minimization conditions (i.e. Eqs. (169a) and (169b)). The final expression is:

$$\frac{\mu^{IE}_{k,pol}}{kT} = \ln\frac{\phi_k}{\delta_k r_k} + \ln\sim\rho - r_k\ln\left(1-\sim\rho\right) - \frac{z}{2}r_k\left(\frac{q}{r}-1\right)\ln\left(1-\sim\rho+\frac{q}{r}\sim\rho\right) + \frac{z}{2}q_k\left(\ln\Gamma_{kk}-\frac{r_k}{q_k}\ln\Gamma_{00}\right) - \frac{q_k}{\sim T_k} - \sum_{\alpha=1}^{m}\left[d^k_\alpha\ln\left(\frac{\nu^\alpha_d}{\nu_{\alpha 0}}\right)\right] - \sum_{\beta=1}^{n}\left[a^k_\beta\ln\left(\frac{\nu^\beta_a}{\nu_{0\beta}}\right)\right] \quad (170)$$

where $\sim\rho$ is calculated using $\rho_P=\rho_{P,\infty}$. The values of Γ_{kk}, Γ_{00}, ν^α_d, $\nu_{\alpha 0}$, ν^β_a and $\nu_{0\beta}$ are calculated by imposing the minimization conditions. It is important to note that, as proposed in the literature [99], it can be commonly assumed that the volume change of formation of an $\alpha\beta$ contact, $V^0_{\alpha\beta}$, is equal to zero.

This assumption allows significant simplifications. In fact, in such a case, the expression of the minimization conditions for Γ_{kk}, Γ_{00}, ν^α_d, $\nu_{\alpha 0}$, ν^β_a and $\nu_{0\beta}$, takes the same form as for the equilibrium NRHB theory (i.e. Eqs. 115a,b). Moreover we have also that:

$$\sim\rho = \rho_{P,\infty}/(\omega_P\rho^*) \quad (171)$$

Where ω_P, is the mass fraction of polymer while, according to NRHB framework,

$$\rho^* = \frac{\sum_{i=1}^{t}x_iM_{w_i}}{rv^*} = \frac{\sum_{i=1}^{t}N_iM_{w_i}}{rNv^*} \quad (172)$$

Consistently with the original version of NETGP theory by Sarti and Doghieri, also in this case the expression of chemical potential of component k in the polymer phase, is independent on pressure.

2.3. Molecular dynamics and Monte Carlo methods

Computer simulations of molecular models provide a viable alternative to theories of Equation of State for polymeric mixtures in view of limitations, approximations and some spurious results of the latter. Atomistic models, with a full chemical detail of molecules, are often extremely demanding in terms of computer resources. The challenging simulation of polymeric system, endowed with intrinsic long range spatial correlations of macromolecules, is then more efficiently tackled by using coarse-grained molecular models that, if one adopts proper effective potentials, can provide a reliable prediction of the phase behavior of various polymeric systems. [185].

The simulation of solution of semiflexible polymers has been performed using Monte-Carlo (MC) algorithms for self-avoiding walk used to describe macromolecules on a Lattice. Among these type of models, we mention here the so-called 'bond fluctuation' model [186–189] where macromolecules are represented, in a coarse-grained picture, as a series of effective monomers connected by bond vectors in a cubic lattice. This approach provided also a reasonable qualitative description of polymer dynamics [188,189].

Simulation of polymer solution has also been performed using off-lattice coarse-grained models, adopting both MC algorithms and MD techniques. A successful example of off-lattice coarse-grained model is that of 'bead spring', where a macromolecule is

represented as an effective chain of beads [185]. A bead represents an effective monomer, integrating in one unit several atoms. The bonds between consecutive beads on a single chain is ruled by the combination of a finitely extensible nonlinear elastic (FENE) potential and by a Lennard-Jones (LJ) potential while between non bonded beads only a LJ potential is acting. In the model picture, a low molecular weight solvent molecule in a mixture with polymer molecules, is represented by a single bead, interacting with all the other beads by a LJ potential.

Approaches based on coarse-grained models, which are less demanding than atomistic simulations in terms of computer resources, can provide valuable information on the phase behavior of polymeric systems, granted that the adopted effective potentials are good enough. Both MD and MC methods can be used to this aim. MD simulations are based on the numerical solution of Newton's equations of motion written for a system of interacting particles. Conversely, MC methods are aimed at the determination of probability distributions, calculated by means of random numbers, to be used to calculate averages of several observables.

Use of MD simulations to investigate phase coexistence in polymeric systems requires the proper choice of the statistical ensemble. In fact, since the number of molecules ($\mathcal{N}$) considered in the simulation is finite, the statistical ensembles are not all equivalent as they would be in the thermodynamic limit (i.e. $\mathcal{N} \to \infty$). The canonical $\mathcal{N}VT$ ensemble can be used, implementing the proper 'thermostat', to study phase equilibria by MD simulation of kinetics of phase separation up to establishment of equilibrium. These procedures become particularly cumbersome in the proximity of critical points and the simulations require large systems and computation times, particularly in the presence of very long macromolecules [185]. MD simulations of phase equilibria in polymer systems can also be performed in the isothermal-isobaric $\mathcal{N}PT$ ensemble, coupling the system to a 'barostat'. The equality of chemical potentials in the phases at equilibrium is imposed by using a procedure based on the Widom virtual particle insertion/deletion technique [190]. Effects associated to a finite size and the assessment of the actual achievement of a true phase equilibrium require a careful analysis of the results to avoid erroneous conclusions when using MD simulations.

By MC method one obtains the probability distribution of the different microstates for a system at equilibrium, to be used to compute the average of a specific observable, realizing artificial moves of the system, from a configuration to another, that have to be submitted to the Metropolis acceptance test [191]. As compared to MD simulations, MC methods allow the use of Grand Canonical and Semi-Grand Canonical ensembles.

Application of coarse-grained MD simulations and MC methods to binary mixtures requires information on interactions between the different species. The simplest predictive approach is to use the Lorenz Berthelot combining rule [192] to predict the parameters of the non-bonded Lennard-Jones binary interaction potential between different species. However, often a fitting correction factor to the Berthelot rule has to be introduced to account for peculiarities of interactions between molecules that are necessarily neglected in the simplified, somewhat blurred, coarse-grained view. Alternatively, one can use the Berthelot rule in combination with nonbonded binary interaction potentials for each species that properly account for specific interactions. In both cases, additive parameters have to be introduced, compromising predictive capability of calculations.

The use of simplified pair potentials is obviously an approximation but provides a reasonable description of the behaviour of real materials. A more rigorous approach should obviously include three-body terms into the expressions of intermolecular interaction.

Overall, the coarse-graining approach can be considered as a useful means to provide a first rough estimate on phase equilibria of polymer solutions, also for polar solvents like CO_2 and NH_3, although is not suited to deal with aqueous solutions, in view of the clustering tendency of water molecules, and of polyelectrolytes.

Investigation of phase equilibria involving polymer solutions is, at this stage, still a challenging task, in view of the large length and time scales to be spanned. Reliable results ae limited to the case of flexible homopolymers with relatively short chains without an all-atom modeling of solvent. Further steps are needed towards a better theoretical understanding of polymer solutions and their properties.

We provide here a few examples of the application of atomistic simulations to gas sorption in polymers. In particular, we mention the case of the simulation of CO_2 sorption in a high free volume polymer of technological interest, the PIM-1 that is a polymer of intrinsic microporosity, performed by Heuchel et al. [193]. These authors, using the Gusev-Suter transition state theory [194,195], overestimated solubility coefficients. Results in close agreement with experiments were instead obtained by Fang et al. [196,197] which applied the Widom Insertion Method. More recently, Kupgan et al. [198] used a combination of Grand Canonical Monte Carlo and Molecular Dynamics simulations to simulate CO_2 sorption in PIM-1 up to 50 atm. There are examples also of simulation of sorption of gas mixtures in polymers. One is the work by Neyertz and Brown [199] which performed large-scale MD simulations to predict the solubility of O_2/N_2 mixtures in ultrathin polyimide films, in good agreement with experimental results.

3. Strategies for model validation and estimation of parameters

3.1. Experimental approaches

In the previous sub-sections we have introduced lattice-fluid and perturbation EoS theories (e.g. NRHB and SAFT) capable of accounting for association phenomena present in mixtures containing highly polar and strongly associating compounds, as are mixtures where self- and cross- hydrogen bonding and Lewis acid/Lewis base type interactions do establish.

In the simplest cases, both classes of models require for pure compounds, in the absence of long-range forces, the knowledge of three scaling parameters (four in the case of SAFT-VR) and of two or three parameters for each kind of self-association interaction. Additive parameters are required when also long-range forces are accounted for (as is the case of SAFT variants accounting for the presence of electrostatic forces). In the case of low molecular weight compounds, the values of all these parameters can be retrieved from liquid and vapor densities and of vapor pressures over a significant range of temperatures. Conversely, in the case of polymers are generally used the PVT data of the compound in the molten state in a wide range of temperature and pressure, when available. These data are obviously unattainable if the polymer degrades before melting. In this event, a viable option could be the extrapolation of the values of the three scaling parameters determined for short chain compounds to polymers, when the chemical structure is similar. Another approach, that has been proposed when using PC-SAFT [154,155,200] is that of combining pure polymer density data with VLE and LLE phase equilibria data for binary mixtures of the polymer of interest with different low molecular weight compounds, to gather the values of both pure polymer parameters and of binary interaction parameter.

For associating compounds, the association parameters, relative to short-range interactions, could also be calculated on the basis of the experimentally determined value of the enthalpy and entropy of interaction, using the liquid-vapor equilibrium data only for the determination of the three scaling parameters. However, it is first necessary to determine the association scheme, i.e. the number and type of association sites.

Please cite this article in press as: G. Mensitieri, G. Scherillo, C. Panayiotou et al. Towards a predictive thermodynamic description of Fsorption processes in polymers: The synergy between theoretical EoS models and vibrational spectroscopy. Mater. Sci. Eng. R (2020), https://doi.org/10.1016/j.mser.2019.100525

As discussed in the description of NRHB and SAFT models, in the case of binary mixtures a binary interaction parameter is introduced (to be used in the combining rules for the calculation of cross interaction energy). Typically, the value of this interaction parameter, in the case of binary mixtures of a polymer and a low molecular weight compound, can be retrieved by using the expression of chemical potentials provided by NRHB or SAFT models to fit phase equilibrium data as, for example, sorption isotherms of the low molecular weight compound within the polymer, preferably determined at several temperatures. Theoretical expressions for the estimation of the binary interaction parameter have also been used [117], but their application is generally limited to binary mixtures of two low molecular weight compounds. For cross-associating binary mixtures, the values of the parameters ruling the cross-interactions are also required. Also in this case, these values can be retrieved by fitting phase equilibrium data, e.g. sorption isotherms. Otherwise, if both compounds are self-associating, calculation of these parameters could be performed by exploiting some combining rules of self-associating parameters, as already discussed in section 2.1.7.1.

In the light of the previous discussion, one appreciates how vibrational spectroscopy can provide experimental data from which the fraction of non-associated molecules, that is a key property in association theories, can be calculated, thus allowing validation and development of these theoretical approaches. It is worth noticing here that, when comparing spectroscopic data with results of theoretical modelling, one should pay attention to compare equal quantities, i.e. site fractions or molecule fractions. Spectroscopic data could also provide useful information to determine what is the most suitable association scheme (i.e. number and type of proton donors and proton acceptors present on a molecule that establishes specific hydrogen bonding). Unfortunately, there are few contributions in the literature addressing these issues, both for mixtures of low molecular weight compounds and for mixtures including polymers.

3.2. Gravimetric methods

The gravimetric method for the measurement of sorption isotherms in polymers is based on the detection of the weight increase/decrease of a polymer sample due to gas or vapor sorption/desorption [201]. The sample is exposed to a controlled environment consisting in a gas or vapor at controlled pressure and temperature.

There are several devices that can be used to measure the weight change of the polymer sample. One of the first to be used is the quartz spring microbalance (McBain balance) [202,203]. In Fig. 4 is reported a schematic of an equipment based on a McBain spring balance. Measurement of spring extension/contraction determined by weight increase/decrease can be converted, by calibration, into mass change values. In a typical sorption experiment, after degassing the sample, pressure is rapidly increased and the elongation of the spring is monitored, relative to a constant length reference rod, using a cathetometer or a camera, till the attainment of sorption equilibrium. Gas or vapor pressure can then be increased stepwise obtaining a sorption isotherm at a fixed value of temperature.

Other devices can be used to monitor the weight change in place of the spring microbalance, such as a Cahn electro-balance [204], a magnetic suspension microbalance [205] or a quartz crystal microbalance [206].

3.3. Pressure decay method

Another experimental technique for the measurement of gas and vapour sorption isotherms is the pressure decay method [201].

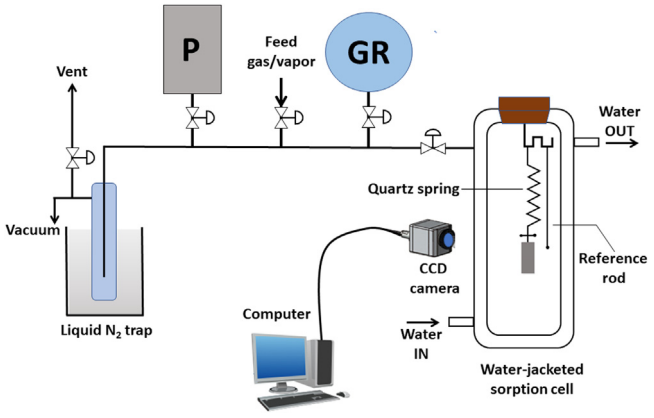

Fig. 4. Schematic representation of a McBain quartz spring sorption apparatus. The polymer sample hangs from the quartz spring located in the sorption chamber. (P: pressure transducer; GR: gas/vapor reservoir).

The evaluation of the amount of absorbed penetrant is based on the measurement of the decrease of gas pressure in the environment around a polymer sample in a closed cell, promoted by the sorption itself. Using a molar balance equation for the penetrant in the gas phase, performed between the time of start of the experiment and after the attainment of sorption equilibrium and based on the values of the volume of the sample and of the measuring cell, to be known with a high accuracy, one can estimate the absorbed amount of penetrant within the polymer sample. Source of errors could be the accuracy of pressure measurement that decreases as the full scale range of the transducers increases, the reliability of the Equation of State for the penetrant in the gaseous or vapor phase, the occurrence of possible swelling of the polymer sample that affects the estimation of the actual headspace volume of the measuring cell and, in the case of vapor sorption, the possible adsorption of the penetrant on the walls of the measuring cell. A discussion of the design criteria for a pressure decay apparatus, in the case of single-volume and dual-volume measuring cell, is reported in [207]. A schematic of a dual-volume pressure decay apparatus is reported in Fig. 5.

Pressure decay apparata were also developed to evaluate gas mixture sorption in polymers, by combining barometric measurements and gas chromatographic analysis [208], see Fig. 6.

3.4. Vibrational spectroscopy and its role in association theories

Infra-red (IR) and Raman spectra arise as a result of transitions between quantized vibrational energy levels. In IR spectroscopy these transitions occur by absorption of electromagnetic radiation of appropriate energy (frequency); in Raman spectroscopy a visible/NIR laser line promotes the system to a high-energy virtual-state which is unstable and quickly decays to the ground state. In a

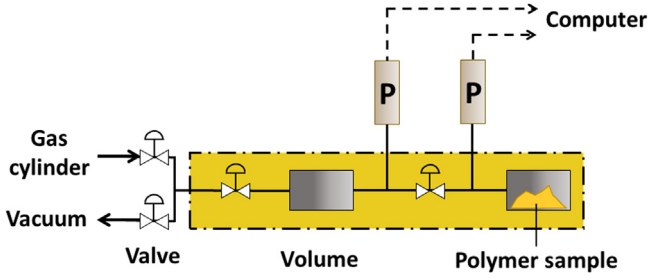

Fig. 5. Schematic of a pressure decay apparatus (dual-volume dual-transducer configuration) (P: pressure transducer). Dashed box indicates a temperature-controlled chamber.

Please cite this article in press as: G. Mensitieri, G. Scherillo, C. Panayiotou et al. Towards a predictive thermodynamic description of Fsorption processes in polymers: The synergy between theoretical EoS models and vibrational spectroscopy. Mater. Sci. Eng. R (2020), https://doi.org/10.1016/j.mser.2019.100525

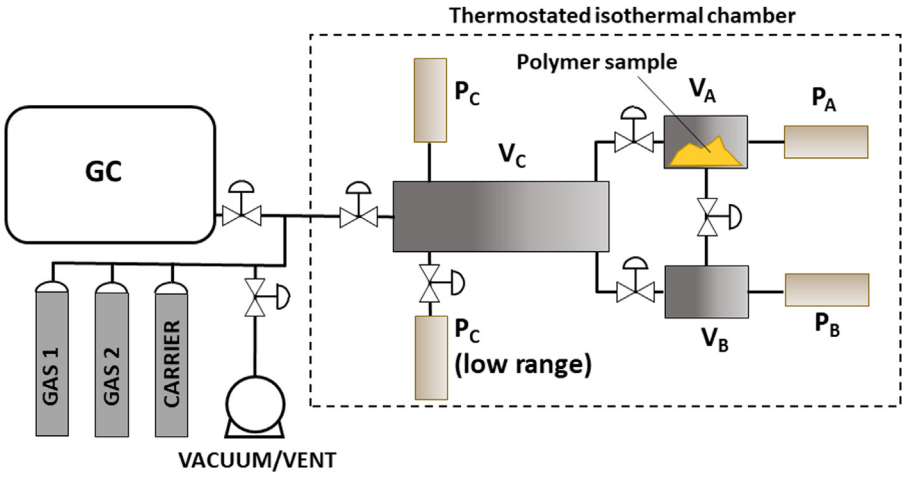

Fig. 6. Scheme of the mixed-gas equipment for the measurement of sorption in polymers. (GC—gas chromatograph; P_A, P_B, P_C – pressure transducers). Adapted from reference [208].

limited number of cases the process ends-up to vibrational energy levels other than the ground state, which produces the so-called inelastic scattering, i.e., scattered radiation with a frequency different from that of the exciting radiation. Collection of inelastically scattered radiation provides information on vibrational energy levels complementary to that given by Infrared spectroscopy [209].

Molecular vibrations can range from the very simple motion of two atoms (the stretching of a bond in a diatomic molecule) to highly complex displacements of every atoms in a polyatomic structure. The vibrational spectra, therefore, become richer of signals (and of information) as the structural complexity increases. The position and intensity of the peaks in IR and Raman spectra are dictated by the geometry of the vibrating unit and the strength of the bonds involved, which is the underlying reason for the usefulness of these techniques in structural analysis. Furthermore, as we will elaborate in the forthcoming paragraph, the signal intensity exhibits a more or less complex functional relationship with the concentration of the absorbing species in a mixture, which forms the basis for developing accurate and reproducible analytical methods [210,211].

The rationale of adopting spectroscopic techniques for investigating the sorption behavior of polymers lies in the wealth of information at molecular level that could be extracted therefrom and that is unavailable when relying on purely gravimetric data. Obviously, the type of information and the level of detail that are accessible depend on the nature of the chosen spectroscopic tool and, in particular, on the time frame of the probing electro-magnetic radiation. Another critical parameter is the bandwidth of the generated signals which dictates the spectroscopic contrast, (i.e. the possibility to discern the signature(s) of the penetrant within the complex pattern generated by the polymer substrate), and the feasibility of multiplexed detection. In both these respects, vibrational spectroscopy provides distinct advantages. Infrared and Raman spectra consist of a highly specific pattern of signals with narrow bandwidths (typically, less than 1 nm against – for example – over 50 nm in fluorescence spectra) which can be regarded as a true fingerprint of the compounds they originate from. In addition, a number of these signals are very sensitive to the establishment of molecular interactions, particularly H-bonding, and this sensitivity can be exploited for identifying the different molecular aggregates being formed in a system. Counterbalancing this advantage, molecular interactions produce considerable band broadening as a consequence of the wide distribution of geometries and force constants occurring in supramolecular aggregates. This effect limits and often prevents full resolution of the different components that make up the observed profiles and, in many instances, one has to resort to resolution-enhancement approaches. These will be discussed in detail in the forthcoming paragraphs.

Another limitation of the vibrational techniques results from the intensity enhancement of the bands [in particular, ν(OH)/ν(NH) modes] upon the establishment of the interaction. This poorly predictable effect complicates the quantitative analysis; several ways to circumvent the problem have been proposed in the literature and will be discussed in detail.

However, among the manifold benefits that vibrational spectroscopy has to offer in the present application, the principal is perhaps its nature of a true solid-state sampling technique coupled with an exceptional sampling flexibility. Thus, commercial films in the thickness range between 200 and 10 μm are readily characterized by FTIR/Raman with little or no post-processing. Whenever thinner films are required for specific applications (i.e., from 0.1 to 5 μm) these may be prepared by suitable spin-coating methods. The open architecture of the FTIR/Raman spectrometers and the remote-sensing capabilities makes it rather straightforward to develop *in-situ*, time-resolved measurements, which are essential to achieve the stability and the quality of data that are mandatory for the present application.

3.4.1. Quantifying the penetrant concentration by vibrational spectroscopy

Quantitative analysis by infrared spectroscopy relies on the relationship between the amount of absorbed electromagnetic radiation and the quantity of absorbing material. This relationship, in its more general form, can be written as:

$$\frac{dP}{P} = -NC_M\sigma_{EXT}dL \tag{173}$$

where P is the incident power (i.e., the number of incident photons per unit time), N the Avogadro's number, C_M the molar concentration of the absorber in the sampling volume, σ_{EXT} the extinction molecular cross-section and L the optical path-length (in the above formula the scattered radiation, i.e., σ_{SC}, is considered negligible). When the measurement is performed on the radiation crossing the sample (transmission mode), integration over the crossed optical path gives:

$$\int_{P_0}^{P_L}\frac{dP}{P} = -N\sigma_{EXT}\int_0^L C_M dL \Longrightarrow ln\frac{P_L}{P_0} = -N\sigma_{EXT}C_T L \tag{174}$$

Please cite this article in press as: G. Mensitieri, G. Scherillo, C. Panayiotou et al. Towards a predictive thermodynamic description of Fsorption processes in polymers: The synergy between theoretical EoS models and vibrational spectroscopy. Mater. Sci. Eng. R (2020), https://doi.org/10.1016/j.mser.2019.100525

where P_0 and P_L are the incident and the transmitted power, respectively and C_T is the total concentration of analyte in the sample.

The Transmittance, *T*, is the ratio between the transmitted and the incident power or, for consistency with most literature notation, the ratio between the transmitted radiation intensity (I_L) and the incident radiation intensity (I_0):

$$T = \frac{P_L}{P_0} = \frac{I_L}{I_0} = \exp(-N\sigma_{EXT}C_T L) = \exp(-\alpha C_T L) \tag{175}$$

the term $\alpha = N\sigma_{EXT}$ is the linear molar absorptivity. In the analytical applications of FTIR spectroscopy the most widely used photometric quantity is Absorbance, *A*, defined as $A = log_{10}(I_0/I_L)$, which allows linearization of Eq. (175) in the well-known Lambert-Beer form (Eq. 179):

$$A = log_{10}\left(\frac{I_0}{I_L}\right) = -log_{10}T = \frac{NC_T\sigma_{EXT}L}{ln10} \tag{176}$$

and, defining the decadic molar absorptivity as:

$$\varepsilon = \frac{N\sigma_{EXT}}{ln10} \tag{177}$$

$$A = \varepsilon L C_T \tag{178}$$

ε is the quantity generally referred to in the literature (omitting the term *decadic*). Other terms have been used to designate this constant and are still encountered nowadays (extinction coefficient, absorption coefficient) which generates a certain degree of confusion; molar absorptivity is the preferred nomenclature [212].

In applying the seemingly straightforward relationship (178) to real-world problems, there are a number of points to be carefully considered.

i) First and foremost, the photometric observable *A* is linearly related to a volumetric concentration. When a correlation is made between spectroscopic and gravimetric measurements of penetrant uptake, the gravimetric values are expressed in terms of weight ratios. These can be converted into molar concentration knowing the density of the system. While for low solubility (1–2 wt %) penetrants the density can be safely considered coincident with that of the pristine sample and invariant with penetrant uptake, this is no longer true when the penetrant uptake becomes conspicuous. Severe nonlinearities in the Beer-Lambert diagrams are often due to neglecting the density variation during a sorption process.

ii) ε is a way of expressing the absorption cross-section of a molecule (see Eq. (177)), which physically corresponds to the effective area of a homogeneous incoming beam from which the molecule will absorb every photon. It is a physical constant (expressed in m^2) related to the structure of and the electronic distribution within the molecule. In particular:

$$\sigma_{EXT} = \frac{\pi}{3c}\left[\left(\frac{\partial\mu_x}{\partial Q_i}\right)^2 + \left(\frac{\partial\mu_y}{\partial Q_i}\right)^2 + \left(\frac{\partial\mu_z}{\partial Q_i}\right)^2\right] \tag{179}$$

where *c* is the speed of light *in vacuo*, μ is the dipole moment of the absorber and Q_i is the normal coordinate of the respective vibrational mode. This quantity must be evaluated for converting *A* into C_T, which is one of the most difficult tasks when applying spectroscopic monitoring to sorption processes. As it is apparent from Eq. (179), σ_{EXT} is a sensitive function of $\partial\mu/\partial Q_i$, the transition dipole moment. Molecular interactions, especially H-bonding, may significantly alter this parameter, which implies a considerable sensitivity of ε to the molecular environment, a sensitivity even greater than peak position, that is customarily employed to evaluate interaction strength. The above argument stresses the need of estimating the respective ε values whenever multiple molecular aggregates are formed, for example, when there exist diferent interaction sites on the polymer backbone. This is not always feasible, which may prevent a complete characterization of the system in terms of species population. Again, assuming an average value for the molar absorptivities of different species, as it is often done, may lead to severe nonlinearities in the *A* vs C_T diagrams.

iii) In the present application the optical path, *L*, corresponds to the sample thickness; it is an experimental variable in transmission measurements, while, as we will see later, it is a fixed quantity in the Attenuated Total Reflection (ATR) mode. In transmission, *L* can be used to adjust the sensitivity (see Eq. (178)) provided the polymer substrate makes no or limited interference in the analytical frequency range. Obviously, the sensitivity increment is achieved at the expenses of the time to equilibration and a trade-off is to be established between sensitivity and experiment duration. As an example, for the case of water sorption in thermoplastic polyesters, where the polymer produces negligible signals in the 3800 – 3000 cm^{-1} range, the sensitivity reaches 100 ppm for a 40 μm thick film that achieves equilibrium in 150 s. In this and in analogous cases the limit of detection can be further improved (if needed) by increasing *L*.

The ATR sampling is based on the detection of the evanescent radiation produced at the boundary between a propagating medium (an ATR crystal, also called internal reflection element, IRE) and a rarer medium (the polymer film). The experimental set-up is schematically depicted in Fig. 7A,B.

The evanescent field is produced in conditions of total reflection, i.e., when the angle of incidence, θ, exceeds the critical angle, θ_c, defined as: $\theta_c = \arcsin(n_2/n_1)$ where n_2 and $n_1$are the refractive indices of the rarer and the denser medium, respectively.

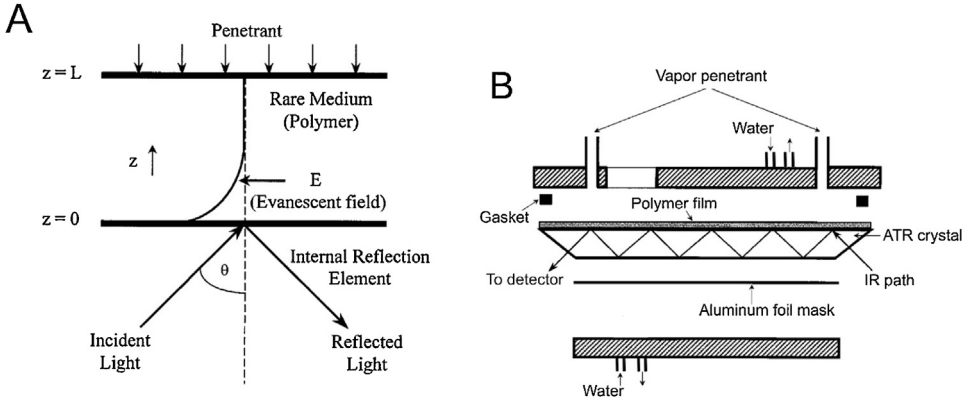

Fig. 7. A): Schematic diagram illustrating the ATR sampling mode. B): experimental setup for diffusion measurements by ATR spectroscopy. Figures reprinted with permission from [213]. Copyright 2002 American Institute of Chemical Engineers (AIChE).

The evanescent field, E, decays exponentially in the rarer medium as:

$$E = E_0 \exp\left\{-\frac{2\pi}{\lambda_1}\left(sin^2\theta - \left[\frac{n_2}{n_1}\right]^2\right)^{\frac{1}{2}} z\right\} \quad (180)$$

where E_0 is the field strength at the boundary, λ_1 is the radiation wavelength in the denser medium and z is the distance from the surface. Eq. (180) can be conveniently re-written as:

$$E = E_0 \exp(-\gamma z) \quad (181)$$

where γ, the electric field amplitude decay constant, is given by

$$\gamma = \frac{2\pi\left[sin^2\theta - \left(\frac{n_2}{n_1}\right)^2\right]^{\frac{1}{2}}}{\lambda_1} \quad (182)$$

When the rarer medium absorbs at specific frequencies, the intensity of the reflected wave will be correspondingly frustrated, which results in an absorption spectrum analogous (but not coincident) with that in transmission. Thus, in analogy with Eq. (173), we may write

$$\frac{dI}{I} = -\alpha C_M dz \quad (183)$$

where I is the radiation intensity and α is the linear molar absorptivity ($\alpha = N{\cdot}\sigma_{EXT}$takes the same values as in transmission). We indicate with the symbol $\mathcal{A}$ the quantity $\ln(I/I_0)$. It is unfortunate that $\mathcal{A}$ is often called Absorbance, especially among the ATR community [213–215], thus generating some confusion with the customary meaning of the term (i.e. the decadic logarithm of the ratio between incident and transmitted intensity). In the present context, $\mathcal{A}$ will be designed as the natural Absorbance to specify its derivation from the natural logarithm. To combine the Beer-Lambert relationship with the field strength Eq. (181) it is necessary to postulate the weak absorption condition:

$$\frac{I}{I_0} = e^{-\mathcal{A}} \cong 1 - \mathcal{A} \,\text{from which}\, dI = -I_0 d\mathcal{A} \quad (184)$$

and, substituting into Eq. (183):

$$d\mathcal{A} = \frac{\alpha}{I_0} C_M I dz \quad (185)$$

which, upon integration, yields:

$$\mathcal{A} = \int_0^d \frac{\alpha}{I_0} I C_M dz \quad (186)$$

d is the distance from the surface travelled by the evanescent wave before vanishing (conventionally, before $E \leq E_0/e$). Putting $\alpha^* = \alpha/I_0$ and since $I = E^2$, we end up with [214,215]:

$$\mathcal{A} = \int_0^d \alpha^* E_0^2 \exp(-2\gamma z) C_M dz \quad (187)$$

Eq. (187) is valid for a single reflection experiment. In case the geometry of the IRE allows for m multiple reflections, the integral in Eq. (187) is to be multiplied by m.

An important consideration is that the quantity d, which resembles the optical path L in transmission measurements, is strongly dependent on the wavelength of the radiation, λ, according to the Harrick equation [216]:

$$d = \frac{\lambda}{2\pi n_1\left[sin^2\theta - \left(\frac{n_2}{n_1}\right)^2\right]^{\frac{1}{2}}} \quad (188)$$

Thus, the depth of penetration changes across the spectrum, typically from around 0.2 μm at 4000 cm^{-1} up to around 10 μm at 450 cm^{-1}, depending on the geometry and the IRE parameters in Eq. (188). This effect makes the ATR spectrum less intense in the higher frequency side and more intense in the lower, in comparison to the transmission spectrum. d can be controlled in a narrow range (compared to L) by adjusting the angle of incidence, θ, (if the experimental setup allows for this), or by choosing an IRE with appropriate refractive index.

Quantitative analysis by Raman spectroscopy is based on the relationship between the intensity of the inelastically scattered radiation and the concentration of scattering centers [217,218]. The problem is best treated by factorizing sample and laser variables with respect to the collection variables. A specific scattering intensity I_{SCA}, expressed in $photons{\cdot}sr^{-1}\,cm^{-2}{\cdot}s^{-1}$ can be conveniently defined as:

$$I_{SCA} = P_D \beta D \ell \quad (189)$$

where P_D is power density of the laser beam ($photon{\cdot}s^{-1}\,cm^{-2}$); $\beta = \frac{d\sigma}{d\Omega}/N$ is the Raman cross section ($cm^2{\cdot}molecules^{-1}\,sr^{-1}$); D is the density of scattering centers in the sampling volume ($molecules{\cdot}cm^{-3}$) and ℓ is the path length illuminated by the laser beam (cm). $\sigma = \Phi/J$ is the ratio between the total scattered power, Φ, and the irradiance of the laser beam, J, Thus, β represents the fraction of the total intensity scattered in a given direction within an infinitesimal element of the whole solid angle, Ω (sr), around the scattering center.

Analogously, an instrumental collection function C ($cm^2{\cdot}sr{\cdot}e^-{\cdot}photons^{-1}$) expressing the fraction of the total scattered light that is collected and measured by the instrument can be defined as:

$$C = A_D \Omega_D T Q \quad (190)$$

where A_D is the area sampled by the spectrometer (cm^2); Ω_D is the collection solid angle of the instrument ($steradians$, sr); T is the instrumental transmission (unitless); Q is the quantum efficiency of the detector [electrons (e^-)·$photons^{-1}$]. Both the instrumental transmission and the quantum efficiency are frequency dependent variables. The observed intensity (in photoelectrons) is:

$$I(\nu) = I_{SCA} C t = (P_D \beta D \ell)(A_D \Omega_D T Q) t \quad (191)$$

where t is the exposure time in seconds. Consider two scattering species i and j producing two separate peaks at frequencies ν_i and ν_j. Their intensity ratio is given by:

$$\frac{I(\nu_i)}{I(\nu_j)} = \frac{\beta_i D_i T(\nu_i) Q(\nu_i)}{\beta_j D_j T(\nu_j) Q(\nu_j)} = K \frac{D_i}{D_j} = K \frac{n_i}{n_j} \quad (192)$$

where $K = [\beta_i T(\nu_i) Q(\nu_i)]/[\beta_j T(\nu_j) Q(\nu_j)]$ is a constant depending only on the choice of the analytical peaks and is invariant with the instrumental parameters provided the two peak are recorded in a single measurement. n_i and n_j represent the number of molecules of the respective species in the sampling volume. According to Eq. (192), quantitative analysis by Raman spectroscopy is never performed on the absolute intensity values of a single analytical peak, as in transmission FTIR, but is always based on intensity ratios.

3.4.2. Monitoring sorption processes by ATR-FTIR spectroscopy

One of the first systematic studies on the use of Infrared spectroscopy for measuring diffusion coefficients in polymers dates back to the early 1980s; the experiments were performed in the attenuated total reflection mode. Remizov and co-workers [219] investigated the transport of low molecular weight compounds (acetone, methyl ethyl ketone and benzene) in

polyethylene. The aim of the study was to demonstrate the feasibility and accuracy of the ATR measurement of diffusion coefficients. Albeit the authors recognized the exponentially decaying nature of the evanescent field, no attempt was made to correct for this effect. The obtained diffusivity values were comparable to those from conventional gravimetric measurements but the spectroscopic data were plagued by a conspicuous degree of scatter. In perspective, it can be readily perceived that the problem originated from the off-line experimental procedure, analogous to the conventional pat-and-weight method, by which the polymer film was removed from the optical element after each measurement. This caused difficulties in establishing a consistent degree of contact between the sample and the IRE, which in ATR spectroscopy is an essential requirement for achieving accurate and reproducible reflectance values. After this seminal contribution, only a limited number of papers appeared in the following decade [220–222]. It was not until the early nineties of the past century that several research groups independently initiated long-term programs on the development of ATR-based methods for investigating small-molecule and macromolecule transport [223]. A steady flow of papers has appeared since then, which constitutes now a consolidated body of knowledge.

The relationship between the photometric observable $\mathcal{A}$ and the penetrant concentration is more involved in ATR than in transmission for it involves the exponentially decaying nature of the evanescent field (Eq. (187)). Thus, in order to simulate the sorption kinetics, it is necessary to postulate a concentration profile to be convoluted with the ATR absorption relationship. Fieldson and Barbari [214] considered the case of a *Fickian* one-dimensional diffusion in a polymer film of thickness $2L$ in contact with an infinite bath of penetrant. If the concentrations at the two interfaces ($z = L$ and $z = -L$) are instantaneously established at a value C_s and the initial concentration of penetrant is zero, then the concentration C at any position in the film, z, and at any time, t, is [224]:

$$\frac{C}{C_S} = 1 - \frac{4}{\pi}\sum_{n=0}^{\infty}\frac{(-1)^n}{2n+1}exp\left[\frac{-D(2n+1)^2\pi^2 t}{4L^2}\right]cos\left[\frac{(2n+1)\pi z}{2L}\right] \quad (193)$$

where D is the diffusion coefficient. Integrating Eq. (193) over the film thickness, one obtains the mass of absorbed penetrant as a function of time:

$$\frac{M_t}{M_\infty} = 1 - \sum_{n=0}^{\infty}\frac{8}{(2n+1)^2\pi^2}exp\left[\frac{-D(2n+1)^2\pi^2 t}{4L^2}\right] \quad (194)$$

where M_t and M_∞ are the mass sorbed within the polymer at time t and at equilibrium, respectively. Often, to simplify the calculations, the short-times and the long-times solutions of the differential mass balance equation are used, respectively written as [214]:

$$\frac{M_t}{M_\infty} = \frac{2}{L}\left(\frac{D}{\pi}\right)^{0.5} t^{0.5} \quad (195)$$

$$\frac{M_t}{M_\infty} = 1 - \frac{8}{\pi^2}exp\left(\frac{-D\pi^2 t}{4L^2}\right) \quad (196)$$

By substituting the *Fickian* concentration profile, $C(z,t)$ obtained from Eq. (193) into the ATR relationship (i.e. substituting for C_M in Eq. (187)) and integrating, one obtains [214]:

$$\frac{\mathcal{A}_t}{\mathcal{A}_\infty} = 1 - \frac{8\gamma}{\pi[1-exp(-2\gamma\cdot L)]}\sum_{n=0}^{\infty}\left\{\frac{exp(g)[fexp(-2\gamma L)+(-1)^n(2\gamma)]}{(2n+1)(4\gamma^2+f^2)}\right\} \quad (197)$$

Where

$$g = \frac{-D(2n+1)^2\pi^2 t}{4L^2}$$

and

$$f = \frac{(2n+1)\pi}{2L}$$

Eq. (197) has been used for regressing *time-resolved* ATR data either in full or in more compact forms after some simplifying assumptions [213–215,225,226]. Experimentally, for measurements of small-molecules diffusion, a polymer film is cast on the surface of the IRE, which provides an optimum interface contact. This assembly is then mounted in an ATR flow-cell, or, in some cases, contacted with a static penetrant reservoir (a filter-paper impregnated by the liquid penetrant). In this experimental configuration great care should be taken to ensure that no deformation/buckling of the cast film occurs upon sorption, which may cause the film surface to loose contact with the IRE, severely affecting the spectrum quality. In Ref [214]. the authors measured the diffusivity of water in poly(acrylonitrile) (PAN) using the long-times approximation (Eq. (196)). The ATR estimation provided D values in good agreement with earlier gravimetric data and demonstrated a significant dependence of the transport properties on the thermal history of the sample. This dependence was attributed to sample annealing which produces a crystalline phase impervious to the penetrant, and to the removal of residual solvent incorporated during film casting. In a further contribution by the same group, *Case II* diffusion was considered and its incorporation into the formulas of evanescent field spectroscopy was implemented [215]. *Case II* transport behavior is unique to polymers and is related to the swelling of a glassy phase by a low molecular weight penetrant. It produces a front of constant penetrant concentration advancing from the polymer-penetrant interface into the polymer bulk at a constant velocity, υ.

For this case, the concentration profile as a function of position and time can be expressed as:

$$C(z,t) = C_L\mathcal{H}(z+\upsilon t - L) \quad (198)$$

where $\mathcal{H}(x)$ is the Heaviside step function, defined as:

$$\mathcal{H}(x) = \left\{\begin{array}{l} 0,\ x<0 \\ 1,\ x\geq 0 \end{array}\right\}$$

Substituting into Eq. (187) and integrating, one obtaines:

$$\frac{\mathcal{A}}{\mathcal{A}_\infty} = \frac{1-exp(2\gamma\upsilon t)}{1-exp(2\gamma L)} \quad (199)$$

for $\upsilon t/L \leq 1$. When the systems behaves as predicted by this simple model, equilibrium is reached when the dimensionless quantity $\upsilon t/L$ goes to unity. A specific feature of Case II diffusion is that $\mathcal{A}/\mathcal{A}_\infty$ approaches unity with an exponential trend, which makes it easy to distinguish, via ATR spectroscopy, *Case II* from *Fickian* behavior. In Ref. [215] the authors examined the diffusion of acetone in polypropylene and of methanol in polystyrene and poly(methyl methacrylate). They demonstrated the ability of ATR spectroscopy to discriminate between diffusion models (i.e. *Fickian* for acetone/polypropylene and methanol/polystyrene, *Case II* for methanol/poly(methyl methacrylate)). The diffusivity data presented therein were unavailable at the time, not only for the investigated systems but also for other common penetrant/polymer pairs of technological relevance, which gave further impetus to the development of the FTIR-ATR method. The methanol-based systems highlighted a further feature of the spectroscopic approach, that is the ability of detecting molecular interactions, especially H-bonding. Although no specific bandshape analysis was performed in this seminal

contribution, the possibility of exploiting the molecular information contained in the *time-resolved* spectra was clearly recognized. Later, the same group examined the diffusion of methyl ethyl ketone (MEK) in poly(isobutylene), comparing the spectroscopic and the gravimetric techniques [226]. The authors developed a setup for the simultaneous measurement of spectroscopic and gravimetric data, which facilitated the comparison between the two approaches. The diffusivities evaluated by the two techniques agreed well ($3.85{\cdot}10^{-8}$ cm^2/s by spectroscopy and $3.72{\cdot}10^{-8}$ cm^2/s by gravimetry). A further benefit of using FTIR-ATR (as well as transmission FTIR) over gravimetry is the possibility of investigating multicomponent diffusion. This advantage was exploited in studies dealing with the transport of vapor mixtures of toluene and MEK in Poly(isobutylene) [227,228]. The mutual diffusion coefficients of the two components were successfully evaluated and it was shown that, under certain experimental conditions, the diffusivity of the fastest penetrant (MEK) was increased by the additional free volume created by the slower penetrant. The solvation process was separated from diffusion in the system MEK/vinyl alcohol-vinyl butyral copolymers [213]. Deconvolution of the carbonyl band of the penetrant allowed measuring the equilibrium constant and the diffusion coefficient simultaneously. Analysis of the time-resolved spectra also allowed the authors to verify and confirm the local equilibrium hypothesis for the investigated copolymers. By separating the H-bonding formation from the effective diffusion process, it was possible to estimate a true diffusivity, which was found coincident with that of a probe (methylene chloride) with a close Lennard-Jones diameter and a negligible interactive character. The diffusion of acrylonitrile in a heterogeneous polymeric membrane (phase-segregated polyurethane) was investigated adopting a similar transport model. The study revealed that the main factors controlling the diffusion process were the surface to volume ratio and the available surface binding sites. Both these factors were successfully quantified by ATR-FTIR spectroscopy [225].

The work of Furlan [229] illustrates the impact of polymer morphology on transport properties. The diffusion of decyl alcohol in hydrogenated polybutadienes was investigated by FTIR-ATR. The sorption was found much slower and the uptake lower that those predicted by a simple two-phase model. The author interpreted these effects as being due to an intermediate phase present in the system to a considerable amount, which behaves in-between a fully accessible amorphous and a completely impervious crystalline phase. Van Alsten and Coburn [230] investigated the transport of water in glassy polyimides differing for cure conditions and backbone structure. They concluded that the main factors affecting the diffusion behaviour were chain stiffness, crystallinity and the density of the amorphous phase. The spectra of absorbed water were found to be significantly sensitive to the macromolecular environment: at least three distinct environments were detected, pointing to a considerable degree of inhomogeneity in the investigated materials. Sammon and co-workers [231] studied by FTIR-ATR spectroscopy the sorption of water and methanol into poly(ethylene terephthalate), PET, of varying crystallinity degrees. The behavior of the H_2O/PET system was found to be *Fickian*, with a marked decrease of diffusivity with increasing crystallinity. No evidence of swelling was observed. Conversely, the sorption of liquid methanol is *non-Fickian* and is accompanied by significant swelling. Increasing the crystallinity reduced the swelling effect, hence the sorption rate, possibly due to a free-volume reduction. The sorption rate of methanol was found to be higher than that of water, likely because of the swelling effect. A very interesting and unique feature of the ATR-FTIR method is the possibility it offers to study interdiffusion of polymers. This phenomenon is challenging to monitor; for instance, the measurement is unfeasible by transmission FTIR. The simplest application of the ATR approach is when the two components are both amorphous and the experiment is performed at a temperature above the respective T_g's. In these conditions, the system displays a *Fickian* behaviour, which can be easily modelled by the relevant ATR/mass transport equations. Jabbari and Peppas [232] investigated the interdiffusion of polystyrene (PS) and poly(vinyl methyl ether) (PVME), a fully compatible polymer pair, below and above the T_g of PS. At 105 °C (T_g +5 °C) the interdiffusion coefficient was $1.1{\cdot}10^{-12}$ cm^2/s, a value intermediate between the self-diffusion coefficients of the two components. At 85 °C (T_g – 15 °C) the behavior deviated severely from the *Fickian* model and was time-dependent. To fit the kinetic data at both temperatures a linear combination of *Fickian* and *Case II* models was adopted. At 85 °C Case II was the dominant contribution (70 %) while at 105 °C Case I prevailed markedly (80 %). The spectroscopic analysis also revealed that, after the establishment of intimate contact, the fastest diffusing component (PVME) swells the slower (PS) prior to starting interdiffusion across the interface [232]. To deepen the fundamental understanding of the macromolecular transport in semicrystalline polymers, Van Alsten and co-workers studied the diffusion of amorphous PS into amorphous and a semicrystalline PS as a function of the molecular weight (i.e., the size) of the polymeric penetrant [233]. In this elegant experimental investigation the spectroscopic contrast for discriminating the penetrant from the substrate was achieved by using monodisperse, perdeuterated atactic PS as diffusant and fully hydrogenated atactic or isotactic PS as substrate. The latter was annealed in different conditions to vary the crystallinity degree. The diffusivity values of the D-PS tracer in PS melts were found in excellent agreement with literature data based on ion-beam experiments. For semi-crystalline samples *non-Fickian* kinetics were observed at low temperatures and high penetrant molecular weight. It was proposed that the permeability of the substrate is controlled by the size and connectivity of the amorphous phase in comparison to the size of the diffusant. Thus, when the dimension of the penetrant approaches that of the amorphous regions between the crystallites, the capacity of the diffusing macromolecules to undergo the required reptation for passing through is hindered, resulting in a reduction of the transport rate [233].

We conclude this section with a brief discussion on what is considered the most relevant application of ATR spectroscopy to polymer/penetrant systems, namely the study of polymer processing by high pressure or supercritical (sc) CO_2. The ATR sampling has unique features that make it an unsurpassed experimental approach for these demanding investigations. Among others, the fact that the electromagnetic probe does not reach the surrounding environment, which removes any interference from the intense signals of the gas phase. A large body of studies has accumulated along the years, starting from the pioneering work of the Kazarian's group, who first described an experimental arrangement for *in-situ* collection and discussed in detail the various issues related to data processing and interpretation [234–237]. One of the open questions for exploiting the potential of $scCO_2$ processing as a green-chemistry approach is a fundamental understanding of the molecular interactions taking place between the functional groups of the diverse polymer substrates and the carbon dioxide. In this respect, major contributions were given for thermoplastic polyesters (PMMA and its co-polymers [234,238], PET [239–241]), syndiotactic polystyrene [242] and poly(ethylene glycol), PEG [243]. A recent, very interesting contribution [244] discusses new insights into the interaction mechanisms and reports the relative thermodynamic parameters obtained by *in-situ* ATR spectroscopy, for numerous polymer systems subjected to high pressure CO_2 processing. The ATR sampling mode offers a further advantage, i.e., the possibility of quantifying concurrently CO_2 sorption and the substrate swelling. This unique feature has been

Please cite this article in press as: G. Mensitieri, G. Scherillo, C. Panayiotou et al. Towards a predictive thermodynamic description of Fsorption processes in polymers: The synergy between theoretical EoS models and vibrational spectroscopy. Mater. Sci. Eng. R (2020), https://doi.org/10.1016/j.mser.2019.100525

exploited in a number of studies on commercial reverse-osmosis membranes [245], coordination polymers [246], poly(dimethyl siloxane) elastomers [237], PEG [243,247], polyketones [248] and hyper-cross-linked polymer sponges [249]. More advanced experimental approaches based on ATR spectroscopy are being actively developed for the present application, owing to its enormous technological interest. Among them, it is worth mentioning the use of ATR-FTIR microspectroscopy, which provides imaging capabilities for the collection of spatially resolved data [250]. The principal results obtained in the last decades on polymer processing by high pressure CO_2 as investigated by ATR-FTIR have been summarized in a recent review article [251].

3.4.3. Development of experiments in the transmission mode

Concurrently with the development of the ATR-FTIR method, other groups explored the possibility of monitoring the sorption process by means of FTIR transmission measurement. This alternative approach, described in detail in Ref. [252], is based on time-resolved FTIR transmission measurements performed on a polymer film placed in a cell where it is exposed to a controlled pressure of a pure penetrant vapor phase and kept at a controlled temperature (see Fig. 8 for a schematic of the apparatus). This experimental approach was developed to respond to a number of drawbacks of the ATR sampling mode. The key factor to ensure the quality of an ATR spectrum — the sample-to-IRE contact — is rather difficult to control, especially in long-term measurements. In fact, while the deformation of the polymer film due to sorption may be tolerated in transmission measurements, it produces a considerable worsening of the spectrum and of the quantitative accuracy in ATR. This problem has often restricted the use of the ATR technique to short time tests, preventing the attainment of a true equilibrium, which had to be extrapolated by suitable diffusion models [215,227,228]. This procedure may induce additional uncertainty in the determination of the diffusivity values. To optimize the contact, films were directly cast on the IRE. This protocol is efficient but has limited applicability for thermosets which are difficult to remove, once cured, without damaging the surface of the expensive crystal.

The Absorbance to concentration relationship is much simpler in transmission than in ATR (compare Eqs. (178) and (187)), as the former does not include the exponential decay term of the evanescent field in the integral over the thickness dimension. Therefore, gravimetric measurements can be directly correlated with their spectroscopic counterparts, irrespective of any concentration gradient along the thickness dimension. On the downside, it should be mentioned that the transmission mode is restricted to sorption of gases or vapors. In fact, contrary to what happens in ATR, in the transmission mode the electromagnetic probe samples both the polymer film and the surrounding environment. Thus, monitoring the diffusion of penetrants in the liquid phase would require extremely thin liquid layers to prevent saturation of the spectrum signals. For the same reason, the transmission mode demands a very careful control of penetrant pressure (and temperature) within the diffusion chamber for a correct background compensation. Luckily, the performances of a diffusion chamber in terms of stability and time to achieve steady conditions, can be monitored photometrically with great accuracy. It has been demonstrated that a well conditioned apparatus is able to reach constant pressure in less than 20 s and that, after this transient, the baseline is very consistent, which allows a reliable monitoring of sorption kinetics in the time scale of hundreds of seconds. This is the normally observed time range for sorption of water vapor in films of thickness from 20 to one hundred μm.

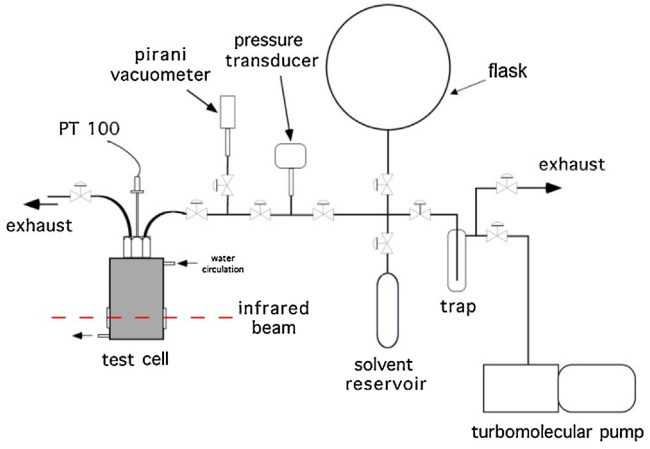

Fig. 8. Schematic representation of an experimental setup for sorption measurements of vapors in polymers by transmission FTIR spectroscopy. Reprinted with permission from [252]. Copyright 2001 Elsevier Ltd.

As an example, in Fig. 9A is reported the time evolution of the baseline (i.e., the single-beam spectrum collected at time t ratioed against the background collected at the end of the run) for a test in which the apparatus is filled with methanol vapor from zero to 6.7 Torr at 35 °C. At time zero (closed valve, green trace in Fig. 9A) the ν(CO) roto-vibrational band of methanol at 1033 cm^{-1} is negative, being the pressure inside the cell lower than the reference pressure. The transient period comprises six spectra collected every 3 s, after which the signal vanishes and a very consistent baseline is recorded for the rest of the run. (2 h long). The noise level at 1033 cm^{-1} is at 8×10^{-4} absorbance units (A.U.), essentially the same value recorded elsewhere (see the inset of Fig. 9A, where the red, blue and green traces were recorded at 21, 1800 and 7200 s). By increasing the test pressure, the time to reach steady conditions decreases further. Fig. 9B displays a typical sorption test by transmission FTIR, of methanol vapor in an amorphous polyimide at a relative pressure, p/p_0, of 0.3 (i.e. 69.95 Torr). In the inset, the data collected at various p/p_0, values are reported in a Fick's diagram [253].

To measure the diffusion of gases, a slightly different set-up has been proposed [254,255], whose schematic diagram is represented in Fig. 10.

In this case, the accessible temperature range was extended to -180 ÷ +350 °C and pressure control was achieved dynamically by a mass-flow controller/pressure-valve system. Provision was made for monitoring the diffusion of gas mixtures (two mass-flow controllers connected in parallel) taking advantage of the spectroscopic contrast among the mixture components. This setup performed comparably to the static diffusion cell in terms of baseline stability but the time to reach constant pressure was higher (100–120 s, depending on the p value), which limits the detection of very fast sorption kinetics. As an example of the diffusion measurement performed with the apparatus of Fig. 10, a sorption/desorption cycle of CO_2 in a commercial polyetherimide is represented in Fig. 11.

3.4.4. The advent of Raman spectroscopy

Raman spectroscopy plays an important role for investigating sorption processes, but has a main drawback in comparison to IR, which is related to its reduced sensitivity. This problem is a direct consequence of the inelastic character of the Raman process, whereby out of a population of 10^6 photons that are scattered elastically (Rayleigh radiation) only one is scattered inelastically. Thus, the Raman cross-section of most analytes is low, and the limits of detection relatively high. For example, CO_2 absorbed in solid/liquid matrices displays a significant IR cross-section (1200 L mol^{-1} cm^{-1} [256]) which makes it readily detectable down to $1{\cdot}10^{-3}$ wt % levels. Conversely, the reduced Raman cross-section renders

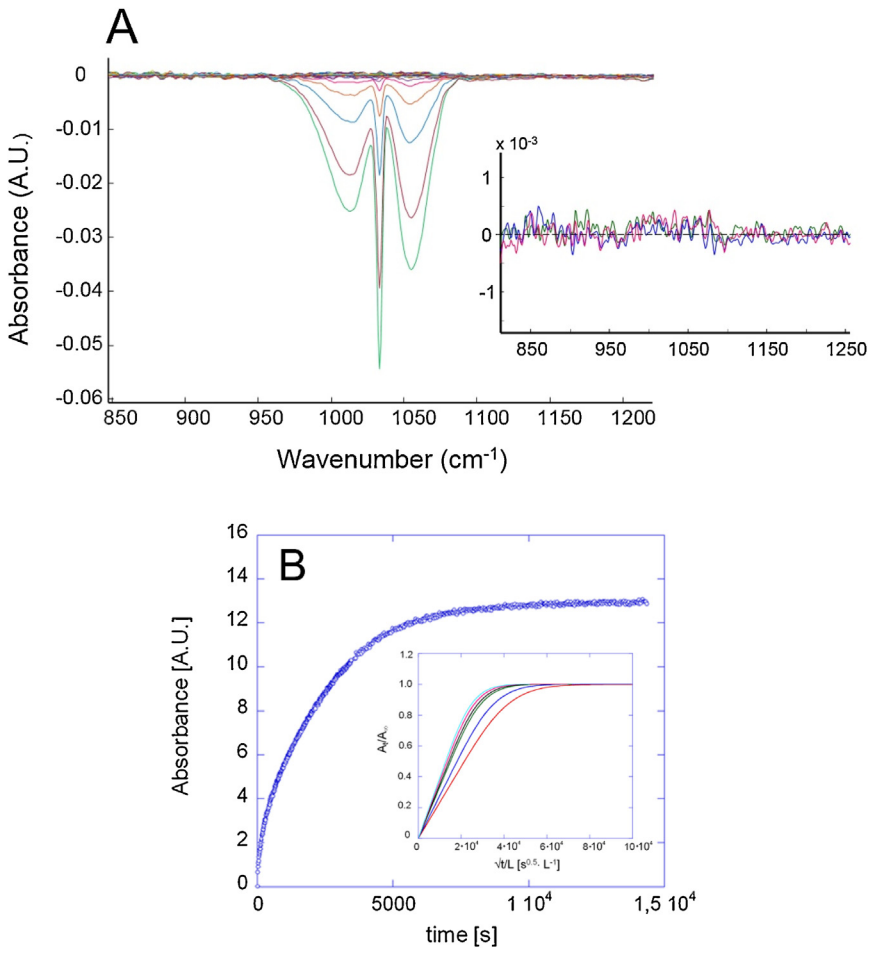

Fig. 9. (A): *Time-resolved* spectra collected in two hours interval to test the baseline stability of the diffusion cell. (B): Monitoring of the sorption of methanol vapor in an amorphous polyimide by transmission FTIR. The inset represents the Fick's diagrams at different p/p_0 values (from the curve with the lower slope to the curve with the higher slope $p/p_0 = 0.1, 0.2, 0.3, 0.4, 0.5, 0.6$).

CO_2 essentially undetectable up to values around 0.5 wt % [257] and allows the usage of the Raman technique only when the amount of absorbed penetrant is large, such as, on exposure to supercritical conditions [258]. The issue of poor sensitivity is partially alleviated in case of analytes exhibiting exceptional Raman activity, such as dyes or fluorescent molecules (which, in turn, may show adverse interfering effects) or when resonance mechanisms may contribute to enhance the spontaneous

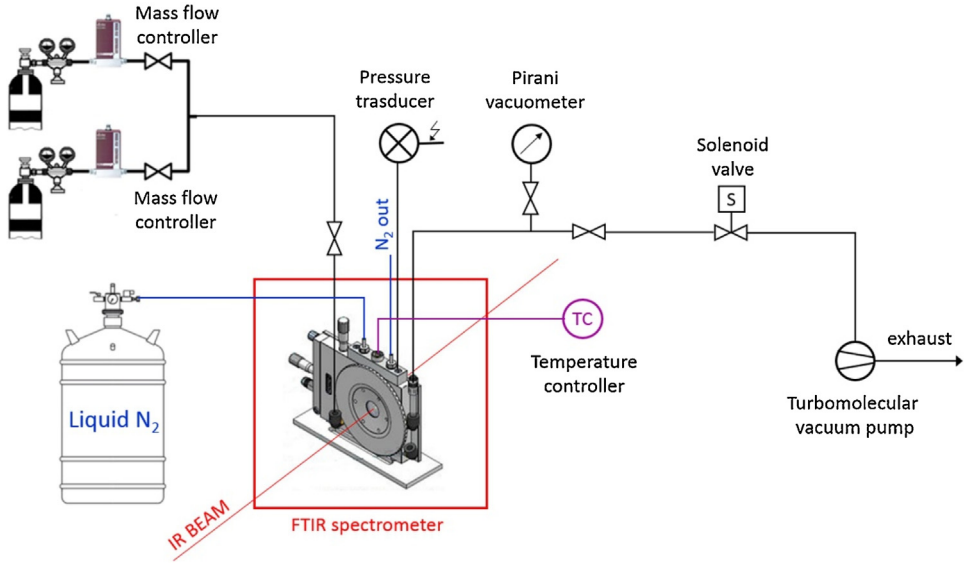

Fig. 10. Schematic representation of an experimental setup for diffusion of gases in polymers by transmission FTIR spectroscopy. Reprinted with permission from [255]. Copyright 2018 Elsevier B.V.

Please cite this article in press as: G. Mensitieri, G. Scherillo, C. Panayiotou et al. Towards a predictive thermodynamic description of Fsorption processes in polymers: The synergy between theoretical EoS models and vibrational spectroscopy. Mater. Sci. Eng. R (2020), https://doi.org/10.1016/j.mser.2019.100525

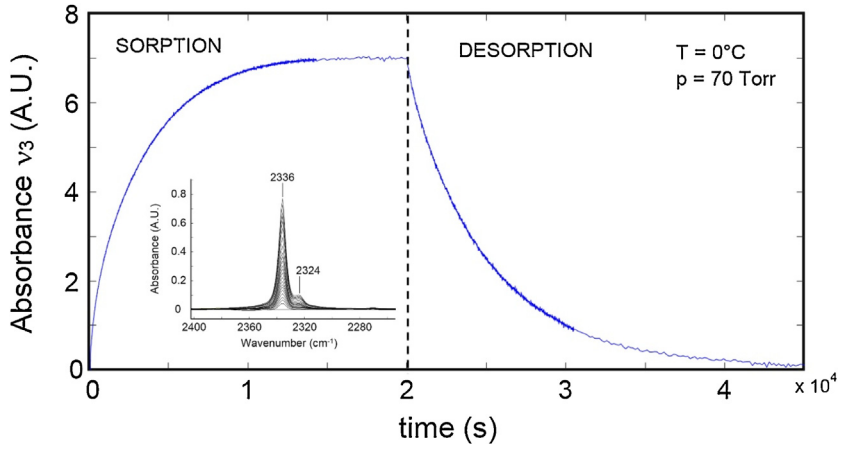

Fig. 11. Monitoring of CO_2 sorption in a commercial polyetherimide (Ultem 1000®) by transmission FTIR. Test performed at T = 0 °C and p = 70 Torr. The inset displays the analytical signal (O=C=O antisymmetric stretching, ν_3) at increasing sorption times.

emission. This is why the study of the diffusion of dyes in films and fibers by Raman approaches has been an active research area in the last two decades. In particular, the investigators took advantage of the capability of contemporary Raman instrumentation (Confocal Raman Microscopes, CRM) of reconstructing a chemical image of the sample by use of the spectroscopic contrast among the components, with a spatial resolution of 1 × 1 μm in the *x-y* plane and of around 2 μm along the *z* dimension. This experimental approach allows the measurement of the concentration gradients developing in a diffusion process, a relevant information that is not straightforward to obtain. Fleming and co-workers [259] measured and modelled the diffusion of the dye Disperse Red 1 (DR1) in a PET film subjected to supercritical CO_2. The concentration profiles of the dye were monitored by confocal Raman microscopy and the effect of the diffraction distortion was minimized by adopting an oil-immersion objective. The authors were able to reconstruct the gradients across the thickness dimension for 230 μm thick slabs and demonstrated the possibility of evaluating diffusion coefficients of DR1 directly from CRM data ($D = 6.75 \pm 1.01 \cdot 10^{-14}\ m^2\ s^{-1}$ at 200 bar and 80 °C). Successful modelling of the data set was achieved by a *Fickian* diffusion mechanism. The authors stressed the non-destructive character of the approach, as opposed to the conventional mechanical sectioning (slicing) procedure, which may alter the polymer morphology and/or the distribution of the diffusant in the matrix.

An analogous approach was applied to PET fibers: the Disperse Yellow 23 dye was incorporated in the fiber by supercritical CO_2 processing. Sizable dye-concentration gradients were detected along the line normal to the fiber surface, which were monitored as a function of dyeing time. The diffusion coefficient evaluated from the CRM data compared favorably with those from literature. It was found that the *z*-scanning mode provided reliable results up do a depth of 45 μm from the fiber surface. The study demonstrated the capability of the technique to monitor concurrently and correlate the dye distribution and the morphological features of the fiber matrix, which represents a significant advantage for the characterization of dyed fibers. It is to be mentioned that in these early studies the measurements were performed off-line, due to the difficulties in coupling the high pressure environment to the microscopic setting. Later on, recognizing the potential of the Raman approach, numerous investigators developed *in-situ* experiments, which were very helpful for a better understanding of a variety of high temperature and high pressure processes, in particular the supercritical CO_2 processing of polymers. The principal results of these endeavors have been recently summarized in a comprehensive review article to which the interested reader is referred [258].

3.4.5. Tools for data analysis

3.4.5.1. Difference spectroscopy and least squares curve fitting. It often occurs that the analytical bandshape is complex and poorly resolved. This effect originates from two concurrent factors: i) the molecular interactions of the probe with the polymer substrate and/or with itself; ii) the occurrence of interfering signals from the polymer substrate in the analytical range.

The first issue is especially severe with H-bonding interactions. In fact, in the ν(OH) range, the signal relative to the proton donor undergoes a downward shift (*red-shift*) by an amount proportional to the interaction strength and a marked increase in intensity, also related to the H-bonding energy. Furthermore, due to the distribution of geometries and force constants that occurs in a supramolecular aggregate, the ν(OH) band broadens considerably in comparison to the signal produced by an isolated molecule. Typically, the FWHH of a H-bonded ν(OH) mode increases by a factor between 5 and 10 with respect to the signal produced by a "free" OH group. Another complication arising for one of the most investigated probes, H_2O, is the mechanical coupling of the two stretching modes, which produces two signals (antisymmetric at higher frequency, symmetric at lower). Thus, the number of active modes in the analytical range is doubled with respect – for example – to an alcohol or a tertiary amine.

As for the second issue, the ν(OH)/ν(NH) range, which is where the most useful signals for monitoring concentration and molecular interactions of H-bonding probes are located, is crowded if the polymer also possesses these functionalities (polyamides, polyols), but is otherwise relatively free from interference. A notable exception is represented by polymers with carbonyl groups (polyesters, polyimides) which exhibit a well resolved peak at around 3450 cm^{-1}, originating from a non-fundamental vibration [1st overtone of the νC=O) for polyesters or a combination ν_{as}(C=O) + ν_s(C=O) for polyimides]. The main approach to eliminate the interfering signal of the substrate is difference spectroscopy (DS). The method relies on the Beer-Lambert relationship (Eq. (178)) and on the absorbance additivity:

$$A_{tot}(\nu) = \sum_{i=1}^{n} A_i(\nu) \tag{200}$$

In the case of a two-component system, Eq. (200) reduces to $A_s(\nu) = A_1(\nu) + A_2(\nu)$ and, if the sample spectrum, A_s ,displays a frequency interval where the component *1* does not contribute, $A_s(\nu) = A_2(\nu)$ for ν comprised in that range. When the spectrum of the component *2*, A_{ref}, is experimentally accessible, we may use it to digitally subtract the contribution of *2* from the sample

spectrum until the above frequency range is reduced to zero (to the baseline). In doing so, the contribution of *2* is eliminated in the whole spectrum range. This process is accomplished by iteratively changing a subtraction factor k, according to:

$$A_D(\nu) = A_s(\nu) - kA_{ref}(\nu) = 0 \tag{201}$$

Combining Eqs. (178) and (201) the meaning of the k factor is apparent:

$$k = \frac{A_s(\nu)}{A_{ref}(\nu)} = \frac{C_2}{C_{ref}}\frac{L_s}{L_{ref}} = \frac{C_2}{\rho_2}\frac{L_s}{L_{ref}} \tag{202}$$

where ρ_2 is the density of component *2* and C_2 is its concentration in the system expressed in the same units as ρ_2. L_s and L_{ref} are the thicknesses of the films used to collect the sample spectrum and the reference spectrum, respectively. Sorption/desorption of a penetrant in a polymer substrate is a special case of two-component systems. Here the component *1* is the penetrant and the component *2* (the one whose FTIR spectrum is experimentally available) is the so called *dry sample*, i.e. the film after the drying protocol. The difference spectrum is representative of the sorbed penetrant and is obtained according to Eq. (201). If the uptake is very limited ($1 \div 2$ wt %) and the swelling is negligible, $C_2 \cong \rho_2$; $L_s \cong L_{ref}$, and, from Eq. (202), $k = 1$. Thus, in the above conditions, the starting spectrum can be directly subtracted from the entire set of spectra collected during a sorption/desorption run. Conversely, in case of density (and hence, thickness) changes, the k value becomes time-dependent and is to be evaluated point-by-point either manually or by suitable regression algorithms. It should be noted that, in the latter case the FTIR experiment will allow - in ideal conditions - to carefully monitor both the swelling (through the k values) and the sorption processes. From the above discussion it follows that the essential requirement for a successful application of DS is a reliable reference spectrum. The *dry sample* may or may not belong to this category, depending on whether or not the penetrant induces significant perturbations to the vibrational response of the substrate. The perturbation is never zero but, in many instances, it can be tolerated. Fig. 12A,B displays the absorbance and the difference spectra in the ν(OH) range (3900–3200 cm^{-1}) of a commercial polyetherimide equilibrated at different water vapor activities [260]. In this interval the substrate exhibits a sharp peak at 3485 cm^{-1} which is the already mentioned ν_{as}(C=O) + ν_s(C=O) combination mode, plus other minor features. DS is effective in isolating the penetrant spectrum but induces an artifact in the form of an apparent maximum at 3475 cm^{-1}, highlighted in Fig. 12B. This feature can be (and has been) confused with an unresolved peak, but is actually a derivative-type profile (i.e., a two-lobe profile, approximately symmetric, with a minimum below the baseline, and a maximum above). The effect is typically observed in DS when a peak in the sample spectrum is shifted with respect to the reference spectrum. A *red-shift* (i.e., towards lower wavenumbers) produces a profile where the minimum precedes the maximum; the sequence is inverted for a *blue-shift*. In the case of the polyetherimide the effect is generated by the shift of the combination peak in the *wet-sample* with respect to the reference position (in the dry sample), which in turn, is a consequence of the H-bonding interactions established between the carbonyl groups and the water molecules. The effect is therefore due to the perturbation brought about by the penetrant; it is subtle in comparison to the overall signal and, once it has been recognized as an artifact, can be safely ignored in the subsequent data analysis (vide infra). In other cases, when the penetrant uptake is larger and more interactions are formed, severe distortion of the analytical band-shape may occur, which can complicate or even prevent full resolution of the components.

When proton donors like OH or NH are present in the polymer substrate, a 3D network is formed by self-association of these units. This is the typical situation in polyamides, polyols or epoxy resins. The above networks produce strong signaling in the ν(OH)/ν(NH) range, in the form of broad bands with complicated and asymmetrical shapes. These profiles reflect the H-bonding equilibrium and, in particular, the length of the H-bonding chains, which affects both the position and the breadth of the resulting signals. If the self-association equilibrium is perturbed (by rising the temperature, for instance) the band-shape changes to a significant extent. The ν(OH) spectrum of a penetrant like water occurs in the same region as the spectrum of the H-bonding network of the substrate and it would require difference spectroscopy to be isolated. However, an H-bonding penetrant may perturb the self-association equilibrium of the substrate with the consequence of modifying substantially its ν(OH)/ν(NH) bandshape. In these situations, the *dry spectrum* is no longer a valid reference to be subtracted from the *wet spectrum*, and this is clearly reflected in the appearance of distorted and/or poorly defined profiles in the DS spectra.

To illustrate the above argument, in Fig. 13, red trace, is reported the spectrum of a fully dried film of a commercial polybenzimidazole (Celazole® S26). The purple trace in the same figure refers to the spectrum of the same film equilibrated at a water vapor activity of 0.5, containing 12.0 wt % of penetrant, while the blue trace is the difference spectrum (*wet-sample* – *dry-sample*) [261]. The DS trace has a distorted profile with a sequence of maxima and minima that is not representative of the true penetrant spectrum but is produced by the shift/widening of the unresolved components of the substrate spectrum after penetrant uptake.

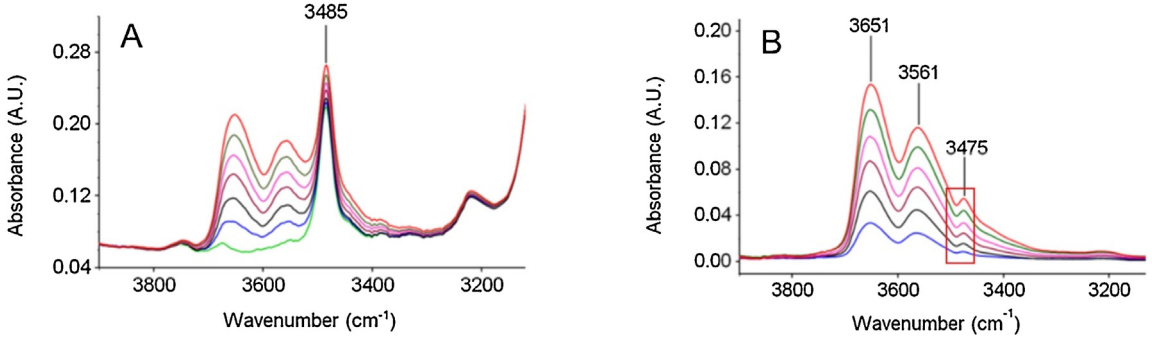

Fig. 12. Absorbance (A) and difference (B) spectra of a commercial polyetherimide (Ultem 1000®) film 37.7 μm thick equilibrated at different relative pressures of water vapor. Traces in (B) represent the spectra of H_2O sorbed in the polymer. Green trace, dry film; blue, $p/p_0 = 0.1$; black, $p/p_0 = 0.2$; dark red, $p/p_0 = 0.3$; magenta, $p/p_0 = 0.4$; dark green, $p/p_0 = 0.5$; red, $p/p_0 = 0.6$. Reprinted with permission from [260]. Copyright 2017 American Chemical Society. (For interpretation of the references to colour in this figure legend, the reader is referred to the web version of this article.)

Please cite this article in press as: G. Mensitieri, G. Scherillo, C. Panayiotou et al. Towards a predictive thermodynamic description of Fsorption processes in polymers: The synergy between theoretical EoS models and vibrational spectroscopy. Mater. Sci. Eng. R (2020), https://doi.org/10.1016/j.mser.2019.100525

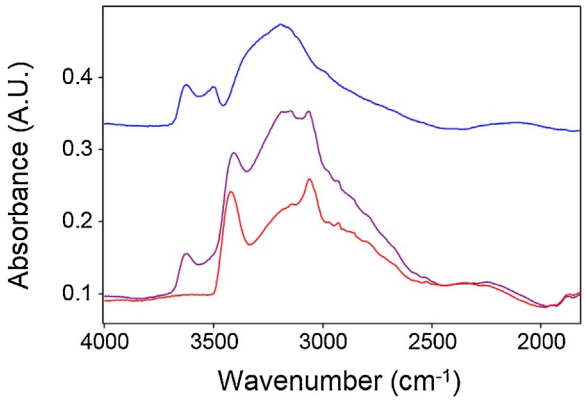

Fig. 13. Red trace; FTIR spectrum in the 4000 – 1900 cm^{-1} range of a thin film (10.8 μm) of a commercial polybenzimidazole (Celazole® S26). The film was fully dried under vacuum at 150 °C [261]. Purple trace: Spectrum of the same film equilibrated at a water vapor activity of 0.5 (H_2O uptake = 12.0 wt %). Blue trace: Difference spectrum *wet-sample – dry-sample*. Red and purple traces are represented in their actual absorbance scale. The difference spectrum is arbitrarily offset along the Y axis to facilitate the comparison. Reprinted with permission from [261]. Copyright 2018 American Chemical Society. (For interpretation of the references to colour in this figure legend, the reader is referred to the web version of this article.)

This is an extreme case in which a conspicuous uptake coupled with a significant perturbation of the polymer spectrum makes the DS tool inappropriate.

DS can be used for purposes other than that of removing the interference of the polymer substrate. When a well-resolved peak of the substrate can be identified whose position is significantly altered by molecular interactions with the penetrant (a typical example is the carbonyl stretching vibration(s) of polyesters or polyimides) this shift-effect can be used to estimate the population of interacting groups. The approach, originally developed by Maréchal [262], was successfully employed in a number of polymer systems with H_2O or methanol as penetrants [260,263,264]. It relies on the circumstance that the observed shift is, in fact, due to the presence of two unresolved components: one originates from the interacting carbonyls and is accordingly located at lower frequency. Its intensity is usually weak in comparison to the main band. The second component arises from the 'free' carbonyls, which absorb at higher frequency. The latter represents the main contribution to the overall signal intensity. The separation between the two components, $\Delta\nu$, is directly proportional to the H-bonding strength. Generally, with penetrants like water or alcohols the resolution is not achieved, nor a clear shoulder is discernible on the right-side of the νC=O peak. This is because the FWHH of the two components is lower than or comparable to $\Delta\nu$. The reference spectrum for DS is experimentally available, being coincident with the νC=O) peak in the fully dried polymer, which can be subtracted out from the *wet-spectrum* to isolate the contribution of interacting carbonyls. The critical point of this procedure is to identify a criterion to correctly evaluate the subtraction factor k, which has now a different meaning than before. A viable criterion is to reduce as much as possible the experimental profile to a horizontal baseline drawn in the high frequency side of the band. When the DS spectrum crosses the baseline producing a negative lobe, oversubtraction has occurred and the k value has gone beyond its true value. An application of the method is illustrated in Fig. 14, relative to a polyimide film containing 2.54 wt % of water [263].

The physical meaning of k is derived from the relationship:

$$A_D = A_s - A_{ref} = L_s\left(\varepsilon_f C_f + \varepsilon_b C_b - k\varepsilon_f C_{tot}\right) \quad (203)$$

where the subscripts f and s refer, respectively, to 'free' and H-bonded carbonyls and C_{tot} is the total (volumetric) concentration of carbonyls in the sample.

In the hypothesis of thickness invariance, the subtraction condition reads:

$$L_s\left(C_f - kC_{tot}\right) = 0 \quad (204)$$

from which

$$k = \frac{C_f}{C_{tot}} \text{ or } \frac{C_b}{C_{tot}} = 1 - k \quad (205)$$

It is noted that the fraction of bound carbonyls is directly accessed via the k value, without prior knowledge of the $\varepsilon_f/\varepsilon_b$ ratio, which is generally $\neq 1$. The fraction of interacting carbonyls represents a relevant information that can be compared with the concentration of H-bonded penetrant evaluated independently

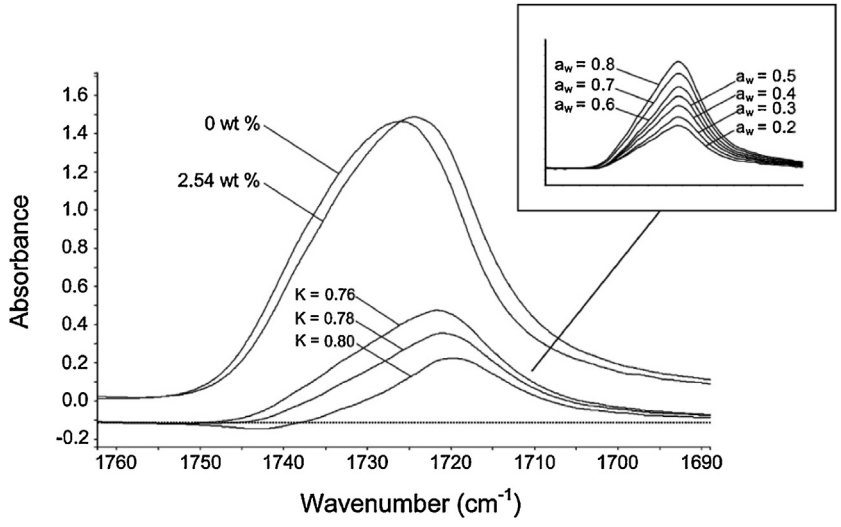

Fig. 14. Difference Spectroscopy on the carbonyl band [ν_{as}C=O)] of a polyimide film containing 2.54 wt % of absorbed water. The figure displays the experimental spectra of the dry and the wet sample (denoted, respectively 0 wt % and 2.54 wt %) and the DS spectra obtained with three values of the k factor, as indicated. Over-subtraction for $k = 0.80$ is apparent in the form of a negative lobe on the left side of the band. The inset displays the difference spectra obtained by the method described in the text for the film equilibrated at the indicated values of water vapor activity (a_w). Reprinted with permission from [263]. Copyright 2007 American Chemical Society.

Please cite this article in press as: G. Mensitieri, G. Scherillo, C. Panayiotou et al. Towards a predictive thermodynamic description of Fsorption processes in polymers: The synergy between theoretical EoS models and vibrational spectroscopy. Mater. Sci. Eng. R (2020), https://doi.org/10.1016/j.mser.2019.100525

from the spectrum in the ν(OH) range to verify the proposed structures of the supramolecular aggregates [260]. The band-shape of proton-donor penetrants like water or methanol as isolated by DS is still complex: it comprises several components more or less resolved depending on the system under scrutiny. Examples of these profiles, relative to water sorbed in a polyester [poly(L-lactic acid), PLLA] and in the polyetherimide Ultem 1000® are reported in Fig. 15A and B, respectively.

Full resolution of the components, which allows one to fully characterize the system at the molecular level, is achieved by application of Least-squares curve fitting (LSCF) methods. The level of confidence of the LSCF results - often questioned - critically depends on the complexity of the bandshape and on partial resolution features like shoulders or slope changes in the experimental profile. It is very useful the synergic use of the results of other resolution-enhancement approaches like 2nd derivative analysis, Fourier self-deconvolution and two-dimensional correlation spectroscopy [266]. The spectra represented in Fig. 15 do not raise specific issues: two out of three components display well defined maxima, while the third can be suitably simulated by a symmetrical bandshape (gaussian). The regression results simulate accurately the experimental data and the LSCF parameters – shape function, FWHH, position – are very consistent within the dataset of any specific system. As evidenced in Fig. 15, the FWHH and the shape-function parameters relative to a specific probe in different polymer substrates also compare favorably. Differences are noted in the position of the components and in the relative intensity of the band at the lowest frequency. As will be discussed in the forthcoming paragraph, the former is a mean-field effect related to the dielectric constant of the medium, while the latter is due to the degree of probe self-association. It has been demonstrated [253,260,263,264] that a proper choice of the shape function is critical for achieving an optimum simulation of the experimental profiles. For H_2O the mixed Gauss-Lorentz model has been used extensively:

$$f(x) = (1 - Lr)Hexp\left[-\left(\frac{x - x_0}{FWHH}\right)^2 4ln2\right] + Lr\frac{H}{4\cdot\left(\frac{x-x_0}{FWHH}\right)^2 + 1} \qquad (206)$$

where x_0 is the peak position, H the peak height and Lr is the fraction of Lorentz character. In several systems it was found that the low-frequency component invariably converges toward a purely gaussian bandshape (i.e., $Lr = 0$), while the intermediate component retains a significant Lorentz character. The high-frequency peak often displays an asymmetrical shape, which makes symmetric functions, as Eq. (206), unsuitable. This effect occurs because, as it will be discussed later, the peak is actually an unresolved doublet. These situations were handled by use of asymmetrical shape-functions as the log-normal model [253,260]:

$$f(x) = H\cdot exp\left\{-\frac{ln2}{(ln\rho)^2}\cdot ln^2\left[\frac{(x - x_0)\cdot(\rho^2 - 1)}{FWHH}\right] + 1\right\} \qquad (207)$$

where ρ is the asymmetry index, i.e., the ratio between left and right half-widths. Considerable improvements in the simulation were achieved by use of this alternative function for the high-frequency component.

Having resolved the band-shape components, one is in the position of converting their intensities into absolute concentration values of the different species that were spectroscopically identified. To this end it is necessary to evaluate the molar absorptivities, ε_i, of each species since, as already noted, ε_i's are very sensitive to the chemical environment. This is a non trivial task and is accomplished by coupling spectroscopic and gravimetric data collected in closely matching conditions. An illustration of the adopted approach for the system H_2O/PLLA (see Fig. 15A) is reported below [265]. Two district water species were identified: i) isolated molecules bound to PLLA carbonyls, commonly referred to in the literature as *first shell* water and ii) molecules self-interacting with the above species forming dimers, *second shell* water. This nomenclature is generally adopted when dealing with sorbed H-bonding probes absorbed in macromolecular systems [267]. The molar absorptivities of the two species were denoted, respectively, ε_{bc} (for *bound to carbonyls*) and ε_{sa} (for *self-associated*). Coupling the Beer-Lambert expression for the total concentration of sorbed water with the mass-balance relationship, one obtains:

$$C_{tot} = \frac{A_{bc}}{\varepsilon_{bc}L} + \frac{A_{sa}}{\varepsilon_{sa}L} \qquad (208)$$

$$C_{tot} = C_{bc} + C_{sa} \qquad (209)$$

$$\frac{A_{bc}}{C_{tot}} = \varepsilon_{bc}L - \frac{\varepsilon_{bc}}{\varepsilon_{sa}}\frac{A_{sa}}{C_{tot}} \qquad (210)$$

The C_{tot} values were taken from the gravimetric measurements as a function of p/p_0. The density of PLLA (1.240 g/cm^3), assumed invariant with H_2O sorption, was employed to convert gravimetric weight ratios into volumetric concentration values. The components at 3575 and 3521 cm^{-1} were selected as analytical peaks for the *bc* and the *sa* species, respectively, for reasons that will become apparent later. Eq. (210) predicts the linearity of the A_{bc}/C_{tot} vs A_{sa}/C_{tot} plot, with a negative slope equal to the molar absorptivities' ratio $\varepsilon_{bc}/\varepsilon_{sa}$ and intercept equal to $\varepsilon_{bc}\cdot L$. The experimental values exhibit the expected behaviour (see Fig. 16) and the

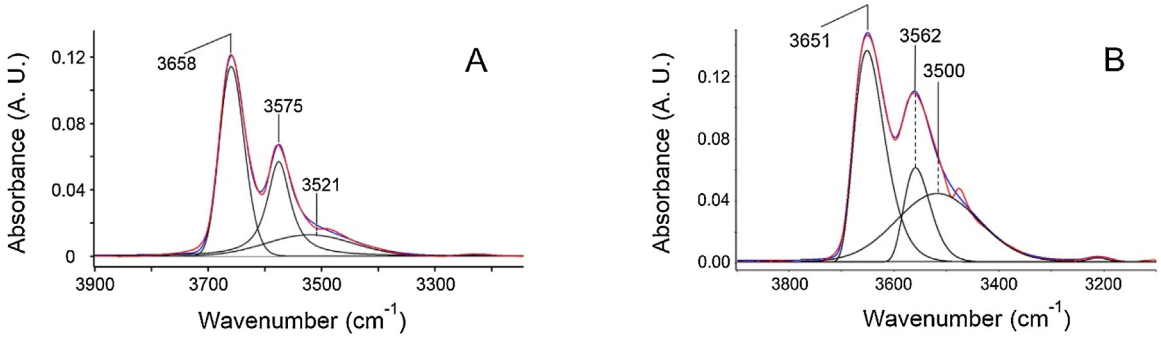

Fig. 15. Curve fitting analysis of the spectrum representative of water absorbed in PLLA (A) and in Ultem 1000® (B). The figures display the experimental profile (red trace), the best-fitting curve (blue trace), and the resolved components (black traces). The samples were equilibrated at $p/p_0 = 0.5$ for PLLA and at $p/p_0 = 0.6$ for Ultem 1000®. (For interpretation of the references to colour in this figure legend, the reader is referred to the web version of this article.)

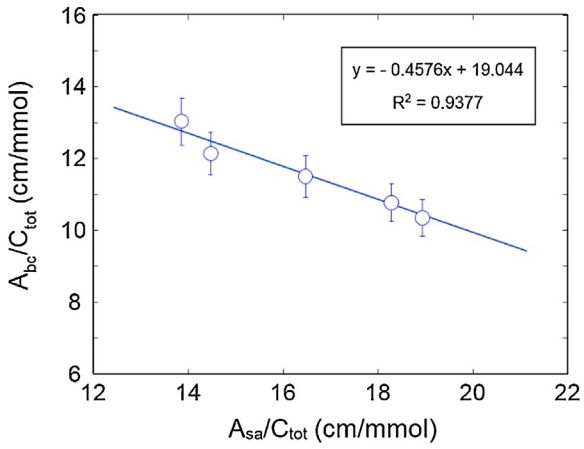

Fig. 16. Plot of A_{bc}/C_{tot} as a function of A_{sa}/C_{tot} for the system H_2O/PLLA.

absorptivity values calculated therefrom were ε_{bc} = 41.3 km/mol and ε_{sa} = 90.2 km/mol. These values compare favourably with those obtained for other systems with H_2O as penetrant [H_2O/Poly(ε-caprolactone): PCL, ε_{bc} = 72.2 km/mol and ε_{sa} = 98.2 km/mol; H_2O/polyetherimide: ε_{bc} = 34.5 km/mol and ε_{sa} = 89.7 km/mol] [260].

3.4.5.2. Two-dimensional correlation spectroscopy. A recently developed approach to improve the resolution of complex bandshapes, which has been demonstrated to be especially effective for H-bonding systems, is Two-dimensional correlation spectroscopy (2D-COS). This technique provides significant resolution enhancements and valuable information about the dynamics of the system. It is a perturbative method that relies on imposing an external stimulus to a system initially at equilibrium. A correlation analysis is then performed on the spectral response of the system, by measuring the covariance of two signals (peaks' absorbance, in the present case) as a function of a third common variable related to the perturbing function (time, in the present case). In view of the relevance assumed by 2D-COS in the spectroscopic analysis of diffusion processes, a brief summary of its principles is given [268]. A time-dependent spectral intensity $y(\nu, t)$ observed for a period $T = T_{max} - T_{min}$ produces a *dynamic spectrum* $\sim y(\nu, t)$, defined as:

$$\sim y(\nu, t) = \begin{cases} y(\nu,t) - \bar{y}(\nu) for\, T_{min} \le t \le T_{max} \\ 0\, otherwise \end{cases} \quad (211)$$

In Eq. (211) $\bar{y}(\nu)$ represents the reference spectrum, which is intended to eliminate the static component of the signal. It can be chosen in different ways depending on the specific response function. For non-periodic functions, the two most convenient choices are the *static* or *time-averaged* spectrum, defined as:

$$\bar{y}(\nu) = \frac{1}{T}\int_0^T y(\nu, t)dt \quad (212)$$

or the *ground-state spectrum,* well before the application of the stimulus (at $t \ll 0$). The complex cross-correlation function between dynamic spectral intensities at wavenumbers ν_1 and ν_2, which represents the basic formula of 2D-COS analysis is given by Eq. (213):

$$\Phi(\nu_1, \nu_2) + i\Psi(\nu_1, \nu_2) = \frac{1}{\pi T}\int_0^\infty \sim Y(\nu_1, \omega) \sim Y^*(\nu_2, \omega)d\omega \quad (213)$$

where $\Phi(\nu_1, \nu_2)$ and $\Psi(\nu_1, \nu_2)$ are the synchronous and the asynchronous 2D spectra, respectively, $\sim Y(\nu_1, \omega)$ is the forward Fourier transform (FT) of the dynamic spectrum at ν_1 and $\sim Y^*(\nu_2, \omega)$ is the conjugate FT of $\sim y(\nu_2, t)$, i.e.,

$$\sim Y(\nu_1, \omega) = \int_{-\infty}^{+\infty} \sim y(\nu_1, t)e^{-i\omega t}dt \quad (214)$$

$$\sim Y^*(\nu_2, \omega) = \int_{-\infty}^{+\infty} \sim y(\nu_2, t)e^{i\omega t}dt \quad (215)$$

In Eqs. (213–215) ω is the Fourier frequency, i.e. $1/t$, not to be confused with the spectral frequency ν. For a number of response functions the integrals in Eqs. (214–215) and their product in Eq. (213) can be solved in closed form. These analytically accessible functions include the exponential decay, one of the most common for chemically or physically evolving systems:

$$\sim y(\nu, t) = \begin{cases} \sim y(\nu, t) = A(\nu)\cdot e^{-k(\nu)t} for\, t \ge 0 \\ 0\, otherwise \end{cases} \quad (216)$$

To simplify the treatment, it is assumed that $T_{min} = 0$ and $T_{max} >> 1/k(\nu)$, which implies that the reference spectrum can be set to zero. In Eq. (216) $A(\nu)$ is the initial absorbance value and $k(\nu)$ is the rate constant for the peak at wavenumber ν. For two peaks at frequencies ν_1 and ν_2 having different values of A and k, Eq. (213) becomes:

$$\Phi(\nu_1, \nu_2) + i\Psi(\nu_1, \nu_2) = \frac{A(\nu_1)A(\nu_2)}{\pi t}\int_0^\infty \frac{k(\nu_1)k(\nu_2) + i[k(\nu_1) - k(\nu_2]\omega + \omega^2}{\left[k^2(\nu_1) + \omega^2\right]\left[k^2(\nu_2) + \omega^2\right]}d\omega \quad (217)$$

Solving the above integral, one obtains:

$$\Phi(\nu_1, \nu_2) = \frac{A(\nu_1)A(\nu_2)}{T}\frac{1}{k(\nu_1) + k(\nu_2)} \quad (218)$$

$$\Psi(\nu_1, \nu_2) = \frac{A(\nu_1)A(\nu_2)}{\pi T}\frac{\ln k(\nu_1) - \ln k(\nu_2)}{k(\nu_1) + k(\nu_2)} \quad (219)$$

If the values of the two decay constants are comparable, i.e. $k(\nu_1) \approx k(\nu_2)$, Eq. (219) further simplifies to:

$$\Psi(\nu_1, \nu_2) = \frac{2A(\nu_1)A(\nu_2)}{\pi T}\frac{k(\nu_1) - k(\nu_2)}{k(\nu_1) + k(\nu_2)} \quad (220)$$

From Eqs. (219–220) it emerges that, for exponential decay dynamics, asynchronicity means that two signals evolve with different rate constants. If the decay constants are equal, no asynchronous correlation develops, regardless of the initial intensities of the signals. This is a very useful feature for it improves the resolution of extensively overlapped peaks by decreasing the total number of components present in the frequency spectrum. A detailed discussion of this effect is reported in ref. [255]. The synchronous map has lower specificity since the resolution enhancement is only due to the spreading of the frequency data over a second wavenumber axis. This effect is often insufficient to separate the components in the profiles of strong H-bonding penetrants like water or methanol [253,263]. The cross-peaks at off-diagonal positions reflect any couple of signals evolving in time; the spectrum along the main diagonal (always positive) is the power or autocorrelation spectrum, which provides information on the signals more susceptible to the external perturbation. According to Eq. (218), the autopeaks, when fully resolved, may afford quantitative estimates of the decay constants.

Further information may be gathered from the sign of the cross-correlation peaks, which reveal dynamic relationships between two signals according to the so-called Noda rules [268,269]. Those

Please cite this article in press as: G. Mensitieri, G. Scherillo, C. Panayiotou et al. Towards a predictive thermodynamic description of Fsorption processes in polymers: The synergy between theoretical EoS models and vibrational spectroscopy. Mater. Sci. Eng. R (2020), https://doi.org/10.1016/j.mser.2019.100525

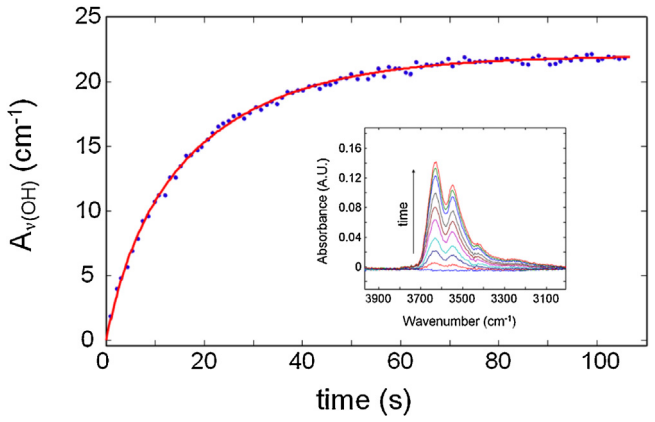

Fig. 17. Integrated absorbance (3720 – 3000 cm^{-1}) of the H_2O band as a function of time for a sorption experiment on the H_2O/PCL system at 30 °C and p/p_0 = 0.6. Solid dots are the experimental data; the continuous line is the regression of the data with a two component exponential of the same form as Eq. (219) (see text). The inset represents the time evolution of the analytical band. Reprinted with permission from [271]. Copyright 2014American Chemical Society.

of interest in the context of diffusion experiments are: i) In the synchronous spectrum the sign of a cross-peak is positive if the correlated signals change in the same direction (they both increase or decrease) and is negative otherwise. ii) In general, if an asynchronous cross-peak located at coordinates ν_1, ν_2 is positive, $\Psi(\nu_1, \nu_2) > 0$, the intensity change at ν_1 is accelerated with respect to the intensity change at ν_2. In the specific case of exponential decay kinetics, this means that $k(\nu_1) > k(\nu_2)$ [269,270]. If $\Psi(\nu_1, \nu_2) < 0$ the opposite relationship between the decay constants holds true. iii) The above relationship remains valid as long as $\Phi(\nu_1, \nu_2)$ is positive; otherwise, it is to be reversed.

It has been demonstrated that any linear transformation of the original response function leaves the sequential order unaltered [269]. This implies that normalization of the kinetic curves is immaterial and that the conclusions drawn for Eq. (216), can be extended to a response function of the type:

$$\sim y(\nu, t) = A(\nu)\left(1 - e^{-kt}\right) \tag{221}$$

which represents the long-term solution of the Fick's model (Eq. 196), expressed in terms of absorbance.

Finally, it is noted that the band-shape of the asynchronous peaks can also provide useful information: a correlation between two sharp components gives rise to a sharp peak, while a correlation between a sharp component and a much broader band results in an elongated shape. A conical feature is observed when the interacting signals are both broad.

As an example of the application of 2D-COS to a real system, in the following we discuss the analysis of the *time-resolved* data gathered during a sorption/desorption experiment on the system H_2O/PCL [271].

The integrated area of the ν(OH) band of sorbed water is reported in Fig. 17 as a function of sorption time. The process can be accurately described in terms of the Fick's equation (Eq. (194)), yielding a diffusion coefficient of $4.93 \cdot 10^{-7}$ cm^2/s, in good agreement with earlier literature values obtained gravimetrically [272]. Phenomenologically, the response function of the system is suitably simulated by a two-component exponential of the same form as Eq. (221) (see Fig. 17, continuous line) i.e.,

$$A(t) = A_1\left(1 - e^{-k_1 t}\right) + A_2\left(1 - e^{-k_2 t}\right) \tag{222}$$

Assuming the two components to be related to distinct species involved in the diffusion process, it is possible to interpret the 2D-COS results in terms of Eqs. (216–220). In Fig. 18A,B are reported, respectively, the synchronous and asynchronous maps obtained by the 2D-COS analysis of the absorbance spectra represented in the inset of Fig. 17.

The synchronous map shows the two components already resolved in the frequency spectra (3628, 3549 cm^{-1}), plus the relative correlations; thus, it does not provide any resolution enhancement. All the synchronous correlations are positive according to the growing trend of both signals. Better-defined features are present in the asynchronous spectrum: in the lower-side region with respect to the main diagonal four cross-correlations are identified (the upper-side features are redundant owing to the antisymmetric character of the asynchronous matrix). These occur at [3595–3635 cm^{-1} (-)], [3550–3595 cm^{-1} (+)], [3456–3635 cm^{-1} (–)], and [3465–3550 cm^{-1} (–)]. The correlation intensity goes to zero at 3635–3550 cm^{-1} and at 3615–3456 cm^{-1}. It is concluded that the four distinct components at 3635, 3595, 3550 and 3456 cm^{-1} are arranged pairwise: the two signals at 3635 and 3550 cm^{-1} evolve synchronously [$\Psi(\nu_1, \nu_2) = 0$] and at a different rate with respect to the doublet at 3595–3456 cm^{-1} which is also correlated synchronously. In particular, from to the sign of the cross-peaks, and according to the Noda rules, in the sorption experiment the doublet at 3635–3550 cm^{-1} grows faster than the doublet at 3595–3456 cm^{-1}. The above information is essential for a correct assignment of the resolved components,

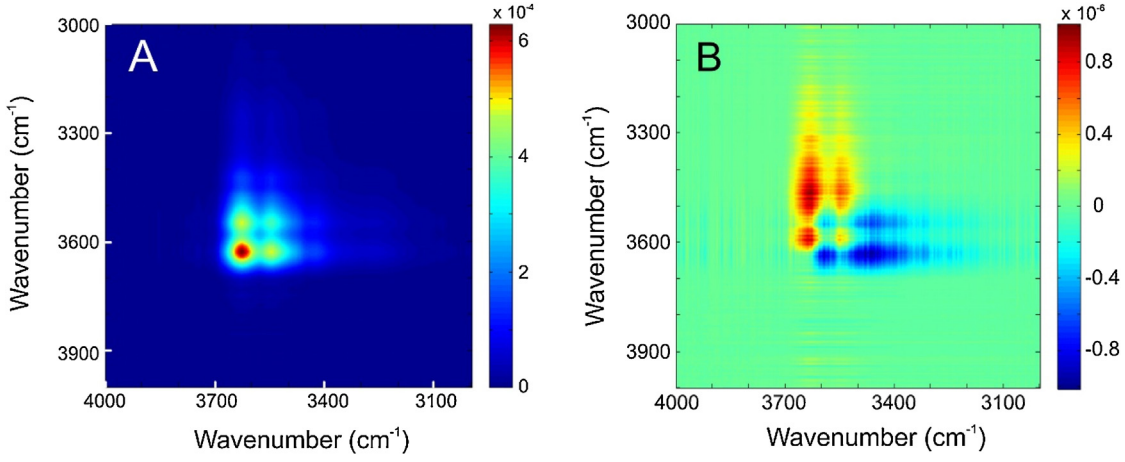

Fig. 18. Synchronous (A) and asynchronous map (B) obtained by 2D-COS analysis of the time-resolved spectra collected during the sorption experiment on the system H_2O/PCL at p/p_0 = 0.6 (sequence shown in the inset of Fig. 17). Reprinted with permission from [271]. Copyright 2014 American Chemical Society.

Please cite this article in press as: G. Mensitieri, G. Scherillo, C. Panayiotou et al. Towards a predictive thermodynamic description of Fsorption processes in polymers: The synergy between theoretical EoS models and vibrational spectroscopy. Mater. Sci. Eng. R (2020), https://doi.org/10.1016/j.mser.2019.100525

insofar as the synchronously correlated signals are likely generated by a single molecular species, while asynchronous correlation implies distinct species. The elongated shape of the cross-peaks at [3456–3635 cm^{-1} (–)] and [3465–3550 cm^{-1} (–)] indicate that the correlation occurs between a sharp signal (at 3635 and 3550 cm^{-1}) with a significantly broader band (at 3456 cm^{-1}). Conversely, the narrower cross-peaks at [3595–3635 cm^{-1} (–)] and [3550–3595 cm^{-1} (+)] reflect the correlation between two sharp components. The whole pattern can be interpreted in terms of two distinct water species, each producing two signals. This conclusion is sound when considering that that a single H_2O molecule produces two ν(OH) modes, (out-of-phase at higher frequency and in-phase at lower frequency). Of the four identified signals, three are sharp (the doublet at 3635–3550 cm^{-1} and the components at 3595 cm^{-1}), the fourth, at 3465 cm^{-1}, is broader. This suggests that the H_2O molecules producing the former doublet have two equivalent O—H bonds, i.e., these molecules retain the original C_{2V} symmetry. Conversely, the species producing the signals at 3595–3465 cm^{-1} has two hydrogens with a distinct chemical environment. In particular, the broad band can be associated with an O—H bond interacting with a proton-acceptor, while the sharp signal is due to a 'free' O––H. As we will discuss later, this doublet is characteristic of self-associated water in the form of dimers. Finally, we note that the asynchronous spectrum obtained in the desorption experiment is coincident with that of Fig. 18 in terms of overall pattern but the sign of all peaks is reversed. This implies that, on desorption, the doublet at 3595–3465 cm^{-1} evolves (decreases) faster than that at 3635–3550 cm^{-1}.

3.4.5.3. Quantum Chemistry methods as a tool for spectral interpretation. The assignment of the numerous components making up the penetrant spectrum and the interpretation of the effects induced on the substrate spectrum by molecularly interacting penetrants is a non-trivial task. One of the most powerful tools to tackle these problems is the *first principle* simulation of the vibrational spectra. By this approach, tentative structures of the supramolecular aggregates are optimized using appropriate model chemistries (mainly, Density Functional Theory, DFT, and second order Möeller-Plesset perturbation theory, MP2). Upon convergence to a meaningful stationary state, the theory provides the complete set of force constants plus the relevant geometric parameters. These are input in a classical Normal Coordinate Analysis (NCA) scheme as the F and G matrices (Wilson GF method), which produces the frequency, the form and the symmetry (if any) of the whole set of normal modes [209]. In addition, modern computational platforms often allow the estimation of infrared and Raman intensities, other relevant parameters for interpretative purposes [273,274]. Once an appropriate simulation of the experimental spectrum has been achieved, the analysis allows one to confirm the proposed structure of the supramolecular aggregate and to establish the vibrational origin of the observed IR/Raman signals. There are numerous issues along the way to get the final solution of the vibrational problem. These issues are to be taken in careful consideration; otherwise, computational approaches may produce meaningless or misleading results. First, the molecular model is to be chosen properly: it should be able to capture the structure (G matrix) and the electron density distribution (F matrix) of the system and, at the same time, remain of a manageable size. This is especially true when computationally intensive calculations such as infrared and/or Raman intensities are required. Thus, polymer chains are simulated by short segments capable of reproducing the chemical environment in terms of interaction sites and steric hindrance around them. Furthermore, molecular models containing aliphatic chains and multiple conformational degrees of freedom, such as aliphatic esters or amides, are known to exhibit shallow Potential Energy Surfaces (PES) [275,276]. A preliminary PES exploration to identify relevant stationary state(s) is a fundamental step in the structure-optimization strategy because any *ab-initio* method will invariably localize the minimum that is closer to the initial input geometry. Conformational searching is generally performed by Molecular Mechanics (MM) using algorithms based on the Metropolis-Montecarlo method. These maximize computational efficiency and afford PES searching of very complex structures in reasonable amounts of time. The stationary state(s) identified by MM represent the starting points for the *ab initio* optimization. The characterization of the relaxed geometry is even more critical when dealing with supramolecular aggregates: in this case, the two interacting units (the substructures) are not linked by a covalent bond with its strict directional and dimensional parameters but are connected by much weaker interactions, which are more difficult to simulate reliably. For instance, H-bonding is not explicitly implemented in several MM force fields. Recent strategies for starting-point setting rely on structural databases analysis [261]: the two substructures, relaxed at the chosen level of theory, are manually arranged so as to occupy the position of maximum likelihood occurrence of the molecular interaction under consideration. This arrangement is obtained by reference to specialized databases [277–279] that display the probability of occurrence and the spatial features of interactions between pairs of functional groups. The databases focus but are not limited to H-bonding interactions; they are composed by searching structural libraries as Protein Data Bank (PBD) and Cambridge Structural Database (CBS) for non-bonded interactions between a contact group (B) and a central group (A). The resulting scatterplot shows the experimentally observed distribution of B around A and provides information about the frequency and directionality of intermolecular contacts. As an example of the above approach, Fig. 19A displays the scatterplot relative to the central group imidazole interacting with the contact group H_2O, which has been employed to set the starting point geometry for the molecular model of the polybenzimidazole hydrate [261].

Fig. 19B is an alternative representation in terms of contour density surfaces, calculated by dividing the space around the central group into a grid and counting the number of contact atoms in each grid volume. The two interacting sites of the imidazole unit are readily recognized in Fig. 19B and the starting-point geometry for *ab-initio* optimization was obtained therefrom by positioning the two H_2O molecules in the red spots of the highlighted areas. Fig. 19C displays the resulting structure relaxed at the B3LYP/6-31 G(d) level of theory in which the two contact groups are localized within the area of maximum likelihood occurrence [261].

The QM/MM approach was employed to identify the molecular aggregates for the case of PCL interacting with two penetrants, namely H_2O and CO_2 [257,271]. The aliphatic ester pentyl hexanoate (PHEX) was selected to mimic the proton-acceptor/electron-rich groups on the polymer chain (C=O and C—O—C) and the steric hindrance in the proximity of these sites.

The structure of the supramolecular aggregate with water (H-bonding interaction), relaxed at the B3LYP/6-31 G(d) level of theory is reproduced in Fig. 20A. It was found that the calculated geometrical parameters of the donor/acceptor pair comply with the general H-bonding formation criteria. The out-of-phase and the in-phase ν(OH) modes of H_2O in Structure of Fig. 20A are shifted downward with respect to the isolated molecule by -41 and -63 cm^{-1} respectively, while the δ(HOH) vibration is shifted at higher frequency by +26 cm^{-1}. These effects are characteristic of water acting as proton donor and represent the signature for the occurrence of H-bonding. The experimentally observed frequencies compare well with those calculated and allowed an unambiguous assignment of the doublet observed at 3635 –

Please cite this article in press as: G. Mensitieri, G. Scherillo, C. Panayiotou et al. Towards a predictive thermodynamic description of Fsorption processes in polymers: The synergy between theoretical EoS models and vibrational spectroscopy. Mater. Sci. Eng. R (2020), https://doi.org/10.1016/j.mser.2019.100525

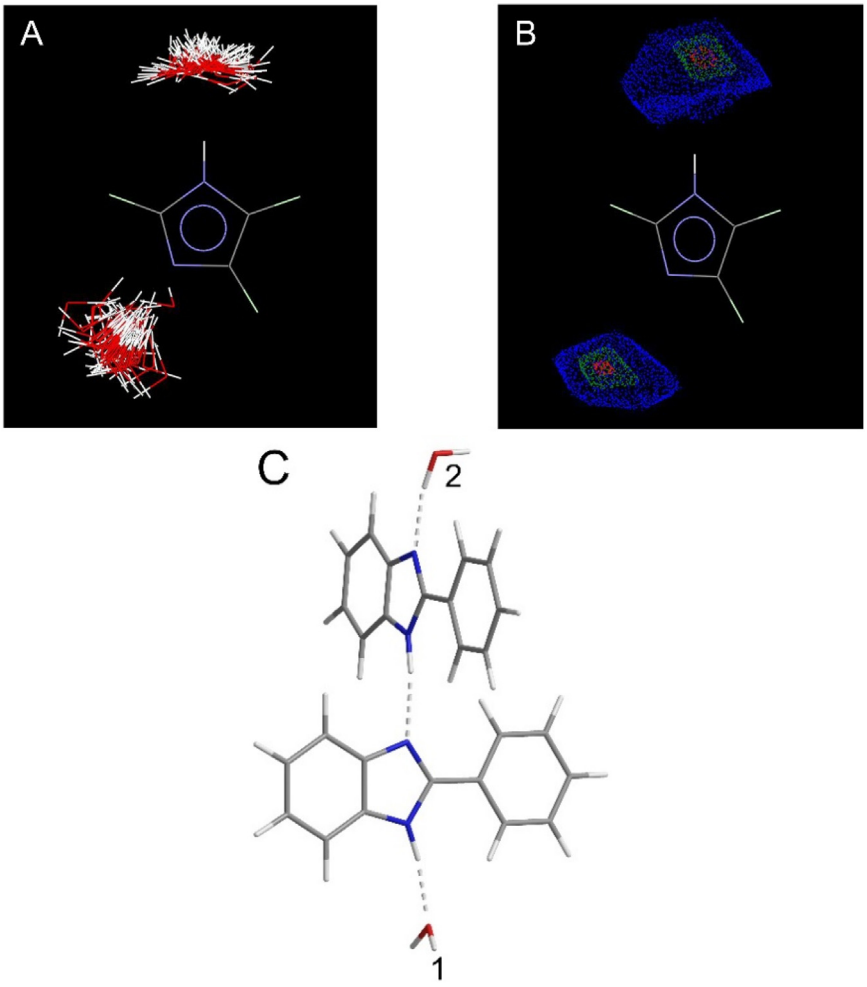

Fig. 19. Scatterplot (A) and density contour plot (B) for the central group imidazole interacting with the H_2O contact group. The density contour plot was employed to identify the position of the contact groups for the starting geometry of the supramolecular model of polybenzimidazole hydrate, whose optimized geometry is reproduced in (C). Reprinted with permission from [261]. Copyright 2018 American Chemical Society.

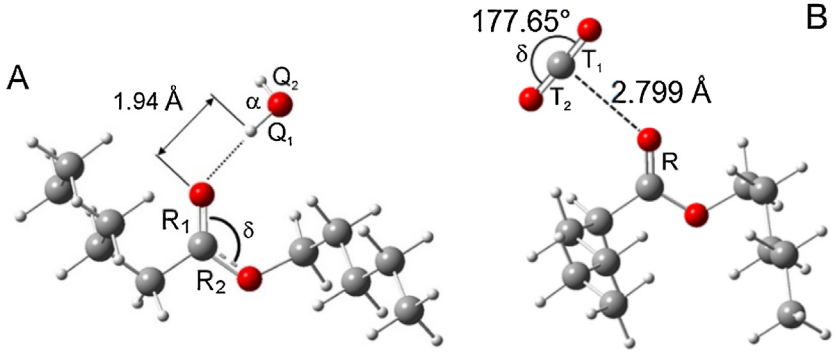

Fig. 20. (A): Optimized geometry of pentylhexanoate/H_2O H-bonding complex, a model for the H_2O/PCL system. Reproduced with permission from [271]. (B): Optimized geometry of pentylhexanoate/CO_2 complex, a model for the CO_2/PCL system. Atoms' color code: white =H; grey = C; red = O. Reprinteed with permission from [257]. Copyright 2016 American Chemical Society. (For interpretation of the references to colour in this figure legend, the reader is referred to the web version of this article.)

3550 cm^{-1} to the ν_{as}(OH) and ν_s(OH) modes of the water molecules H-bonded to the PCL carbonyls. On the basis of the QM/NCA results it was also possible to rule out the involvement of the ether-like oxygens in H-bonding with water [271].

To reproduce reliably the properties of the CO_2/PCL system, which involves weak interactions of the Lewis-acid/Lewis-base type (LA-LB), higher-level theories than DFT were required [280–282]. In particular, the MP2 /6-31(d) model chemistry was selected as a suitable compromise between accuracy and computational cost [257,283,284]. The QC/NC analysis confirmed LA–LB as the main interaction mechanism, but also highlighted the occurrence of weak H-bonds acting cooperatively to stabilize the supramolecular complex. The LA-LB contacts were identified almost exclusively on PCL carbonyls because of steric factors. The determined optimized

Please cite this article in press as: G. Mensitieri, G. Scherillo, C. Panayiotou et al. Towards a predictive thermodynamic description of Fsorption processes in polymers: The synergy between theoretical EoS models and vibrational spectroscopy. Mater. Sci. Eng. R (2020), https://doi.org/10.1016/j.mser.2019.100525

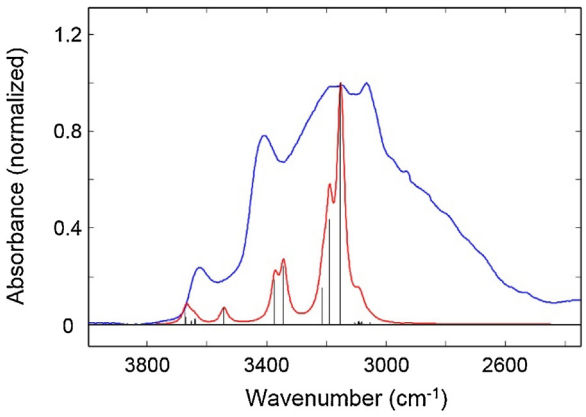

Fig. 21. Comparison between the experimental spectrum (blue trace) of PBI equilibrated at a water vapour activity of 0.1 and the calculated spectrum (red trace) of the hydrate model of PBI. (For interpretation of the references to colour in this figure legend, the reader is referred to the web version of this article.)

geometry of the supramolecular aggregate with CO_2 is reproduced in Fig. 20B. The vibrational origin of the doublet observed at 676 – 648 cm^{-1} in the Raman spectrum of sorbed CO_2 and its diagnostic character were identified. In fact, this feature appears only upon the interaction establishment as a consequence of the loss of the original $D_{\infty h}$ symmetry by the CO_2 molecule. The perturbation effects brought about by the penetrant on the PCL spectrum were also interpreted in the light of the vibrational analysis.

The QC/NCA is even more informative when extensive self-association in the polymer substrate takes place because of the presence of OH/NH groups on the backbone. As already mentioned, this complicates the analysis and makes the computational results a primary support towards a proper interpretation. An example of such a situation is represented by the system H_2O/polybenzimidazole (PBI) [261]. PBI is a high-performance technopolymer capable of forming an extended and rigid H-bonding network through NH···N interactions. This is reflected in the complex bandshape observed in the 3900 – 2500 cm^{-1} range (see Figs. 13 and 21).

The IR spectrum of the hydrate model of PBI, calculated at the B3LYP/6-31 G(d) level of theory (red trace in Fig. 21) was in good agreement with the experimental spectrum and allowed the interpretation of the complex pattern. In particular, the analysis provided the unambiguous assignment of three bands of absorbed water at 3628, 3550 and 3174 cm^{-1}. Furthermore, the theoretical evaluation of the absolute intensities for these ν(OH) components allowed the identification of selected signals to be correlated with gravimetric data for calibration purposes, and made available a means for evaluating the absolute concentration of specific H_2O species.

3.4.6. A synergic approach combining NRHB modelling, gravimetry, FTIR in situ spectroscopy and spectral interpretation

Equilibrium and dynamic experimental results obtained from gravimetric measurements and from in-situ vibrational spectroscopy along with the elaboration of the spectra by performing subtraction spectroscopy, LSCF and 2D-COS, provide a wealth of qualitative and quantitative information on the interactions established in the penetrant/polymer system exposed to a gaseous or a vapor phase of a low molecular weight penetrant. The experimental outcomes consists in the amount and type of self- and cross-interactions established in the system and in the identification of the groups involved. This information can be effectively used to tailor the structure of the terms accounting for interactions in NRHB or SAFT models and to verify the quantitative theoretical predictions regarding the amount of established interactions. In section 4 several examples illustrating in detail this procedure will be provided.

To compare the IR quantitative analysis with the simulations performed using the NRHB and NETGP-NRHB approaches, the volumetric concentration of different penetrant species from IR is to be transformed into the moles of self and cross specific interactions per mass of polymer occurring within the penetrant/polymer system, that are provided by the models.

The relationships between the above quantities depend on the specific system and could be highly complex in view of the multiplicity of interacting species that can, in addition, be characterized by a dual nature (e.g. they may act both as a proton donor and a proton acceptor). When the number of species is limited, full molecular characterization of the occurring interactions can be gathered from IR spectra.

To illustrate the general methodology, we confine our attention to relatively simple H_2O/PLLA binary system discussed previously. In this case, the IR quantitative analysis provides the concentration of *first-shell* and *second-shell* water species, in terms of moles/cm^3. The molecular aggregate is illustrated in Fig. 22 along with the frequencies of the relative signals. In the figure the *first-shell* water is denoted 'bc' (bound to carbonyls) and the *second-shell* is referred to as 'sa' (self-associated).

The relationships between the volumetric concentration of a penetrant species and the corresponding moles of established Hydrogen Bonds, take the following form:

$$f_{ss}\frac{C_{ss}}{\rho_{pol}}=\frac{n_{11}}{m_{pol}};\ f_{fs}\frac{C_{fs}}{\rho_{pol}}=\frac{n_{12}}{m_{pol}} \tag{223}$$

where C_{fs} and C_{ss} are, respectively, the volumetric concentration of *first-* and *second-shell* water species provided by IR analysis, ρ_{pol} is the density of the polymer in the mixture, m_{pol} is the mass of polymer in the mixture, n_{11} represents the moles of self-HB interactions established by water molecules (subscript '1' refers to water in the NRHB model framework) and n_{12} represents the moles of cross-HB occurring between the proton donor groups of water molecules and the proton acceptor groups (carbonyls) present on polymer backbone (subscript '2' refers to polymer in the NRHB model framework). f_{ss} and f_{fs} represent 'stoichiometric' factors that account for the number of interactions formed by a single water species. In the present system (see Fig. 22), $f_{ss}=1$ and $f_{fs}=2$. The value of these stoichiometric factors may change with the system considered and with the penetrant concentration. Information on these factors can be gathered by vibrational spectroscopy.

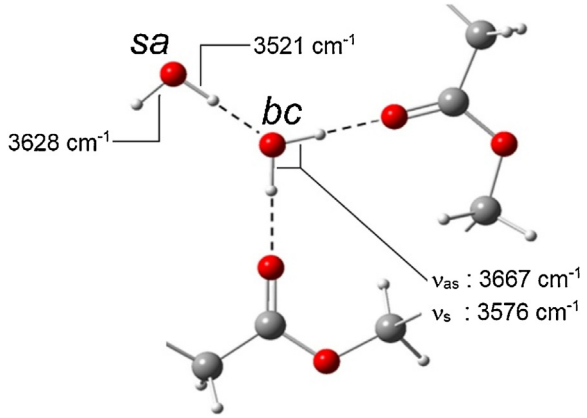

Fig. 22. Schematic representation of the two water species identified in the H_2O/PLLA system. 'bc' stands for bound to carbonyls, corresponding to *first-shell* water; 'sa' stands for self-associated water, corresponding to *second-shell* water.

Please cite this article in press as: G. Mensitieri, G. Scherillo, C. Panayiotou et al. Towards a predictive thermodynamic description of Fsorption processes in polymers: The synergy between theoretical EoS models and vibrational spectroscopy. Mater. Sci. Eng. R (2020), https://doi.org/10.1016/j.mser.2019.100525

3.5. Inverse gas chromatography

In this sub-section we review the essentials of the Inverse Gas Chromatography method for the determination of key thermodynamic properties of materials. The main reason for this is to appreciate the capacity of a new approach to solution thermodynamics, the Partial Solvation Parameter (PSP) approach, for material characterization, which is exposed in section 3.8.1.

Inverse Gas Chromatography (IGC) is a relatively simple yet powerful technique for the investigation of material, especially, polymer properties or for material characterization through material interaction with low molecular weight solvent – probes [285–288]. It is based on measurement of retention times, t_R, of the probes injected into the gas chromatography column containing as immobile phase the investigated material (polymer, drug, ionic liquid, etc). A probe non-retained or non-interacting with the immobile phase is also used and its retention time, t_M, is subtracted from the corresponding time of the interacting probes. This corrected retention time is the key IGC datum out of which the specific retention volume, V_g, of the probe per unit mass of the material is determined. The neat retention volume, V_N, is first determined from the flow rate of the carrier gas, F_C, through the equation [285–288]:

$$V_N = F_C(t_R - t_M) \tag{224}$$

and the specific retention volume, reduced to 273 K, is obtained from the defining equation:

$$V_g = \frac{273.15}{T}\frac{V_N}{w} \tag{225}$$

where, w is the mass of the investigated material (say, polymer) in the column.

As long as we may assume that the probe sorption in the bulk of the studied material (liquid) phase has reached equilibrium, V_g may be used for obtaining a number of useful thermodynamic properties of the investigated material. The sorption enthalpy is obtained from the temperature dependence of V_g through the following equation [285–288]:

$$\Delta H_S = -R\frac{dlnV_g}{d(1/T)} \tag{226}$$

In the majority of cases, IGC experiments are conducted at infinite dilution of the probe (component 1 or solute) in the studied material (immobile) phase (component 2 or solvent). This is convenient since probe – probe interactions may be neglected, and Henry's law applies. At infinite dilution of the probe and at equilibrium with the stationary liquid phase, a most useful thermodynamic quantity, namely, the mole fraction activity coefficient, $(a_1/x_1)^\infty$, is obtained through the equation [285–289]:

$$ln\gamma_1^\infty = ln\left(\frac{273.15R}{p_1^0 V_g M_2}\right) - \frac{p_1^0}{RT}(B_{11} - V_1) \tag{227}$$

M_2 in Eq. (227) is the molar mass of the immobile phase, while p_1°, V_1, and B_{11} are the saturated vapor pressure, molar volume and second virial coefficient of the solute-probe at T.

Quite often, the molar mass M_2 is not easily defined, such as in the cases of crosslinked polymers or composite materials [290]. In these cases it is more convenient to obtain, instead, the weight fraction activity coefficient, $(a_1/w_1)^\infty$, from the following equation [290]:

$$ln\Omega_1^\infty = ln\left(\frac{273.15R}{p_1^0 V_g M_1}\right) - \frac{p_1^0}{RT}(B_{11} - V_1) \tag{228}$$

where, now, M_1 is the molecular weight of the solute – probe.

Once the activity coefficient of the solute is known, the excess chemical potential or the partial molar excess free energy are obtained through the classical equation:

$$\frac{\overline{g}_1^{E,\infty}}{R\cdot T} = ln\Omega_1^\infty \tag{229}$$

In practice, however, when the investigated material is a polymer, the quantity of key interest is the Flory-Huggins χ interaction parameter or the residual mole fraction activity coefficient at infinite dilution, which, in the present context is obtained from the following equation [44,287–291]:

$$\chi = ln\gamma_1^\infty - 1 - ln\frac{V_1}{V_2} = ln\left(\frac{273.15Rv_2}{p_1^0 V_g v_1}\right) - 1 - \frac{p_1^0}{RT}(B_{11} - V_1) \tag{230}$$

Where, v_1 and v_2 are the specific volumes of probe and polymer, respectively.

Partial molar excess enthalpy and entropy may be also obtained through the classical equations:

$$\frac{\overline{h}_1^{E,\infty}}{R} = \frac{\partial\left[\overline{g}_1^{E,\infty}/(RT)\right]}{\partial(1/T)} = \frac{\partial ln\Omega_1^\infty}{\partial(1/T)} \tag{231}$$

and

$$\overline{g}_1^{E,\infty} = \overline{h}_1^{E,\infty} - T\overline{s}_1^{E,\infty} \tag{232}$$

IGC is widely used for the determination of the solubility parameter, δ_2, of the investigated material. Unfortunately, this is most often done on the basis of Hildebrand's Regular Solution Theory (RST) [292,293] through the equation:

$$\chi = \frac{V_1}{RT}(\delta_1 - \delta_2)^2 \text{ (RST)} \tag{233}$$

Guillet and coworkers [294,295] have rearranged Eq. (233) as follows:

$$\left(\frac{\delta_1^2}{RT} - \frac{\chi}{V_1}\right) = \left(\frac{2\delta_2}{RT}\right)\delta_1 - \left(\frac{\delta_2^2}{RT}\right) \text{ (RST)} \tag{234}$$

Eq. (234) is, then, the working equation for obtaining δ_2 by plotting the left-hand side quantity versus the probe solubility parameter, δ_1. A straight line is presumably obtained and δ_2 is obtained either from its slope or the intercept. It is crucial to stress the point that RST Eqs. (233) and (234) cannot apply when χ is negative, as is often the case when the studied material interacts via strong specific forces such as hydrogen-bonding or acid-base interactions. A drastically different approach should be followed in this case [42,55,296,297], as explained in the sub-section devoted to Partial Solvation Parameters.

IGC is also used for the surface energy characterization of solid stationary phases. In the case of polymers, this would imply IGC experiments at temperatures below glass transition temperature, T_g. Both, weak dispersive (d) as well as strong specific (sp) surface energy interactions are obtained via IGC. The adsorption free energy change, ΔG_{ad}, is related to the neat retention volume through the following equation [298–300]:

$$-\Delta G_{ad} = -\left(\Delta G_{ad}^d + \Delta G_{ad}^{sp}\right) = RTlnV_N + C \tag{235}$$

The constant C is related to the reference states and its value is not required in practical applications.

When inert n-alcane probes are used, the adsorption free energy is related to the dispersion surface energy components, γ^d,

through the Fowkes equation [301–303]:

$$-\Delta G_{ad} = -\Delta G^{d}_{ad} = 2N_A a\sqrt{\gamma^{d}_{2}\gamma^{d}_{1}}\,(\text{inert probe 1}) \tag{236}$$

where, N_A is Avogadro's number and a is the cross-section area of the probe molecule. Combining Eqs. (235) and (236), the following working equation is obtained:

$$RTlnV_N = 2N_A a\sqrt{\gamma^{d}_{2}\cdot\gamma^{d}_{1}} - C\,(\text{inert probe 1}) \tag{237}$$

By plotting the left-hand side of Eq. (237) versus the square root of the known dispersion surface energy of the probe, one obtains the corresponding dispersion surface energy component of the studied solid, $\gamma_2{}^d$, (Schulz method). In the alternative Dorris-Gray method [304], the contribution of the methylene group of n-alcane probes is considered only by plotting the left-hand side of Eq. (237) versus the number of probe carbon atoms. From such a plot one obtains the increment per CH_2 group in the sorption free energy through the equation:

$$\Delta G^{CH_2}_{ad} = -RTln\left(\frac{V_N^{C_nH_{2n+2}}}{V_N^{C_{n+1}H_{2n+4}}}\right) \tag{238}$$

The final working equation of the Dorris-Gray method is:

$$\gamma^{d}_{2} = \frac{1}{4\gamma^{d}_{CH_2}}\left(\frac{-\Delta G^{d}_{CH_2}}{N_A a_{CH_2}}\right)^2 \tag{239}$$

where [305]:

$$\gamma^{d}_{CH_2} = 35.6 + 0.058(293.15 - T) \tag{240}$$

Specific or acid-base surface energy components are also obtained from IGC though in a less approximate manner [305,306].

In essence, IGC belongs to sorption measurement methods and its main task is the estimation of the partition coefficient between the gas and the stationary phase. When Henry's law is obeyed by the sorption isotherm, IGC gives for the solubility coefficient in units of cm^3(STP)/atm cm^3 [307,308]:

$$s_1 = \frac{V_g\rho_2}{p^s} \tag{241}$$

where, p^S = 1 atm is the standard outlet pressure of the column and ρ_2 is the density of the stationary phase. At infinite dilution, then, the NELF model [50] (cf. section 2.2.1) gives for the solubility of solute-probe 1 in glassy polymer 2 the following expression (STP: standard temperature and pressure conditions):

$$lns_1^{\infty} = ln\left(\frac{T^{STP}}{P^{STP}T}\right) + r_1^0\left\{\left[1 + \left(\frac{v_1^*}{v_2^*} - 1\right)\frac{\rho_2^*}{\rho_2^0}\right]ln\left(1 - \frac{\rho_2^0}{\rho_2^*}\right) + \left(\frac{v_1^*}{v_2^*} - 1\right) + 2\xi_{12}\frac{\rho_2^0 T_1^*}{\rho_2^* T}\sqrt{\frac{P_2^*}{P_1^*}}\right\} \tag{242}$$

The only adjustable parameter in the NELF model is ξ_{12}, and, as shown, it may be determined from simple IGC measurements.

3.6. PVT properties and dilatometry

In the case of polymers, pure component EoS parameters are typically obtained by nonlinear regression of equilibrium volumetric data of the material in a molten-rubbery state. In the following we report in some detail the generally adopted experimental procedure.

In Fig. 23 is reported the scheme of a common commercial apparatus specifically designed to measure Pressure-Volume-Temperature (PVT) relationships of polymeric fluids (GNOMIX high pressure dilatometer, Boulder, CO, USA). This equipment is based upon the well-established bellow technique: an hydrostatic pressure is imposed over a sample whose volume is known at the starting pressure and temperature of the dilatometric experiment. The volume change of the sample is calculated by measuring the volume of the cell containing the sample surrounded by a confining fluid (typically mercury), by means of a linear variable differential transformer mounted beneath the pressure vessel. The corresponding volume changes of the sample, induced by the applied pressure, are calculated after subtraction of the volume change of the confining fluid from the total volume of the cell. This technique is extensively described in [309]. This dilatometer provides only measurements of volume change so that, in order to determine the actual value of the volume, it is required the knowledge of the polymer density at a known temperature and pressure condition (being known the polymer mass inserted within the instrument).

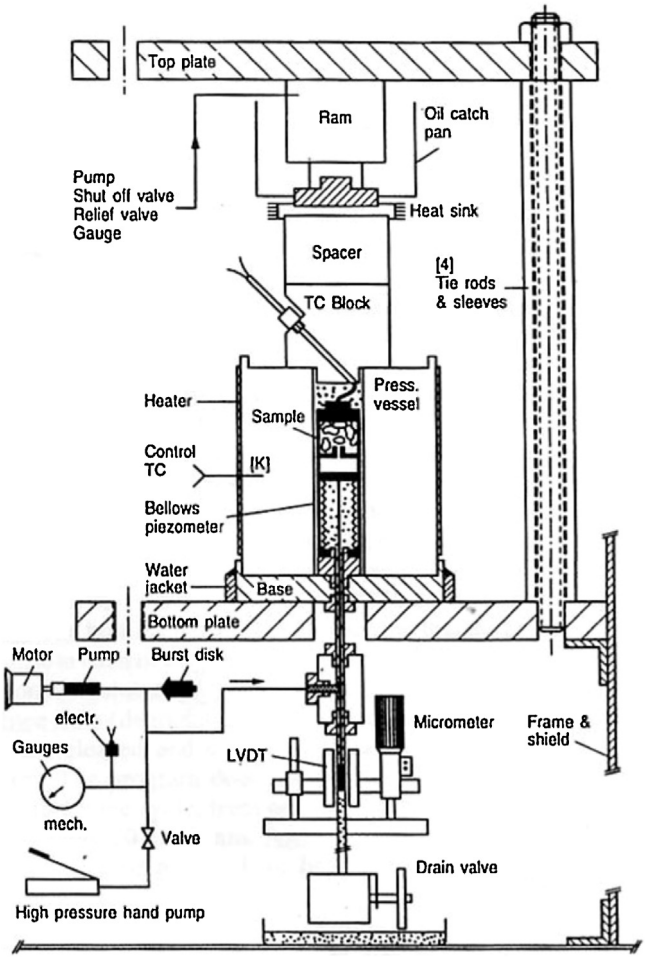

Fig. 23. Schematic representation of GNOMIX high pressure dilatometer.

The required value of density can be, for instance, measured by helium pycnometry. The pycnometer evaluation of the sample density can be also combined with gravimetric sorption tests in the case that the amount of gas adsorbed within the sample significantly affects the measurement of the pressure in the pycnometer gas phase, thus inducing an intrinsic error in the sample volume estimation. An alternative method to measure the density of a polymeric sample at room pressure and fixed temperature is based on the Mohr-Westphal balance. In this case the polymeric sample is first immersed in a liquid phase, (e.g. deionized water) at controlled temperature conditions, then the liquid phase density is adjusted by adding a second component (in

Please cite this article in press as: G. Mensitieri, G. Scherillo, C. Panayiotou et al. Towards a predictive thermodynamic description of Fsorption processes in polymers: The synergy between theoretical EoS models and vibrational spectroscopy. Mater. Sci. Eng. R (2020), https://doi.org/10.1016/j.mser.2019.100525

the case of water can be typically used salts, such as $CaCl_2$) until the density of the liquid solution matches that of the sample, i.e. until the neutral flotation condition of the sample is attained. Finally, the fluid density is measured by the Mohr-Westphal balance. Also in this case a possible source of error in the estimate of sample density is the adsorption of liquid solution within the sample. In such event, one should account for liquid sorption on the basis of the sorption isotherm.

It is worth noting that, for both the techniques briefly described above, further error in the density estimations could arise if the gas or the liquid solution induce a significant swelling of the sample. Actually, the use of helium gas picnometry, at a pressure of around 1 atm, is not expected to promote a significant swelling of the sample.

The dilatometric measurements using the GNOMIX apparatus can be performed by following different protocols. One consists in an isothermal compression procedure, performed by increasing the pressure in a stepwise manner. With a standard equipment, such as the one described in Fig. 23, it is possible to span pressures ranging from 0.1 MPa up to 200 MPa and set temperature values from 25 °C up to 450 °C. At each value of pressure several measurements are performed, for statistical averaging purposes.

The EoS model parameters for pure polymers, can be retrieved by a concurrent nonlinear regression of equilibrium volumetric data at different pressures and temperatures. In this respect, it is worth reminding that the pure component scaling parameters of the NETGP extension of a given equilibrium EoS theory, are the same as ones of the equilibrium EoS itself.

In the case of non crystallizable polymers, the volumetric data are collected for coupled values of temperature and pressure at which the material is in a "rubbery" state, i.e. above the glass transition temperature, T_g, at the test pressure. In the case of semi-crystalline polymers, data need to be collected for coupled values of temperature and pressure at which the polymer sample is in a melt state, i.e. above the melting temperature, T_m, at the test pressure. It is worth noting that both T_g, and T_m of a pure polymer significantly increase with the applied pressure.

As an example, in Fig. 24 is reported a set of dilatometric data obtained by means of a GNOMIX apparatus for a pure polyetherimide (PEI) [310]. These data were used to retrieve the EoS parameters, by a performing a concurrent fitting with the NRHB model. In the case of PEI, the model provides an excellent fitting of the experimental results in the whole range investigated. Since no specific self-interactions are expected for this polymer, as also suggested by the results of vibrational spectroscopy analysis [260], the adopted version of NRHB model contains only the *physical* contribution and the only fitting parameters involved are the lattice fluid scaling parameters.

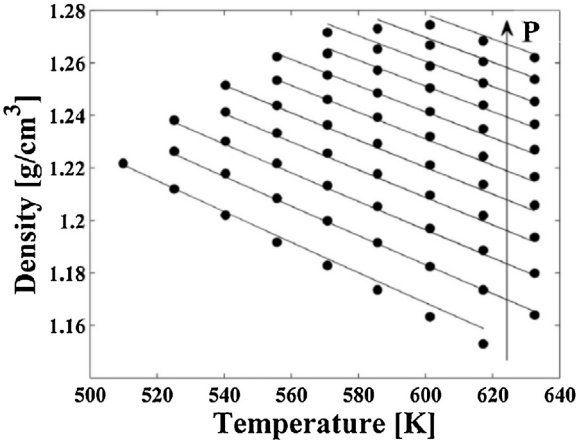

Fig. 24. Experimental equilibrium volumetric data for PEI (full circles) and best fitting curves obtained by using NRHB model.

Table 4
Values of scaling parameters of the NRHB model retrieved from concurrent fitting of dilatometric data for molten PEI. The parameter 's' (the value of surface to volume ratio) was not obtained from fitting but has been calculated using the UNIFAC group contribution scheme [87,88].

ε_s^* [J/mol]	ε_h^* [J/mol]	$v_{sp,0}^*$ [cm^3/mol]	s
6775.2	5.503	0.7228	0.743

The values of NRHB scaling parameters for pure PEI obtained from the fitting procedure i.e. ε_s^*, ε_h^* and $v_{sp,0}^*$, are reported in Table 4.

A difficulty arises in the determination of the pure polymer parameters of the EoS models belonging to the SAFT family. In fact, since for polymers are available only density data in the molten state as a function of temperature and pressure, this limitation affects the reliability of the energy related parameter to be used in binary mixture calculations. For this reason, the evaluation of SAFT parameters for a pure polymer is performed by complementing the pure polymer data with experimental phase equilibrium data for binary mixtures involving a penetrant and the polymer of interest (see, for example [115,311].

3.7. Vapor-liquid phase equilibrium

The pure EoS parameters for low molecular weight compounds can be retrieved by a non-linear regression of vapor-liquid phase equilibrium data. As an example of such procedure, in Fig. 25 are reported vapor pressure and density data for methanol at vapor-liquid phase equilibrium used to determine pure methanol NRHB parameters.

Each methanol molecule presents an OH group, which acts both as a proton donor and a proton acceptor site so that specific self HB interactions are established within each pure methanol phase. Hence, besides the scaling parameters, NRHB modelling of pure methanol phases requires the knowledge of the energy (E_{11}^0) and the entropy (S_{11}^0) of formation of this self hydrogen bonding. In the case that no ab initio calculation or in situ spectroscopic determination of such HB parameters are available, a feasible alternative procedure consists in including E_{11}^0 and S_{11}^0 as additional adjustable parameter to be used for data fitting. The results of this fitting procedure is illustrated in Fig. 25 and the corresponding best fitting parameters are reported in Table 5. The NRHB model provides an excellent fitting capability in a wide range of temperatures, sufficiently lower than the methanol critical point. Actually, the NRHB parameters provided by this simultaneous fitting procedure can be successfully used to reproduce also data in supercritical conditions (results not shown for the sake of brevity), remarking that, as expected, EoS model only fails in the proximity of critical conditions, due to the first neighbour interaction approximation.

Concerning the EoS of SAFT family, for non-associating components there are three pure-component parameters to be determined, two of which represent a geometrical description of the molecular structure while the third is related to the attractive interactions. These parameters, in the case of low molecular weight compounds, are again determined by simultaneous fitting of vapor-liquid phase equilibrium data (i.e. vapor pressure and densities) and are available in the literature for numerous compounds [116,134,312].

It is worth noting here, that the performances of EoS-based theories in interpreting sorption thermodynamics depend significantly upon the quality of model parameters for pure components. In particular, as shown in the literature [313], the capability of pure

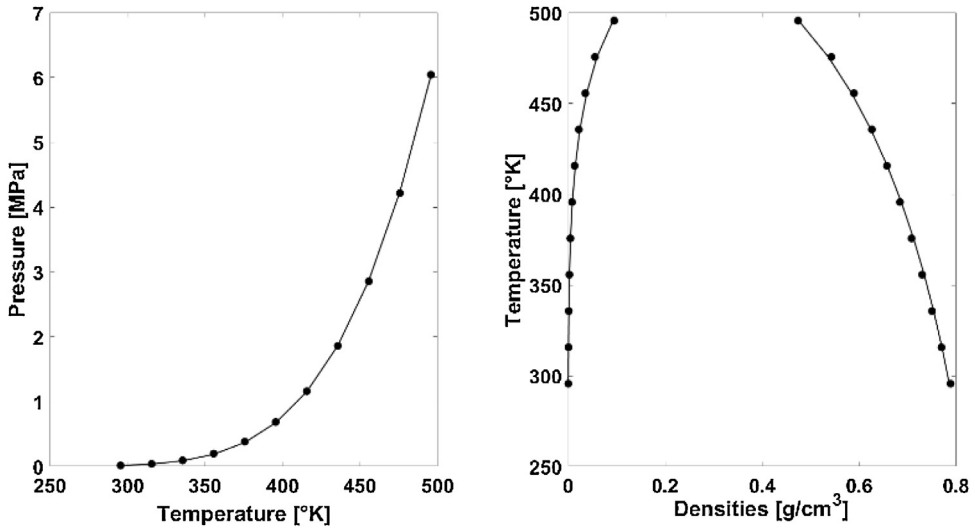

Fig. 25. Vapor-liquid equilibrium data for pure methanol. Experimental data (full circles) and curves resulting from best-fitting with NRHB model (solid lines). Experimental data from https://webbook.nist.gov/chemistry/fluid/ (accessed on November 9, 2012)].

Table 5
Values of scaling parameters of the NRHB model retrieved from concurrent fitting of vapor-liquid phase equilibrium data for methanol. The parameter s (the value of surface to volume ratio) was not obtained from fitting but has been calculated using the UNIFAC group contribution scheme [87,88].

ε_s^* [J/mol]	ε_h^* [J/mol]	$v_{sp,0}^*$ [cm^3/mol]	s	E_{11}^0 [J/mol]	S_{11}^0 [J/(mol K)]
4186.7	0	1.210	0.941	−23857	−20.4243

fluid parameters in the SL model to allow good modelling of pure fluid properties is reflected in the degree of efficacy of the model predictions for the multicomponent mixture thermodynamics. In general, a single set of parameters is not capable of providing good interpretation of experimental results in a large range of pressures and temperatures and, in particular, outside the range where they have been estimated. Actually, several sets of SL pure component parameters can be found in the scientific literature for the same compounds. The detailed discussion provided by von Konigslow [71] for the case of CO_2, highlights the effect of the selected set of SL parameters for the pure compound on the performances of SL model in interpreting sorption thermodynamics of CO_2 in rubbery polymers.

Moreover, another important issue is that any model should not be used to fit experimental data in regions where it is not expected to provide good results (e.g. near critical points, in the case of models adopting mean-field approximation) or related to properties that are not expected to be well interpreted by the model itself (e.g properties associated to internal molecular degree of freedom in the case of SL model).

Finally, also the intrinsic quality of the experimental data has a considerable effect on the reliability of estimated pure components parameters. Unfortunately, information on the quality of data, typically carried by the statistical estimate of their error bounds, is not always available.

3.8. Predictive approaches

Quantum Mechanics (QM) or Quantum Chemistry (QC) calculations can be used to estimate the values of pure component model parameters in association theories (e.g. SAFT and NRHB). For the theories belonging to the SAFT family, methods have been developed to determine the association parameters as well as the 'physical parameter' (number of segments, segment energy and segment diameter) as well as to define the combining rules in mixtures [117]. In the following it is illustrated in some detail the procedure based on Partial Solvation Parameter (PSP) approach [40–44,53–55] to determine parameters of the NRHB theory. To this aim are used expressions bridging molecular descriptors, predicted by means of the PSP approach, to the EoS parameters.

3.8.1. The Partial Solvation Parameter (PSP) approach in polymer solution thermodynamics

The Partial Solvation Parameter (PSP) approach is a novel predictive thermodynamic framework, which combines elements from the Solubility Parameter approach [293,314–317], the Solvatochromic/LSER approach [317–323] and the COSMO-RS theory of solutions [105,108,324]. It retains the simplicity of the Solubility Parameter approach and it has molecular descriptors that can be mapped one-to-one to the Abraham/LSER descriptors. Alternatively, these descriptors may be derived from the moments of the quantum-mechanics based COSMO-RS σ-profiles. Because of this combination, the PSP approach has a broader range of applications compared to each of the above three approaches. In what follows, we will briefly present the PSP essentials. Details may be found in the recent relevant literature [40–44,53–55].

Originally [40–44], PSPs were heavily based on cosmoments and COSMO-RS database [105,108,324]. In the more recent developments [53–55], PSPs are based on the freely available Abraham's QSPR/LSER molecular descriptors [322,323,325]. Due to space limitations, we will confine ourselves here to these more recent developments. However, some key concepts should be clarified first.

3.8.1.1. Key concepts and definitions. The cohesive interactions in a pure compound are, in general, different from its solvation interactions with solvents. Some molecules may self-associate in their pure state via hydrogen bonding interactions while some others cannot self-associate but can only cross-associate with different molecules. The cohesive energy, then, or the heat of vaporization cannot be used to determine the hydrogen bonding capacity of these latter molecules. This is why PSPs are focusing on solvation rather than on cohesion. The compounds are divided into two major classes, the homo-solvated and the hetero-solvated ones. The homo-solvated molecules are the molecules in which all types of intermolecular interactions are operational in pure state as well as in solution. In contrast, in hetero-solvated molecules the

Please cite this article in press as: G. Mensitieri, G. Scherillo, C. Panayiotou et al. Towards a predictive thermodynamic description of Fsorption processes in polymers: The synergy between theoretical EoS models and vibrational spectroscopy. Mater. Sci. Eng. R (2020), https://doi.org/10.1016/j.mser.2019.100525

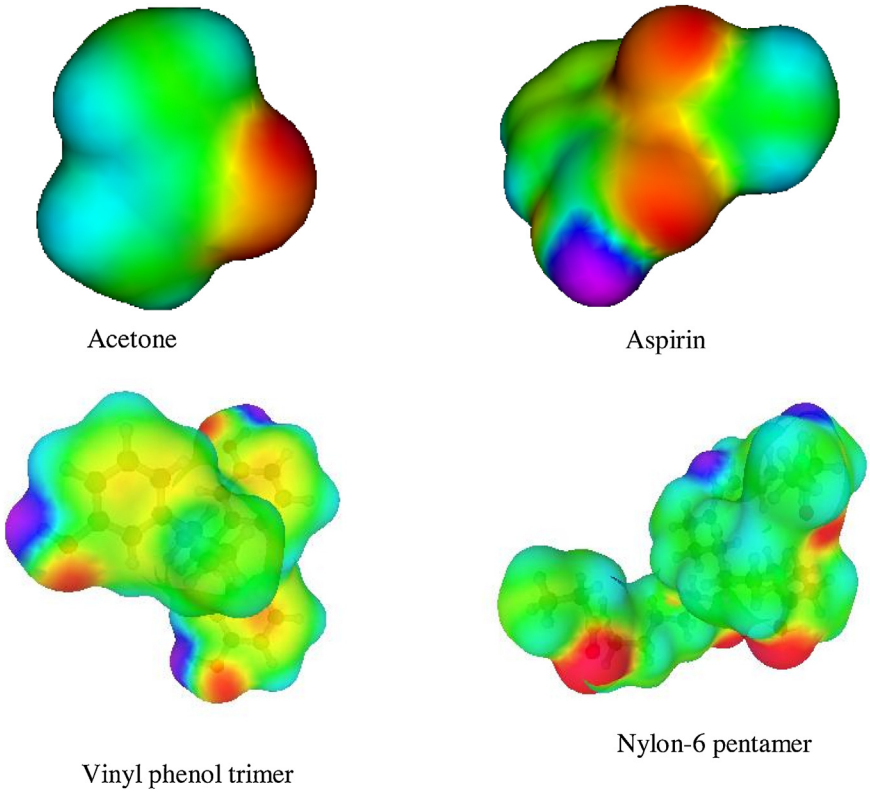

Fig. 26. Surface charge distribution in representative molecules.

types of operational intermolecular interactions in solution may be different from those in pure state. Typical representatives of homo-solvated and hetero-solvated compounds are aspirin and acetone, respectively, as shown graphically in the upper part of Fig. 26. The surface charge (σ) profile of aspirin contains, both, acidic (blue) as well as basic (red) surface areas and may self-associate, while acetone does not possess acidic areas and can only cross-associate with another acidic compound This distinction leads to the distinction between the well known cohesive energy density (ced) and the solvation energy density (sed):

$$\sigma_W^2 + \sigma_{pz}^2 + \sigma_{hb}^2 = \sigma_{total}^2 = sed \tag{243}$$

In the PSP framework, each compound / molecule is characterized by four major PSPs, which have the same dimensions as the solubility parameters ($MPa^{1/2}$).

The first PSP, σ_d, is called dispersion PSP, it reflects cavity effects, hydrophobicity, and dispersion or weak non-polar interactions, and maps McGowan volume, V_x, and excess refractivity, E, LSER descriptors [322,323,325] of the compound through the following equation [54,55]:

$$\sigma_d = 100\sqrt{\frac{3.1V_x + E}{V_m}}(\text{dispersion PSP}) \tag{244}$$

V_m in this equation is the molar volume of the compound.

The polarity PSP, σ_p, reflects dipolar (Debye-type as well as Keesom-type) interactions and maps the polarity, S, LSER descriptor [322,323,325] of the compound through the following equation [54,55]:

$$\sigma_p = 100\sqrt{\frac{S}{V_m}}(\text{polarity PSP}) \tag{245}$$

These two PSPs, when combined, give the non-hydrogen-bonding PSP of the compound:

$$\sigma_{nhb} = 100\sqrt{\frac{3.1V_x + E + S}{V_m}}(\text{Non} - \text{Hydrogen Bonding PSP}) \tag{246}$$

The rest of PSPs and LSER descriptors reflect the stronger or specific interactions of the hydrogen-bonding type or the Lewis acid / base interactions. The hydrogen bonding donor or acidity PSP is defined as follows [54,55]:

$$\sigma_{Ga} = 100\sqrt{\frac{A}{V_m}}(\text{acidity PSP}) \tag{247}$$

Similarly, the hydrogen bonding acceptor or basicity PSP is defined as follows [54,55]:

$$\sigma_{Gb} = 100\sqrt{\frac{B}{V_m}}(\text{basicity PSP}) \tag{248}$$

These are free-energy descriptors as indicated by the subscript, G.

The above definitions serve a dual purpose. First, they establish the one-to-one mapping of LSER descriptors into PSPs and, second, they act as the vocabulary for translating the PSP thermodynamic framework for mixtures [54,55] into an equivalent framework exclusively in terms of LSER descriptors. One might, then, utilize efficiently the rather large body of freely available information on LSER descriptors in the open literature [325] for the prediction of thermodynamic properties in a vast range of systems, conditions, and system complexities. In the next subsection we will recall the essentials of the mixture formalism [54,55] but in terms of the above LSER descriptors.

Please cite this article in press as: G. Mensitieri, G. Scherillo, C. Panayiotou et al. Towards a predictive thermodynamic description of Fsorption processes in polymers: The synergy between theoretical EoS models and vibrational spectroscopy. Mater. Sci. Eng. R (2020), https://doi.org/10.1016/j.mser.2019.100525

3.8.1.2. Mixture thermodynamics with PSPs. The activity coefficient is considered here to be a product of the combinatorial and residual contributions. Following our previous practice [42,53–55], we will adopt the classical Guggenheim – Staverman expression [1,86] for the combinatorial contribution to the activity coefficient (superscript, *C*):

$$\ln\gamma_i^C = \ln\left(\frac{\phi_i}{x_i}\right) + \frac{z}{2}q_i\ln\left(\frac{\theta_i}{\phi_i}\right) + \frac{\phi_j}{r_j}\left(l_i r_j - l_j r_i\right) \tag{249}$$

In the infinite dilution limit of solute *i* in solvent *j*, Eq. (249) reduces to:

$$\ln\gamma_{i/j}^{c,\infty} = \ln\frac{r_i}{r_j} + \frac{z}{2}q_i\ln\frac{q_i r_j}{q_j r_i} + \frac{z}{2r_j}\left(q_j r_i - q_i r_j\right) + \left(1 - \frac{r_i}{r_j}\right) \tag{250}$$

In the LSER/PSP framework, we will have three separate contributions to the residual activity coefficient arising from the dispersion, the polar, and the hydrogen-bonding or acid/base intermolecular interactions. The first two contributions are of the classical quadratic form of solubility parameter or cohesive energy density differences, which, when expressed in terms of LSER descriptors, take the following form [54,55]:

$$\ln\gamma_1^{VE} = \frac{10000V_{x,1}\phi_2^2}{RT}\left(\sqrt{3.1 + \frac{E_1}{V_{x,1}}} - \sqrt{3.1 + \frac{E_2}{V_{x,2}}}\right)^2 \tag{251}$$

and

$$\ln\gamma_1^{S} = \frac{10000V_{x,1}\phi_2^2}{RT}\left(\sqrt{\frac{S_1}{V_{x,1}}} - \sqrt{\frac{S_2}{V_{x,2}}}\right)^2 \tag{252}$$

As observed, these two contributions are always positive. Negative contributions (γ values less than unity) may arise from the third contribution only (hydrogen-bonding or acid-base interactions) to be discussed next. It is also important to notice that, for these two contributions, we need the E/V_x and S/V_x ratios for component 2 and not the absolute *E* and *S* values.

The third residual contribution to the activity coefficient arises from the hydrogen-bonding (or Lewis acid/base) interactions in the system. In the LSER/PSP framework homo-solvated or self-associated compounds [40–44] are compounds that possess, both, acid and base sites. Compounds which possess just one type of such moieties (either proton donors or proton acceptors – acid or base groups) are called hetero-solvated compounds [40–44]. They exhibit some kind of "chameleonic" behavior, that is, they behave with different polar interaction capacity depending on the compound they interact with. However, in the present case, where hydrogen-bonding will always be present in the system, all compounds are characterized by a single set of their LSER descriptors. In Table 6 are reported the LSER descriptors of some common compounds.

In the general case, both components, solute and solvent have donor as well as acceptor groups and the contribution to the activity coefficient may be obtained by applying Veytsman's statistics [35,36,54,55], as described above.

In our typical case of a mixture of solvent (component 2) with the solute (component 1) both possessing donor and acceptor sites, the equation for the hydrogen-bonding contribution to the activity coefficient takes the following simple form:

$$\ln\gamma_1^H = \left[r_1\nu_H - \ln\frac{x_1}{x_1 - r_1\nu_{11} - r_1\nu_{12}} - \ln\frac{x_1}{x_1 - r_1\nu_{11} - r_1\nu_{21}}\right]_{mixture} - \left[r_1\nu_{11} + 2\ln(1 - r_1\nu_{11})\right]_{pure1} \tag{253}$$

Table 6
The LSER-type Molecular Descriptors of Common Solvents [54,55].

Solvent	V_x	*E*	*S*	*A*	*B*
n-PENTANE	0.813				
n-HEXANE	0.954				
n-HEPTANE	1.095				
n-OCTANE	1.236				
n-NONANE	1.377				
n-DECANE	1.518				
CYCLOHEXANE	0.845	0.410	0.007		
CARBON TETRACHLORIDE	0.739	0.460	0.244		
BENZENE	0.716	0.610	0.266		
TOLUENE	0.857	0.600	0.320		
ETHYLBENZENE	0.998	0.610	0.363		
ACETONE	0.547	0.191	0.703		0.493
METHYL ETHYL KETONE	0.688	0.170	0.697		0.510
METHYL ACETATE	0.606	0.140	0.640		0.450
ETHYL ACETATE	0.747	0.110	0.618		0.450
n-PROPYL ACETATE	0.888	0.090	0.597		0.450
n-BUTYL ACETATE	1.028	0.071	0.597		0.449
TETRAHYDROFURAN	0.622	0.291	0.524		0.479
1,4-DIOXANE	0.681	0.330	0.744		0.635
CHLOROFORM	0.617	0.430	0.481	0.150	
DICHLOROMETHANE	0.494	0.390	0.574	0.100	
DIIODOMETHANE	0.766	1.325	0.690	0.05	0.2
METHANOL	0.308	0.280	0.439	0.539	0.804
ETHANOL	0.449	0.250	0.419	0.537	0.964
1-PROPANOL	0.59	0.228	0.420	0.580	1.033
1-BUTANOL	0.731	0.220	0.420	0.607	1.128
1-PENTANOL	0.872	0.220	0.420	0.620	1.052
1-HEXANOL	1.013	0.210	0.420	0.576	1.004
1-HEPTANOL	1.154	0.209	0.422	0.568	1.024
1-OCTANOL	1.295	0.200	0.421	0.574	1.067
ISOPROPANOL	0.59	0.210	0.366	0.526	1.030
2-BUTANOL	0.731	0.220	0.370	0.543	0.991
CYCLOHEXANOL	0.904	0.461	0.557	0.505	1.090
PHENOL	0.775	0.808	0.880	1.066	0.526
ETHYLENE GLYCOL	0.508	0.400	0.833	1.118	1.763
DIMETHYL SULFOXIDE	0.613	0.520	1.72		0.970
WATER	0.167	0.000	0.450	1.168	1.168

The corresponding hydrogen-bonding contribution at infinite dilution, takes the following approximate analytical form:

$$\ln\gamma_1^{hb,\infty} = \frac{r_1}{r_2}N_{HB,2} - \ln\frac{1 + A_{H,12} - N_{HB,2}}{A_{H,12}} - \ln\frac{1 + A_{H,21} - N_{HB,2}}{A_{H,21}} - \left\{N_{HB,1} + 2\ln\left(1 - N_{HB,1}\right)\right\} \tag{254}$$

where, the N_{HB}s are given by:

$$N_{HB,ij} = \frac{A_{H,ij} + 2 - \sqrt{A_{H,ij}\cdot\left(A_{H,ij} + 4\right)}}{2} \tag{255}$$

and

$$A_{H,\,ij} = \frac{V_{m,2}}{9.75}\cdot exp\left(\frac{G_{ij}^H}{R\cdot T}\right) \tag{256}$$

$G_{a\beta}^H$is the free-energy change upon formation of one α-β hydrogen bond (or one *i*-*j* hydrogen bond since, in our case, the types of donors and acceptors are associated with the types of molecules *i* and *j*). It is this quantity which requires the knowledge of the hydrogen-bonding LSER descriptors, A_i and B_j. With known descriptors, this free energy change is obtained from the following simple equation [54,55]:

$$G_{ij}^H = -20000\sqrt{A_i B_j}\,(\text{at T} = 25^\circ\text{C}) \tag{257}$$

This equation is sufficient for calculations at ambient conditions. In order to extend it to remote conditions of temperature one has to insert in it the entropic contribution. On adopting the universal value of $-26.5\ \text{J}\cdot\text{K}^{-1}\,\text{mol}^{-1}$ for the entropy change upon

hydrogen bond formation [54,55] for alkanols (average energy change −23000 J·mol^{-1}) and the assumption that the entropy becomes zero when the hydrogen bonding energy is zero, the working equations become:

$$E_{Hb} = -30450\sqrt{AB} \tag{258}$$

$$S_{HB} = -35.1\sqrt{AB} \tag{259}$$

and the general equation for the free energy change at any temperature T:

$$G_{HB} = -(30450 - 35.1T)\sqrt{AB} \tag{260}$$

The above equations may, now, be combined in order to obtain the final working equation for the residual activity coefficient or:

$$\ln\gamma_1^{residual} = \ln(\gamma_1^{VE}\gamma_1^{S}\gamma_1^{H}) =$$

$$= \frac{10000V_{x,1}\phi_2^2}{RT}\left\{\left(\sqrt{3.1+\frac{E_1}{V_{x,1}}}-\sqrt{3.1+\frac{E_2}{V_{x,2}}}\right)^2+\left(\sqrt{\frac{S_1}{V_{x,1}}}-\sqrt{\frac{S_2}{V_{x,2}}}\right)^2\right\}$$

$$+\left[r_1\nu_H - \ln\frac{x_1}{x_1 - r_1\nu_{11} - r_1\nu_{12}} - \ln\frac{x_1}{x_1 - r_1\nu_{11} - r_1\nu_{21}}\right]_{mixt}$$

$$-[r_1\cdot\nu_{11} + 2\ln(1 - r_1\cdot\nu_{11})]_{pure1} \tag{261}$$

This is the desired working equation, which is a most useful equation in handling phase equilibria and related properties in systems of solutes with solvents. Detailed numerical examples of calculations with PSPs and further explanations may be found in recent publications [326,327].

3.8.1.3. Equation-of-state considerations and solubility parameters. Volumetric or PVT data over a broad range of temperature and pressure are usually highly accurate and, thus, they constitute a valuable source of information for the characterization of fluids. This information is extracted from PVT data through an appropriate equation-of-state framework. The exchange of information between equation-of-state scaling constants and PSPs was discussed recently [328] by using the above equation-of-state model. The same model will be used in order to inter-relate LSER descriptors with its scaling constants.

As mentioned above, in the NRHB approach each fluid is characterized by two scaling constants, the hard-core density (or, equivalently, the hard-core specific volume), $\rho_i^* = 1/v_{sp,i}^*$, and the average per segment van der Waals interaction energy, ε_i^*. Both scaling constants may be considered to be temperature dependent but these temperature corrections cancel out at 25 °C, which is the reference temperature for the PSP definitions.

The potential energy of a homo-solvated compound consists of two parts. The first part arises from all types of intermolecular interactions except hydrogen bonding and the second part arises from the hydrogen bonding interactions. Thus, the cohesive energy density (square of solubility parameter, δ_s) or the potential energy per unit volume is given by the following equation [54,55,328]:

$$ced = \delta_s^2 = \frac{E_P}{V_m} = \frac{s\theta\varepsilon^*\Gamma - \nu_H\Delta E_{hb}}{9.75\sim v} = \sigma_{nhb}^2 + \sigma_{hb}^2 \tag{262}$$

where:

$$\theta = \frac{s}{s+\sim v-1} \tag{263}$$

PSPs have the same dimensions as solubility parameter (MPa$^{0.5}$) and, thus, σ_{hb} and σ_{nhb} may be considered as alternative estimations of $\delta_{s,hb}$ and $\delta_{s,nhb}$ components.

In the simpler Lattice-Fluid (LFHB) version (s = Γ = 1) [27], Eq. (262) reduces to the simpler form:

$$\frac{\delta_s^2 = \sim\rho^2\varepsilon^* - \nu_H\sim\rho\Delta E_{hb}}{9.75 = 10000\frac{3.1V_x+E+S}{V_m} - \left(\frac{N_H}{N}\right)\frac{\Delta E_{hb}}{V_m} = \sigma_{s,nhb}^2 + \sigma_{s,hb}^2\ (\text{LFHB})} \tag{262a}$$

Eq. (262) (or Eq. (262a)) is a most useful equation, bridging the LSER/PSP with the equation-of-state approach. We should underline, here, two points: First, the nominator in Eq. (262) may be estimated (with the equation of state) for the liquid and for the vapor phase at the same external conditions and, from their difference, one may obtain the heat of vaporization of the compound. Second, the hydrogen bonding contribution to the molar potential energy (and to heat of vaporization) is obtained from the product of the interaction energy change upon formation of one hydrogen bond, ΔE_{hb}, with the total number of such hydrogen bonds, $N_H/N = r\nu_H$. The equation-of-state calculations with PSP require the knowledge of ρ^* or of V^* for each compound. The latter quantity is linearly related with V_x or V_{vdw} or V_{cosm} or with their combination and, of course, it may be obtained directly from molar volume data.

This PSP formalism can be used for both concentrated as well as infinitely dilute systems, for small molecules as well as for high polymers and copolymers. It may, in particular, be used for the surface characterization of polymer and other solid surfaces. In fact, it may be used in order to obtain the corresponding surface energy components, γ_{SVE}, γ_a, and γ_b, of the solid surfaces [54,55]. The contact angle θ of a liquid L on a polymer surface P is given by the quadratic equation [54,55]:

$$\gamma^L(1+\cos\theta) = 2\left(\sqrt{\gamma_{SVE}^P\gamma_{SVE}^L} + \sqrt{\gamma_a^P\gamma_b^L} + \sqrt{\gamma_b^P\gamma_a^L}\right) \tag{264}$$

The range of applications of the PSP approach is rather vast. It may be used for the prediction of phase equilibria in highly non-ideal systems, for the solubility of solids, such as drugs, in various solvent systems over an extended range of temperatures, or for the sorption of solvent vapors on polymer surfaces. Various examples are reported in reference [54,55]. It may, in particular, be used for the complete thermodynamic characterization of solid surfaces via a novel method exposed in reference [55]. The way by which inverse gas chromatography (IGC), volumetric PVT data, or contact angle data may be combined for the integral characterization of polymeric materials is schematically shown in Fig. 27.

Having the PSPs of a polymer, one may predict its Flory-Huggins interaction parameter, χ_{12}, not only with a solvent but also with another polymer. This, then, may be used for the prediction of polymer – polymer miscibility – a subject of high technological importance. It may, as an example, predict the effect of copolymer

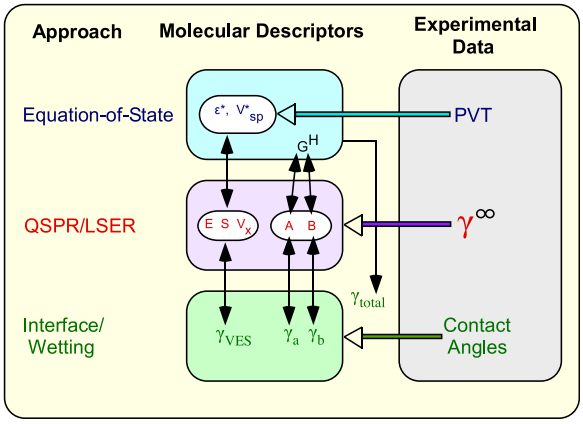

Fig. 27. The interconnection of molecular descriptors of the various thermodynamic approaches and their typical provenance.

composition on its miscibility with another polymer or copolymer. It may also use experimental or theoretical information on oligomers or low molecular weight analogs in order to characterize high polymers [44,55].

The significant advantage of the current PSP/LFHB combination is the simplicity of the key bridging Eq. (262a), which maps PSPs onto equation of state scaling constants and hydrogen-bonding parameters. Any other equation-of-state framework, such as the various SAFT-type variants, should seek the analogous of Eq. (262a) and then apply the above methodology in order to make phase equilibrium calculations.

4. Case studies and applications

4.1. Gas and vapor sorption

4.1.1. Sorption themodynamics in rubbery polymers

4.1.1.1. Applications of Sanchez-Lacombe theory. Several authors investigated sorption equilibria in amorphous binary rubbery polymer-penetrant mixtures in a wide range of temperature and pressure, up to penetrant supercritical conditions. In particular, many of these studies were focused on polymer-gas systems of interest for foaming, packaging or separation processes, in which the mean field interactions contribution was sufficient to properly describe the interactions among the components. As expected, in these cases the SL model showed a satisfactory (correlation) capability in interpreting the sorption thermodynamics of the polymer-penetrant mixtures investigated when the temperature, pressure and penetrant concentration conditions guarantee that such mixtures are in a rubbery state. Among these studies we mention here the relevant work of Sato et al. [329–331] and Tomasko et al. [332] dealing mainly with polymer-supercritical gas systems of interest for gas foaming processes.

For instance, Sato et al. [329] investigated the solubilities of nitrogen and carbon dioxide in an amorphous polystyrene (PS) under high temperatures and pressures interpreting the results with SL theory. In particular, the authors selected a range of temperatures and pressures which assured that the analyzed polymer-penetrant mixtures were in rubbery conditions when in equilibrium with the pure penetrant. To this aim were selected temperatures which were above the pure polymer glass transition temperature and the pressures were small enough so that the mechanical effect of the penetrant pressure on the polymer chains mobility was negligible as compared to the plasticization effect induced by the sorption of penetrant in the mixture. In Fig. 28 are reported the sorption isotherms for the systems polystyrene-carbon dioxide and polystyrene-nitrogen along with curve fitting performed using the SL model, assuming a temperature dependent mean field binary interaction parameter.

The pure component penetrant LF scaling parameters were retrieved by a non-linear regression of equilibrium properties. As evident in Fig. 28, the SL model provided a fully satisfactory correlation capability. From these and other investigations, SL model emerged as a well-established tool suitable for correlation of sorption isotherms of gases and vapors in rubbery amorphous polymer systems, not displaying a significant contribution of polar and/or specific interactions.

Condo et al. [333] assessed the SL model capability to correlate multiple equilibrium thermodynamics properties of polymer-penetrant systems. In particular, they investigated the sorption thermodynamics of CO_2 in poly(methyl methacrylate) (PMMA) and polystyrene (PS). To this aim, once the pure component LF scaling parameters were retrieved by fitting pure components equilibrium data, the authors used the SL model to correlate the sorption isotherms for each of the two amorphous rubbery binary mixtures by using only the corresponding binary interaction parameters for fitting purposes. Then, the authors used the SL model in combination with the Gibbs-Di Marzio (GD) entropy criterion [172,334] to predict glassy-rubbery state maps that compared well with available experimental data. In section 4.2 this issue is specifically addressed.

In a following paper [335] the procedure of Condo et al. [333] was extended, adopting the SL theory to correlate equilibrium volumetric data, solubility data and glass-rubbery state maps for the system PMMA-CO_2. Due to the reduced number of equilibrium dilation data available in the literature for polymer-penetrant mixtures (and in particular for the one selected in this work), the authors developed an innovative technique based upon ADSA (axisymmetric drop shape analysis) to optically measure volumetric properties of polymer-penetrant mixtures in situ during sorption/desorption tests. More in detail, the experimental swelling and sorption isotherms data collected for the system investigated ranged from 40 °C up to 200 °C and the pressure ranged from atmospheric pressure up to 100 atm. The pure component LF parameters were retrieved by performing a non linear regressions of the corresponding equilibrium data and a temperature dependent mean field interaction parameter was introduced in the mixing rule of the binary system. The value of this parameter was retrieved by a non-linear regression of isothermal equilibrium volumetric data and the results are reported in Fig. 29a,b. A preliminary investigation was carried

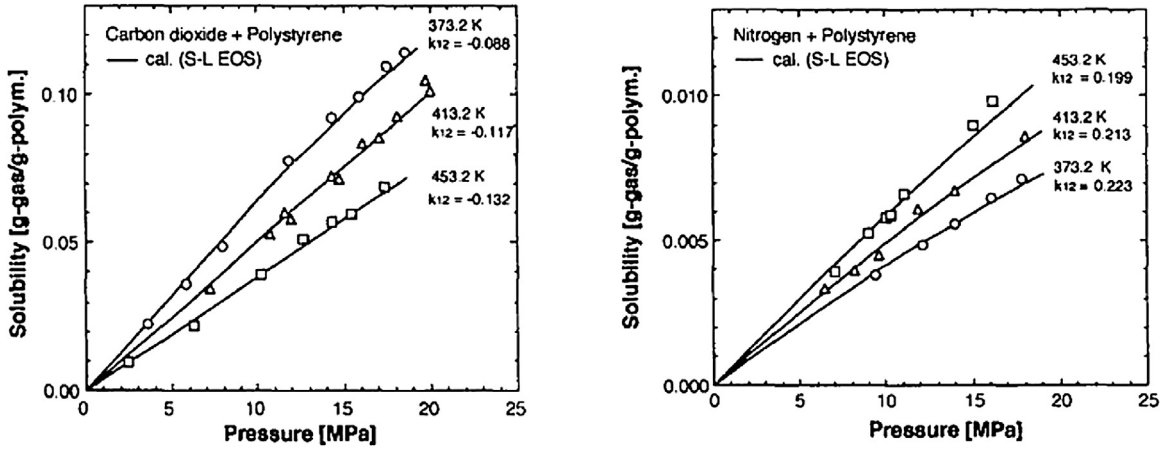

Fig. 28. Experimental sorption isotherms and curve fitting using SL model for the systems polystyrene-carbon dioxide (left) and polystyrene-nitrogen (right). Reprinted with permission from [329]. Copyright 1996 Elsevier B.V.

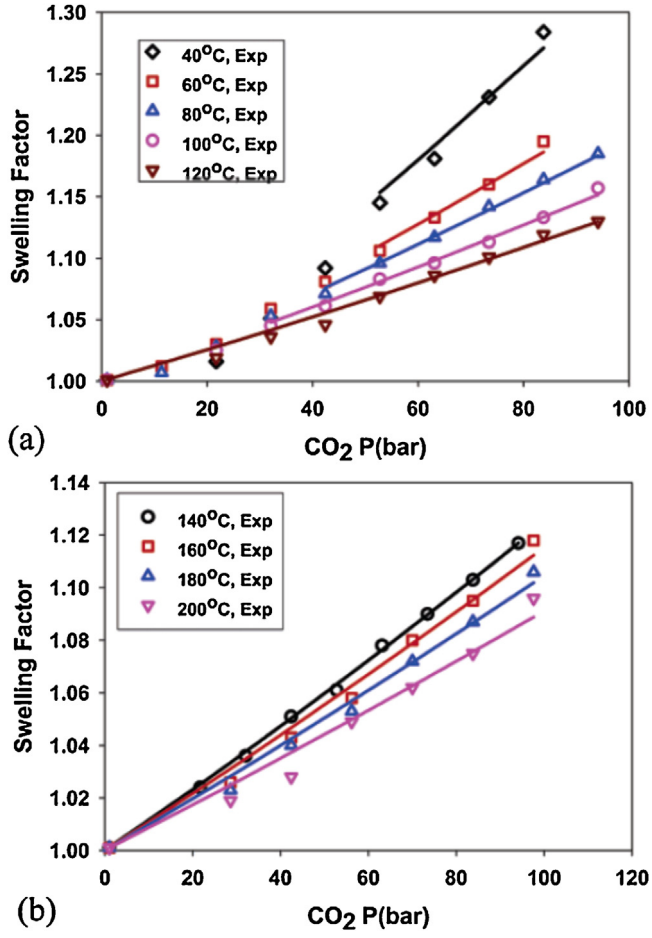

Fig. 29. a,b. Experimental data for equilibrium swelling induced by CO_2 sorption in PMMA at various temperatures. Solid lines represent the results of curve fitting using SL model. Reprinted with permission from [335]. Copyright 2005 American Chemical Society.

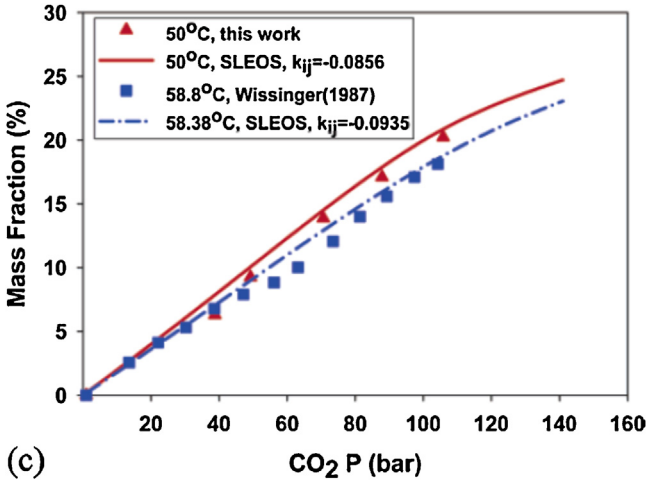

Fig. 30. Experimental sorption isotherms for the system PMMA- CO_2. Blue symbols represent data collected by Wissinger et al. [336]. Lines represents the predictions obtained by SL theory. Reprinted with permission from [335]. Copyright 2005 American Chemical Society. (For interpretation of the references to colour in this figure legend, the reader is referred to the web version of this article.)

out in order to estimate, at each temperature, what was the pressure range which assured the PMMA-CO_2 system to be in a rubbery state. As evident in Fig. 29a,b, the SL model provided a very good correlation of experimental equilibrium swelling data (equilibrium swelling was defined as the ratio equilibrium volume mixture to the equilibrium volume of pure polymer at the same temperature and at 1 atm).

Once the mean field interaction parameter, k_{ij}, was determined as a function of temperature, the SL model was again used in combination with the GD entropy criterion to predict the glass transition depression induced by the penetrant (see section 4.2 for a discussion of the issues related to the GD criterion). Model predictions were also validated against experimental data retrieved in literature by using an high pressure DSC. In addition, using the calculated value of k_{ij} and of its temperature dependence, the authors predicted, by means of the SL model, the equilibrium sorption isotherms that were compared with experimental gravimetric sorption isotherms. In Fig. 30 is reported, as an example, the comparison between the SL predictions and the experimental data at 50 °C in a pressure range which assured that the PMMA- CO_2 system was in a rubbery state.

Sanly and Erkey [337] adopted the SL EoS theory to model the demixing pressures of a binary mixture of amorphous rubbery hydroxy-terminated poly(dimethylsiloxane) and carbon dioxide (PDMS(OH))-CO_2) at various temperatures. More in details, polymer samples with two different molecular weights were selected and, for both of them, the demixing pressures were experimentally obtained by using a constant volume view cell at three temperatures (313.2 K, 323.2 K and 333.2 K), in a wide range of compositions (up to 0.718 polymer weight fraction). Two different types of phase separation were observed in the system during the depressurization process, depending on the composition: respectively a bubble point or a cloud point. Finally, a mixture critical point was also determined for one of the two systems investigated. The bubble points data were correlated by using the SL model, adopting a temperature dependent mean field interaction parameter as the only fitting parameter. As usual, pure component LF scaling parameters of the two components were retrieved as by their corresponding equilibrium data. The SL model provided an acceptable correlation capability of the experimental results, despite the fact that self Hydrogen Bonding interaction between the terminal OH groups of the polymer are expected to occur within the system and, in addition, that acid/base Lewis cross-interactions could occur between the penetrant and the silanol groups on the polymer backbone. In particular, the model correlation exhibited a full satisfactory qualitative agreement with the trends observed for both the systems investigated, reproducing the observed LCST behavior. However, the quantitative agreement was less satisfactory with a relative error concerning the bubble point data ranging from 2 % up to 30 %.

The same authors also investigated, by using the SL model, the bubble point data reported by Garg et al. [338] for the system (PDMS(CH_3))-CO_2. For this system the SL theory is expected to be suitable, in view of the absence of hydrogen bonding interactions. Indeed, the results concerning the bubble point data at a given temperature reported in Fig. 31 confirms the quite satisfactory correlation capability of the SL EoS for this system. In particular, the higher deviation between the experimental data and the model calculations at high penetrant concentration, were partially attributed by the authors to the inherent difficulty to measure correctly the bubble points in such conditions.

EoS models with a more complex structure than random mean field lattice fluid models are required to deal with systems involving specific interactions, as will be illustrated in sub-sections 4.1.1.2 and 4.1.1.3.

4.1.1.2. Applications of PHSCT and SAFT. Gross and Sadowski [115,154] demonstrated the quite good capability of SAFT and, even better, of PC-SAFT, in predicting (i.e. using $k_{12} = 0$) the vapor

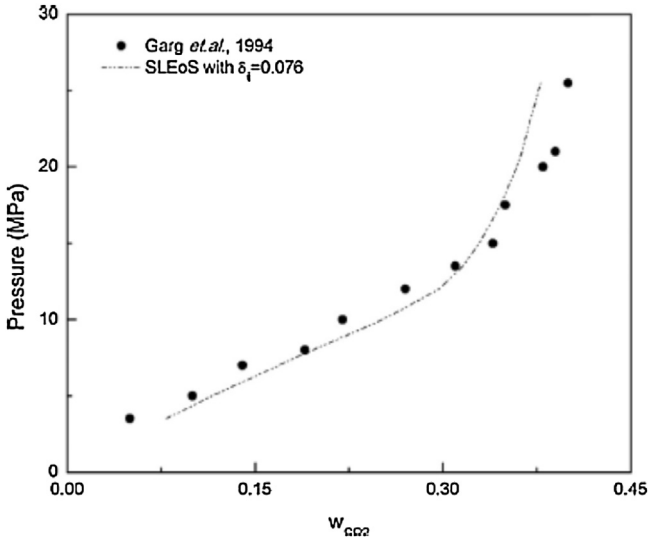

Fig. 31. SL model predictions of bubble point data at T = 323.13 K, for the system (PDMS(CH_3))-CO_2 (polymer molecular weight 308.000 g/mol). The SL mean field interaction parameter is indicated in the caption of the figure as δ_{ij}. Reprinted with permission from [338]. Copyright 1994 American Chemical Society.

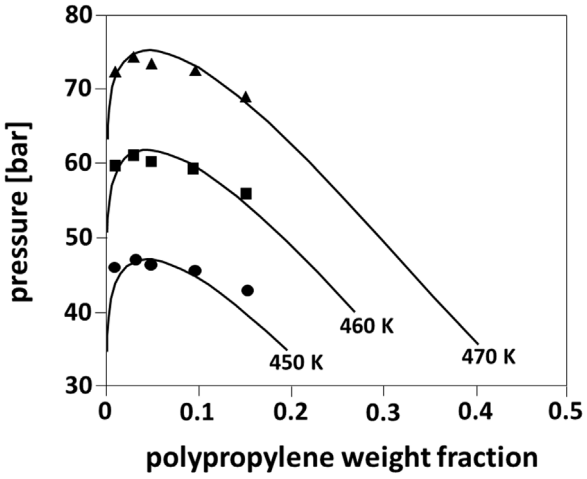

Fig. 33. Liquid-liquid phase equilibrium for the polypropylene/n-pentane system at T = 450, 460 and 470 K. Pressure is reported vs weight fraction of polypropylene. Comparison of experimental cloud points (symbols) with PC-SAFT calculations (k_{ij} = 0.0137, assumed to be independent of temperature). M_w of polypropylene is 50.4 kg/mol and M_w/M_n = 2.2. The polymer was assumed to be monodisperse in the calculations. Adapted from [115].

liquid equilibrium for the non-associating polyethylene/toluene system, assuming that no polyethylene is present in the vapor phase and using only experimental information on pure components (see Fig. 32).

Good correlation capability was also obtained using PC-SAFT in the more challenging case of liquid-liquid equilibrium for the non-associating polypropylene/n-pentane system [115]. In this case PC-SAFT approach provided a correct interpretation of the experimental results (see Fig. 33) at three temperatures by using, as fitting parameter, only the temperature-independent binary interaction parameter.

Another example of successful interpretation of liquid-liquid phase equilibrium is the case of HDPE–butyl acetate system [340], that has been modelled using simplified PC-SAFT approach to correlate data (k_{ij} = 0.0156) (see Fig. 34). The system displays both upper and lower critical solution temperature (UCST and LCST), behaviour that is qualitatively well described by the model. The two set of data for HDPE of two different molecular weights are both interpreted using a single binary interaction parameter.

In [155] are shown the rather good performances of PC-SAFT in describing the cloud point data for LDPE in several solvents, using as fitting parameter a binary interaction parameter for each LDPE/solvent system.

PC-SAFT has been used to predict phase behaviour of ternary systems, assuming that the thermodynamics is still dominated only by binary interactions. Predictions were obtained based on model parameters determined from pure components data and on binary interaction parameters determined from experiments performed on binary subsystems. An example is the successful interpretation of the phase behaviour of PMMA/MMA/CO_2 ternary system [341].

Application of PC-SAFT to interpret the phase behaviour of copolymer/solvent systems requires the calculation of pure copolymer segment parameters from the corresponding homopolymers. Moreover three binary parameters are needed: two

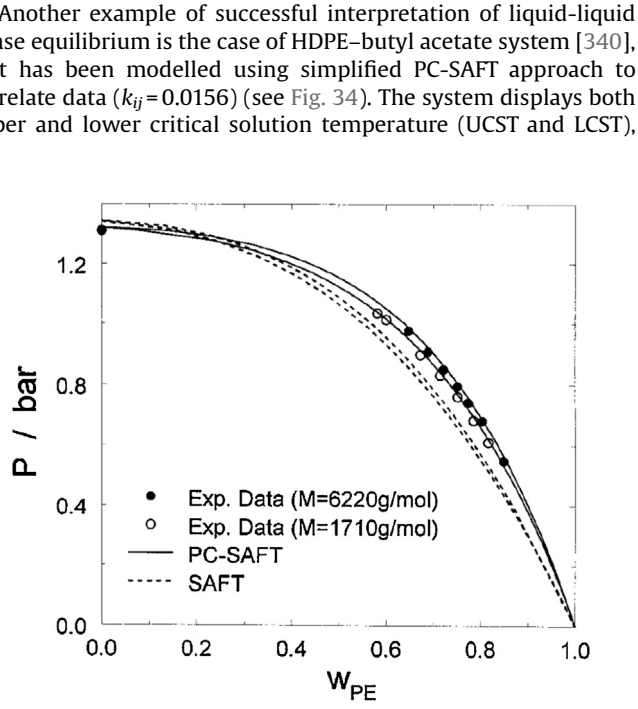

Fig. 32. Vapor-liquid phase equilibrium for the olyethylene-toluene system at T = 120 °C. Pressure is reported vs weight fraction of polyethylene. Experimental data (black and white circles) are from [339]. Lines represent predictions (k_{ij} = 0) obtained using SAFT and PC-SAFT models. Reprinted with permission from [154]. Copyright 2002 American Chemical Society.

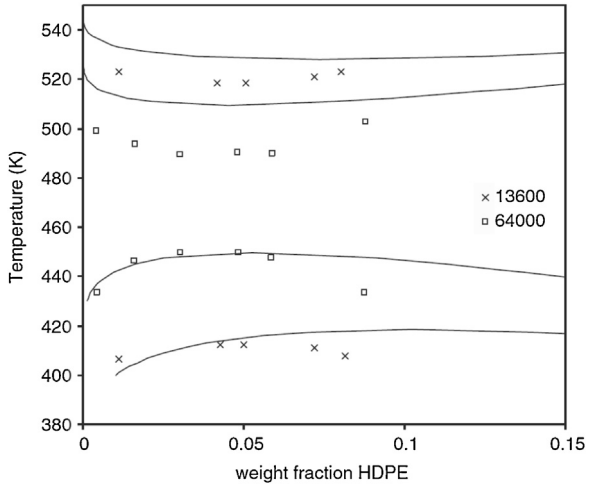

Fig. 34. LLE data for the HDPE–butyl acetate system. Lines are curve fitting with simplified PC-SAFT. Reprinted with permission from [340]. Copyright 2004 Elsevier B.V.

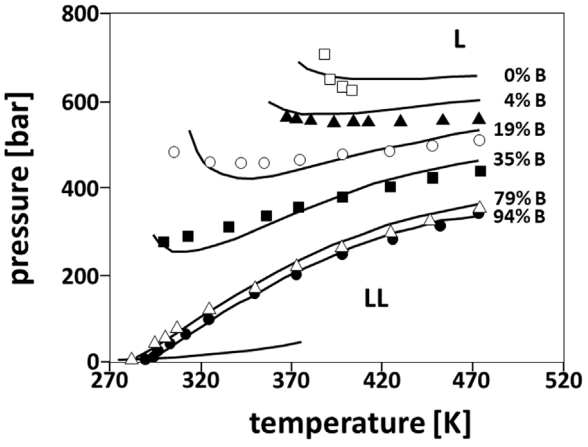

Fig. 35. Cloud point pressure vs temperature (in K) for the poly(ethylene-co-1-butene)/propane system. B indicates the mole percent of butene in the copolymer. Polymer weight fraction is about 0.05 %. Symbols represent experimental data and lines are the results of PC-SAFT calculations. Adapted from [115].

parameters account for the interactions of the solvent with each of the monomer and can be retrieved from homopolymer/solvent systems, while a third parameter accounts for the interactions between unlike monomer segment of the copolymer and has to be retrieved from copolymer/solvent data. In Fig. 35 are reported the experimental data for cloud point pressure of the poly(ethylene co-1-butene)/propane system along with curves calculated by using the PC-SAFT approach extended to the case of copolymers [167]. The pure-component parameters for the copolymer were calculated from those of poly(ethylene) (HDPE) and poly(1-butene) and the HDPE/propane and poly(1-butene)/propane binary parameters for were determined for the homopolymer systems. The 'internal' interaction parameter accounting for interactions between an ethylene segment and a butene segment was retrieved from a one point fitting of the cloud-point curve of the copolymer containing 35 % butene monomers. The model has then been used to predict the behaviour of the copolymer/solvent system in the whole range of copolymer compositions (curves reported in Fig. 35).

An example of application of simplified PC-SAFT to the case of associating compounds is the polyethylene glycol 1500 (PEG 1500)/water system (see chap. 14 in ref. [117]). Satisfactory results (see Fig. 36) were obtained with simplified PC-SAFT with a binary parameter $k_{ij} = 0$ and using pure component parameters for PEG entirely based on low-molecular weight homologues. The −OH and −O− groups have been assumed to be the association sites on PEG molecule. The association parameters (association volume and energy) are assumed to be constant for PEG of different molecular weights.

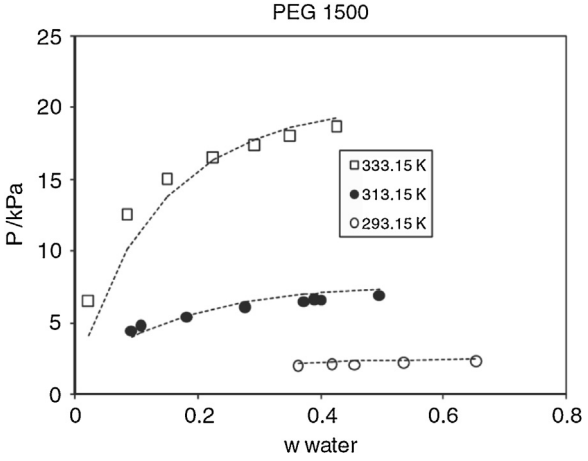

Fig. 36. Vapor-liquid equilibrium (sorption isotherms) for the PEG 1500-water system. Symbols are experimental data and lines are predictions with simplified PC–SAFT ($k_{ij} = 0$). Reprinted with permission from [117]. Copyright 2010 John Wiley and Sons.

Arce and Aznar [342] compared the modelling capability of SL EoS and of PC-SAFT in the case of mixtures of a polymer and a low molecular weight compounds. To this aim, they investigated the phase behavior of several commercial biodegradable polymers and copolymers in supercritical fluids (SCF). In particular, they selected binary systems formed by poly(D,L,Lactide) with, respectively, dimethyl ether, carbon dioxide, chlorodifluoromethane, difluoromethane, trofluorometane,1,1,1,2-tetrafluoroethane. In addition, they also investigated the poly(butylene) succinate-carbon dioxide and poly(butylene)succinate-co-butylene adipate-carbon dioxide systems and the ternary system poly(D,L, Lactide)-dimethyl ether-carbon dioxide.

Following well-established procedures (described in section 3), which can be applied in general for any EoS model, the pure fluid scaling parameters for the low molecular weight compounds were retrieved by fitting pure component VLE data, while the pure polymers scaling parameters were obtained as best fitting parameters of dilatometric pure component equilibrium data. In view of the types of chemical groups involved in these systems, no specific interactions were introduced in the PC-SAFT modelling approach. Hence, only the binary mean field interaction parameters have been considered for data best fitting. In the case of the ternary system it was also determined the binary mean field interaction parameter for the carbon dioxide-dimethyl ether couple, by performing non-linear regressions of VLE data. For all the binary polymer-SCF fluid systems investigated the PC-SAFT model provided an excellent modelling capability, with particular reference to the determination of cloud point isopleths, whereas the SL modelling performances were less good, but still satisfactory.

Once all the corresponding binary interaction parameters were determined, the authors also applied the two models, in a purely predictive fashion, to the case of ternary system formed by poly(D, L, Lactide)-carbon dioxide-dimethyl ether. In Fig. 37 are compared the modelling predictions for this ternary system with

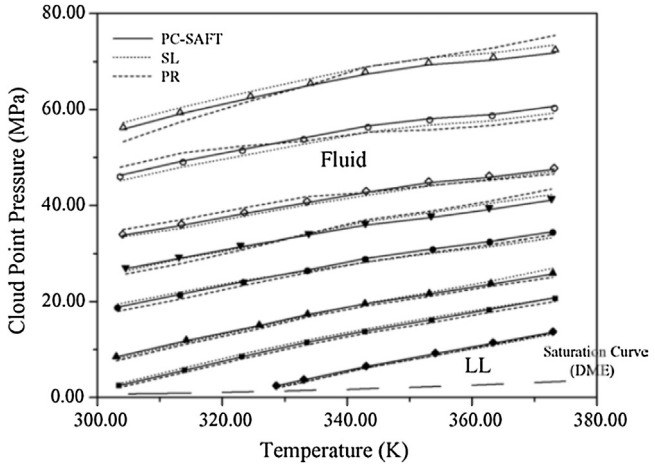

Fig. 37. Cloud point isopleths of polyD,L, Lactide M.W. = 30,000 g/mol in solvent mixtures of carbon dioxide and dimethyl ether, at different carbon dioxide mass fractions (ω_{CO_2}). (◆ $\omega_{CO_2} = 0.0000$; ■ $\omega_{CO_2} = 0.01283$; ▲ $\omega_{CO_2} = 0.02127$; ● $\omega_{CO_2} = 0.03280$; ▼ $\omega_{CO_2} = 0.04222$; ◇ $\omega_{CO_2} = 0.04955$;○ $\omega_{CO_2} = 0.06310$; $\omega_{CO_2} = 0.07279$). Results of calculations performed using the semi-empiric Peng Robinson (PR) equation of state are also reported [343]. Reprinted with permission from [342]. Copyright 2005 Elsevier B.V.

Please cite this article in press as: G. Mensitieri, G. Scherillo, C. Panayiotou et al. Towards a predictive thermodynamic description of Fsorption processes in polymers: The synergy between theoretical EoS models and vibrational spectroscopy. Mater. Sci. Eng. R (2020), https://doi.org/10.1016/j.mser.2019.100525

experimental data. In particular, the authors compared several cloud points isopleths, reported in Fig. 37 in terms of pressure vs temperature. Each isopleth was referred to an equilibrium of phase in which the same assigned carbon dioxide concentration occurs within one of the two coexisting phases. In particular, each calculation refers to an assigned temperature, the assigned carbon dioxide concentration of one of the isopleths experimentally detected and an additional assigned value (experimentally measured) of concentration in one of the two-coexisting phases, so that all the other concentration and the pressure were calculated as dictated by phase equilibrium and mass balance. This procedure demonstrated how the PC-SAFT model is a valuable tool to predict the phase equilibria behavior of a ternary system starting from the evaluation of the relevant model parameters for the corresponding binary systems. Conversely, the predictive performances of the SL theory resulted less effective, but still satisfactory.

Comparison of the performances of models of the SAFT family with SL was also provided by Chen et al. [344]. The authors interpreted the sorption thermodynamics of several subcritical and supercritical fluids in molten rubbery polymers, as well as in semi-crystalline polymers displaying amorphous rubbery domains, comparing the performances of the SL, the PC-SAFT and the CK-SAFT theories. For the sake of comparison, the authors also performed calculations with the empiric cubic equation of state proposed by Sako, Wu and Prausnitz (SWP) [345]. 21 binary systems were considered, formed by several polymers (PMMA, LDPE, HDPE, PIB, PVAc, PTFE, PVDF, PBS, PS, PBMA) with several low molecular weight compounds (N_2, CO_2, C_2H_4, C_4H_{10}, iso-C_4H_{10}). Each of these systems was reasonably well modelled assuming that no specific interactions are present in the pure components systems as well as in the corresponding binary mixtures so that the two SAFT-type models were implemented in the form which disregard the self- and cross-association terms allowing a more consistent comparison with pure mean field EoS models. Moreover, for all the systems investigated it was reasonably assumed that each of this high monodisperse molecular weight polymer was not dissolved in the external fluid phase. Following the usual procedure the pure fluid model parameters were determined by a non-linear regression of VLE equilibrium data for the low molecular weight compounds and were retrieved by a non-linear regression of dilatometric equilibrium data in the case of polymers. Finally, the models were used to correlate sorption equilibrium isotherms, assuming only a temperature-dependent binary interaction parameter, k_{ij}, as best fitting parameter.

In the case of polymer-penetrant mixtures in which the polymeric phase is semicrystalline, the common biphasic assumption was made, so disregarding the contribution of non-homogeneous interphase domains. In addition, the crystalline domains were assumed to be impervious to the penetrant. On the basis of this extensive modelling investigation, the authors concluded that, for the investigated systems, both PC-SAFT and SL EoS provided a satisfactory correlation capability in the case of amorphous polymers. As an example, in Fig. 38 is reported the case of the system PVAc-CO_2.

These results are reasonable when dealing with systems where no specific interactions take place and it is in line with the results provided by similar comparative investigation between the SL theory and a SAFT-type model reported above. A notable result of such investigation is that PC-SAFT represents an improvement, compared to the CK-SAFT model, for the description of sorption thermodynamics of polymer-penetrant mixtures. In particular, the two models differ only in the way the dispersion term is obtained according to the perturbation approach. In the case of CK-SAFT, the Helmholtz energy is built starting from the properties of Argon as reference fluid, assuming the latter as being formed by single

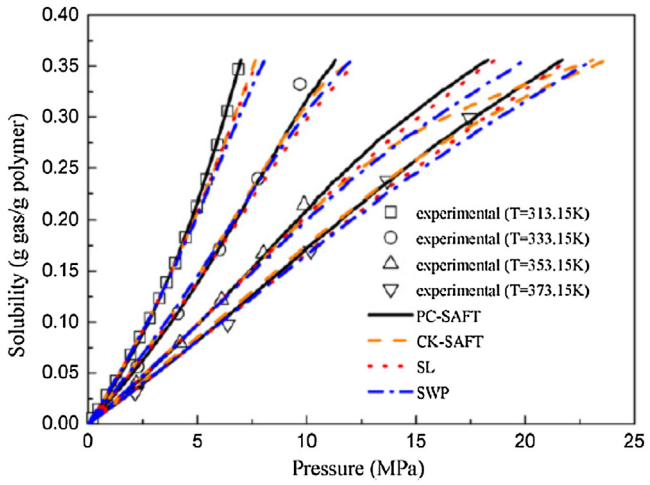

Fig. 38. Experimental sorption isotherms of CO_2 in PVAc. Data taken from ref. [346]. Reprinted with permission from [344]. Copyright 2009 Elsevier B.V.

spheres. Conversely, the PC-SAFT dispersion term is obtained according to the second order perturbation theory of Barker and Henderson [347,348], assuming therefore a bonded sphere chain as reference fluid. On this basis, it is expected that the PC-SAFT model is better suited to deal with equilibrium thermodynamics of mixtures involving high molecular weight compounds.

More recently Markocic et al. [349] have investigated the solubility of supercritical carbon dioxide within polyethylene glycol of various molecular weights, by correlating the sorption isotherms respectively with the SL model and the SAFT model in the version proposed by Huang and Radosz [49,116]. In particular, in the implementation of SAFT model, no specific interactions within the system were taken into account, so that the only fitting parameter was in both the models the corresponding mean field binary interaction parameter. The authors found that, assuming a temperature and pressure dependent values of k_{ij}, both the models exhibited a substantially equivalent and reliable correlation capability, which was able to account for the observed different behavior exhibited by the system as a function of the molecular weight of the polymer.

In [350] the SAFT, in the version proposed by Huang and Radosz [49, 116,] and the PC-SAFT [134] models, were tested by correlating the thermodynamics of polymer-solvent mixtures over a wide range of temperatures and pressures. To this aim polymer-solvent phase equilibria involving homopolymers (polyolefins) as well as copolymers were investigated. As already pointed out, the models of the SAFT family allow to explicitly account for different polymer properties that affect significantly the phase behavior. Among these properties are included the molecular weight, the polydispersity and the macromolecular architecture, with particular reference to hetero-bonded chains. This extensive validation investigation led the authors to conclude that the deviations of the best-fitting PC-SAFT correlations from the experimental data were only marginally smaller as compared to the case of SAFT model, resulting in both cases quite satisfactory.

The case of mixtures endowed with association interactions was addressed in a paper by Kouskoumvekaki et al. [351]. The authors adopted the version of the simplified PC-SAFT EoS theory proposed by Von Solms et al. [135] to deal with mixtures endowed with association contribution (i.e. hydrogen bonding) with the aim of modeling the thermodynamics of binary and ternary mixtures of polyamide 6 with several solvents (water, ε-caprolactam, ethyl benzene and toluene). In particular, in the investigated systems, the water and the ε-caprolactam are hydrogen bonding self-associating compounds so that both self- and cross-association

Please cite this article in press as: G. Mensitieri, G. Scherillo, C. Panayiotou et al. Towards a predictive thermodynamic description of Fsorption processes in polymers: The synergy between theoretical EoS models and vibrational spectroscopy. Mater. Sci. Eng. R (2020), https://doi.org/10.1016/j.mser.2019.100525

terms need to be accounted for. The main purpose of this investigation was to reproduce, in a purely predictive fashion, the equilibrium thermodynamics of the polyamide 6/ ε-caprolactam/water ternary system, since it is of interest for the modelling of one of the most common processes for the synthesis of polyamide 6 based on a hydrolytic polymerization route. To this aim the authors firstly obtained the pure component parameters of the model. For the self-associating compounds, besides the three scaling parameters two additional parameters have to be introduced, i.e. the association energy (well depth), ε_{AB} and the dimensionless association co-volume k_{AB}. The pure ε-caprolactam system was considered to be endowed with hydrogen bonding specific interactions occurring between the N—H group and the C=O group present on the aromatic ring, so that the model parameters required for it were a total of five and were retrieved by a non linear regression of pure component VLE data. Due to the fact that the energy of HB interaction established within the system was comparable with the mean field values, multiple solutions was provided by this fitting procedure, including one obtained by disregarding such association interaction. For this reason, to assess which was the most reliable set of parameters for pure ε-caprolactam, they were tested by correlating VLE data of several binary systems of ε-caprolactam respectively with octane, decane, dodecane, and acetic acid. For each of these four compounds the pure component parameters were already well established in the literature, with the alkanes not displaying any association parameter and with specific self interactions being present only in the case of acetic acid. The simplified PC-SAFT provided a satisfactory correlation capability for the four binary systems investigated, (the corresponding k_{ij} being the only fitting parameter for any binary system).In particular, in the case of ε-caprolactam/alkanes systems the corresponding k_{ij} was fixed equal to zero. In the case of the ε-caprolactam-acetic acid mixture, different kinds of cross hydrogen bonding interactions are expected to occur, in addition to the two self association interactions of the two pure compounds. In this respect for each kind of cross specific interaction established within the mixtures considered, the corresponding association term were obtained according to Elliot's mixing rule [352] so that they were predicted as a function of the corresponding pure component parameters and of the concentration. Once the most reliable set of parameters for pure ε-caprolactam have been successfully identified by this procedure, the binary system of interest for this study, i.e. the one formed by water and ε-caprolactam, was investigated. Two sets of VLE isothermal equilibriium data were simultaneously correlated quite satisfactory by assuming as only best fitting parameter the corresponding temperature independent k_{ij} parameter (k_{ij} = -0.07). The five parameters of self associating water were taken by the literature and again Elliot's mixing rule was adopted to obtain the parameters of the two types of cross association interactions which were expected to establish within the binary system (i.e the one among N—H groups and O—H groups and the one among C=O groups and O—H groups).

Having fully characterized the binary water/ε-caprolactam system, the other two binary systems of interest (i.e. polyamide 6/ water and polyamide 6/ε-caprolactam) were investigated, first determining the pure polymer parameters. To this aim, it has been assumed that one proton donor site (N-H) and one proton acceptor site (C = O) are present on each repeating unit. The pure polymer component parameters were then validated against VLE data of two binary systems (i.e. polyamide 6/toluene and polyamide 6/ ethyl benzene) for which the second component parameters were already well established in literature. The model correlations for the two systems considered, were fully satisfactory adopting the corresponding k_{ij} parameters as the only optimization parameter and were quite acceptable even assuming k_{ij} = 0. Once the parameters of the polymer were succesfully validated, the authors investigated the two binary systems of interest, i.e. polyamide 6/ water and polyamide 6/ε-caprolactam, in order to obtain the corresponding k_{ij} by best-fitting procedures (still assuming Elliot's mixing rule for cross association parameters). In Fig. 39 is reported, as an example, the result for the system polyamide 6/water in phase equilibrium with pure water. The model provided a quite satisfactory interpretation of data for both the binary systems obtaining from the best-fitting procedure of binary data a temperature-independent value of k_{ij}= -0.011 for the polyamide 6/ε-caprolactam system and a temperature dependent k_{ij} for the polyamide 6/water system (k_{ij}=-0.04 at T = 543.15 K).

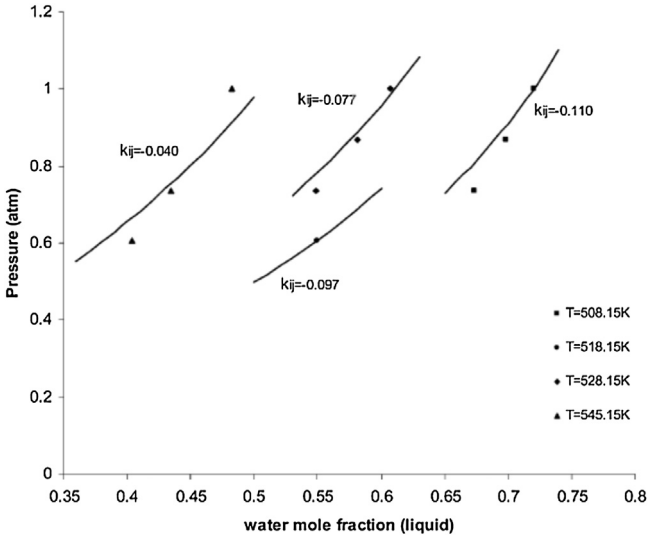

Fig. 39. VLE data (liquid refers to the polymer-water phase exposed to pure water vapor phase) for the binary system polyamide 6/water. Solid lines represent results of best fitting performed using simplified PC-SAFT with the temperature dependent k_{ij} as fitting parameter. Experimental data taken from [353]. Reprinted with permission from [351]. Copyright 2004 American Chemical Society.

Finally, once all the pure compound scaling parameters and each k_{ij} of the three associated binary sub-systems had been carefully estimated, the simplified PC-SAFT model was applied to predict the thermodynamics of the phase equilibrium between the binary water/ε-caprolactam vapor phase and the polyamide 6/ ε-caprolactam /water ternary system.

In Fig. 40 is reported the curve predicted by the model using the k_{ij}'s obtained from the respective binary systems the model predictions and the experimental data at T = 543.15 K. These calculations were performed at different assigned composition of the water/ε-caprolactam vapor phase and for a given experimentally measured concentration of one of the two penetrant within the ternary system, so that the other penetrant composition and the equilibrium pressure were calculated by imposing the phase-equilibrium conditions dictated by the equivalence of penetrant chemical potential in the two co-existing phases. In addition, in the same figure, is also reported the curve obtained by fitting the equilibrium data for ternary equilibrium using the binary k_{ij} for the polyamide 6/water system as fitting parameter (the value of k_{ij} was in this case estimated to be equal to -0.11, that is higher than the value obtained from the correlation of the polyamide 6/water binary data at the temperature of interest (i. e. -0.04 at545.15 K). In this case a much better accordance with data was obtained.

4.1.1.3. Applications of panayiotou-vera and NRHB. In this subsection, are presented some applications of Panayiotou and Vera, PV, and Non-Random Hydrogen Bonding, NRHB, models to

Please cite this article in press as: G. Mensitieri, G. Scherillo, C. Panayiotou et al. Towards a predictive thermodynamic description of Fsorption processes in polymers: The synergy between theoretical EoS models and vibrational spectroscopy. Mater. Sci. Eng. R (2020), https://doi.org/10.1016/j.mser.2019.100525

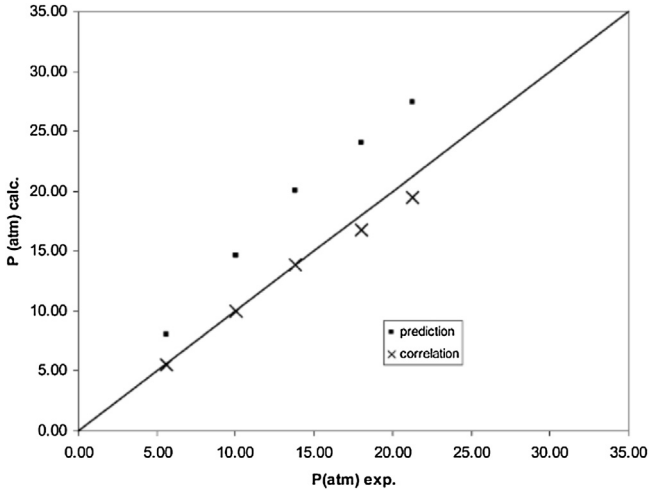

Fig. 40. Predicted and correlated and experimental total pressure data for the ternary system polyamide 6/water/ε-caprolactam at T = 543.15 K 543.15 K ((1) ε -caprolactam; (2) water (3) polyamide 6). Symbol ■ refers to model prediction, symbol x refers to model correlation using the k_{ij} parameter for the binary polyamide 6/water system as fitting parameter. The binary interaction parameters are k_{12} = - 0.07, k_{13} = - 0.04, k_{23} = -0.011 (prediction) and k_{12} = - 0.07, k_{13} = - 0.11, k_{23} = - 0.011 (correlation).Solid line represents the straight line P_{calc}=P_{exp}. Experimental data taken from [354]. Reprinted with permission from [351]. Copyright 2004 American Chemical Society.

polymer-penetrant systems endowed or not with inter- and intramolecular interactions.

Performances of the PV model [68,69] were compared to those of SL model in the paper by Garg et al. [338] in the case of polymer melts in phase equilibrium with a gaseous pure penetrant phase, ranging from low penetrant pressures up to supercritical conditions. In particular they focused on the poly(dimethyl siloxane) (PDMS)-carbon dioxide and on the polystyrene (PS)-1,1 difluoroethane systems. Due to the high solubility of the penetrants, in both cases a significant swelling of polymer melts occurs, so that at the temperature values characterized by the highest solubility of penetrant (at the lower temperatures), S-shaped solubility isotherms were found. After determination of the Lattice Fluids scaling parameters for pure penetrant and polymer, both the models were used to correlate different sorption isotherms, by assuming as best fitting parameter the binary mean field interaction parameter (assumed to be temperature dependent). The SL correlation capability was quite satisfactory, but a clear improvement was exhibited when using the PV model. Since the cross-mean field interactions differ significantly from the arithmetic mean value of the self-mean field interaction energies at the investigated temperatures, this results in a tendency to non-random distribution of contacts which is accounted for by the PV model but not by the SL model, which assumes random mixing. As an example of such comparative investigation, in Fig. 41a,b is reported the sorption isotherms of PDMS-CO_2 system along with curve fitting performed using SL and PV models.

In macromolecular systems, possible hydrogen bonding interactions influence rather strongly their thermodynamic properties. In Figs. 42 and 43 are presented vapor – liquid equilibrium data for polymer – solvent systems endowed with both self- and cross-association interactions, along with predictions (i.e. with k_{ij} = 0) and correlations (using k_{ij} as fitting parameter) provided by the NRHB model. Pure fluid parameters were taken from [99]. These results show that the NRHB model is able to satisfactorily predict (i.e. without the use of any binary adjustable parameter) the VLE of such binary mixtures, while, using one fitted binary interaction parameter, the model very accurately describes the solvent solubility in the liquid phase.

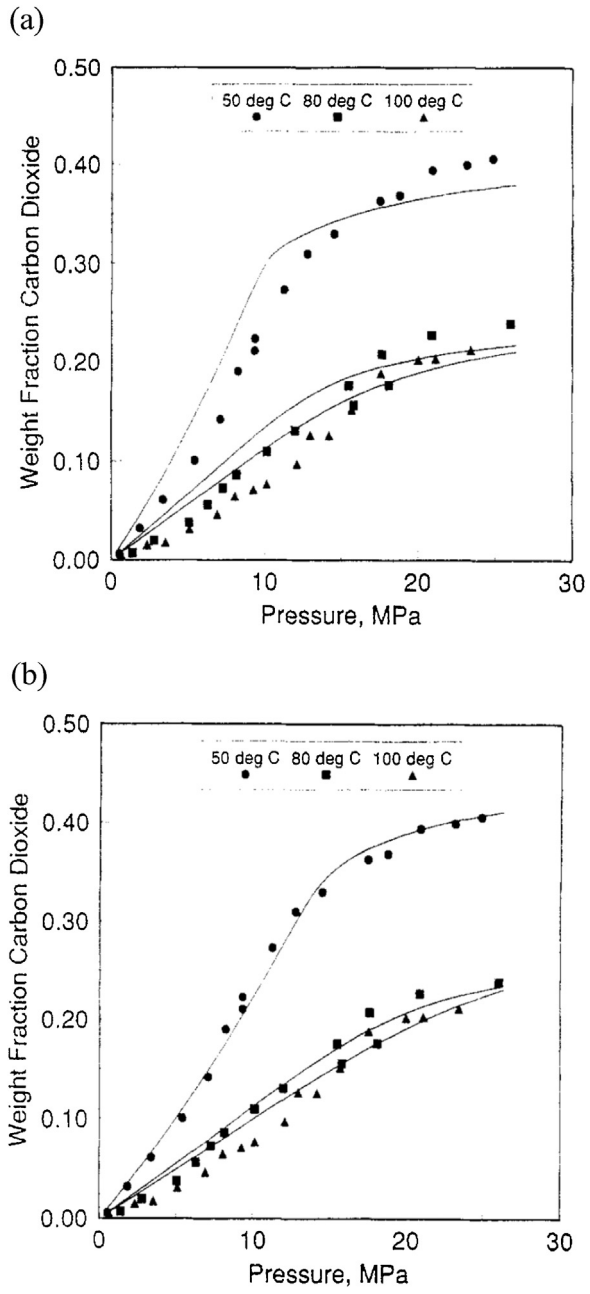

Fig. 41. (a) Sorption isotherms of CO_2 in PDMS. Solid lines represent best-fitting curves obtained with SL model. Reprinted with permission from [338]. Copyright 1994 American Chemical Society. (b) Sorption isotherms of CO_2 in PDMS. Solid lines represent best-fitting curves obtained with PV model. Reprinted with permission from [338]. Copyright 1994 American Chemical Society.

Missopolinou et al. [92,93] used a slightly different version of the NRHB, which assumes that the intersegmental energy, ε*, and the close packed volume, v_{sp}* are temperature independent, while the segment volume v* is an adjustable fluid-specific parameter. They applied the model to systems with alkoxy-alkanols, compounds which are capable for both intra- and inter-molecular association. In particular, they applied the NRHB model to interpret data for excess enthalpies of binary mixtures of 2-ethoxyethanol with several hydrocarbons. Examples of the curve fitting of the heat of mixing are reported in Figs. 44 and 45. Fitting parameter were the binary interaction parameter used in the Berthelot-type combining rule for cross interaction energy, ξ_{12}, and the binary parameter, ζ_{12}, used for the calculation of the cross term, v^*_{12},

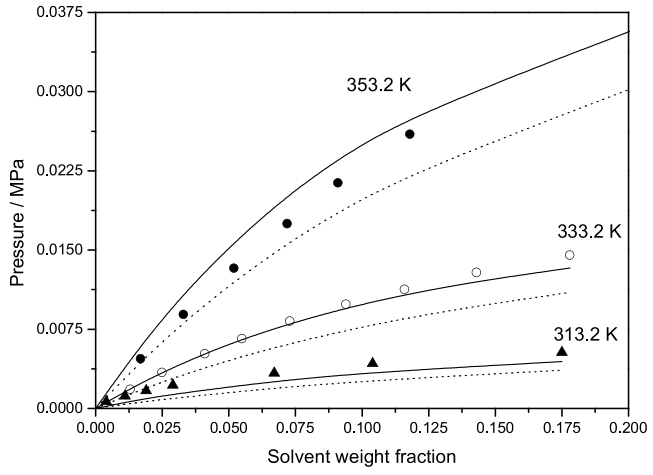

Fig. 42. Butanol – poly(vinyl acetate) VLE. Experimental data [355] (points), NRHB predictions (dotted lines, k_{ij} = 0) and correlations (solid lines, k_{ij} = 0.01372). Pure fluid parameters from reference [99].

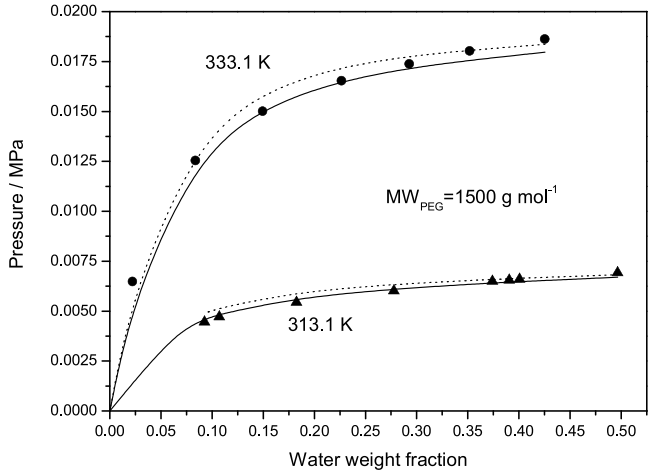

Fig. 43. Water – Poly(ethylene glycol) VLE. Experimental data [356] (points), NRHB predictions (dotted lines, k_{ij} = 0) and correlations (solid lines, k_{ij} = 0.01238) with pure fluid parameters from reference [99].

appearing in the expression for the average segmental volume calculations, v^*, according to the following equations that are specific for the adopted version of NRHB model [93]:

$$v^* = \phi_1 v_1^* + 2\phi_1\phi_2 v_{12}^* + \phi_2 v_2^* \quad (265)$$

$$v_{12}^* = \zeta_{12}\left(\frac{v_1^{*}1/3 + v_2^{*}1/3}{2}\right)^3 \quad (266)$$

After the fitting procedure, the model was used to calculate the separate contributions from non-hydrogen-bonding (dispersion and polar) interactions, from intermolecular, as well as from intramolecular hydrogen bonds, also shown in Figs. 44 and 45.

Interestingly, the behaviour of the binary mixture with benzene is different in two points: the maximum and the shape of the H^E curve. The maximum value is about half the values of the systems with the n-alkanes. The decreased maximum value for the benzene system could be explained on the basis of the occurrence of σ-π hydroxyl – aromatic ring interactions (exothermic process). The asymmetric shape of the H^E curve could be explained by the difficulty of breaking the interactions in the 2-ethoxyethanol - rich region: In this region, the low presence of benzene fails to break the interactions of the pure 2-ethoxyethanol, while in the benzene-rich region the breakage of the intermolecular hydrogen bonding is rather extensive.

As observed in Figs. 44 and 45, the contribution of the intramolecular hydrogen bonds to the heats of mixing of the studied systems is by no means negligible. The important point is that its contribution is negative (exothermic). An explanation of this negative contribution comes from spectroscopic data [79], that indicated that at low concentration, the degree of intramolecular hydrogen bonding is increasing with increasing mole fraction of 2-ethoxyethanol much more than the degree of intermolecular hydrogen bonding. It is also known that, at the low concentration region, the inert solvent does not influence essentially the intramolecular hydrogen bonds, while it causes the destruction of the intermolecular bonds, as the interacting molecules fail to come close together (proximity condition).

The prediction of the NRHB model for the contribution of intermolecular hydrogen bonding is positive for all binaries, while the contribution of the van der Waals interactions are negative (exothermic) for the system with benzene but positive (endothermic) for the other systems with *n*-alkanes, which corroborates the above established picture.

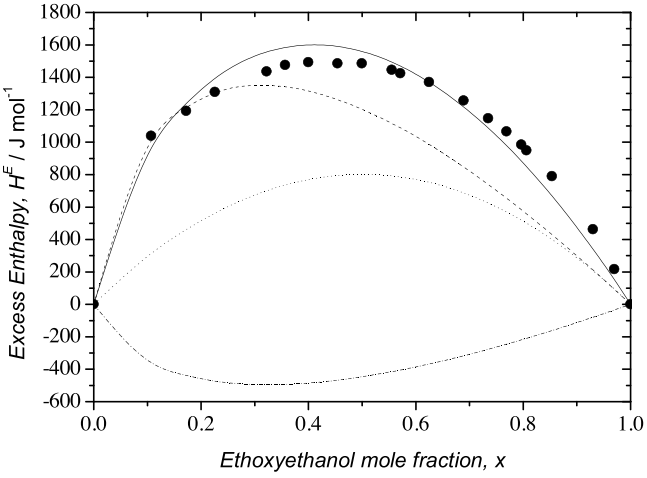

Fig. 44. Experimental (points) [93] and calculated (lines) heats of mixing for the system *x* 2-ethoxyethanol + (1-*x*) n-octane at 318.15 K. The contributions from intermolecular hydrogen bonds (dash,—), dispersive interactions (dot,···), and intramolecular hydrogen bonds (dash dot,-·-·-) are shown by separate lines.

Please cite this article in press as: G. Mensitieri, G. Scherillo, C. Panayiotou et al. Towards a predictive thermodynamic description of Fsorption processes in polymers: The synergy between theoretical EoS models and vibrational spectroscopy. Mater. Sci. Eng. R (2020), https://doi.org/10.1016/j.mser.2019.100525

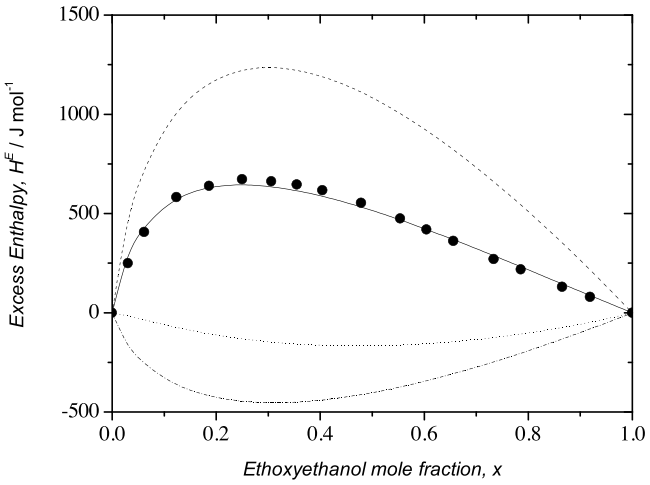

Fig. 45. Experimental (points) [93] and calculated (lines) heats of mixing for the system *x* 2-ethoxyethanol + (1-*x*) benzene at 318.15 K. The contributions from intermolecular hydrogen bonds (dash,—), dispersive interactions (dot,···), and intramolecular hydrogen bonds (dash dot,-·-·-) are shown by separate lines.

In binary mixtures of benzene with plain ethers there are no hydrogen bonding interactions. It is worth pointing out that the enthalpies of mixing for these binaries are negative. Typical examples are the mixtures of 1,4-dioxane with benzene at different temperatures [357] and of 1,2-dimethoxyethane (an isomer to 2-ethoxyethanol) with benzene [358,359]. The latter experimental data are compared with the predictions of the NRHB model for the system *x* 2-ethoxyethanol + (1-*x*) benzene in Fig. 46 and, as is shown, the experimental values for the binary mixture with 1,2-dimethoxyethane coincide with the calculated contribution of the dispersive (non-hydrogen bonding) interactions. From literature data we also see positive enthalpies of mixing in binaries of n-alkanes or cycloalkanes with ethers. Typical examples are the mixtures of n-hexane or cyclohexane with 1,2-dimethoxyethane [360]. This further supports the validity of NRHB model.

An example of the synergic use of gravimetric and spectroscopic experimental analyses in combination with NRHB model to interpret sorption thermodynamics for the case of a rubbery polymer endowed with specific interactions (associations) by hydrogen bonding, is the case of water sorption in poly propylene sebacate (PPSeb) [362]. PPSeb is a biodegradable semicrystalline aliphatic polyester with a glass transition temperature and a melting temperature respectively equal to -53.1 °C and 56.8 °C [363]. Sorption isotherms have been determined gravimetrically at several temperatures while qualitative and quantitative information on water and polymer self-hydrogen bonding and water-polymer cross associations established in the polymer-water mixture, at phase equilibrium with pure water vapor at different pressures, have been gathered by means of in-situ FTIR transmission spectroscopy. The structure of the association adducts has been investigated, highlighting several kinds of water 'species' and identifying the chemical groups of the macromolecule actually involved in the specific self-association and cross-interaction with absorbed water molecules. This information has been used to tailor the structure of the NRHB equations adopted to interpret sorption thermodynamics, identifying the specific association to be accounted for. The model has been used to fit water sorption isotherms and then to predict the amount of different types of self-hydrogen bonding (i.e. water-water and polymer-polymer) and cross-hydrogen bonding (i.e. water-polymer) established within the water-polymer mixture, that have been compared to the corresponding values calculated on the basis of FTIR spectroscopy.

It is worth mentioning that the NRHB model has been developed for amorphous polymers. The use of this theoretical approach in the case of semi-crystalline PPSeb has been justified by assuming [362,364] that the crystalline phase is impervious to water and thus a simple rescaling of the overall solubility is adopted to account for the fraction of amorphous phase. However, there is the possibility that the crystalline phase, even being actually not able to sorb water molecules, exerts a constrain effect that could partially affect the predictive capability of the NRHB approach.

The water-PPSeb system is endowed with a number of possible specific interactions. Self-HB establish among proton donors, PDs, and proton acceptors, PAs, groups present on water molecules (it is assumed that each water molecules carries two proton donors, that are the two hydrogen atoms, and two proton acceptors, i.e. the two lone electron pairs on the oxygen atom) that is identified as '11' interaction. Self-HB interactions can involve also polymer molecules. In fact, possible interactions are those between terminal OH groups acting both as PA and PD, (OH/OH interaction labelled as' 33') and those between the carbonyl groups along the chain, acting as PA, and the terminal OH groups acting as PD (OH/C=O interaction labelled as' 32'). Cross-HB establish between PD groups on water molecules and the carbonyls in PPSeb backbone (H_2O/C=O interaction labelled as' 12'). Two further interactions are those between terminal OH groups of the macromolecule acting as PD and oxygen atom of a water molecule acting as PA (OH/H_2O interaction labelled as' 31') and between terminal OH groups of the macromolecule acting as PA and hydrogen atoms of a water molecule acting as PD (H_2O/OH interaction labelled as' 13').

The results of the FTIR analysis, performed at 30 °C, point to the involvement of terminal hydroxyls on PPSeb in a medium strength H-bonding interaction, as proton donors, with C=O acceptors present on the backbones. This self-interaction does not seem to be significantly perturbated by the presence of sorbed water. Based on the analogies of the H_2O/PPSeb system with the H_2O/PCL system [271] and exploiting the information gathered from complementary spectroscopic approaches (i.e. 2D-COS and LSCF analyses of the OH band of absorbed water for the difference spectra as well as ab-initio, quantum chemistry calculations), authors interpreted the outcomes of vibrational spectroscopy concluding that two water 'species' are present: first shell, '*fs*', water molecules bridging, by hydrogen bonding, two carbonyl groups ('12'

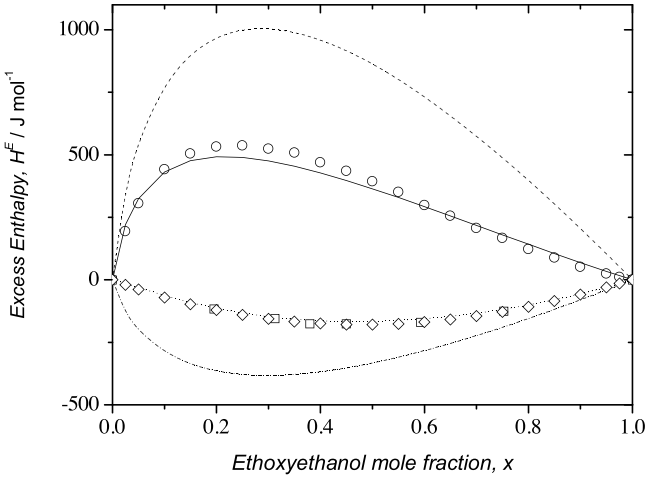

Fig. 46. Comparison of the experimental [361] excess molar enthalpies, H^E, at 298.15 K for the system *x* 2-ethoxyethanol + (1-*x*) benzene, ○, with the predictions of the NRHB model for the contributions from intermolecular hydrogen bonds (—), dispersive interactions (···), intramolecular hydrogen bonds (-·-·-) and the total H^E ( ). The contribution of dispersive interactions is compared with the experimental H^E for the system *x* 1,2-dimethoxyethane + (1-*x*) benzene: □, data from ref. [358]; ◇, data from ref. [359].

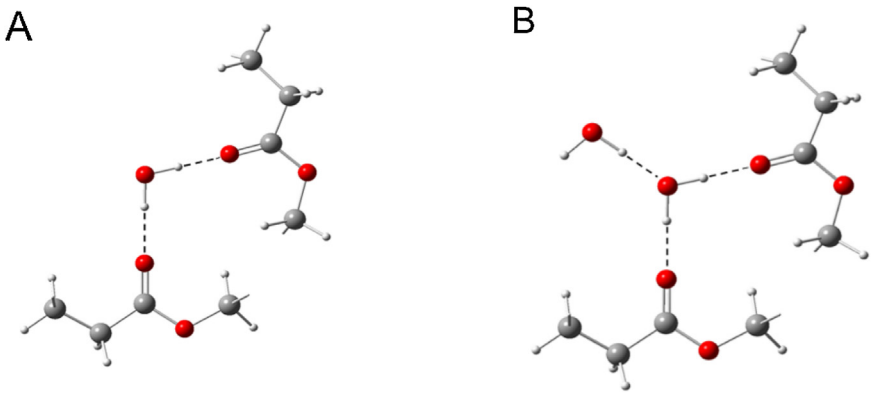

Fig. 47. Schematic representation of the two water species identified by the spectroscopic analysis of the H_2O/PPSeb system: (A) *first shell* water, (B) *second shell* water.

interaction) and second shell, '*ss*', water molecules self-associated to first shell water molecules via HB-interaction involving an hydrogen atom of an *ss* water molecule and the oxygen atom of a *fs* water molecule ('11' interaction). The two kinds of molecular aggregates are schematically represented in Fig. 47.

Quantitative assessment of the concentration of each of the two water species (C_{fs} and C_{ss}) was obtained by elaborating the analytical peaks attained by the LSCF analysis of the OH band of absorbed water. To this aim, the same molar-absorptivity values ((ε_{fs} and ε_{ss}) as determined in the case of the H2O/PCL system [271] were used, in view of the mentioned close similarities between the two systems. The concentrations of the two water species at 30 °C, evaluated by using this procedure, are reported in Fig. 48 as a function of the relative pressure of H_2O vapour in phase equilibrium with the H_2O/PPSeb mixture. In the same figure are also reported the sum of the concentrations of the two water species evaluated spectroscopically and the sorption isotherm evaluated gravimetrically. There is a perfect coincidence between the spectroscopic and the gravimetric estimates providing evidence that the possible contribution of other molecular species (i.e. other interactions involving water molecules) are below the detection limit of the adopted technique.

Water sorption thermodynamics was interpreted by using the NRHB model. In the implementation of the model, the molar volume change upon formation of any type of hydrogen bonding has been assumed to be equal to zero. In the case of water, lattice fluid scaling parameters and the E^0_{11} and S^0_{11} self HB parameters (i.e. '11' interaction) have been taken from the literature [365]. In the case of PPSeb, the lattice fluid scaling parameters were calculated by fitting PVT data (see Fig. 49) while the HB self-interaction parameters (i.e. '32' and 33' interactions) were taken from the literature [95,365,366]. Regarding the cross-interactions, the parameters associated with cross HB '31' (i.e. E^0_{31} and S^0_{31}) and '13' (i.e. E^0_{13} and S^0_{13}) have been calculated as geometric mean of the corresponding parameters for the '33' and '11' interactions [366] (as a consequence, $E^0_{31} = E^0_{13}$ and $S^0_{31} = S^0_{13}$). The only parameters used to fit gravimetric sorption isotherms were the mean field interaction parameter, k_{12}, and the molar internal energy of formation and entropy of formation of '12' interaction, respectively E^0_{12} and S^0_{12}. The NRHB model provided an excellent concurrent fitting (see Fig. 50) of the water sorption isotherms at four different temperatures (25, 30, 35 and 40 °C) with the following values of the parameters: k_{12} = -0.092, E^0_{12} = -12.715 kJ/mol and S^0_{12} = -10.23 J/(mol K). Fitting performed by using only E^0_{12} and S^0_{12} as fitting parameters and imposing k_{12} = 0, resulted to be significantly worse (see Fig. 50).

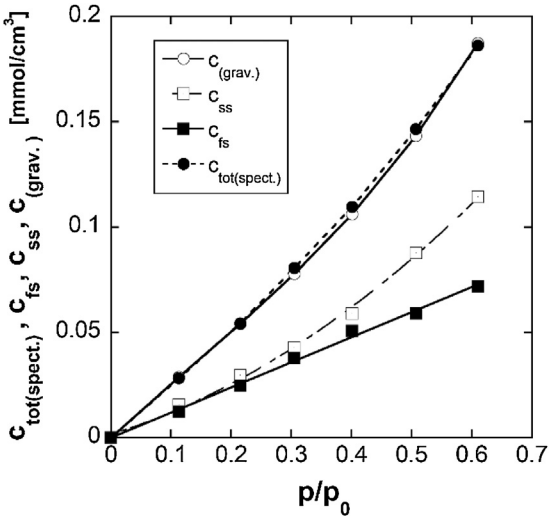

Fig. 48. H_2O/PPSeb system at phase equilibrium with water vapour at different relative pressures, at T = 30 °C. Total concentration of water absorbed in PPSeb as estimated spectroscopically ($C_{tot\ (spect.)}$) and from gravimetric measurements ($C_{(grav.)}$), concentration of first shell water (C_{fs}), concentration of second shell water (C_{ss}), reported as a function of the relative pressure of water vapour. Reprinted with permission from [362]. Copyright 2016 Elsevier Ltd.

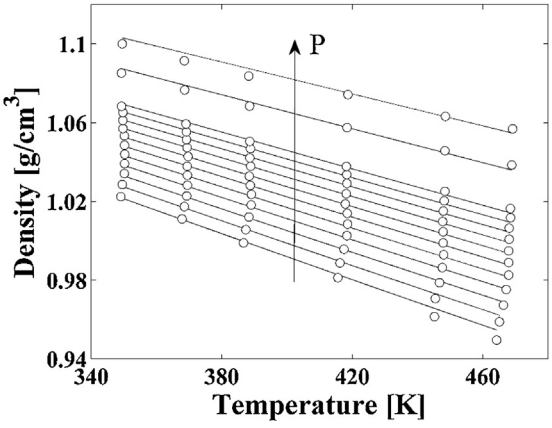

Fig. 49. PVT behaviour of PPseb. Comparison between experimental densitytemperature isobars of PPseb in amorphous equilibrium state (points) and the best fitting prediction of the NRHB model (lines). Isobars pressure values are equal to 0.101325, 10,20, 30,40, 50, 60, 70,80, 90, 100, 150 and 200 MPa. Reprinted with permission from [362]. Copyright 2016 Elsevier Ltd.

Please cite this article in press as: G. Mensitieri, G. Scherillo, C. Panayiotou et al. Towards a predictive thermodynamic description of Fsorption processes in polymers: The synergy between theoretical EoS models and vibrational spectroscopy. Mater. Sci. Eng. R (2020), https://doi.org/10.1016/j.mser.2019.100525

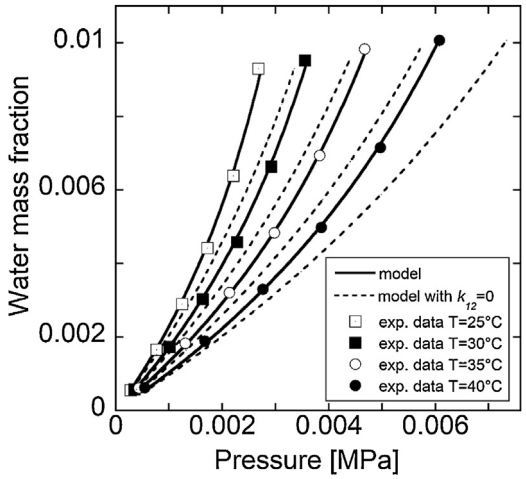

Fig. 50. Water sorption isotherms in PPseb at T = 25, 30, 35 and 40 °C. Points represent experimental data determined gravimetrically. Continuous and dotted lines represent, respectively, best fitting curves provided by the NRHB model including k_{12} as fitting parameter and by the NRHB model with k_{12} = 0. Reprinted with permission from [362]. Copyright 2016 Elsevier Ltd.

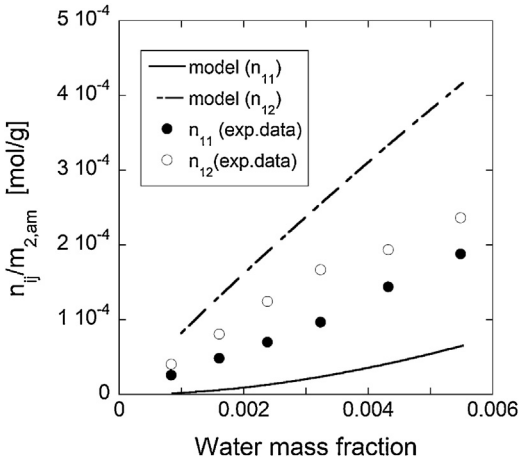

Fig. 52. Comparison of predictions of NRHB model with results of spectroscopic analyses for the amount of self-HB ('11') and cross-HB ('12') established by water molecules in the H_2O/PPSeb at 30 °C. Reprinted with permission from [362]. Copyright 2016 Elsevier Ltd.

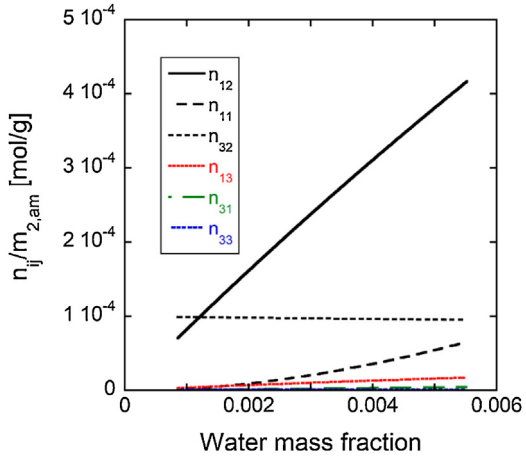

Fig. 51. NRHB predictions for the amount (expressed in moles per gram of amorphous polymer) of the different types of HB contacts established in the PPseb-water mixture at equilibrium with water vapour at several values of relative pressure, at 30 °C. Reprinted with permission from [362]. Copyright 2016 Elsevier Ltd.

The use of NRHB model to perform fitting of isotherms, besides providing estimates of model parameters, supplied also quantitative estimates of the amount of the different kinds of hydrogen bondings established in the H_2O/PPSeb system (see Fig. 51). These estimates are in qualitative agreement with the outcomes of vibrational spectroscopy analysis. In fact, the prevailing self-interactions are the OH/C=O (i.e. '32'), that remain rather constant in value and unaffected by the presence of water, as also indicated by the results of vibrational spectroscopy investigation. The other significant self-interaction is of the H_2O/H_2O type (i.e. '11') while most of the cross-interactions are the H_2O/C=O (i.e. '12').

In particular, in Fig. 52 the estimates of the concentration of self-HB H_2O/H_2O contacts (i.e. '11' interaction) and of the concentration of cross-HB H_2O/C=O (i.e. '12' interaction) provided by the NRHB model are compared with the results of spectroscopic analyses (after proper transformation of the amount of the different water species in terms of amount of hydrogen bonds). The model is able to capture the qualitative behaviour detected spectroscopically, although the quantitative matching is not entirely satisfactory. The reason of this quantitative mismatch has been tentatively attributed by the authors to the presence of interphase regions, characterized by sorption thermodynamics properties that are in-between those of rubbery amorphous regions and of crystalline domains. Another possible source of this partial discrepancy has been identified in the molecular weight distribution of the investigated PPSeb samples, caused by the polymerization process, that does not allow a reliable estimate of the amount of terminal OH groups.

NRHB modelling of sorption thermodynamics has also been used to investigate the CO_2/PCL system [257], in combination with Raman spectroscopy and with quantum chemistry calculations followed by complete normal coordinate analysis for the calculation of the Raman spectra.

CO_2 sorption in molten PCL (T = 353 K) at elevated pressures (up to 7.1 MPa) has been investigated experimentally using a Raman line-imaging setup, suitably arranged to allow, after proper calibration, the quantitative assessment of carbon dioxide concentration in both the time-resolved and the space-resolved modes. The resulting perturbation of the spectral features with respect to reference systems were analysed to investigate the effects of carbon dioxide – polymer interactions on the vibrational pattern. A schematic illustration of the experimental set-up is reported in Fig. 53. A laser beam is focused onto a pendant drop of molten PCL located in a temperature controlled and optically accessible pressure chamber, allowing the detection of the 90°-scattered light. The chamber is connected, by service lines, to a syringe pump that pressurizes the CO_2 and to a pressure transducer. The laser power is concentrated in an approximately cylindrical volume with a diameter of 100 μm ca. The Raman signals are detected from several positions along the waist of the laser beam focus, through the detection part of the Raman line imaging setup. The set up allows resolving the length of the measurement volume in 40 increments of 64 μm length each. The inelastically scattered light from each of these 40 measurement positions is dispersed in its wavelength components resolving a wavelength range of 546 nm up to 605 nm, corresponding to a Raman shift range of 480 cm^{-1} up to 2270 cm^{-1} (collection of 40 Raman spectra).

In Fig. 54 are compared the spectrum collected for the neat PCL at 353 K and atmospheric pressure and the spectrum of the CO_2/PCL mixture at 353 K at equilibrium with gaseous CO_2 at 6.2 MPa.

Please cite this article in press as: G. Mensitieri, G. Scherillo, C. Panayiotou et al. Towards a predictive thermodynamic description of Fsorption processes in polymers: The synergy between theoretical EoS models and vibrational spectroscopy. Mater. Sci. Eng. R (2020), https://doi.org/10.1016/j.mser.2019.100525

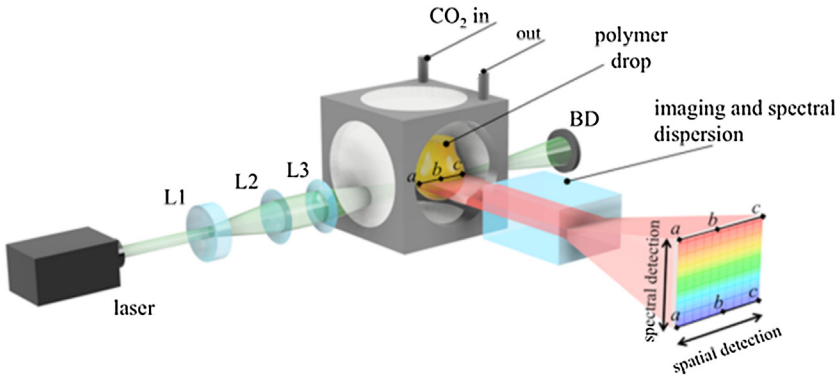

Fig. 53. Schematic illustration of the experimental setup for Raman line-imaging. Reprinted with permission from [257]. Copyright 2016 American Chemical Society.

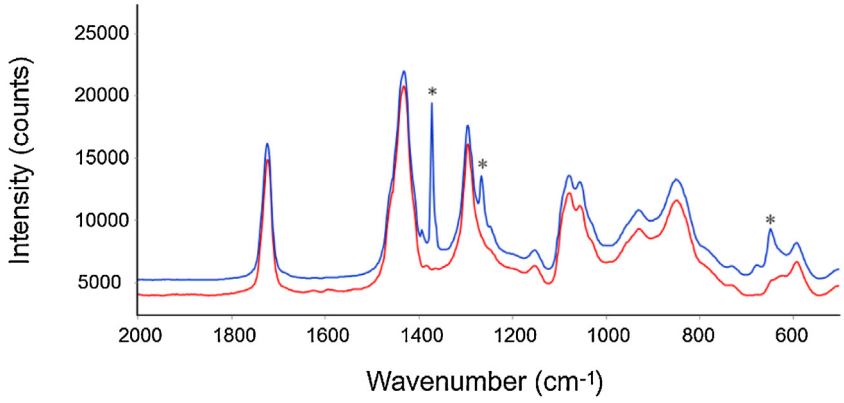

Fig. 54. Raman spectra collected for neat PCL (red trace) and for a PCL/CO_2 mixture after equilibration with gaseous CO_2 at 353 K and 6.2 MPa (blue trace, arbitrarily shifted for comparison purpose). Reprinted with permission from [257]. Copyright 2016 American Chemical Society. (For interpretation of the references to colour in this figure legend, the reader is referred to the web version of this article.)

Both spectra were collected at the centre of the drop. Three fully resolved peaks at 1294, 1430, and 1722 cm^{-1} are evident for the neat PCL while, in the case of the polymer equilibrated in gaseous CO_2, characteristic peaks of the absorbed carbon dioxide are identified at 1371 1264 and at 676 – 648 cm^{-1}. The spectrum of dissolved carbon dioxide was isolated by subtracting the spectrum of neat PCL from that of CO_2/PCL mixture. In Fig. 55 is compared the subtraction spectrum for the case of CO_2/PCL mixture equilibrated at 6.2 MPa with the spectrum of gaseous CO_2 at 6.2 MPa, at T = 353 K. In the difference spectrum it is evident a derivative type feature, centred at 1722 cm^{-1}, associated to a *blue shift* of the C=O stretching vibration of PCL. The couple of signals at 1371 and 1264 cm^{-1} in the difference spectrum is a Fermi dyad. These two components appear to be *red-shifted* in the PCL solutions with respect to the gas phase. Based on the values of these shifts – corrected to properly account for Fermi resonance effects which perturb the true vibrational frequencies of the original transitions - the authors estimated that the partial molar volume of CO_2 in the PCL solution amounts to 39.8 cm^3/mol, being constant in the whole investigated range of pressure.

By combining a spectroscopically available quantity (i.e. the ratio of the intensity of the peak at 1371 cm^{-1}, the upper Fermi-dyad, and of the intensity of the carbonyl peak at 1722 cm^{-1}, I_{uFd}/I_C) with gravimetric sorption isotherm, it was possible to convert the spectroscopic signals into absolute concentration values of CO_2.

Quantum chemistry calculation on model PCL/CO_2 aggregates and Raman spectroscopy analysis indicated that the most relevant interaction is of Lewis acid–Lewis base (LA–LB) type and involves the carbon of CO_2 as electron acceptor and the oxygen of the > C = O unit on PCL as electron donor. On this basis, the NRHB model used to interpret sorption thermodynamics has been structured to account only for the LA-LB interaction involving the carbonyls. The model provides a very good fitting of gravimetric sorption isotherm data at 353 K, collected up to 5 MPa, using as fitting parameters the mean-field binary interaction parameter, k_{12} (= 0.182) and the molar Helmholtz energy of formation of the specific CO_2–carbonyl interaction (= −11,000 J/mol [367].

The NRHB model has been used to predict the molar volume of PCL/CO_2 mixtures (see Figs. 56A,B) in equilibrium with gaseous CO_2. The predictions are in excellent agreement with available data [367,368]. The EoS model provided also estimates for the values of partial molar volume of CO_2 in the polymer mixture. The average value predicted for partial molar volume of CO_2, in the range of interest, was 3809 cm^3/mol, that is close to the value of 39.8 cm^3/mol, calculated from the vibrational spectroscopy analysis (see Fig. 57).

Finally, based on ab-initio calculations and Normal Coordinate Analysis (NCA) - performed on an appropriate low molecular-weight model compound (the chosen molecule was Pentylhexanoate, PHEX), suitably selected to mimic the chain segments where the relevant conformational degree(s) of freedom is (are) localized - the authors identified the most stable supramolecular complex and the preferential site of interaction on the polymer backbone, and evaluated theoretically the Raman spectra of the adduct according to the normal coordinate method. This analysis indicated that the stability of the supramolecular complex is controlled more by the accessibility of the donor than by its electron-density and evidenced also the role played by the

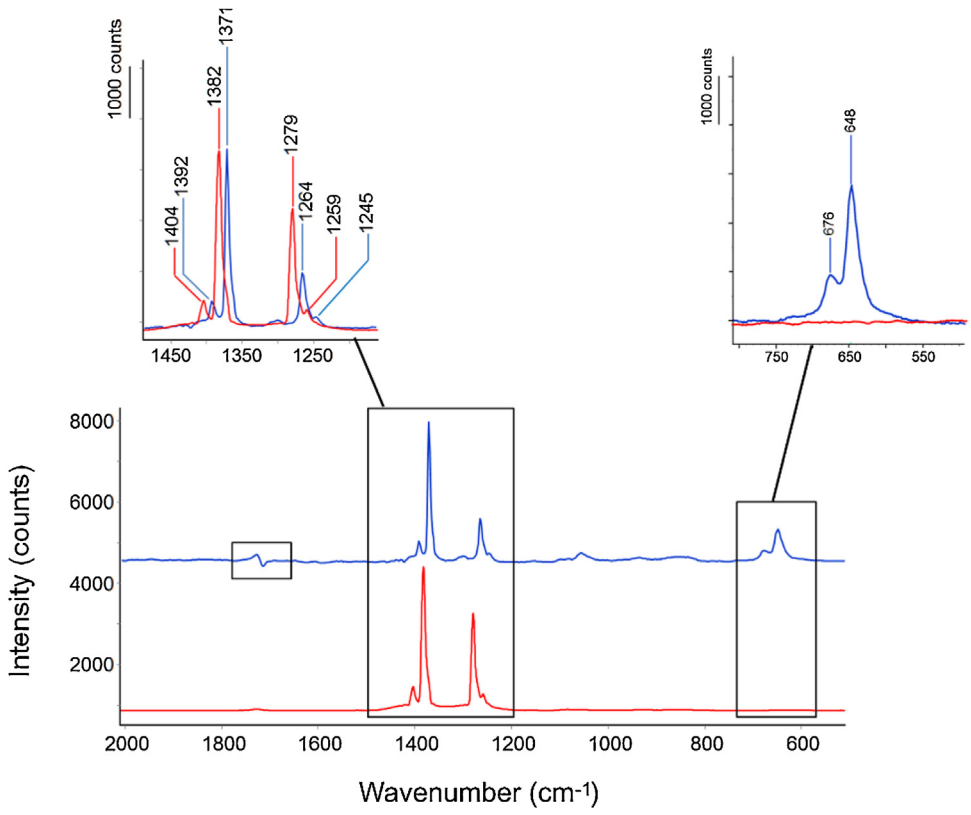

Fig. 55. Red trace: Raman spectrum of gaseous CO_2 (at 353 K 6.2 MPa) collected in the region surrounding the drop. Blue trace (shifted for comparison purposes): Difference spectrum (at 353 K and 6.2 MPa). The difference spectrum is representative of CO_2 dissolved in PCL. The insets report a comparison of the difference spectrum with the gas-phase spectrum in selected ranges. Reprinted with permission from [257]. Copyright 2016 American Chemical Society. (For interpretation of the references to colour in this figure legend, the reader is referred to the web version of this article.)

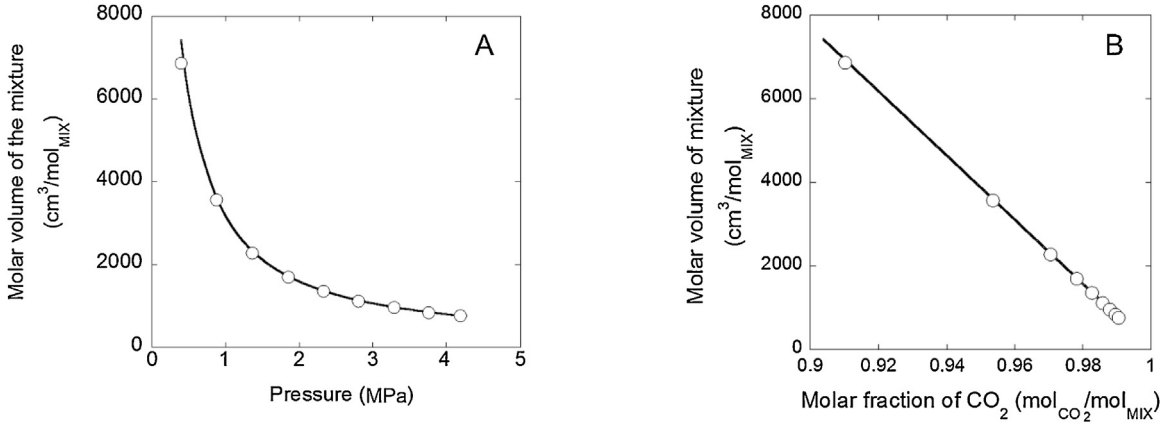

Fig. 56. Experimental values (empty circles) of molar volume of the PCL/CO_2 mixtures [367,368] and theoretical predictions provided by NRHB model (continuous line) reported as function of: (A) pressure at sorption equilibrium and (B) molar fraction of dissolved carbon dioxide at sorption equilibrium. Reprinted with permission from [257]. Copyright 2016 American Chemical Society.

occurrence of weak H-bonds acting cooperatively to stabilize the supramolecular Lewis acid – Lewis base complex. These calculations confirmed that the CO_2/PCL interactions involve preferentially PCL carbonyls identifying as most likely geometry for the interaction complex the one reported in Fig. 58. Another relevant outcome of this analysis is that the doublet appearing at $676 - 648\ cm^{-1}$, in the spectra of the PCL/CO_2 solutions, is generated by the bending modes of carbon dioxide and is to be considered as a specific signature for the occurrence of an attractive interaction of the CO_2 with PCL since it appears as a consequence of a significant distortion from linearity of the molecule induced by the interaction.

4.1.1.4. Comparing NRHB theory and the SAFT family of models. On the basis of the structure of the two main classes of models discussed in this review, the NRHB model and the SAFT 'family' of models, in our opinion, the two approaches display similar performances when using the same number of parameters. The SAFT models, thanks to the possibility of adding up several types of Helmholtz energy contributions, is more flexible and able to deal

Please cite this article in press as: G. Mensitieri, G. Scherillo, C. Panayiotou et al. Towards a predictive thermodynamic description of Fsorption processes in polymers: The synergy between theoretical EoS models and vibrational spectroscopy. Mater. Sci. Eng. R (2020), https://doi.org/10.1016/j.mser.2019.100525

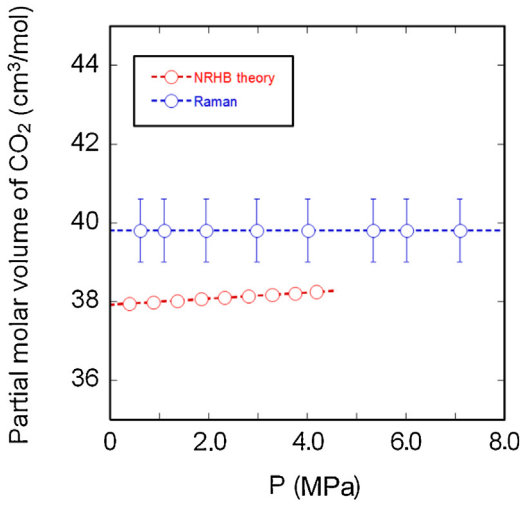

Fig. 57. Partial molar volume of carbon dioxide in PCL – CO_2 mixtures at sorption equilibrium with gaseous CO_2 at different pressures. Values predicted by the NRHB theory (red symbols) and values calculated from Raman spectroscopy (blue symbols). Reprinted with permission from [257]. Copyright 2016 American Chemical Society. (For interpretation of the references to colour in this figure legend, the reader is referred to the web version of this article.)

with more complex systems, although at the expenses of a higher calculation complexity and a higher number of parameters to be determined.

At the best of our knowledge, there are no contributions available in the literature comparing systematically the performances of these two classes of models for systems involving polymer species. There are, however, a few manuscripts where the performances are compared in the case of mixtures involving low molecular weight compounds. These results are briefly summarized in the following.

A first investigation aimed at comparing the performances of NRHB model with those of the CK-SAFT model [49,116] was performed by Tsivintzelis et al. [95]. The authors investigated the phase behaviour of different low molecular weight binary and ternary systems, including also systems displaying polar and associating (hydrogen bonding) interactions. On the bases of this investigation, the authors claimed that NRHB model provides in many cases more accurate correlations for pure components and for binary systems involving self-associating components, whereas

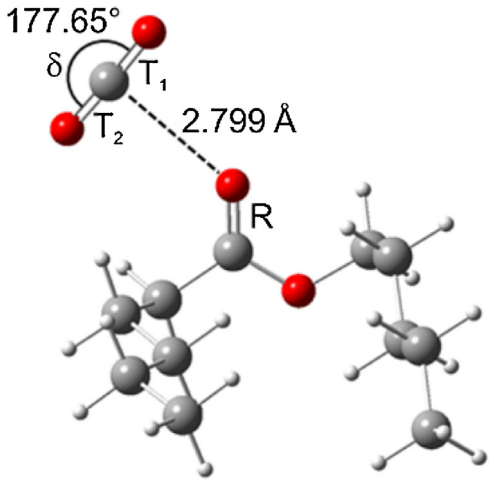

Fig. 58. Optimized structure of the PHEX/CO_2 complex. Color code: white = H; grey = C; red = O. (For interpretation of the references to colour in this figure legend, the reader is referred to the web version of this article.)

the two models display similar performances in describing phase equilibria correlation of highly asymmetric binary non-polar systems.

Afterwards, a more extensive comparison on the modelling capability of NRHB approach and of sPC-SAFT theory [135] was reported by Grenner et al. [94] and by Tsivintzelis et.al. [96].

In the first contribution, the authors investigated more than 100 different binary mixtures of low molecular weight compounds, considering systems whose components were respectively non-polar, weakly polar, strongly polar and/or endowed with hydrogen bonding specific interactions, and focusing, in particular, on the modelling capability of vapor-liquid equilibria. To this aim the models were also used to retrieve pure components parameters from vapor-liquid equilibria. The performances of both approaches were substantially equivalent.

In the second paper, the authors selected several binary mixtures of low molecular weight compounds endowed with polar and/or hydrogen bonding specific interactions, focusing on the corresponding liquid-liquid equilibria. The overall conclusion derived from this extensive investigation is that both models provide satisfactory and quite similar results in terms of fitting and predictive capability on the phase equilibria behaviour. In particular, for liquid-liquid equilibria, NRHB provides more accurate correlations, whereas the sPC-SAFT provides more accurate predictions. Moreover, both the models provided similar predictions for the fraction of non hydrogen bonded molecules in different systems, ranging from pure alkanols a to alkanols-n-hexane mixtures.

A further, more challenging comparison of the predictive capability of the NRHB model respect to the PC-SAFT model in its version for polar fluids, i.e the Perturbed-Chain Polar statistical associating theory (PCP-SAFT), has been performed by Paduszynski et al. [369]. In particular, the authors modelled the phase diagrams of several binary complex associating systems formed by an ionic liquid (PMPIP][NTf2] and an alcohol of different chain length (ranging from butan-1-ol to undecane-1-ol). To this aim, according to a previous work of Tsioptsias et al. [370], NRHB model was implemented by explicitly accounting for physical (dispersive) interactions and, in addition, treating ionic, polar and HB specific interactions established within the mixture, as strong specific interactions all described by means of Veytsman statistics. Conversely, in the implementation of PCP-SAFT, the dipolar interactions were independently accounted for by adding the Gross-Vrabec term (which does not introduce further parameters) to the residual Helmholtz energy. Moreover, ionic interactions were described associating a permanent dipole moment to the ionic liquid molecule. The authors found that both the models displayed similar performances in predicting the pure fluid properties of ionic liquids (with one set of pure component parameters) as well as in describing the liquid-liquid equilibria phase diagrams for each of the different binary systems investigated.

4.1.2. Sorption themodynamics in glassy polymers

4.1.2.1. Applications of NELF (NETGP-SL) theory. To deal with sorption thermodynamics in non-equilibrium glassy polymers one needs to use suitable modelling approaches accounting for the out-of-equilibrium nature of the material. In this sub-section we analyse in some details the NELF theory, that is able to cope with the glassy nature of the polymer for systems that are not endowed with specific interactions.

As discussed in sub-section 2.2.1 of this review the Non-Equilibrium Lattice Fluid (NELF) model was developed by applying the NETGP procedure to extend the equilibrium SL model to deal with polymer-penetrant systems in a glassy state [50]. Further

development was the application of NETGP procedure, respectively, to a version of the SAFT equation of state which did not account for specific interactions and to the Perturbed Hard Sphere Chain Theory (PHSCT). These two extensions will be discussed in sub-section 4.1.2.2.

In sub-section 2.2.1 it has been illustrated that a key point in the implementation of NETGP is that this procedure relies on the knowledge of the polymer density in the polymer-penetrant mixture, i.e. the value of $\rho_{P,\infty,}$ that is asymptotically attained under phase PE conditions, at each imposed pressure, temperature and concentration of the penetrant phase in contact with the polymer sample, or, for the case of binary systems, at each penetrant pressure and system temperature. We start analysing here the first example of application of NELF model, that illustrates the fundamentals of such procedure. Sarti and Doghieri [50,52,371], first applied the NELF model to predict the PE sorption isotherms of several binary polymer-penetrant systems: CO_2, N_2 and C_2H_4 in Bisphenol A-Polycarbonate (PC) and in Hexafluoro Polycarbonate (HFPC), CO_2 in Polymethylmethacrylate (PMMA) and Polystyrene (PS) and N_2 and CH_4 in Tetramethylpolycarbonate (TMPC). In these investigations the effectiveness and reliability of the model was properly tested in a merely predictive way by selecting binary systems for which both solubility and volumetric data of the mixture in PE of phase conditions were available in the literature. In fact, the LF scaling parameters of the SL model for each penetrant were obtained by a non-linear regression of pure penetrant vapor-liquid equilibrium data while, for the polymers, were retrieved by a non-linear regression of PVT equilibrium data, according to the procedure discussed in sub-section 3.6. The binary "mean field" interaction parameter Ψ of the NELF model, was set equal to 1 (ideal geometric mixing rules for the component characteristic LF pressures). All the PE isotherms investigated referred to temperatures well below the pure polymer glass transition temperature T_g. In view of the limited penetrant solubility, also the polymer-penetrant mixture was assumed to be frozen in a glassy state. As for the value of $\rho_{P,\infty}$ at any penetrant pressure, it was determined on the basis of volumetric data retrieved from the literature, so that no adjustable parameters were introduced in the prediction of penetrant sorption isotherms in the polymers. Once the value of density $\rho_{P,\infty}$ was experimentally available, the NELF model provided for all the investigated systems a powerful tool to predict the phase PE conditions. In Fig. 59a,b are reported some examples of the investigated systems.

Once the model has been tested on such model binary polymer-penetrant mixtures, in a series of following papers its application was extended to several systems, proposing also a predictive procedure to be used in the quite common case that no volumetric data on the polymer-penetrant glassy mixture are available. To this aim, in two seminal papers [182,373] the authors performed an extensive experimental campaign on PE sorption isotherms for several amorphous polymer-penetrant systems, (with penetrant ranging from light gases to low molecular weight hydrocarbons) working at temperatures well below the T_gs of the pure polymers. One of the conclusions of these investigations was that, as expected, in the limit of low penetrant concentrations (i.e, in the limit of low penetrant pressures), the value of $\rho_{P,\infty}$ can be assumed substantially equal to the one of the pure polymer right before it is exposed to the penetrant, since both "instantaneous elastic" dilation effect and the mechanical compression effects induced by the penetrant, can be considered in such case negligible. In addition, the authors observed that for polymer-penetrant mixtures well below the T_g and in the case that no significant specific interactions are involved, the relevant excess of free volume inherently associated to the glassy nature of the system plays a dominant role in determining penetrant solubility as compared to the effect of the parameter Ψ, so that the latter could be set, as a first approximation, to be equal to one.

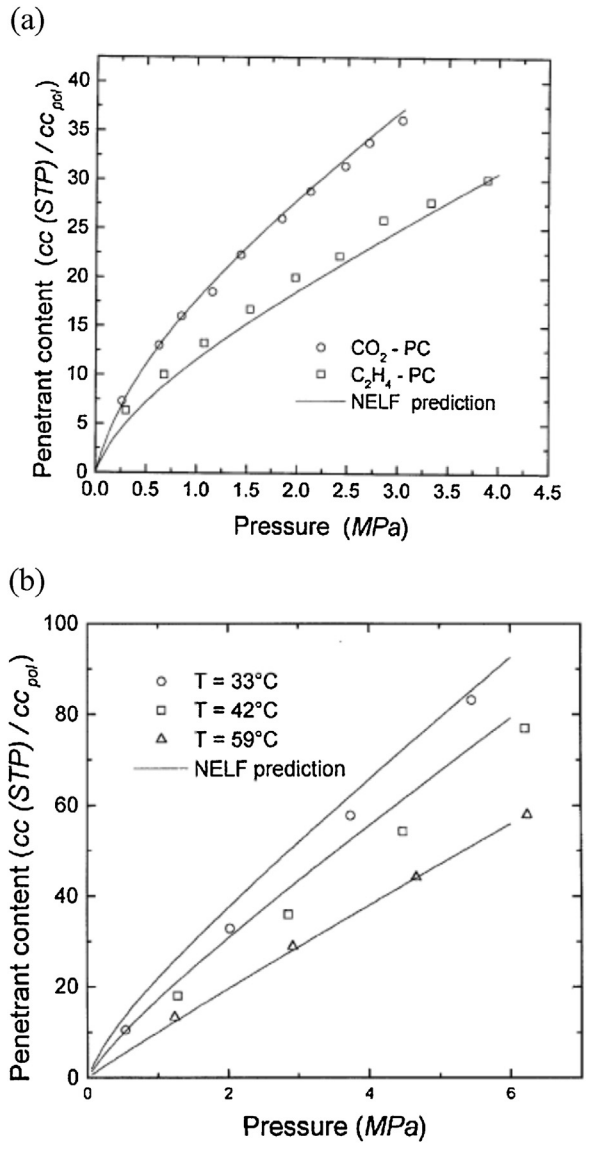

Fig. 59. (a) Sorption isotherms of CO_2 and C_2H_4 in PC at T = 35 °C. Symbols are experimental data by Jordan and Koros [372]; lines represent NELF model predictions. Reprinted with permission from [52]. Copyright 1998 Elsevier Science Ltd. (b) Sorption isotherms of CO_2 in PMMA at T = 33, 42 and 59 °C. Symbols are experimental data by Wissinger and Paulatis [336]; lines represent NELF model predictions. Reprinted with permission from [52]. Copyright 1998 Elsevier Science Ltd.

The same authors have later proposed an operative procedure to extend the effective range of applicability of the NELF model to the case of high penetrant pressures, in the frequent occurrence of lacking of dilation data for the mixture. To this aim, they analysed several experimental data [336,372,373] inferring that, for polymer-penetrant mixtures well below their glass transition temperature, the following empiric equation holds:

$$\rho_{P,\infty} = \rho_P^0(1 - k_{SW}p) \tag{267}$$

where ρ_P^0 represents the starting pure PE polymer density at pressure p = 0 atm (i.e. right before starting the sorption test) and k_{sw} is a swelling coefficient which depends upon the polymer-penetrant couple and is itself a non-equilibrium parameter, which

Please cite this article in press as: G. Mensitieri, G. Scherillo, C. Panayiotou et al. Towards a predictive thermodynamic description of Fsorption processes in polymers: The synergy between theoretical EoS models and vibrational spectroscopy. Mater. Sci. Eng. R (2020), https://doi.org/10.1016/j.mser.2019.100525

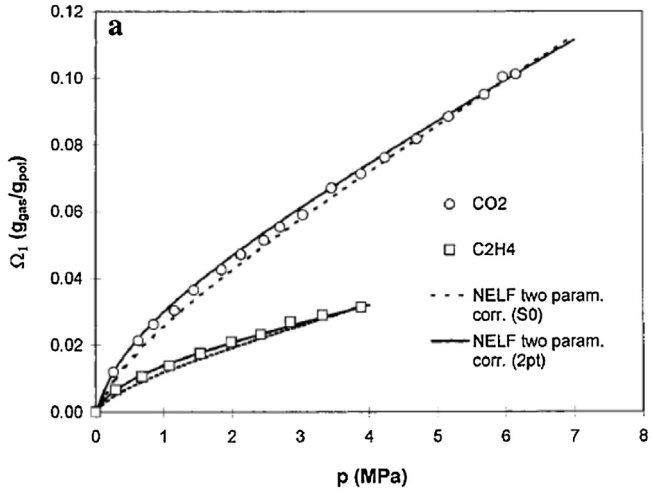

Fig. 60. Comparison of experimental sorption isotherms for C_2H_4 and CO_2 in PC at 35 °C and the results of NELF calculations using the 'two points parameters correlation strategy' and the S_o two parameters correlation'. Reprinted with permission from [182]. Copyright 2001American Chemical Society.

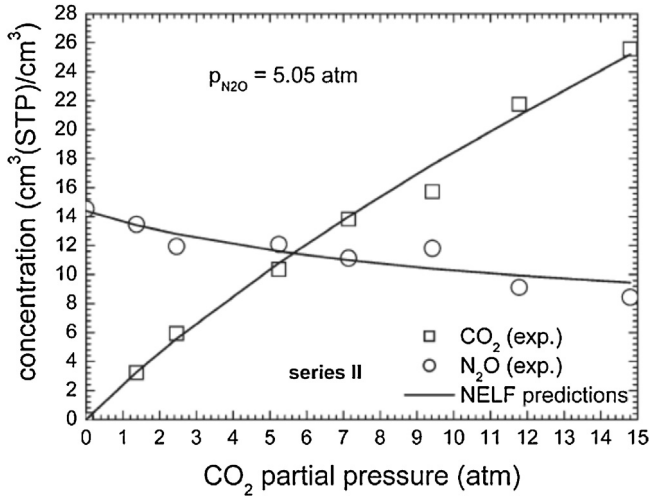

Fig. 61. Solubility of N_2O and CO_2 in PMMA at 35 °C; as a function of CO_2 partial pressure at a fixed N_2O partial pressure of 5.05 atm. Experimental data taken from [377]. Lines represent predictions of NELF model for ternary systems. Reprinted with permission from [376]. Copyright 2011 American Chemical Society.

depends on both thermomechanical and sorption history of the specific polymer sample [374].

In view of the linearity of Eq. (267), to retrieve the PE density values of the polymer in the mixture required for the NELF model calculations at each pressure, it is sufficient to know only two values for density: i) a value for $\rho_{P,\infty}$ at a selected pressure, that can be calculated by using the phase PE equations if the absorbed penetrant concentration at that pressure is experimentally available and by setting the value of the interaction binary parameter, Ψ, equal to 1; ii) the experimental value of ρ_P^0,i.e. the density of the pure polymer before the sorption tests or, alternatively, another value for $\rho_{P,\infty}$ at a different selected pressure, at which the penetrant concentration of the penetrant in the polymer at phase PE is available from experiments. The authors defined as 'two points parameters correlation strategy' the procedure based on the calculation of two values for $\rho_{P,\infty}$.

A second proposed procedure was based on the knowledge of the infinite dilution solubility of penetrant within the polymer, S_o, and of a value for $\rho_{P,\infty}$, referred to as 'S_o two parameters correlation'.

Other alternative procedures were also proposed by the same authors, based on a non linear fitting of the sorption isotherms using three parameters, i.e. Ψ, k_{sw} and ρ_P^0 or two parameters, i.e. Ψ and k_{sw}, in the case that ρ_P^0 is available from experiments. This last option has recently emerged as the one to be preferentially adopted [374,375].

In [182,373] it has been tested the reliability of the different procedures. In Fig. 60 is reported, as an example, the comparison between the 'two points parameters correlation strategy' and the 'S_o two parameters correlation'.

On each investigated system, the authors found that these two approaches show a satisfactory correlation capability. In particular, the authors, as a consistency check, found a substantial agreement between the value of pure polymers density calculated using the two approaches and the corresponding experimental values.

Obviously, it would be desirable to have available the experimental values for polymer density, as a pure component and in the mixture. However, while the pure polymer density, ρ_P^0, can be easily determined by performing helium picnometry measurements or using other standard techniques, the experimental set-up for a direct volumetric measurements on a polymer-penetrant mixture is quite complex and requires in-situ optical and/or spectroscopic techniques.

The multicomponent version of NELF model [183] was also successfully employed to model solubility of gas mixtures in glassy polymers, as is the case of solubility of CH_4/CO_2 mixtures in poly (2,6-dimethyl-1,4-phenylene oxide)(PPO) and of CO_2/C_2H_4 and N_2O/CO_2 mixtures in poly(methyl methacrylate) (PMMA) [376]. To this aim, the NELF model was first used to correlate the sorption isotherms of the corresponding polymer-gas binary sub-systems, retrieving the two polymer-penetrant binary interaction parameters, Ψ_i, and the two binary swelling parameters, $k_{sw,i}$. As for the binary interaction parameter of gas pairs, it could be estimated by non-linear regression of experimental data of the gas mixtures by using the SL model, but in that investigation [376] it was simply set equal to 1. In addition, the value of density of pure polymers before sorption tests was taken from experimental measurements. Regarding the density of polymer in the ternary mixtures, an additive behavior has been assumed, i.e.:

$$\rho_{P,\infty} = \rho_P^0(1 - k_{SW,1}p_1 - k_{SW,2}p_2) \tag{268}$$

where p_i represent the partial pressure of penetrant i and the $k_{sw,i}$ swelling parameters are those determined for the corresponding binary sub-systems.

Once all the binary adjustable parameters were estimated, the NELF model was used in a fully predictive fashion in order to predict the solubility for the corresponding ternary systems. This full predictive approach was possible in view of the adopted mixing rules, which do not introduce any ternary parameter. Actually, this was the main purpose of such investigation, since generally the evaluation of solubility in ternary system requires an experimental set-up and test procedures that are more complex as compared to the ones used for the gravimetric determination of sorption isotherms in binary systems. In Fig. 61 is reported an example of application of such approach for the prediction of solubility in the case one of the ternary systems investigated in [376], that confirms the reliability of the illustrated predictive procedure.

The NELF model was also used by Sarti et al. to interpret sorption thermodynamics of pure penetrants in polymer blends [378]. A procedure was proposed to model the phase PE of gases and vapors in glassy amorphous miscible polymeric blends of polystyrene (PS) and tetramethyl polycarbonate (TMPC). The gases investigated were, respectively, methane (as a non-swelling penetrant) and carbon dioxide (as a swelling penetrant). Also in this case was made the reasonable assumption that the external

Please cite this article in press as: G. Mensitieri, G. Scherillo, C. Panayiotou et al. Towards a predictive thermodynamic description of Fsorption processes in polymers: The synergy between theoretical EoS models and vibrational spectroscopy. Mater. Sci. Eng. R (2020), https://doi.org/10.1016/j.mser.2019.100525

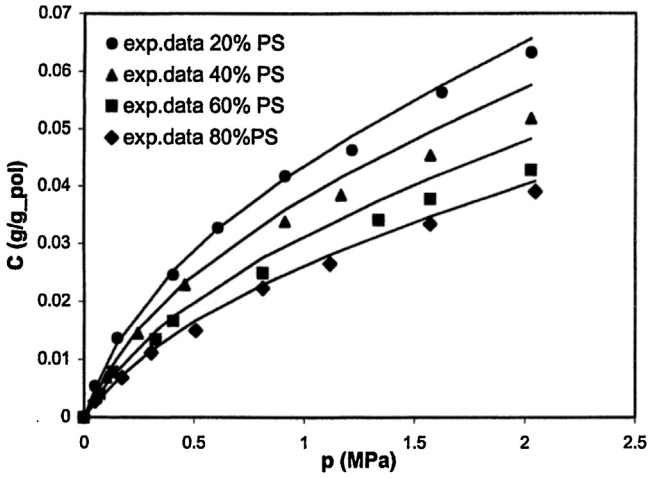

Fig. 62. Sorption isotherms of CO_2 in PS-TMPC blends. Data from [379]. Continuous lines are NELF model predictions based on the binary parameters and swelling coefficients obtained for each of the polymers. Reprinted with permission from [378]. Copyright 2004 American Chemical Society.

phase is only formed by the low molecular weight compound so that, once the mass fraction of the two polymeric component is fixed in a given blend-penetrant system, mass balance allows the straightforward expression of the density of the two polymeric components in the mixture, ρ_i, as a function of the overall blend density in the mixture, ρ_p. Consequently, this latter variable was selected as the only internal state variable for the out-of-equilibrium blend-penetrant glassy system. According to the mixing rules of NELF model for ternary systems, three mean field interaction parameters are needed. The binary interaction parameter for the polymer couple was taken as equal to 1. In addition, in the case of CO_2 (swelling gas), it was assumed that the value of k_{sw} for the blend is the volume average of the two swelling parameters of the two for the binary polymer-CO_2 sub-systems. The curve fitting parameters (for methane, the two "mean field" polymer-penetrant binary interaction parameters and, for carbon dioxide, the two "mean field" polymer-penetrant binary interaction parameters and the two k_{sw} parameters) were retrieved by a nonlinear regression procedure of PE solubility isotherms of the corresponding polymer-penetrant binary sub-systems. Finally, the NELF model was applied to predict the PE solubility isotherms of blend with different PS/TMPC ratio. A very good agreement with experimental data was found, as shown in Fig. 62, where is reported the case of solubility of CO_2 in PS/TMPC, for a PS/TMPC mass ratio ranging from 0.2 up 0.8.

Very recently, Mensitieri et al. [254] combined NELF modelling with FTIR analysis to gather an insight, also from a molecular perspective, on the sorption thermodynamics of CO_2 in PEI, at pressures ranging from 40 to 160 Torr and at several temperatures.

Subtraction spectroscopy analysis was performed on both thick (37.7 μm) and thin (2.6 μm) PEI films, in the spectral region that contains the signals associated, respectively, to the absorbed CO_2 molecules and to the macromolecules, with specific attention on the intense carbonyl bands of PEI. With reference to absorbed CO_2 molecules, there are two signals centered respectively at 2336 and 655 cm^{-1}. The main band 2336 cm^{-1} is associated to the antisymmetric stretching mode (ν_3), while a satellite peak, present at 2324 cm^{-1}, is a non fundamental transition associated to the same species that generated the main absorption at 2336 cm^{-1}. The signal at 655 cm^{-1} is associated to the CO_2 bending mode (ν_2) is a quite weak signal that is also superimposed onto intense polymer bands. Hence, to perform a quantitative analysis and to gather information at the molecular level, it has been selected the signal at 2336 cm^{-1}. The integrated absorbance of the 2336 cm^{-1} band has been collected at several values of pressure of CO_2 in contact with PEI, as a function of time up to the attainment of sorption equilibrium. In Fig. 63A are reported the subtraction spectra collected at sorption equilibrium at different values of CO_2 pressure and at 35 °C, collected in the spectral region where are located the signals associated to the antisymmetric stretching mode of carbon dioxide. In Fig. 63B is reported the correlation between the integrated absorbance of the ν_3 band and the carbon dioxide percent uptake, as measured gravimetrically, collected at the same values of pressure.

2D-COS analysis was performed on the time resolved subtraction spectra collected in the 2250–2420 cm^{-1} range, for the sorption experiment performed at 150 Torr and at T = 35 °C. The elaborated synchronous and asynchronous spectra are reported in Fig. 64A,B. There is evidence of a main component in the frequency spectrum at 2336 cm^{-1}, plus a weak, fully resolved feature at 2324 cm^{-1}. The synchronous map displays off-diagonal wings that indicate the occurrence of a further component significantly broader than the main peaks, pointing to the presence of a broad Gaussian component superimposed onto a sharper component of larger intensity. The asynchronous peak is featureless, thus indicating that all the components in the ν_3 profile evolved synchronously. These results led the authors to the conclusion that a single molecular species produced all the observed components.

The dynamics of CO_2 molecules absorbed in PEI, emerging from these spectral features, has been preliminarily assumed to consist in very short free-rotation regimes (the Gaussian component, barely detectable in the frequency spectrum) interspersed with the formation of specific type of interaction of a single molecular

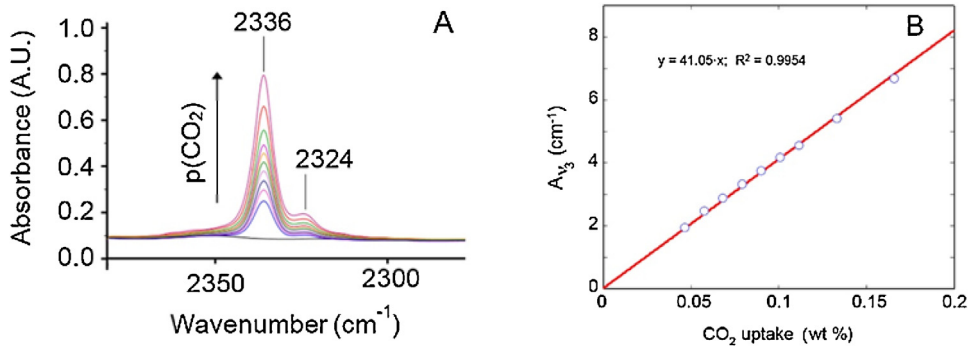

Fig. 63. (A): The ν_3 band of CO_2 after sorption equilibrium at different pressures. (B): Absorbance of the ν_3 band as a function of sorbed CO_2 as evaluated gravimetrically at 35 °C. Adapted from [254].

Please cite this article in press as: G. Mensitieri, G. Scherillo, C. Panayiotou et al. Towards a predictive thermodynamic description of Fsorption processes in polymers: The synergy between theoretical EoS models and vibrational spectroscopy. Mater. Sci. Eng. R (2020), https://doi.org/10.1016/j.mser.2019.100525

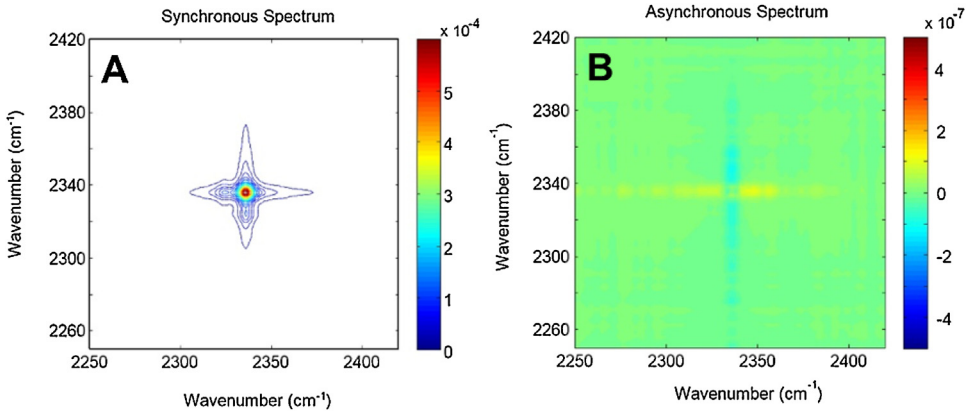

Fig. 64. Synchronous (A) and asynchronous (B) spectra obtained from the time-resolved spectra collected during the sorption experiment performed at 150 Torr and at 35 °C on the CO_2/PEI system. Adapted from [254].

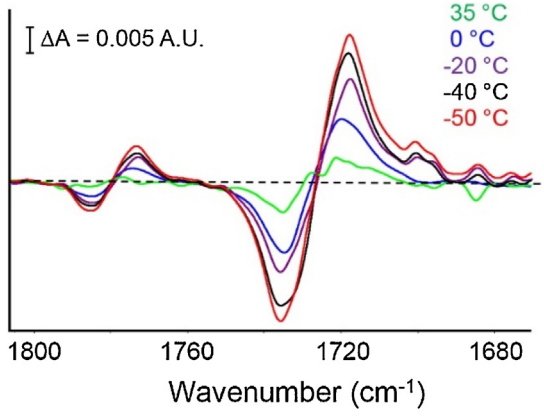

Fig. 65. Difference spectra in the PEI carbonyl range obtained for thin PEI films equilibrated at several temperatures with CO_2 at a pressure of 150 Torr. Adapted from [254].

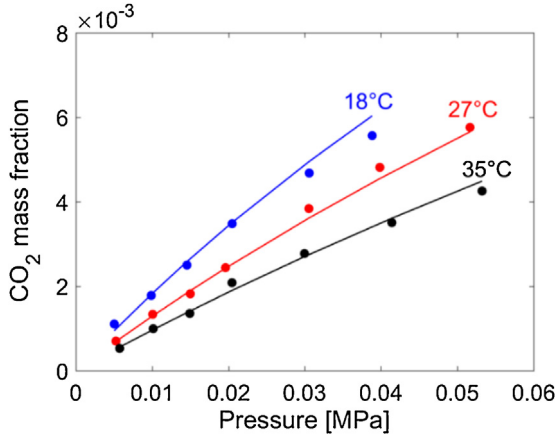

Fig. 67. Gravimetric sorption isotherms of CO_2 in PEI at 18, 27, and 35 °C. Results of data fitting performed concurrently for the three isotherms and provided by NELF model are reported as continuous lines. Adapted from [254].

species of CO_2 with the polymer substrate (the main sharp component).

Further analysis was directed to the identification of the functional group(s) of the PEI backbone that was (were) involved in the formation of the adduct with CO_2. In fact, the interaction of the absorbed molecules with functional groups of PEI determine a perturbation to the spectrum of the substrate consisting in peak shifts and/or band-shape distortion, that can be used to gather information on the geometry and on the electron-density distribution of the molecular aggregate. Involvement of imide carbonyls in specific interactions with absorbed CO_2 molecules, albeit rather weak, is witnessed by limited red-shifts (maximum shift of the main carbonyl component = 0.25 cm^{-1}) occurring for the peaks associated to the in-phase, ν_{ip}(C=O), and out-of-phase stretching, ν_{oop}(C=O), of the imide carbonyls, that evidence a lowering of the peaks frequency (see Fig. 65, where are reported the difference spectra obtained in the PEI carbonyl frequency range, i.e. 1820–1660 cm^{-1}, at a pressure of 150 Torr and at the different temperatures, on thin polymer films). The carbon atom of the carbon dioxide molecule establishes a weak Lewis acid/Lewis base interaction with the imide carbonyls, as schematically represented in Fig. 66. Conversely, the bands associated to C—O—C stretching modes as well as aromatic peaks remained unaffected, thus indicating that both the ether oxygens and the aromatic rings are not involved in specific interactions with absorbed CO_2 molecules.

In view of the weakness of the Lewis acid/Lewis base interactions established by CO_2 molecules with PEI carbonyls, sorption thermodynamics in glassy PEI was interpreted using the NELF approach, with no account for any specific interaction. The model provided a good concurrent fitting of experimental gravimetric sorption isotherms determined at 18, 27, and 35 °C,

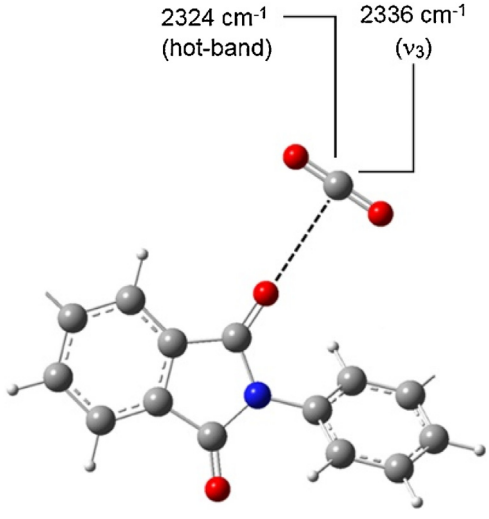

Fig. 66. Schematic representation of the CO_2/C = O interaction. Adapted from [254].

Table 7
Non-equilibrium polyetherimide (PEI) density [310].

Temperature (°C)	Density (g/cm^3)
18	1.2700 ± 0.0006
27	1.2680 ± 0.0006
35	1.2663 ± 0.0006

Table 8
Scaling parameters of Sanchez–Lacombe equation of state (EoS) for PEI [254] and CO_2 [50].

Substance	T^* (K)	P^* (MPa)	ρ^* (g/cm^3)
PEI	893	545	1.354
CO_2	300	630	1.515

up to ca. 400 Torr (0.05 MPa), see Fig. 67, using as fitting parameter only the binary interaction parameter, χ_{12}. A value of $\chi_{12} = 0.0313 \pm 0.003$ was estimated, with a small deviation from the geometric mixing rule for characteristic pressure. The adopted scaling parameters for the Sanchez-Lacombe EoS of pure PEI and CO_2 are reported in Table 7. The (non-equilibrium) density values of neat PEI, $\rho_{P,\infty}$, at each temperature (assumed here to be time-independent) used in the model, were taken from the literature [310] and are reported in Table 8.

The group of Sarti has also used the NELF approach to analyse a system endowed with hydrogen bonding interactions [380]. Water sorption in an amorphous glassy Polylactic (PLA) at different temperatures was investigated, comparing gravimetric and "in situ" time-resolved FTIR-ATR spectroscopic data with predictions of NELF model. To this aim, the authors assumed that the binary interaction parameter, Ψ, of NELF model, takes the same value both for the rubbery and the glassy state of PLA, being related only to the nature of polymer-penetrant interaction. Hence, they retrieved its value performing a nonlinear regression with SL model of water sorption isotherms, at temperatures above the T_g of neat PLA. As for k_{sw}, optical dilation measurements on the glassy PLA-water mixture confirmed that its effect was negligible, as expected in view of low water sorption amount and of the glassy state of the system. Once both Ψ and k_{sw} were available and ρ_p^0 had been measured, the NELF model was used to predict water sorption isotherms. Since the NELF model does not take into account for the presence of HB interactions within the polymer-penetrant mixture, it showed a quite good predictive capability only at relatively low water activities ($a_w < 0.65$) at the different temperatures investigated. In particular, the model is not able to reproduce the upward concavity of water sorption that is associated to the onset of the formation of HB water clusters within the system, which involve more than just dimeric water, as confirmed by the FTIR-ATR measurements.

Similar results were obtained in a following paper [368] dealing with the sorption of water in poly(methyl methacrylate) (PMMA) at several water vapor activities (0 – 0.85), at T = 25, 35, and 45 °C. The swelling coefficient was taken to be zero ($k_{sw} = 0$) while the binary interaction parameter was retrieved by best fitting of sorption data at 35 °C, obtaining a value k_{12} = - 0.05.

Using this value were predicted the water sorption isotherms at T = 25 and 45 °C, assuming the binary interaction parameter to be temperature independent. A good agreement of predictions with experimental data was found up to a water activity of about 0.5, above which significant deviations were evident at all the investigated temperatures, as evident in Fig. 68. The mismatch between model predictions and experimental data at a_w>0.5 was attributed to the occurrence of self-association of water molecules

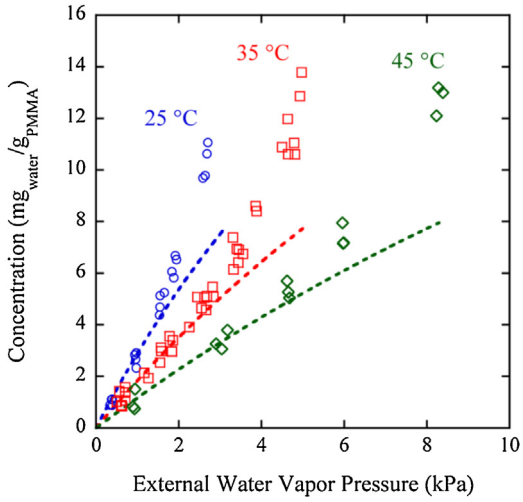

Fig. 68. Water vapor sorption isotherms in PMMA at 25, 35, and 45 °C. Symbols represent experimental data. Dashed lines are predictions provided by NELF model (dashed lines). Reprinted with permission from [381]. Copyright 2013 American Chemical Society.

that is not accounted for by NELF theory. The occurrence of water self-association and of formation of clusters at higher activities was confirmed by time-resolved FTIR-ATR spectroscopy measurements.

These last results clearly indicate that models explicitly accounting for specific self- and cross-interactions have to be used for sorption thermodynamics in glassy systems endowed with hydrogen bonding as is the case of NETGP-NRHB approach reported in section 4.1.2.3.

4.1.2.2. Applications of NETGP-PHSCT and NETGP-SAFT. NETGP-PHSCT and NETGP-PC-SAFT models, if applied to systems that are not endowed with specific interactions and associations, provide performances which are similar to the simpler NELF model. As an example, the experimental solubility isotherms of C_2H_6 and C_2F_6 in Teflon AF1600 and 2400 at 35 °C were interpreted using NETGP-PHSCT (with the perturbation term, which represents the contributions of mean-field forces, that is of the van der Waals type [124]) and NETGP-PC-SAFT models [177]. The density of the two polymers in the binary mixtures were available from volumetric dilation data. Both models provided a quite good predictions (i.e. with no adjustable parameters, assuming $\Psi = 1 - k_{ij} = 1$) of solubility data for C_2F_6 in the two fluoropolymers, while, in the case of C_2H_6, a binary interaction parameter, k_{ij}, equal to about 0.10 had to be introduced to fit the experimental isotherms. Similar results were also obtained using the NELF model. The need, for all the three model, to introduce a value of $\Psi \neq 1$ has been attributed to the failure of the geometric mean rule, that is based on the assumption made by London that the values of first ionization potentials are similar for all the substances [382].

The performances of two NETGP-PHSC models, characterized by different expressions for the perturbation term representing the mean field interaction potential, were compared for the analysis of sorption of CH_4 in poly(ethylmethacrylate) (PEMA), of CO_2 in polycarbonate (PC) and of N_2, CH_4, C_2H_6 and C_3H_8 in Teflon AF2400 [370]. Both the models do not account for association terms and use a different pair interaction potentials between chain segments. In fact, the NETGP-PHSC(VdW) model includes a perturbation term that is of the van der Waals type (van der Waals type of interaction potential) [384]. Conversely, the NETGP-PHSC(SW) model includes a second order perturbation term for a square well potential of

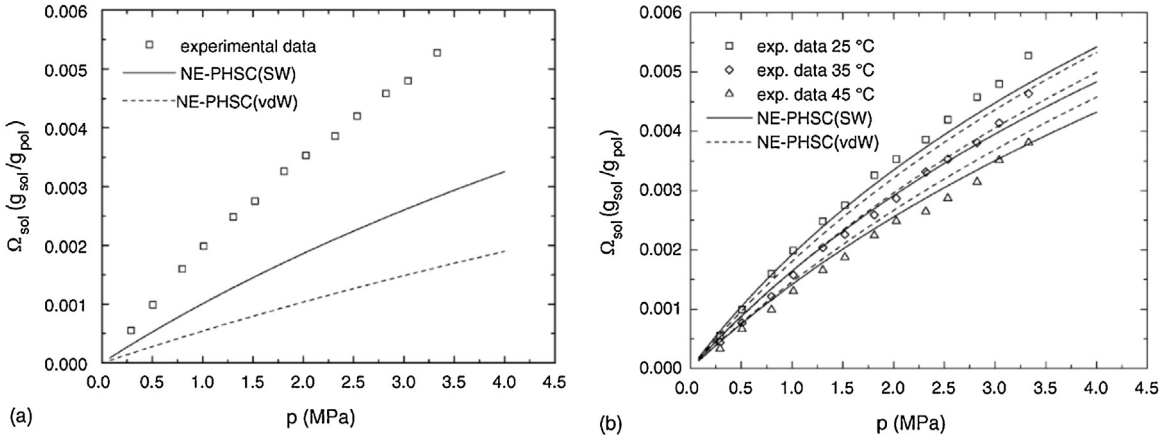

Fig. 69. (a): Sorption isotherms of CH_4 in PEMA at T = 25 °C. Continuous line and dashed line represent, respectively, the predictions (k_{ij} = 0) provided by NETGP-PHSCT(SW) and by the NETGP-PHSCT(VdW) models. (b): Sorption isotherms of CH_4 in PEMA at T = 25, 35 and 45 °C. Continuous lines and dashed lines represent, respectively, the results of best-fitting correlations performed with the NETGP-PHSCT(SW) (k_{ij} = -0.040) and the NETGP-PHSCT(VdW) (k_{ij} = -0.095) models. Reprinted with permission from [383]. Copyright 2006 Elsevier B.V.

variable width (square well form of interaction potential) [127]. The two models provide a representation of the dependence of gas solubility on temperature and pressure that is consistent with experimental data. In most of the cases, a value of the interaction parameter, k_{ij}, different from 0 needs to be used. As an example, in Fig. 69 is reported the case of sorption of CH_4 in PEMA, proving the poor predictive capability (i.e. with k_{ij} = 0) of the two models.

Overall, the NETGP-PHSCT(SW) provides a better interpretation of experimental sorption isotherms in the glassy state of polymers as compared to NETGP-PHSCT(VdW).

Afterwards, Davis and Elabd [381] have investigated water vapor sorption within glassy PMMA. The NETGP-SAFT model was used to interpret sorption thermodynamics, accounting for self-hydrogen bonding interactions among water molecules by introducing two additional pure-component parameters (ε_{AB}/k and κ_{AB}) for water, whose values were taken from the literature [116]. As for the case of NELF, already discussed in the previous sub-section, the swelling coefficient has been taken to be zero (k_{sw} = 0), while the binary interaction parameter was retrieved by best fitting of sorption data at 35 °C, obtaining a value k_{12} = 0.006. Using this value, the water sorption isotherms at T = 25 and 45 °C were predicted, assuming the binary interaction parameter to be temperature independent. As evident in Fig. 70A, this model provides an excellent prediction of experimental data, that at high activities is significantly better than that provided by NELF model. The same approach was adopted to describe water sorption thermodynamics in PLA. Also in this case, at high water activities, NETGP-SAFT performs better than NELF (see Fig. 70B). A good agreement between NETGP-SAFT theoretical predictions and experimental water sorption isotherms was also found for other four glassy polymers, i.e. polyacrylonitrile, PAN, polyethylene terephthalate, PET, polyvinylchloride, PVC, and polystyrene, PS, thus proving that NETGP-SAFT, with an association term accounting for water self-association, does provide a reliable interpretation of water sorption in hydrophobic glassy polymers.

As underlined, the previous implementation of NETGP-SAFT model accounts only for penetrant specific self-interactions and is limited to the cases in which no cross polymer-penetrant and polymer self-interactions do establish within the glassy mixture. Later, Liu and Kentish [385] have applied the NETGP approach to a version of PC-SAFT model, including an association term (short range association interactions, i.e. hydrogen bonding, according to

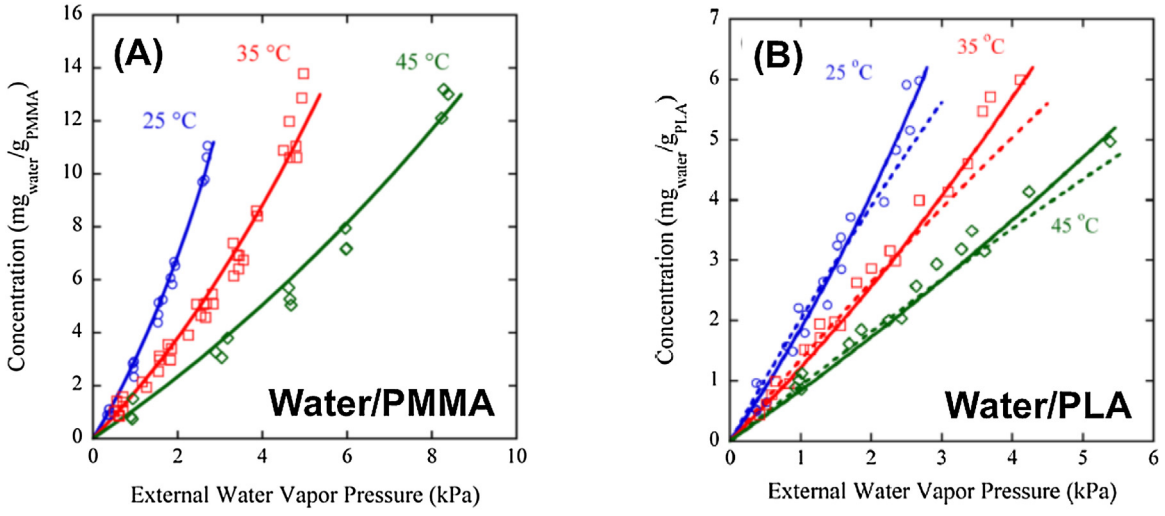

Fig. 70. (A): Water sorption isotherms in PMMA at T = 25, 35 and 45 °C. Continuous lines are predictions obtained using the NETGP-SAFT model. (B): Water sorption isotherms in PMMA at T = 25, 35 and 45 °C. Dashed lines and continuous lines are, respectively, predictions obtained using the NELF and NETGP-SAFT models. Reprinted with permission from [381]. Copyright 2013 American Chemical Society.

Please cite this article in press as: G. Mensitieri, G. Scherillo, C. Panayiotou et al. Towards a predictive thermodynamic description of Fsorption processes in polymers: The synergy between theoretical EoS models and vibrational spectroscopy. Mater. Sci. Eng. R (2020), https://doi.org/10.1016/j.mser.2019.100525

a model proposed by Champan et al. [45] and an induced-association term (according to an approach proposed by Kleiner and Sadowski [166]) to deal with sorption thermodynamics in glassy PLA and PMMA.

In particular, the NETGP PC-SAFT model (without association and induced-association terms) was first successfully employed to describe CO_2 sorption in PMMA using a best fitting procedure to estimate the binary interaction parameter, k_{ij}, and the swelling coefficient, k_{sw}. Conversely, PC-SAFT did not provide, as expected, an acceptable interpretation of data, since it does not account for the non-equilibrium glassy state of the polymer.

In the case of water sorption in PLA and PMMA the authors used the PC-SAFT and NETGP-PC-SAFT approaches, both accounting for water self-association and for polymer-water induced association. In contrast to the case of CO_2 sorption, they found that the PC-SAFT model, although generally valid only for rubbery polymers, provides an excellent fit of water sorption isotherms both in PLA and PMMA, using as fitting parameter only the binary interaction parameter, k_{ij}. The authors postulated that this unexpected result was due to the negligible effect that, in the case water sorption, has the excess free volume on the total water sorption, as compared to the prevailing role of polymer-water induced-association. Moreover, they also concluded that accounting only for water self-association and disregarding induced-association, leads to significant underestimation of the total amount of water sorbed by using PC-SAFT.

Also NETGP-PC-SAFT (with $k_{sw} = 0$) model, including the water self-association and the polymer-water induced association terms, exhibited a satisfactory fitting capability in the case of water-PLA system. In contrast, a reasonable fitting, but worse than that obtained with PC-SAFT model, could be obtained with NETGP-PC-SAFT, in the case of water sorption in PMMA, only by introducing k_{sw} as adjustable parameter. These results are in contrast with those of Davis and Elabd [381,368], which found that the NETGP-SAFT model provides satisfactory results without any induced-association contribution. This discrepancy was tentatively attributed, by Liu and Kentish, to the different association scheme (number of association sites) adopted for water molecules in the two works.

4.1.2.3. Applications of NETGP-NRHB model. In this sub-section we discuss some applications of NETGP-NRHB model to the case of systems where both specific self- and cross-interactions are expected to occur. All these interactions are properly accounted for in the modelling and, notably, a careful assessment of the qualitative and quantitative consistency between the theoretical predictions and the outcomes of vibrational spectroscopy is performed, in terms of amount and type of specific interactions established in the polymer-penetrant systems.

Water sorption thermodynamics in a series of polyimides (PIs) with an increasing fluorine content has been investigated [267,386] by combining vibrational spectroscopy analysis, gravimetry and NETGP-NRHB modelling. Using in-situ FTIR measurements, coupled with gravimetric determination of sorption isotherms, the authors gained relevant experimental information useful in developing the structure of the NETGP-NRHB model. Vibrational spectroscopy has been exploited to determine the type of interactions established in the different H_2O/PI systems, the involved interacting sites on the polymer backbone and a quantitative estimate of the concentration of different water 'species' (i.e. water molecules characterized by different kinds of self- and cross-HB interactions). In particular, the spectroscopic results have been analysed by using difference spectroscopy, LSCF and 2D-COS. By coupling this information with the results of gravimetric measurements, it was possible to evaluate the molar absorptivity of each water 'species', thus allowing the quantification of their populations.

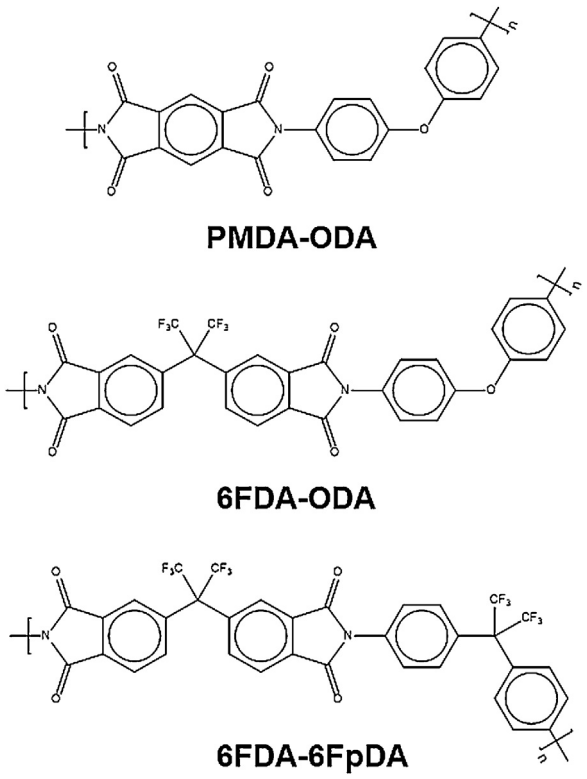

Fig. 71. Repeating units of the different investigated PIs. Reprinted with permission from [267]. Copyright 2012 American chemical Society.

The repeating units of the investigated PIs are reported in Fig. 71.

Difference spectra (i.e. water saturated PI – dry PI) in the OH stretching region, ν_{OH} (i.e. wavenumber range 3800–3200 cm^{-1}), representing absorbed water, are compared in Fig. 72 for the three investigated PIs at phase PE with water vapor, at a relative pressure $p/p_0 = 0.6$ and at T = 30 °C. The complexity of the band profiles reflects the occurrence of different water species. As evident, the amount of absorbed water significantly decreases as the fluorine content increases, as also confirmed by gravimetric water sorption isotherms reported in Fig. 73.

To gather further insight on the interactional issues, 2D-COS investigation in the 3800–3200 cm^{-1} wavenumber range has been performed on the time-resolved spectra collected in-situ during sorption at different relative pressure of water vapor. In Fig. 74 are reported the asynchronous correlation maps for the three PIs at a

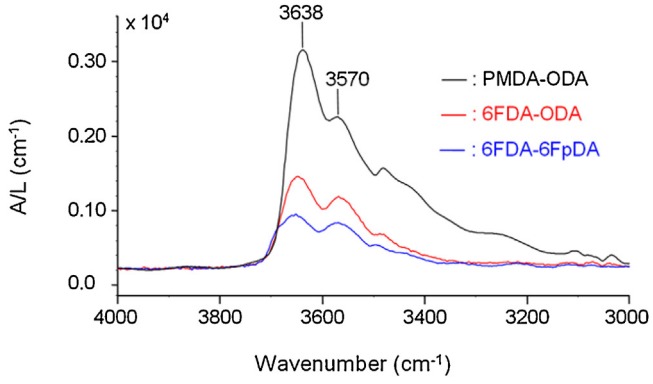

Fig. 72. Difference spectra, normalized for the sample thickness, in the ν_{OH} region for the H_2O/PI systems at sorption equilibrium with water vapor at $p/p_0 = 0.6$ and 30 °C. Reprinted with permission from [267]. Copyright 2012 American Chemical Society.

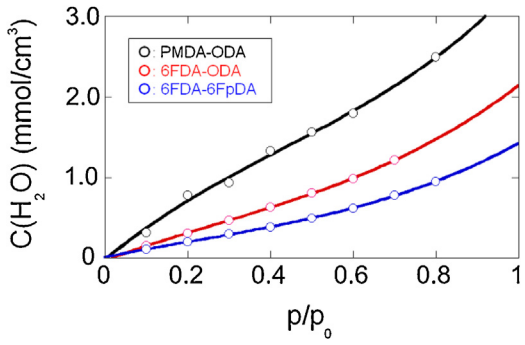

Fig. 73. Gravimetric water vapor sorption isotherms for the three investigated PIs. Reprinted with permission from [267]. Copyright 2012 American Chemical Society.

relative pressure equal to 0.6. The analysis of the asynchronous spectra, for the case of PMDA-ODA, evidenced the presence of two couple of signals, one at 3660–3570 cm^{-1} and the other at 3616–3456 cm^{-1}, that have been interpreted as an indication of the occurrence of two different water species. A similar pattern has been found for the case of 6FDA-ODA. In the case of 6FDA-6FpDA a third, additional, component at 3700 cm^{-1} has been found, that evolves at the same rate as the doublet at 3616–3456 cm^{-1}.

The identification of polymer sites actually involved in the HB interactions was based on the investigation of the perturbation of PI spectrum determined by the absorbed water. In Fig. 75 are reported the fully dry IR spectra for PMDA-ODA and 6FDA-ODA (blue trace) and for the same PIs after equilibration with water vapor at $p/p_0 = 0.6$ (red trace). In the same figure are also reported (in an expanded scale) the difference spectra (i.e. wet-dry). The spectra are reported in three different spectral regions, where are positioned relevant peaks associated to potential proton acceptor groups on the backbone.

In the 1800–1680 cm^{-1} region it is evident the *red-shift* (also confirmed by the two derivative type features present in the difference spectrum, with the negative lobe preceding the positive one) of both the asymmetric and symmetric stretching modes of the imide carbonyls (i.e. ν_{as}(C=O) and ν_s(C=O)). This evidence indicates the involvement of carbonyls in HB interactions, that determines a lowering of the force constant of the double bond. This picture is also consistent with the blue shift observed for the 1378 cm^{-1} band. In fact, this band is essentially associated with the in-plane deformation of the N—C—O group, that displays a stiffer force constant upon establishment of HB involving the carbonyls. Another significant outcome of this spectral analysis is that the relevant band at 1244 cm^{-1}, associated to the asymmetric stretching vibration of the C—O—C bond, remains practically unaffected by the presence of absorbed water, thus indicating that the involvement of ether oxygens as proton acceptors in HB can be safely ruled out, confirming previous experimental results [387] and molecular dynamics simulations [388].

The results of vibrational spectroscopy were used to figure out the HB aggregates formed in the H_2O/PI systems. In detail, the couple of signals at 3660 and 3570 cm^{-1} have been attributed to the out-of-phase and in-phase stretching of water molecules interacting by HB with carbonyls (structure I in Fig. 76, water belonging to the so-called 'first shell' hydration layer) while those at 3616 and 3470 cm^{-1} have been associated to self-associated water (structure II in Fig. 76, water belonging to the so-called 'second shell' hydration layer), i.e. water molecules forming, prevalently, dimers with water molecules interacting with carbonyls. The signal at 3616 cm^{-1} has been assigned to the OH stretching of the OH bond not involved in the interaction while the signal at 3470 cm^{-1} has been assigned to the OH stretching of the interacting OH bond. It is worth noting that the wavenumber values reported here refer to the specific case of PMDA-ODA, slightly different values are detected in the case of 6FDA-ODA and 6FDA-6FpDA. The signal at 3700 cm^{-1}, detected only in the case of SFDA-6FpDA has been associated to self-associating water molecules (structure III in Fig. 76) by HB that involves their oxygen atom.

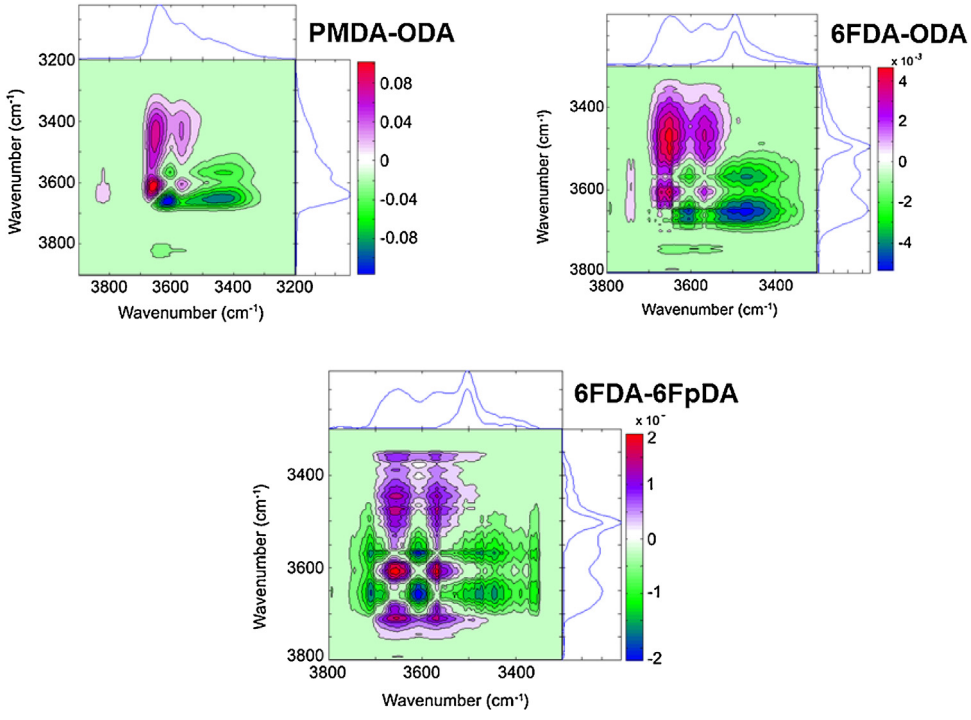

Fig. 74. 2D-COS asynchronous spectra obtained by elaborating time-resolved spectra acquired during water sorption at $p / p_0 = 0.6$ for the three investigated PIs. Reprinted with permission from [267]. Copyright 2012 American Chemical Society.

Please cite this article in press as: G. Mensitieri, G. Scherillo, C. Panayiotou et al. Towards a predictive thermodynamic description of Fsorption processes in polymers: The synergy between theoretical EoS models and vibrational spectroscopy. Mater. Sci. Eng. R (2020), https://doi.org/10.1016/j.mser.2019.100525

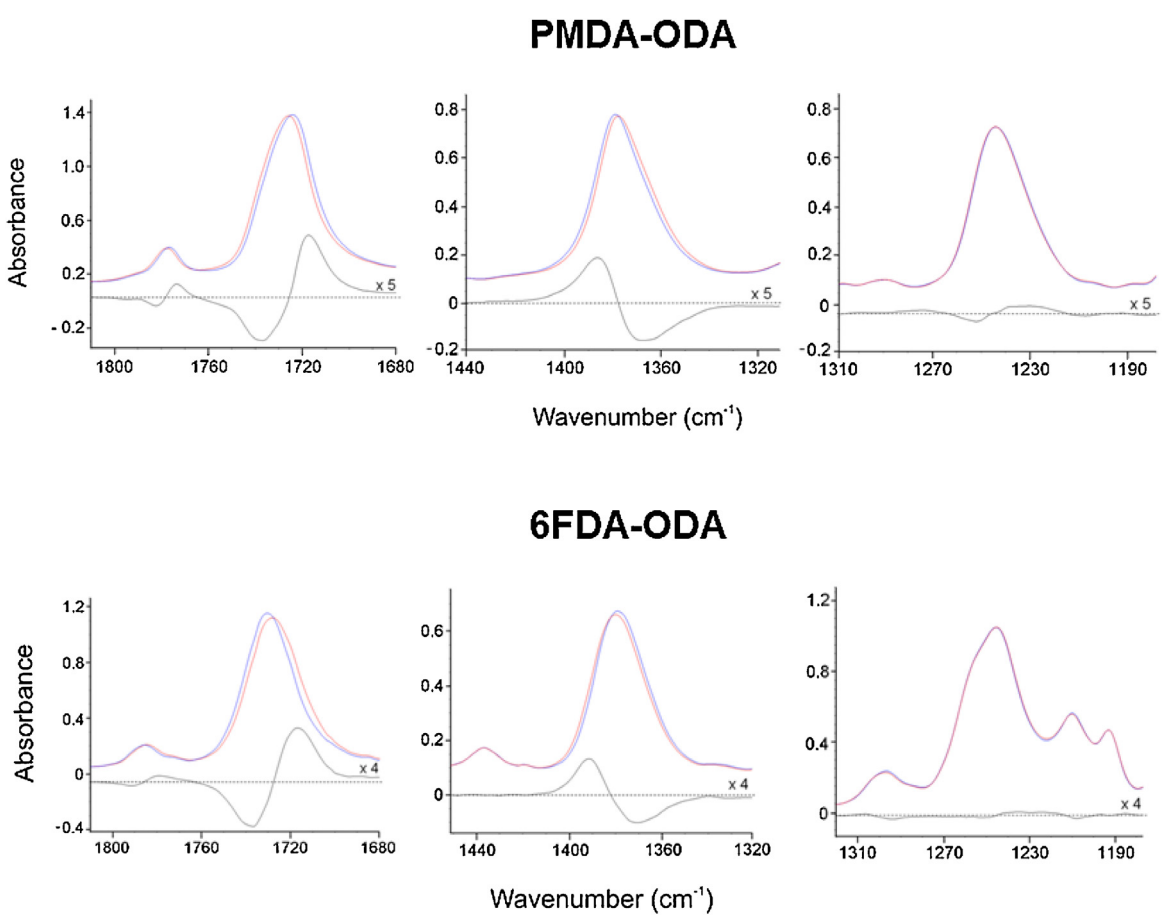

Fig. 75. Spectra of PMDA-ODA and 6FDA-ODA in three different regions. Blue traces refer to dry PIs while red traces refer to PIs after equilibration with water vapor at p / p_0 = 0.6. Difference spectra (wet-dry) in the same regions are also reported (black trace). Reprinted with permission from [267]. Copyright 2012 American Chemical Society. (For interpretation of the references to colour in this figure legend, the reader is referred to the web version of this article.)

Based on arguments used to interpret sorption thermodynamics of a similar system (i.e. H_2O/PEI), that will be illustrated later, one can conclude that the 'first shell' water molecules actually bridge two carbonyls (see scheme I). It corresponds to a 1:2 stoichiometry interaction between water and carbonyls. In fact, there is no evidence of a sharp component at around 3690 cm^{-1}, that is a fingerprint of water molecules interacting with only 1 carbonyl (i.e. 1:1 stoichiometry interaction) [389]. Moreover, the 2D-COS analysis confirms that the water species producing the signals at 3660 – 3570 cm^{-1} have two equivalent O—H bonds, as it is expected in the case of 1:2 stoichiometry interaction.

With the aim of obtaining a quantitative estimate of the two different water 'species', LCSF analysis of the water band profile in the OH stretching wavenumber range has been performed, guided by the results of 2D-COS analysis to identify the number of components and the relative peak positions to be considered. Two analytical peaks were chosen, one representative of the 'first shell' water (i.e. the peak at 3568 cm^{-1}, for the case of 6FDA-ODA) and the other representative of 'second shell' water(i.e. the peak at 3495 cm^{-1}, for the case of 6FDA-ODA). The sum of the two integrated absorbances of each component, normalized by the sample thickness, L, are reported in Fig. 77 for the three investigated PIs as a function of total water concentration as determined gravimetrically. All the values lie on a single curve. The evident non linearity is associated to the fact that the molar absorptivity of 'first shell' water (ε_{fs}), whose concentration prevails at low total water concentration and low values of p / p_0, is smaller than molar absorptivity of 'second shell' water (ε_{ss}), whose relative concentration increases as the value of total water concentration and values of p / p_0 increase. From the initial linear behaviour, the value of ε_{fs} has been estimated to be 670 ± 50 km/mol, from which a quantitative estimate of the concentration of 'first shell' water was obtained as:

$$C_{fs} = \frac{A_{3568}}{\varepsilon_{fs} L} \tag{269}$$

The concentration of 'second shell' water, C_{ss}, has been obtained by the difference between the total water concentration evaluated gravimetrically and C_{fs}. From this value the ε_{ss} was estimated to be equal to 1700 ± 100 km/mol.

In Fig. 78 are reported, for the three PIs, the values of the concentration of 'first shell' and 'second shell' water at 30 °C as a function of p/p_0. The values of the ratio of the concentration of first-shell and second-shell water are collectively reported for the three PIs vs total water concentration in Fig. 79. Interestingly, all the values display a common trend.

Water sorption thermodynamics in PIs was interpreted using NETGP-NRHB approach [386] only for 6FDA-ODA and 6FDA-6FpDA since, in the case of PMDA-ODA, the polymer degrades near its glass transition temperature and the scaling parameters of the EoS for the pure polymer cannot be retrieved from fitting PVT data above the glass transition temperature. The NRHB parameters used for pure 6FDA-ODA and 6FDA-6FpDA as well as for water are reported in Table 9. Results of fitting of gravimetric sorption isotherms at 30 °C are reported in Fig. 80. The two fitting parameters were the binary interaction parameter, ψ_{12} = (1 –

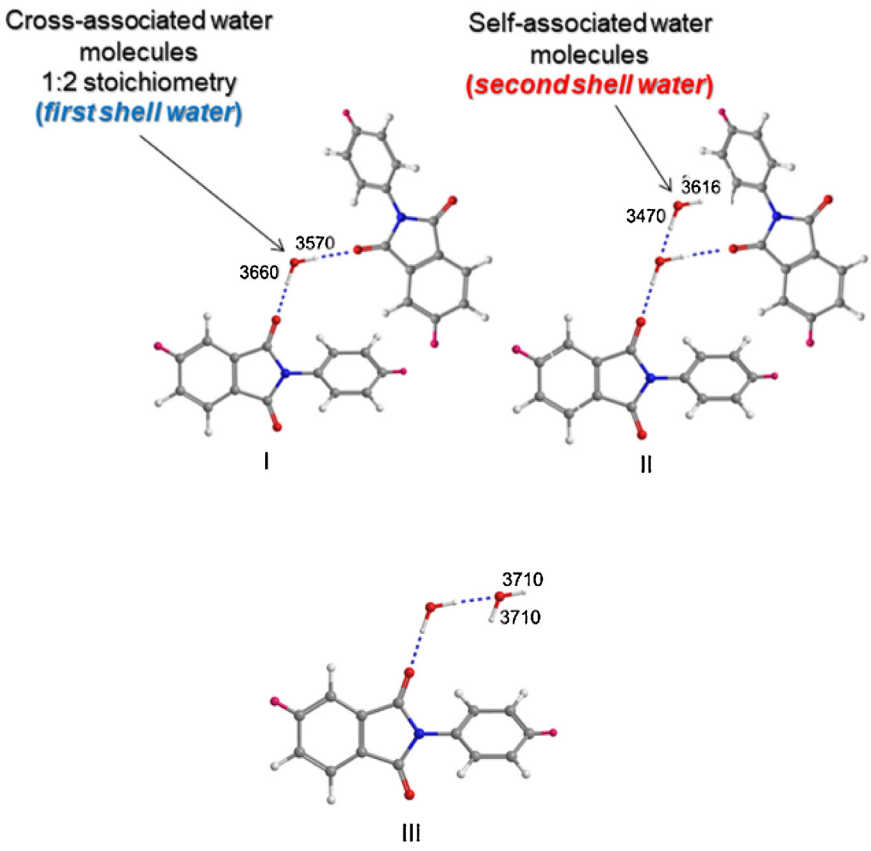

Fig. 76. Schematic representation of the HB interactions in the investigated H_2O/PI systems. Atoms color codes: white = H; grey = C; red = O, blue = N; cyan = dummy. The structures represented are those of the 6FDA-ODA and the 6FDA-6FpDA polyimides. Also indicated, are the frequencies of the stretching vibrations of the O—H bonds for the different water species. Reprinted with permission from [267]. Copyright 2012 American Chemical Society. (For interpretation of the references to colour in this figure legend, the reader is referred to the web version of this article.)

k_{12}), and the molar Helmholtz energy of formation of polymer/water HB interaction, A^0_{12} (numerical values are reported in Table 10). Based on the spectroscopic results the model accounted for the presence of four proton acceptor groups (carbonyls) per repeating unit of polymer. Each water molecule was assumed to carry two proton donor and two proton acceptor groups. The densities of the two polymers have been assumed to keep a constant, frozen-in, non-equilibrium value, equal to that of the starting dry material, assuming that absorbed water does not affect them. Fitting of sorption isotherms by NETGP-NRHB model provided also a quantitative estimate of the amount of each of the different hydrogen bonding adducts that form within the polyimide-water mixture at phase equilibrium with water vapor at different relative pressures. In Figs. 81 and 82, for the case of 6FDA-ODA and of 6FDA-6FpDA, these estimates are compared with the outcomes of vibrational spectroscopy (after their conversion in terms of moles of self-HB occurring between water molecules and moles of cross-HB occurring between water molecules and polymer backbone, both normalized per mass of polymer). An excellent matching was found between model predictions and experimental results.

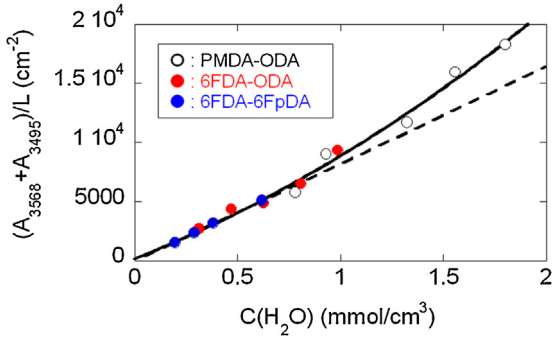

Fig. 77. $(A_{3568} + A_{3495})/L$ as a function of water concentration in the investigated PIs. Curve is intended for eye guidance only. Reprinted with permission from [267]. Copyright 2012 American Chemical Society.

A system with similar thermodynamic characteristics is the water/polyetherimide (water/PEI). It has been investigated [260] adopting the same approach as for the case of water/PIs, based on the combination of gravimetry, vibrational spectroscopy and modelling of sorption thermodynamics by means of the NRHB model. Further molecular details on the type and amount of adducts formed by hydrogen bonding were also provided by molecular dynamics simulations.

The repeating unit of PEI is reported in Fig. 83. Difference spectra were obtained by performing subtraction spectroscopy (subtraction of dry PEI spectrum from the spectra collected for the H_2O/PEI system). Time evolution of the difference spectra was available for each sorption test up to attainment of water sorption equilibrium. Of particular interest, in the present context, is the region of the ν(OH) band that conveys spectral information on absorbed water. Difference spectra, collected at sorption equilibrium conditions at several relative pressure of water vapor, are reported in Fig. 84. The OH-stretching region is characterized by similar features as for the case of the H_2O/PIs systems illustrated before, with an analogous fine structure that has been interpreted as an indication of the presence of different water species.

Please cite this article in press as: G. Mensitieri, G. Scherillo, C. Panayiotou et al. Towards a predictive thermodynamic description of Fsorption processes in polymers: The synergy between theoretical EoS models and vibrational spectroscopy. Mater. Sci. Eng. R (2020), https://doi.org/10.1016/j.mser.2019.100525

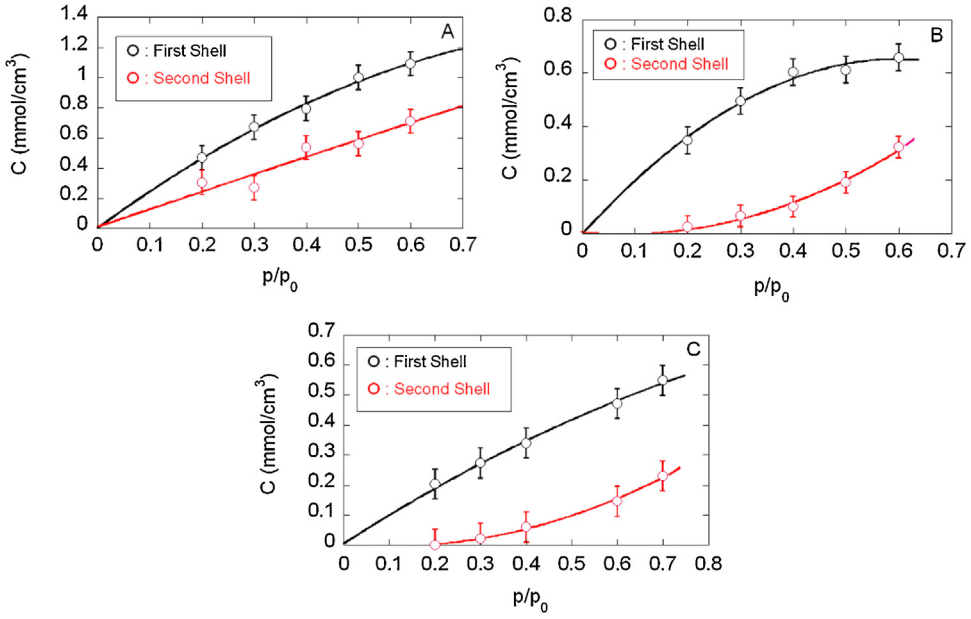

Fig. 78. Equilibrium concentration of first- and in the second-shell water molecules vs p / p_0. A) PMDA-ODA; B) 6FDA-ODA; C) 6FDA-6FpDA. Curves are intended for eye guidance only. Reprinted with permission from [267]. Copyright 2012 American Chemical Society.

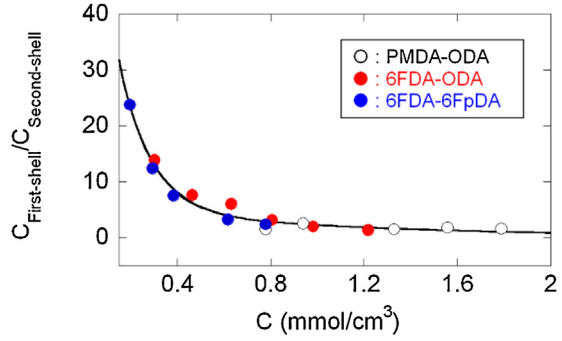

Fig. 79. The ratio $C_{First-shell}/C_{Second-shell}$ as a function of the total water concentration for the three PIs. Curve is intended for eye guidance only. Reprinted with permission from [267]. Copyright 2012 American Chemical Society.

2D-COS was performed on the time-resolved sorption measurement carried out at $p/p_0 = 0.6$, obtaining the asynchronous map reported in Fig. 85. Four different components were detected, arranged pairwise: the 3655–3562 cm^{-1} couple evolving synchronously at a faster rate as compared to the 3611–3486 cm^{-1} couple, also evolving synchronously. These results indicated that two distinct water species are present, each of them producing two OH-stretching modes (in phase at lower frequency and out of phase at higher frequency).

Information on which interacting groups on the polymer backbone are actually involved in interactions has been gathered from subtraction spectroscopy performed on thin polymer films. Interpretation of the spectra was carried out also relying upon full Normal Coordinate Analysis (NCA) based on quantum chemistry methods rooted on Density Functional Theory (DFT). As for the case of H_2O/PIs systems, the results of this analysis highlight the involvement of the imide carbonyls as proton acceptors in H-bonding. Conversely, the involvement of ether oxygens in interactions was found to be negligible. In Fig. 86 are reported the difference spectra (subtraction of dry polymer spectrum from the spectra of PEI equilibrated with water vapor) collected in the frequency range 1820–1660 cm^{-1}, at different relative pressures of water vapor. It is evident a *red shift* of both the peaks associated to the symmetric and antisymmetric stretching modes of the imide carbonyls, at all the relative pressures. This effect is caused by the electron-density withdrawing operated by the proton which, in turn, determines a lowering of the C=O force constant.

In the light of the outcomes of vibrational spectroscopy, the authors propose that the two peaks at 3655–3562 cm^{-1} are respectively associated to asymmetric and symmetric stretching modes of isolated water molecules interacting with the PEI carbonyls with a 2:1 stoichiometry of the carbonyl-to-water interaction. It means that each of these water molecules bridges two carbonyls belonging to different imide groups and that only a negligible fraction of H_2O molecules forms a single H-bonding with an imide carbonyl. Conversely, the two peaks at 3611–3486 cm^{-1} are associated to water molecules self-interacting with the above water species. In Fig. 87 are reported the proposed architectures of the two aggregates along with the associated peak frequencies.

A quantitative estimation of the concentration of the two water species at sorption equilibrium has been obtained by combining LCSF analysis of the spectral profiles in the ν(OH) region with the gravimetric sorption isotherm. The following equation has been

Table 9
NRHB parameters for pure polyimides and pure water [386].

Component	ε_s^* [J/mol]	ε_h^* [J/(mol K)]	$v_{sp,0}^*$ [cm^3/g]	E_{11}^{0w} [J/mol]	S_{11}^{0w} [J/(mol K)]	V_{11}^{0w} [cm^3/mol]
6FDA-ODA	5988.5	4.3186	0.5736			–
6FDA-6FpDA	5471.1	3.8652	0.5174			–
Water	5336.5	−6.506	0.9703	−16100	−14.7	0

Please cite this article in press as: G. Mensitieri, G. Scherillo, C. Panayiotou et al. Towards a predictive thermodynamic description of Fsorption processes in polymers: The synergy between theoretical EoS models and vibrational spectroscopy. Mater. Sci. Eng. R (2020), https://doi.org/10.1016/j.mser.2019.100525

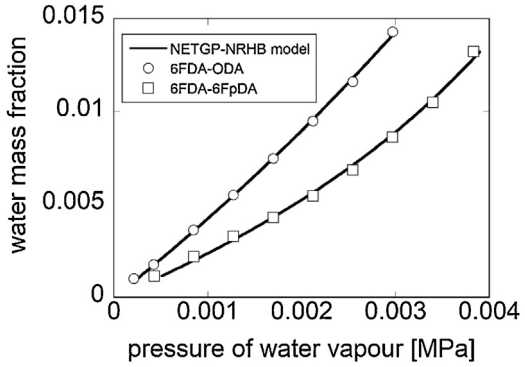

Fig. 80. Fitting by using NRHB model of Water sorption isotherms determined gravimetrically at 30 °C for 6FDA-ODA and 6FDA-6FpDA polyimides.

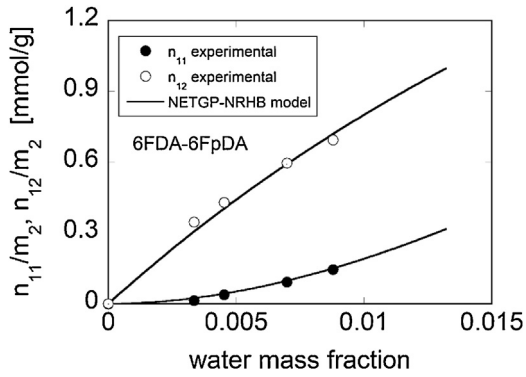

Fig. 82. Self- and cross- Hydrogen Bonding established in 6FDA-6FpDA/water mixture as a function of absorbed water mass fraction.

Table 10
NETGP-NRHB fitting parameters for the two PIs/H_2O systems [386].

System	ψ_{12}	A^0_{12} [J/mol]
6FDA-ODA/water	0.787	−12,400
6FDA-6FpDA/water	0.869	−12,100

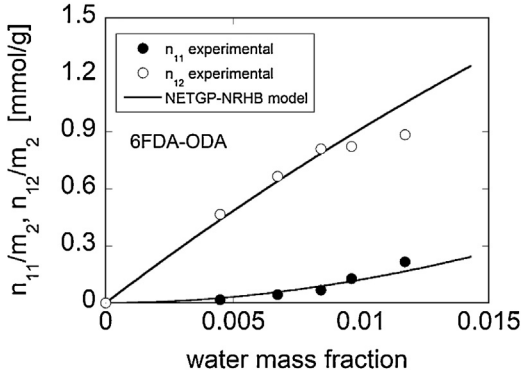

Fig. 81. Self- and cross- Hydrogen Bonding established in 6FDA-ODA/water mixture as a function of absorbed water mass fraction.

used to retrieve the molar absorptivity of first- and second-shell water (ε_{fs} and ε_{ss}):

$$\frac{A_{fs}}{C_{tot}} = \varepsilon_{fs} L - \left(\frac{\varepsilon_{fs}}{\varepsilon_{ss}}\right)\frac{A_{ss}}{C_{tot}} \tag{270}$$

where L is the sample thickness, A_{fs} and A_{ss} are the integrated absorbances (A_{fs} and A_{ss} are, respectively referred to the analytical signals at 3562 and 3468 cm^{-1}), C_{tot} is the volumetric concentration as evaluated at equilibrium at each water vapor activity. In Fig. 88 are reported the results of LSCF analysis performed on the subtraction spectrum along with (see the inset) the A_{fs}/C_{tot} vs A_{ss}/C_{tot} data and their fitting with Eq. (270) curve for evaluating the absorptivities of the analytical peaks (ε_{fs} = 34.5 km/mol and ε_{ss} = 89.7 km/ mol). It was then possible to use the Lambert-Beer relationship (i.e. $C_{fs}=A_{fs}/(L\cdot e_{fs})$ and $C_{ss}=A_{ss}/(L\cdot e_{ss})$) to estimate the absolute concentration of each water species at sorption equilibrium. These values are reported in Fig. 89A as a function of mass fraction of water at equilibrium. Moreover, based on the spectroscopic analysis performed on thin films, it was achieved a quantitative evaluation of carbonyl groups involved in HB interactions, see Fig. 89B. As shown in the same figure, the concentration of interacting carbonyls is identical to the double of concentration of first shell water, consistently with a 2:1 stoichiometry of the carbonyl-to-water interaction.

Quantitative estimates supplied by MD simulations for the values of C_{fs}, C_{ss} and of concentration of carbonyls involved in HB interactions, compare very well with the results of FTIR spectroscopy (see Figs. 89A,B). MD simulations provided also an interesting insight on the bridging of carbonyls by first-shell water. From this analysis it emerged that intramolecular bridges prevail (see Fig. 90). First-shell water molecules prevalently form HBs with two consecutive carbonyl oxygens. Interchain water bridges are less frequent, although their number increases with water concentration.

Water sorption thermodynamics in PEI has been again described by NETGP-NRHB model. Polymer density has been assumed to be time-invariant, taking the same value as that of the dry polymer at the temperature of each of the isotherms. Sorption isotherms at four temperatures (30, 45, 60 and 70 °C) have been determined gravimetrically and are reported in Fig. 91. Based on the results of vibrational spectroscopy, in the building of the model, only one type of proton acceptor groups (the imide carbonyls) has been accounted for. The values of EoS scaling parameters for pure PEI and of water and of self HB parameters for pure water were already available [310]. The curves resulting from the concurrent fitting of PE sorption data with the NETGP-NRHB model are reported in Fig. 91. Three fitting parameters were used: the energy and entropy of formation of water – polymer cross-HB (E^0_{12} and S^0_{12}) and the mean field binary interaction parameter (ψ_{12} = 1-k_{12}). As for the case of PIs, the volume of formation of water – polymer cross-HB has been taken to be equal to zero. The values determined for the thee parameters are reported in Table 11.

As for the case of polyimides, quantitative estimates of the amount of each of the different hydrogen bonding adducts that form within the PEI-water mixture at phase equilibrium with water vapor at different relative pressures have been obtained from the fitting procedure of the experimental sorption isotherms. In Fig. 92 these estimates are compared to the outcomes of vibrational spectroscopy and of MD simulations (after their conversion in terms of moles of self-HB occurring between water molecules and moles of cross-HB occurring between water molecules and polymer backbone, both normalized per mass of polymer), achieving a reasonable agreement.

4.2. Retrograde vitrification

EoS approaches can be effectively exploited to predict glassy and rubbery domains for amorphous polymers exposed to low molecular weight compounds at different values of temperature and pressure. Occurrence of glass transition in a polymer –

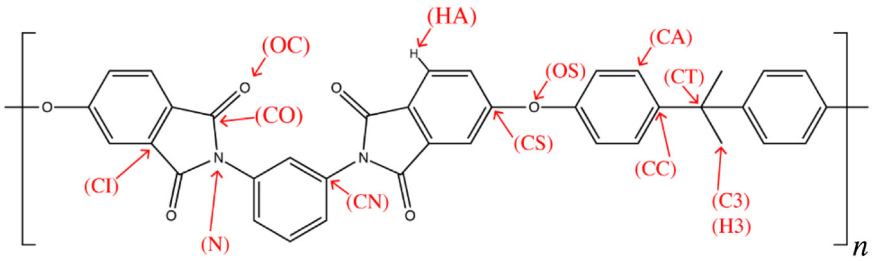

Fig. 83. Repeating unit of PEI. Different atom types are explicitly labeled. Reprinted with permission from [260]. Copyright 2017 American Chemical Society.

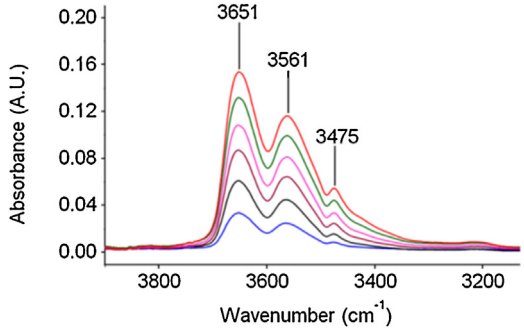

Fig. 84. Difference spectra of a PEI film at sorption equilibrium with water vapor at different relative pressures (Greentrace, dry film; blue, $p/p_0 = 0.1$; black, $p/p_0 = 0.2$; dark red, $p/p_0 = 0.3$; magenta, $p/p_0 = 0.4$; dark green, $p/p_0 = 0.5$; red, $p/p_0 = 0.6$) at T = 30 °C. Reprinted with permission from [260]. Copyright 2017 American Chemical Society. (For interpretation of the references to colour in this figure legend, the reader is referred to the web version of this article.)

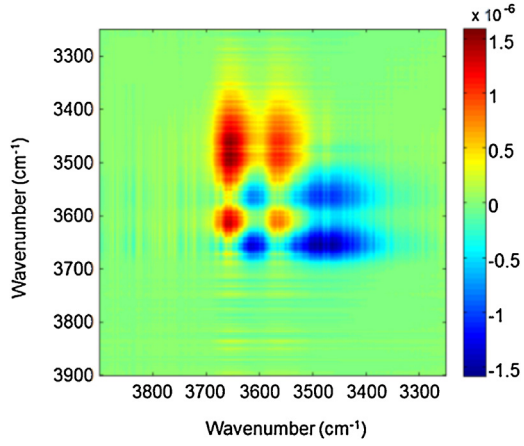

Fig. 85. 2D-COS Asynchronous map referred to time-resolved spectra collected I water sorption experiments performed at $p/p_0 = 0.6$ and T = 30 °C. Reprinted with permission from [260]. Copyright 2017 American Chemical Society.

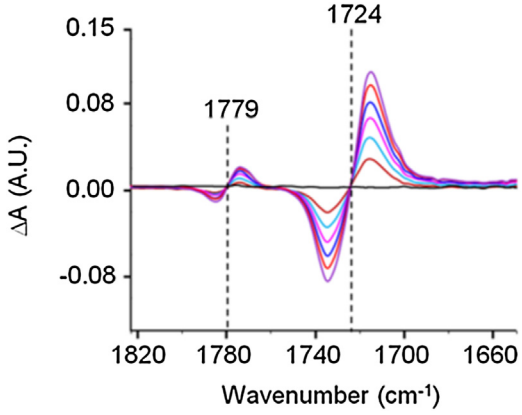

Fig. 86. Difference spectra collected in the1820 – 1660 cm^{-1} range for PEI film with a 3.0 μm thickness after equilibration at different relative pressures of water vapor. Red navy trace: $p/p_0 = 0.1$; light blue: $p/p_0 = 0.2$; purple: $p/p_0 = 0.3$; blue: $p/p_0 = 0.4$; red: $p/p_0 = 0.5$; violet: $p/p_0 = 0.6$. T = 30 °C. Reprinted with permission from [260]. Copyright 2017 American Chemical Society. (For interpretation of the references to colour in this figure legend, the reader is referred to the web version of this article.)

penetrant system is ruled by penetrant pressure and system temperature. In fact penetrant pressure has a direct mechanical effect on the glass transition temperature (T_g) and an indirect effect associated to the plasticizing action of dissolved penetrant that, in turn, is related to the dependence on temperature and pressure of the solubility of the penetrant itself within the polymer (the higher is the concentration of the penetrant the higher is the depression of T_g of the system).

Condo et al. [333] modelled the dependence of the T_g of the polymer-penetrant system on the pressure of penetrant in contact with the polymer, on the basis of the Gibbs – Di Marzio criterion for glass transition [171,334], stating that at T_g the configurational mixture entropy is zero. This approach is rooted on the interpretation of glass transition as a second order thermodynamic transition, i.e. on the existence an ideal glass transition temperature, T_2, that occurs in a polymer, kept constant all the other conditions, at infinitely slow cooling starting from a rubbery state. The adopted expression of the configurational entropy was provided by Sanchez-Lacombe EoS [5]. Four different types of T_g vs penetrant pressure diagrams were identified, ranging from type I to type IV [333]. The so-called *retrograde vitrification* relevant phenomenon was evidenced consisting in the occurrence of a rubbery-to-glass transition as temperature increases. As an example, under isobaric conditions, for a polymer-penetrant mixture at equilibrium with a penetrant fluid phase, the phenomenon occurs when an increase in temperature determines an increase in polymer segmental mobility that is overcome by a reduction of this mobility determined by a decrease of penetrant solubility within the polymer phase. This phenomenon is schematically represented in Fig. 93, in the case of a type IV behavior [390].

Pierleoni et al. [391], for the case of thin films of atactic polystyrene (aPS) exposed to toluene vapor, adopted dynamic desorption/sorption experiments to create a T_g vs pressure diagram, obtaining a map for rubbery and glassy states of the polymer that displays a type IV behavior. The experimental set-up was arranged to control with high accuracy the rate of change of the temperature of the system and/or of the pressure of the vapor phase. In Fig. 94 are schematically illustrated the experimental patterns of the three types of scan of temperature and pressure values: isobaric, isothermal and iso-activity tests. An example of the results of isothermal dynamic desorption/sorption experiments is reported in Fig. 95.

Please cite this article in press as: G. Mensitieri, G. Scherillo, C. Panayiotou et al. Towards a predictive thermodynamic description of Fsorption processes in polymers: The synergy between theoretical EoS models and vibrational spectroscopy. Mater. Sci. Eng. R (2020), https://doi.org/10.1016/j.mser.2019.100525

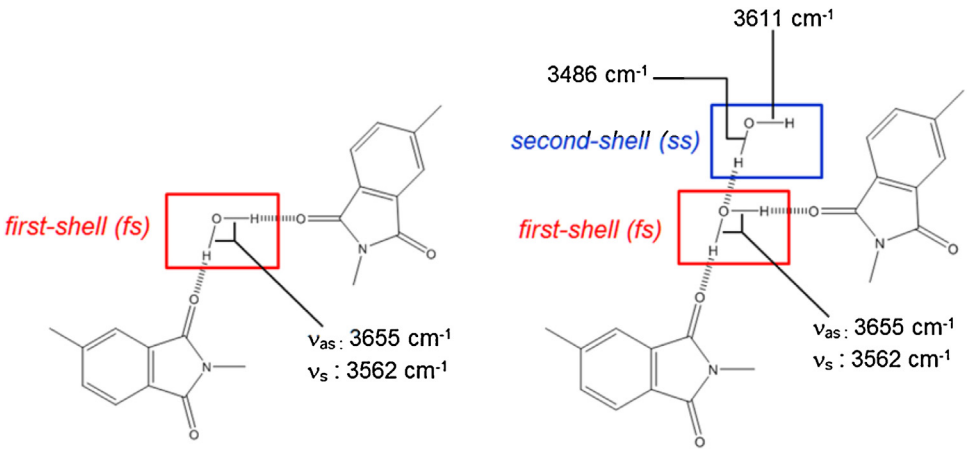

Fig. 87. Representation of two water species proposed for the PEI/H_2O system. On the left side are depicted the isolated water molecules belonging to the first hydration layer of penetrant (first shell) and, on the right side, are depicted the self-associated water molecules belonging to the second-shell hydration layer (second shell). Reprinted with permission from [260]. Copyright 2017 American Chemical Society.

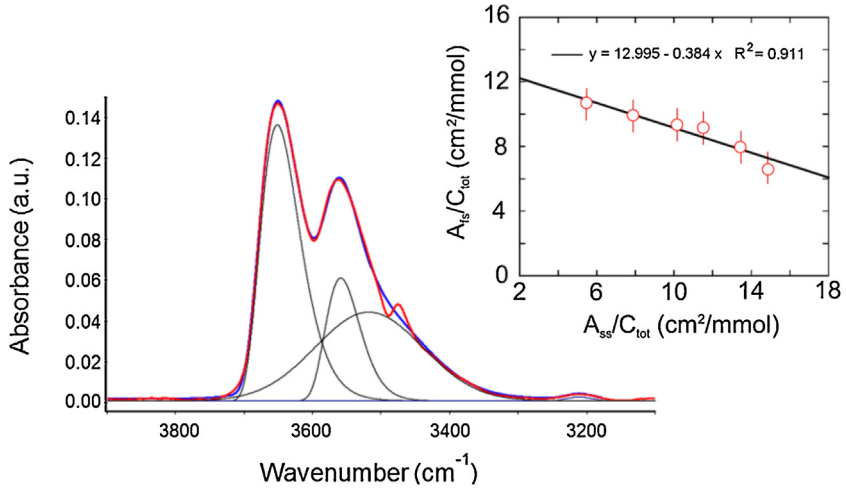

Fig. 88. LCSF analysis of the subtraction spectrum in the OH-stretching region for PEI-H_2O system at water sorption equilibrium at $p/p_0 = 0.6$ and 30 °C. Are reported the experimental profile (red trace), the best-fitting curve (blue trace) and the resolved components (black traces). In the inset are reported data for A_{fs}/C_{tot} vs A_{ss}/C_{tot} and the fitting performed using Eq. (270) curve for evaluating the absorptivities of the analytical peaks. Reprinted with permission from [260]. Copyright 2017 American Chemical Society. (For interpretation of the references to colour in this figure legend, the reader is referred to the web version of this article.)

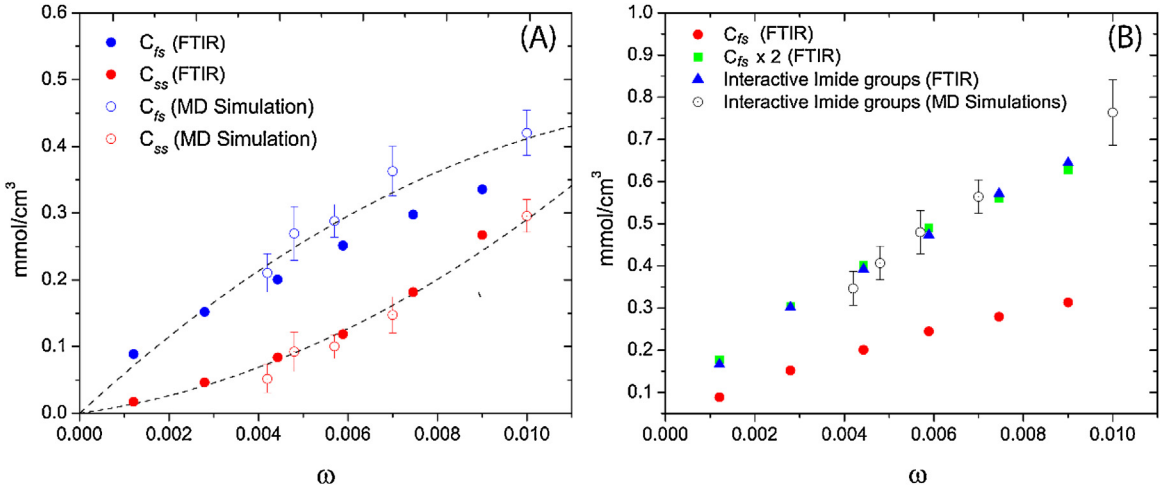

Fig. 89. (A): Values of C_{fs} and C_{ss} estimated from FTIR spectroscopy and from MD simulation, reported as a function of relative pressure of mass fraction of water in the water-PEI mixture at equilibrium with water vapor at different p/p_0. Dotted lines are a guide for the eye. (B): Concentration of interacting carbonyls of imide groups determined from FTIR spectroscopy and resulting from MD simulations are reported as a function of mass fraction. Experimental values of C_{fs} and $2xC_{fs}$ are also reported for comparison purposes. Reprinted with permission from [260]. Copyright 2017 American Chemical Society.

Please cite this article in press as: G. Mensitieri, G. Scherillo, C. Panayiotou et al. Towards a predictive thermodynamic description of Fsorption processes in polymers: The synergy between theoretical EoS models and vibrational spectroscopy. Mater. Sci. Eng. R (2020), https://doi.org/10.1016/j.mser.2019.100525

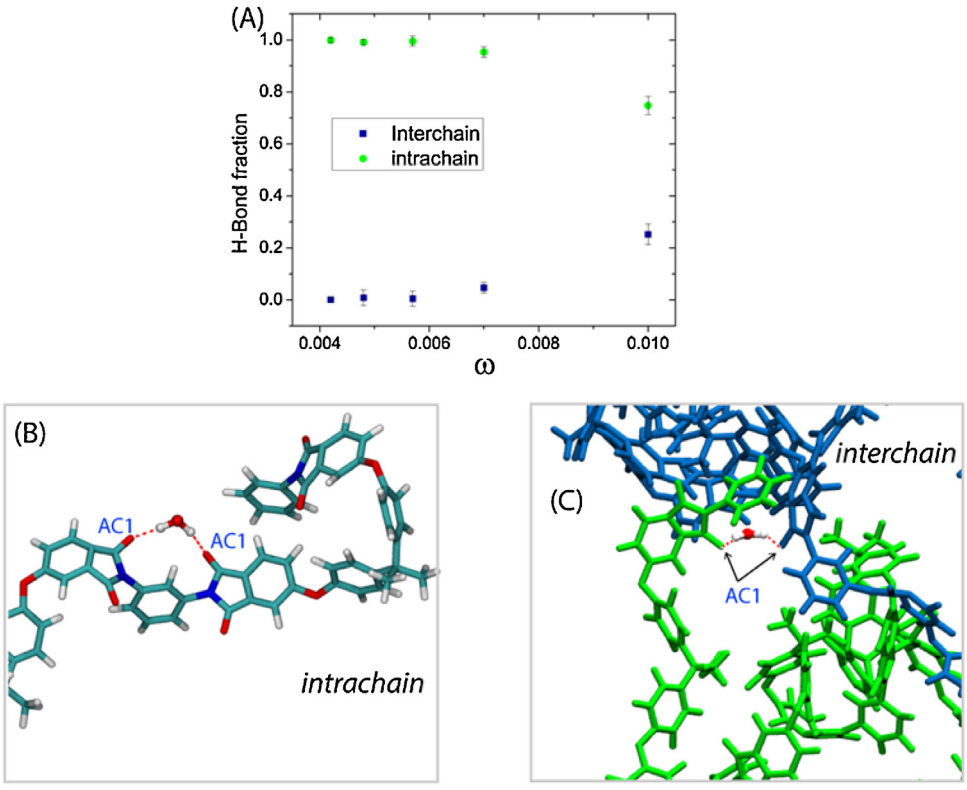

Fig. 90. (A) Fractions of intrachain and interchain H-Bond formed by first-shell water molecules with imide carbonyls (AC1) as a function of water mass fraction in PEI, at equilibrium with water vapor at several values of p/p_0. (B): Snapshot of an intrachain hydrogen bond. (C): Snapshot of an interchain hydrogen bond; the two different chains are reported in blue and green, respectively. Reprinted with permission from [260]. Copyright 2017 American Chemical Society. (For interpretation of the references to colour in this figure legend, the reader is referred to the web version of this article.)

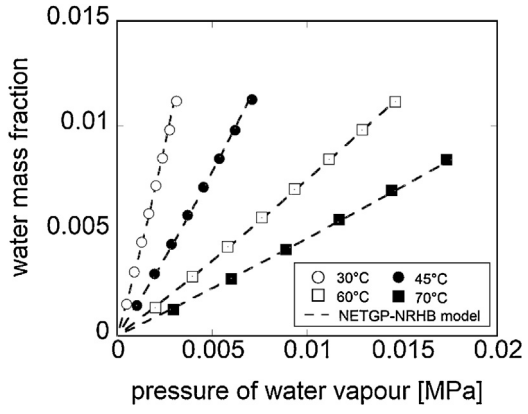

Fig. 91. Gravimetric water sorption isotherms in PEI. Symbols are experimental points. Dotted lines are the results of concurrent curve-fitting of the four isotherms using NETGP-NRHB.

The authors, considering the glass transition as being a second order thermodynamic transition, provided a proof of the fact that, if such a transition occurs in a rubbery polymer mixture in equilibrium with a penetrant in the vapor state (first order equilibrium curve), at the junction between the first order and second order equilibrium curves one observes discontinuities in the values of the derivatives of mass fraction of penetrant in the polymer mixture as a function of temperature or pressure. On this basis they were able, starting from the identification of such discontinuities in dynamic desorption/sorption experiments, to construct the rubbery-glassy map for the toluene-aPS system.

Table 11
NETGP-NRHB fitting parameters for the PEI/H_2O system [260].

ψ_{12}	E_{12}^{0wp} [J/mol]	S_{12}^{0wp} [J/(mol·K)]	V_{12}^{0wp} [cm³/mol]
0.879 ± 0.005	−13,264 ± 200	−6.107 ± 0.100	0

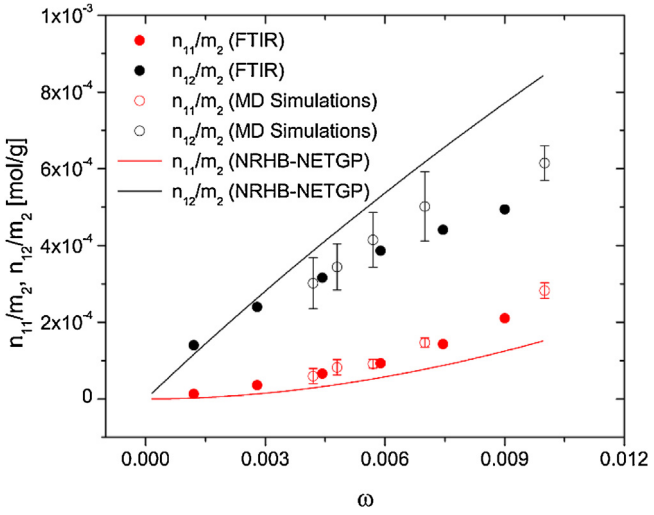

Fig. 92. Comparison of the predictions of the NETGP-NRHB model for the amount of self- and cross-HBs with the outcomes of FTIR spectroscopy and of MD simulations. Reprinted with permission from [260]. Copyright 2017 American Chemical Society.

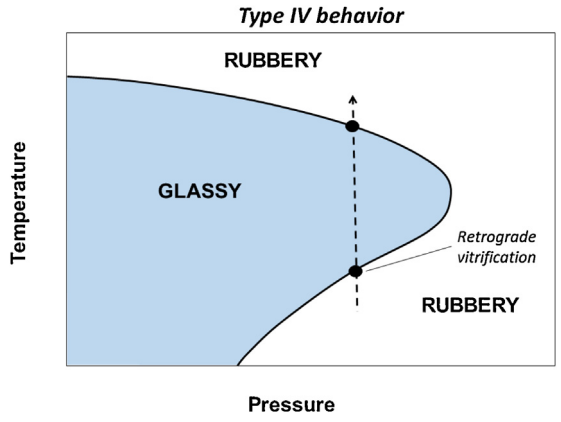

Fig. 93. Schematic glass transition temperature – pressure plot reporting a type IV behavior and associated *retrograde vitrification* phenomenon for a mixture of a polymer with a low molecular weight penetrant. Reprinted with permission from [390]. Copyright 2018 American Chemical Society.

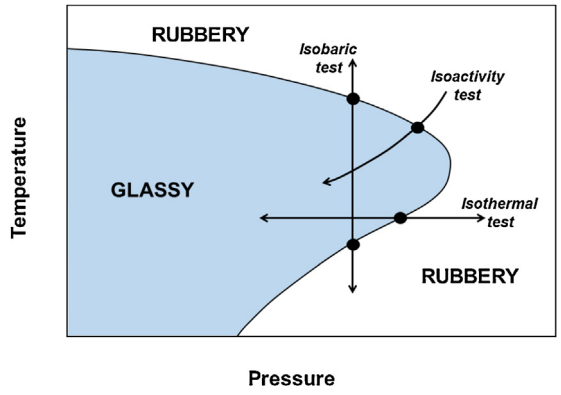

Fig. 94. Schematic illustration of the patterns of the three different types of 'dynamic' sorption tests performed by Pierleoni et al. [391]. Reprinted with permission from [390]. Copyright 2018 American Chemical Society.

In a companion paper [390], were presented rubbery-glassy maps for the toluene/aPS system predicted theoretically by using the NRHB model, without the terms accounting for specific interactions. The model was first used to perform a concurrent fitting of toluene sorption isotherms in PS at several temperatures (ranging from 40 to 110 °C), obtaining an excellent agreement. The only fitting parameter was the mean field interaction parameter, k_{12} (= -0.0015 ± 0.0002). NRHB scaling parameters for toluene and PS were taken from the literature [39,95]. Expressions for entropy of the mixture were those of the NRHB model. It is to be noted that in the NRHB theory, as for any lattice theory, the only entropy accounted for is the configurational one. As a consequence, the application of the GD criterion consists in taking equal to zero the total equilibrium entropy of a polymer-penetrant binary mixture calculated using NRHB model. According to the NRHB approach the total (configurational) entropy is:

$$S_{tot} = S_{LF} + S_{HB} = S_{LF,R} + S_{LF,NR} + S_{HB} \quad (271)$$

where S_{tot} is the total configurational entropy of the system, that is made of a 'lattice fluid' contribution, S_{LF}, and an 'Hydrogen Bonding' contribution, S_{HB}, that is neglected in the case of toluene/PS system. S_{LF} contribution is, in turn, the sum of a *random* contribution, $S_{LF,R}$ (this would be the total lattice fluid contribution in the case of random mixing) and of a term accounting for non-random distribution of site contacts in the lattice, $S_{LF,NR}$.

The random term has the following expression:

$$S_{LF,R} = S^{C}_{LF,R} + S^{INT}_{LF,R} \quad (272)$$

$S^{C}_{LF,R}$ is an external 'configurational' contribution that is expressed as:

$$S^{C}_{LF,R}/(RrN) = (1 - \sim\nu)ln(1 - \sim\rho) + (l + ln(r\sim\nu))/r - \sum_i x_i lnx_i + (z/2)(\sim\nu - 1 + q/r)(1 - \sim\rho + q/r) \quad (273)$$

while $S^{INT}_{LF,R}$ is an 'internal' or 'molecular flexibility' contribution to entropy [392], expressed as:

$$S^{INT}_{LF,R}/(RrN) = \sum_i \left(\frac{\phi_i}{r_i}\right) ln\delta_i \quad (274)$$

where δ_i is the so-called *chain flexibility parameter* [172,333,393,394].

The non-random lattice fluid contribution is given by [395]:

$$S_{LF,NR}/(RrN) = \frac{z}{2}\left[-(\sim\nu - 1)\cdot ln(\Gamma_{00}) - \frac{q_1}{r_1}\phi_1 \cdot ln(\Gamma_{11}) - \frac{q_2}{r_2}\phi_2 \cdot ln(\Gamma_{22}) + (\sim\nu - 1)(\Theta_1 \cdot \Theta_r \cdot ln(A_{01}) \cdot \Gamma_{01} + \Theta_2 \cdot \Theta_r \cdot ln(A_{02}) \cdot \Gamma_{02}) + \frac{q_1}{r_1}\phi_1 \cdot \Theta_2 \cdot \Theta_r \cdot ln(A_{12}) \cdot \Gamma_{12}\right] \quad (275)$$

The expression of the S_{HB} term is not reported here since is not relevant for the toluene/aPS system. In Eqs. (273–275), x_i represents the molar fraction of species i, and $A_{ij} = e^{\left(\frac{\Delta\varepsilon_{ij}}{kT}\right)}$ where $\Delta\varepsilon_{ij} = \varepsilon_{ii} + \varepsilon_{jj} - 2(1 - k_{12})(\varepsilon_{ii}\varepsilon_{jj})^{0.5}$ and $\varepsilon_{ii} = \varepsilon^{*}_{i}\frac{2}{z}$. Here i, j = 0,1,2 and $\varepsilon^{*}_{0} = 0$. Finally, $\Theta_r = \frac{q/r}{(q/r + \sim\nu - 1)}$.

Details and relevant issues related to the calculation of δ_i for each component of the mixture are reported in [390]. It suffices here to mention that its value is related to the so-called *flex energy* for bonds within the molecules of the two components. The *flex energy* for each of the components is assumed to be neither dependent on temperature nor on composition. Its value could be calculated by zeroing the equilibrium entropy of a pure component - polymer or penetrant - at T_2. Since this temperature is virtually unattainable, for all practical purposes, in the case of a polymer,

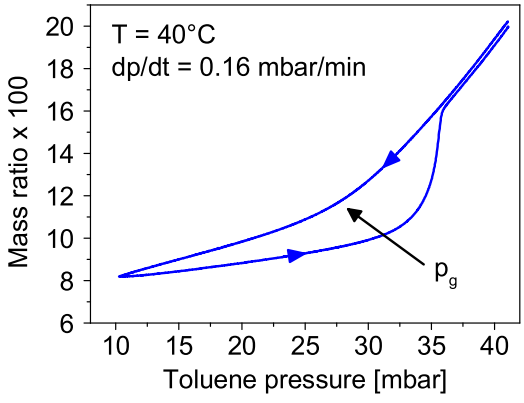

Fig. 95. Isothermal dynamic desorption/sorption experiments performed on PS in contact with toluene vapor at 40 °C of toluene in PS and at constant rate of change of the pressure of toluene vapor equal to 0.16 mbar/min. Rubbery to glassy state transition during dynamic desorption step is highlighted by an arrow. Reprinted with permission from [391]. Copyright 2017 American Chemical Society.

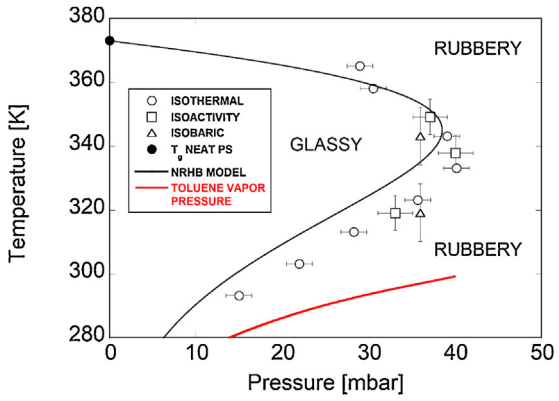

Fig. 96. Comparison of experimental data for T_g vs P taken from ref. [391] with theoretical predictions obtained using the NRHB model. Reprinted with permission from [390]. Copyright 2018 American Chemical Society.

one may retrieve the value of *flex energy* from the experimentally accessible glass transition temperature, T_g (see ref. [396] for arguments in support of this choice). In the case of the low molecular weight penetrant, the assumption of full flexibility is adopted, i.e. of zero *flex energy*. NRHB model was then used to obtain theoretical predictions of glass transition temperature as a function of fluid pressure. To this aim it was solved the set of equations including the phase equilibrium condition between polymeric mixture phase and toluene vapor (i.e. the equivalence of chemical potentials of the two components in the two phases), the equations of state for pressure for each of the two phases, and the equation expressing the zeroing of equilibrium configurational entropy of the mixture. The solution of this set of equations provides information on the couples of values of temperature and pressure of the vapor phase at which the equilibrium configurational entropy is zero for a rubbery polymer-penetrant mixture in phase equilibrium with an external fluid phase.

In Fig. 96 are reported the NRHB model predictions obtained as described above [390] compared with results obtained by performing isothermal, isoactivity and isobaric dynamic desorption/sorption experiments at a pressure change rate of 0.16 mbar/min [391]. Theoretical predictions were very close, qualitatively and quantitatively, to the experimental outcomes.

At this point, some remarks on the procedure illustrated above to predict the glass transition temperature are appropriate. The theoretical approach of Gibbs and DiMarzio is rooted on the physical interpretation of glass transition upon cooling as emerging from a significant reduction of the number of accessible configurational states related to the increase of rigidity of polymer chains. Relevant successful quantitative predictions obtained from application of this approach are reported in the literature [397,398]. The role of the "configurational entropy" S^C (i.e. the contribution to the total entropy of the fluid related to the number of distinct configurational states, with exclusion of vibrational contributions) is pivotal in the GD theory. Unfortunately, it is rather difficult to gather a fully reliable quantitative estimate of S^C from experiments or from numerical simulations.

Dudowicz et al. [399], in the contribution where they propose a generalization of the classic entropy approach to glass formation starting from an analysis of previous entropy theory, provide a review of the strengths and weaknesses of the GD theory. In their contribution, Dudowicz et al. highlight as the vanishing of S^C upon cooling has been suggested to actually result from the intrinsic inaccuracy of the meanfield calculations of the GD theory and report as even the identification of a vanishing S^C with a second-order phase transition and of the glass transition temperature with the temperature of this hypothetical transition has been criticized.

The zero entropy GD criterion has been also challenged by Wittmann and by Binder et al. [400–402] that questioned the Gibbs-Di Marzio interpretation that the experimentally accessible glass transition reflects the vanishing of configurational entropy at a temperature T_2 in the case of a quasi-static cooling. In particular, Wittmann, adopting an improved lattice fluid framework, demonstrated that the hypothesized transition temperature, T_2, (i.e. the lowest temperature at which the configurational entropy of the system is non-negative) vanishes as the coordination number of the lattice diverges, thus inferring that the existence of such a transition is likely a consequence of the approximations introduced by the statistics associated to development of the partition function.

However, Dudowicz et al. [399], as final assessment, suggest that the concept that glass formation results from an 'entropy catastrophe' still provides a viable model for a qualitative picture of polymer glass transition, as also supported by mean-field calculations for spin models [403–405] that are in line with results generated from GD theory. According to Dudowicz et al. [399] it can be inferred that S^C does not vanish but becomes critically small near T_2 and the conceptual issues of GD theory can be largely overcome by considering the configurational entropy of the lattice model to represent the excess configurational entropy relative to the entropy of the glass.

In the light of these arguments and of the fact that the GD theory deals with an 'ideal glass transition temperature' (thus disregarding its difference with the experimentally accessible T_g) we can comment on the physical soundness of the approach proposed, in the publications reviewed in this section, to predict the dependence of glass transition temperature of a binary polymer-penetrant system. As discussed, this approach is based on the combination of the GD criterion of zeroing of configurational entropy at the transition with the expression of S^C provided by a compressible lattice fluid theory. Actually, it has to be considered as an empirical method, guided by the 'entropy catastrophe' concept, to scale the experimentally accessible glass transition temperature of the pure polymer to the case of polymer-penetrant mixtures.

4.3. Bubble nucleation and polymer foaming

Porous polymers or polymer foams are attracting particular attention as candidate materials in numerous applications such as, scaffolding for tissue engineering, thermal and sound insulation, packaging, sporting equipment, airplane and automotive parts, microelectronic and optical devices [392,406–410]. Supercritical fluids (mainly CO_2 and N_2) are often used for polymer foaming either in batch or in continuous processes. There is, then, a series of issues to be addressed for a rational design of polymer foaming [411]. Apart from the solubility of the blowing agent in the polymer matrix, one has to account for interfacial phenomena, viscosity/viscoelasticity issues and, especially, for the peculiar phenomenon of retrograde vitrification [333,411]. The very formation of pores inside the matrix may be done by triggering nucleation either by pressure induced phase separation or solvent induced or even temperature induced phase separation. It is then of primary importance to have a reliable and versatile equation-of-state model as a guide for the rational design of the production of porous polymers with the appropriate pore size and pore size distribution [411]. NRHB theory is particularly suited for this purpose [412].

In this sub-section, we will first recall the essentials of the classical theory of homogeneous nucleation and, subsequently, we will see how NRHB may assist in the design of porous polymer structures. Heterogeneous nucleation also occurs when nuclei are produced on two-phase boundaries, i.e. on the surface of solid particles (fillers or impurities), on preexisting gas cavities, or

Please cite this article in press as: G. Mensitieri, G. Scherillo, C. Panayiotou et al. Towards a predictive thermodynamic description of Fsorption processes in polymers: The synergy between theoretical EoS models and vibrational spectroscopy. Mater. Sci. Eng. R (2020), https://doi.org/10.1016/j.mser.2019.100525

between areas of different density due to dispersed crystallites. However, in most cases of neat polymer foaming the results are discussed assuming homogeneous nucleation.

The first step in polymer foaming is the dissolution of the blowing agent (say, carbon dioxide) in the polymer matrix. The saturated system is, subsequently, destabilized thermodynamically by pressure reduction, as an example. According to the classical homogeneous nucleation theory, the change in the system free energy due to gas nuclei formation inside the metastable polymer matrix can be written as the sum of the free energy gain related to the new phase formation and the cost (increase) of the free energy due to the formation of the interface. Thus, in a closed isothermal system in equilibrium, the free energy change per unit volume due to the formation of new phase cluster is given by the following equation [413,414]:

$$\Delta G = -\frac{4\pi r^3}{3}\Delta P + 4\pi r^2 \gamma \tag{276}$$

In this equation, r is the radius of the spherical cell or cluster, γ the interfacial tension, and ΔP the pressure difference due to the supersaturation of the system. Eq. (276) is derived assuming homogeneous nucleation and that the new cluster phase has bulk phase properties at the same physical state. When ΔG is plotted against cluster size, a curve is obtained exhibiting a maximum at a critical radius r_c, or:

$$\frac{d\Delta G}{dr} = 0 \Rightarrow r_c = \frac{2\gamma}{\Delta P} \tag{277}$$

The maximum ΔG value for homogeneous nucleation is obtained by substituting Eq. (277) into Eq. (276), resulting in the following key equation:

$$\Delta G^*_{hom} = \frac{16\pi\gamma^3}{3\Delta P^2} \tag{278}$$

The main difficulty of applying Eq. (278), is that the interfacial tension between a nucleus with critical size and the metastable polymer matrix is not directly measurable [415]. Thus, in most cases, in order to apply the classical nucleation theory, this interfacial tension is approximated with the corresponding interfacial tension of the macroscopic interface at equilibrium.

Besides γ, much attention should be paid to ΔP in Eq. (278). This ΔP is the pressure difference due to supersaturation of the system. According to Gibbs [416], this pressure difference, $\Delta P = P_\beta - P_\alpha$, is the difference of the pressure, P_β, that the nucleating phase would have at the same temperature and chemical potential with the metastable phase, minus the actual pressure, P_α, of the metastable phase [417]. Very often, this pressure difference is approximated by the actual pressure drop (quench) during the rapid depressurization of the system [392,418]. However, with this approximation the energy barrier for nucleation is rather underestimated [417]. On the other hand, this pressure difference, $\Delta P = P_\beta - P_\alpha$, can be quite well estimated using an appropriate equation of state model through the following phase equilibrium condition [416]:

$$\mu_{g,\alpha}(T, P_\alpha, x_{g,\alpha}) = \mu^o_{g,\beta}(T, P_\beta) \tag{279}$$

where, T is the temperature, x_g is the mole fraction of the gas inside the metastable polymer phase (usually, set equal to the equilibrium solubility at saturation conditions), μ_g is the chemical potential of the gas; subscripts α and β denote the metastable phase, α, and the nucleating phase, β, respectively, while superscript, o, denotes pure substance (here, the nucleating phase is pure gas).

Having the free energy barrier for nucleation, Eq. (278), the nucleation rate, N_o, which represents the number of stable nuclei produced in the system per unit time and unit volume, is given by

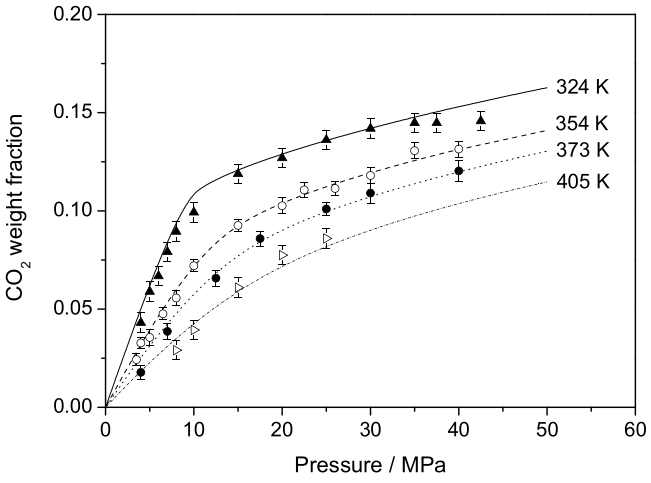

Fig. 97. Sorption of CO_2 in polystyrene. Symbols represent experimental data [420] and lines NRHB calculations.

the following Arrhenius-type equation:

$$N_o = J_k \exp\left(\frac{-\Delta G^*_{hom}}{kT}\right) \tag{280}$$

where, k is the Boltzmann constant and J_k a kinetically determined pre-exponential constant.

From the above exposition and Eqs. (276–279), it is clear that application of the nucleation theory requires a sufficiently accurate estimation of the dissolved amount of fluid (foaming agent) in the polymer matrix, and also the estimation of the induced plasticization of the polymer matrix, of the interfacial tension between the gas nuclei and the polymer phase, as well as of the chemical potentials of all components in the metastable polymer and nucleating phases. As mentioned already, NRHB model can be of much assistance here.

First of all, NRHB and its variations (LFHB, QCHB, COSMO-NRF, LFCOSMO), as an equation-of-state model, is well suited for the estimation of solubilities and phase equilibria over a broad range of pressure and temperature. Second, it is able to describe well the polymer matrix plasticization and the retrograde vitrification. In addition, it may be used for a satisfactory estimation of the effect of

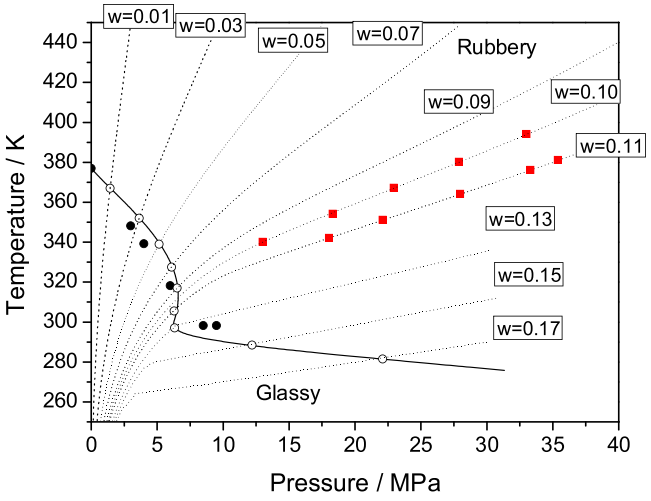

Fig. 98. The plasticization behavior of CO_2 – PS system. Experimental data (solid circles, •) and NRHB predictions (solid line). Open circles (○) show the calculated glass transition point and w the weight fraction of CO_2 on every sorption isopleth. The pressure and temperature conditions used for the foaming experiments that refer to constant sorption conditions are also shown (solid squares, ■) on the $w = 0.10$ and $w = 0.11$ isopleths [419].

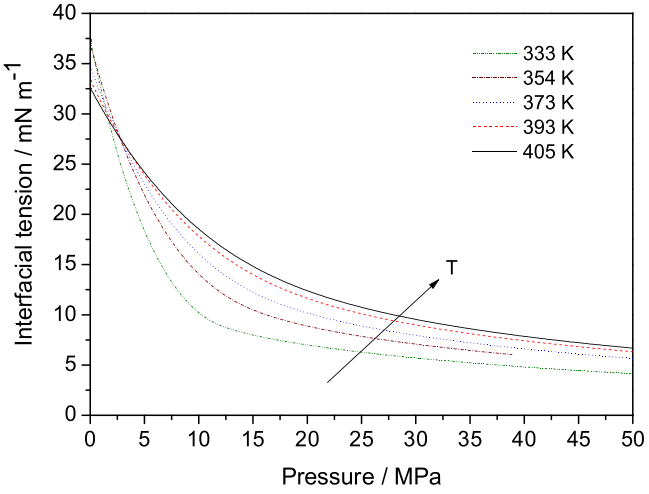

Fig. 99. Surface tension of a polystyrene matrix with dissolved CO_2 at equilibrium [419].

external conditions on interfacial tensions. All the above may apply to highly non-ideal systems including systems interacting with strong specific forces. In what follows, we will present some relevant applications.

Tsivintzelis et al. [419] have studied the foaming of polystyrene with CO_2. Solubility data over a broad range of T and P, were obtained previously by Pantoula et al. [420]. NRHB correlates rather well the experimental data, as shown in Fig. 97. This fitting provides also with the binary adjustable parameter) and, thus, the model may now be used for predictive calculations. The PS plasticization by CO_2, including retrograde vitrification, was calculated by adopting the Gibbs-DiMarzio assumption of zero entropy at the glass transition, as discussed by Tsivintzelis et al. [392]. These experimental glass transition temperatures are compared with the model predictions in Fig. 98. In the same figure are also shown the NRHB predictions for the sorption isopleths (dot lines) and the points on those isopleths (solid squares), which were selected for performing the constant sorption foaming experiments [420].

Assuming that the surface tension of the pure supercritical CO_2 is zero, and that the polymer – dissolved CO_2 system is a

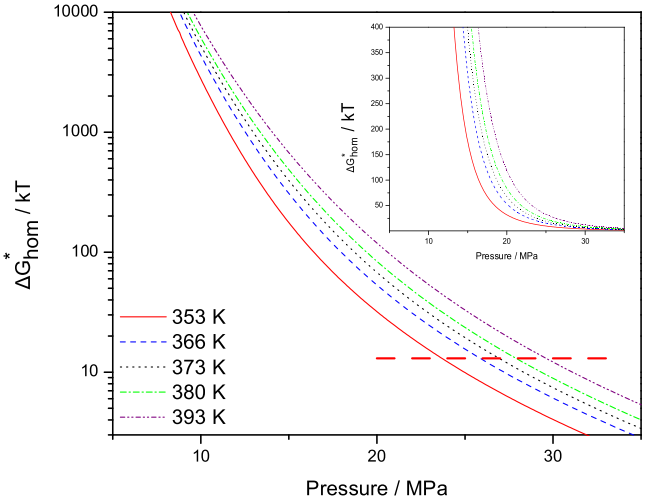

Fig. 100. Energy barrier for nucleation against saturation pressure in the polystyrene-CO_2 system assuming a very rapid isothermal depressurization to ambient pressure. The dash horizontal line denotes the conditions used for performing foaming experiments at a constant energy barrier for nucleation.

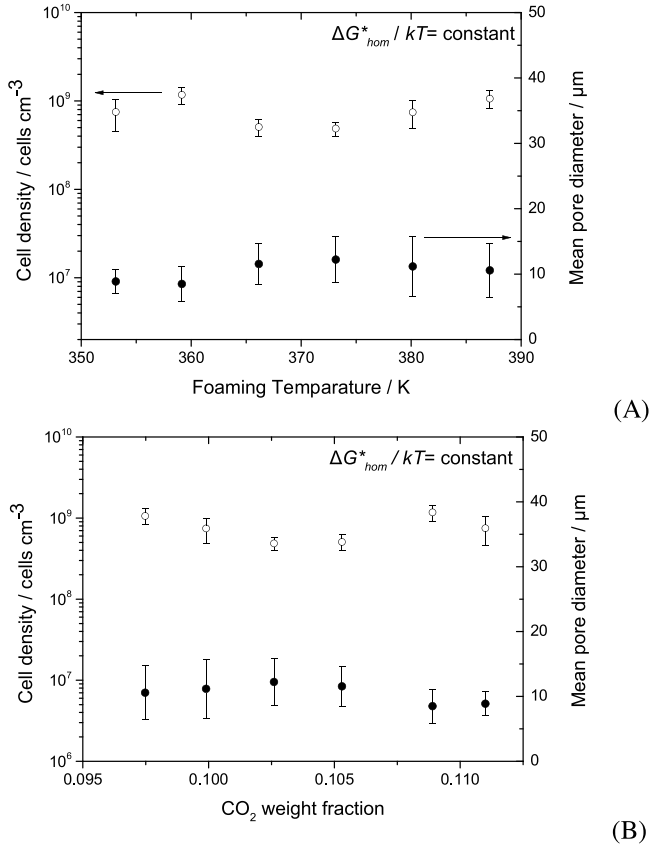

Fig. 101. Average pore diameter and cell population density for porous structures obtained at pressure and temperature conditions that refer to a constant energy barrier for nucleation [419], reported as a function of foaming temperature (A) and of CO_2 weight fraction.

homogenous liquid mixture, the interfacial tension between the polymer (plus dissolved CO_2) phase and the pure CO_2 gas was calculated, following Reid et al. suggestion [421], as:

$$\gamma_{mix}^{1/13} = (1 - w_{CO2})\gamma_{pol}^{1/13} \quad (281)$$

These calculations, over a range of temperatures, are shown in Fig. 99. With the above information, we may now apply Eq. (278) and calculate the energy barrier for nucleation. These calculations, over a range of temperatures and pressures, are shown in Fig. 100 [419]. This is a most useful plot for the rational design of polymer foaming. This plot was used to explain successfully the observed porous structures along the isopleths of Fig. 98 [419].

In Fig. 100 are also reported, by a dashed line, the experimental conditions (T, P) for performing foaming experiments under constant nucleation barrier. Under these conditions we expect similar porous polymer structures. Indeed, the obtained cell densities and mean pore diameters were fairly constant over the studied temperature range and the range of foaming agent content (dissolved CO_2 or external pressure), as shown in Fig. 101.

The above calculations are indicative of the capacity and usefulness of NRHB model for the design of polymer foaming process and porous polymer products for a variety of applications.

4.4. Gel swelling and collapse

NRHB or LFHB are particularly suited to handle the swelling of equilibrium amorphous network structures, either by ordinary solvents or by solvents in the near critical or supercritical state. What is needed is the addition to the physical and hydrogen-

bonding terms in the partition function, of a third term accounting for the rubber elasticity. Equivalently, one may write for the Gibbs energy of the network structure the following equation:

$$G = G_{Ph} + G_H + G_{el} \tag{282}$$

Various expressions may be used for G_{el} [422–425] or for the elastic factor in the partition function [423,424]. For convenience, the interpolation expression of Birshtein et al. [425] for the most common tetrafunctional cross-links will be used here:

$$G_{el} = kT\frac{3\nu_e}{2}\left(\alpha_s^2 + \frac{1}{\alpha_s^2} - 2 + \ln\alpha_s\right) \tag{283}$$

The key quantity in Eq. (283) is the swelling ratio, $\alpha_s{}^3$, that is the ratio of the equilibrium total volume of the swollen structure to the equilibrium volume of pure polymer at same temperature and pressure of the system, or:

$$\alpha_s^3 = \frac{V}{V_2} = \frac{rN\sim \nu v^* + \sum_{\alpha=1}^{m}\sum_{\beta=1}^{n}\left(N_{\alpha\beta}^H V_{\alpha\beta}^0\right)}{r_2N_2\sim \nu_2 v_2^* + \sum_{\alpha=1}^{m_2}\sum_{\beta=1}^{n_2}\left(N_{\alpha\beta}^H V_{\alpha\beta}^0\right)} = \frac{V_{Ph}+V_H}{V_2} \tag{284}$$

In the previous expressions, ν_e is the effective number of crosslinks in the rubber network. V_{Ph} and V_H are the non-hydrogen-bonding and the hydrogen bonding contributions, respectively, to the total volume of the system. Subscript '2' refers to the pure (unswollen polymer). All the other symbols have been defined in the section 2.

The "elastic" contribution to the equation of state (the extra term due to Eq. (283)) is:

$$\sim T\left[v^*\frac{\nu_e}{V_2}\left(\alpha_s^2 - \frac{1}{\alpha_s^2} + \frac{1}{2}\right)\frac{1}{\alpha_s^3}\right] \tag{285}$$

Thus, as an example, the full LFHB equation of state of swollen networks is:

$$\sim P + \sim T\left[\ln(1-\sim\rho) + \sim\rho\left(1-\frac{1}{\bar{r}}\right) + \frac{s}{2}\ln\Gamma_{00} + \left[v^*\frac{\nu_e}{V_2}\left(\alpha_s^2 - \frac{1}{\alpha_s^2} + \frac{1}{2}\right)\frac{1}{\alpha_s^3}\right]\right] = 0 \tag{286}$$

Of course, the presence of the elastic term modifies the hydrogen-bonding minimization conditions, which now become:

$$\frac{\nu_{\alpha\beta}}{\nu_{\alpha 0}\nu_{0\beta}} = \sim\rho\exp\left(\frac{-G_{\alpha\beta}^0}{kT} - \frac{\nu_e}{V_2}\left(\alpha_s^2 - \frac{1}{\alpha_s^2} + \frac{1}{2}\right)\frac{V_{\alpha\beta}^H}{\alpha_s^3}\right) = \frac{r}{A_{\alpha\beta}} \text{ for each } \alpha,\ \beta \tag{287}$$

In a similar manner, in the case of a binary system, the contribution to the chemical potential of the solvent (indicated by subscript '1'), due to the elastic term is:

$$r_1\sim \nu v_1^*\frac{\nu_e}{V_2}\left(\alpha_s^2 - \frac{1}{\alpha_s^2} + \frac{1}{2}\right)\frac{1}{\alpha_s^3} \tag{288}$$

In the general case of f-functional crosslinks the '$^1/_2$' in the parentheses in Eqs. (286–288) should be replaced by the ratio '2/f'.

In the case of charged (hydro)gels, an electrostatic contribution to the above formulae should be added. For small charge densities and m charged segments per network chain, a good approximation is the van't Hoff equation for the electrostatic effect, or:

$$G_{ion} = -kTm\nu_e ln(rN) \tag{289}$$

In the case of a binary system, the electrostatic contribution to the chemical potential of the solvent is given by:

$$-mr_1\sim \nu v^*\frac{\nu_e}{V_2}\frac{V}{V_{Ph}\cdot\alpha_s^3} \tag{290}$$

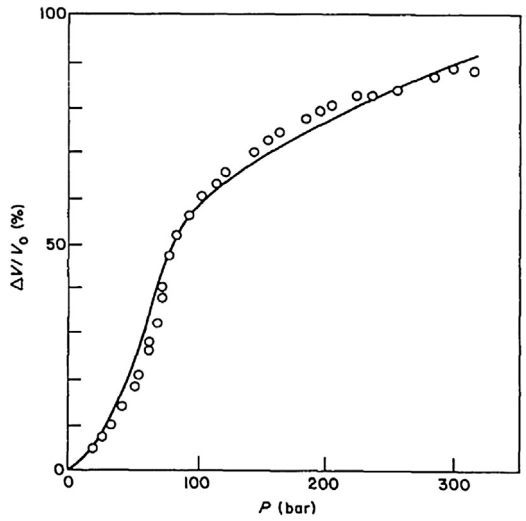

Fig. 102. Swelling ratio of PDMS rubber with supercritical carbon dioxide at 35 °C. Comparison of experimental data (symbols) [428] with calculations (solid line). Reprinted with permission from [424]. Copyright 1992 Elsevier Ltd.

One may further use the classical Donnan equilibrium theory in order to correct the expression for the chemical potential if the surrounding water of the charged (hydro)gel may be considered a dilute electrolyte solution. The above formalism is sufficient for handling swelling and collapse of network structures over a broad range of external conditions. In practical calculations, the equilibrium swelling ratio is obtained by setting μ_1-μ_1° = 0 and solving for polymer volume fraction. It should be mentioned that Eqs. (283–285) and (288–290) (or the corresponding equations if Flory's expressions for the elastic term are chosen) may also be used with the plain PV equation of state [72,73,113,426,427] – a precursor of NRHB model.

In Fig. 102 is reported a first comparison of experimental [428] swelling ratios with calculations based on the above formalism [424]. As shown, the agreement is quite satisfactory up to rather high external pressures.

In Fig. 103 are compared similar calculations with experimental data on the swelling capacity of poly(ethylene oxide) (PEO) gels in

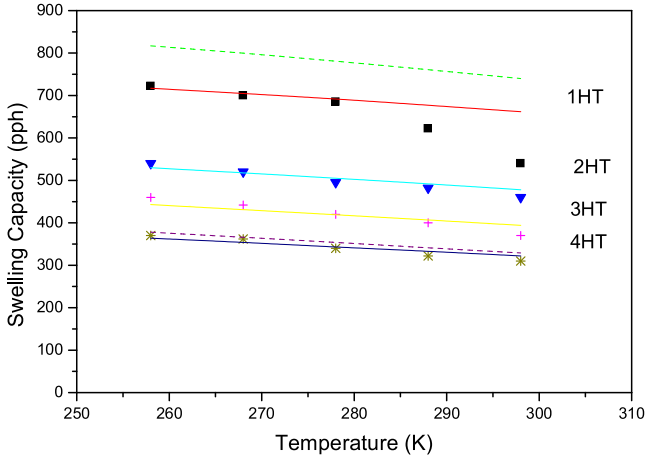

Fig. 103. Swelling capacities of PEO gels of different cross-link densities in chloroform as a function of temperature. Symbols are experimental data [429]. The two dashed lines are the predictions of the model for the lowest (upper curve) and the highest (lower curve) cross-link densities. Solid lines are calculated by slightly varying the binary interaction parameter.

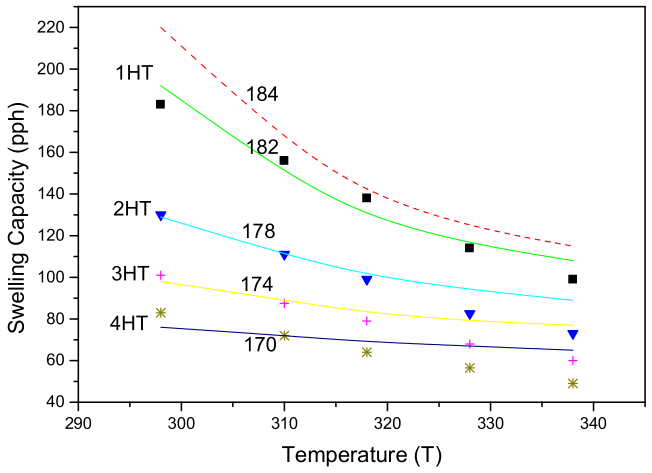

Fig. 104. Swelling capacities of PEO gels of different cross-link densities in water vs. temperature. Symbols are experimental data [429]. The dashed line is the prediction of the model for the lowest cross-link density assuming availability for hydrogen bonding of all oxygens of PEO chains. Solid lines are calculated by varying the number of available oxygen sites per PEO chain (numbers near each line).

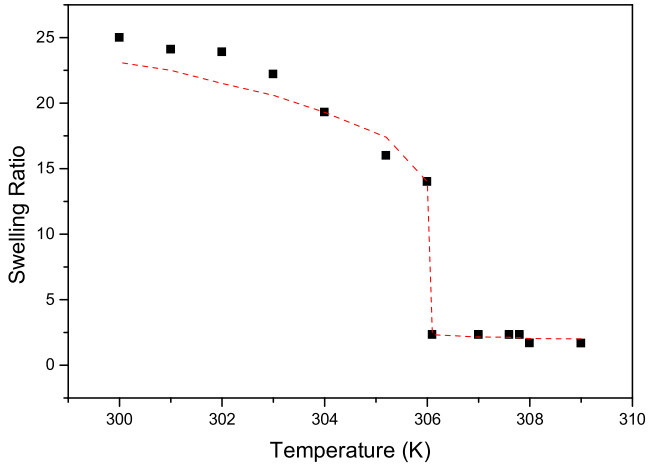

Fig. 105. Swelling ratio of water + PNIPA gel as a function of temperature. Symbols are experimental data from Marchetti et al. [430]. The dashed line are the LFHB model calculations by Lele et al. [429]. Adapted from [429].

chloroform as a function of temperature for four values of cross-linking densities [429]. The two dashed lines in Fig. 103 are pure predictions of the model for the two extreme cross-linking densities. In view of the complexity of the systems, the agreement is rather satisfactory.

Lele et al. [429] have also measured the swelling capacity of the above crosslinked PEOs in water. It is assumed that the water molecule carries two proton acceptor sites per oxygen atom in PEO chains. It is expected that the number of available oxygen sites for hydrogen-bonding will diminish as the degree of crosslinking of the PEO chains increases. This number is not known but the model could be used to estimate it. These calculations and predictions are compared with experimental data [429] in Fig. 104 displaying a good agreement.

A most interesting application of the model is the description of gel collapse shown in Fig. 105. The studied gel is the poly(n-iso propyl acrylamide) (PNIPA) hydrogel. Lele et al. [429] have assumed that the scaling constants of PNIPA are equal to those for poly(methyl methacrylate) and were able to calculate, by the LFHB model, the swelling ratio as a function of temperature. As shown in Fig. 105, the model can reproduce well the volume phase transition (gel collapse) near 306 K.

5. Conclusions

Sorption thermodynamics of low molecular weight compounds in rubbery and glassy polymers is of relevance for numerous technological and engineering applications. To this end, the predictive capability of thermodynamic models would be highly desirable for material design purposes.

Reliable theoretical approaches need to account for several complex phenomena, such as penetrant and polymer self- and cross-associations and nonequilibrium nature of the glassy state. The Equation of State theories, discussed in this review, provide a consistent framework to build reliable models for sorption thermodynamics, able to deal with these complexities providing not only the interpretation of sorption isotherms but also of other relevant features, that include volumetric behavior of rubbery polymers, interfacial properties of polymer mixtures, enthalpy of sorption and plasticization phenomena.

In this review the attention has been focused on several EoS approaches, ranging from equilibrium random mixing compressible lattice fluid theories, accounting only for mean field interactions, to equilibrium theories explicitly accounting for several kinds of association phenomena and interactions. Sorption thermodynamics for the out-of-equilibrium polymers below T_g, has also been addressed, illustrating an effective procedure that is used to extend equilibrium theories to the case of non-equilibrium glassy mixtures. Overall, the illustrated class of models actually provide a rather reliable framework for interpretation of absorption phenomena for which an increasing number of predictive capabilities is being developed.

In this regard, a relevant issue is related to the evaluation of the values of model parameters. This topic has been treated, illustrating both experimental and predictive methods to retrieve these values. A promising approach to gather qualitative and quantitative information on self- and cross-interactions is based on vibrational spectroscopy. The provided examples show the possibility of detecting the chemical groups actually involved in the interactions and the quantification of the amount of the different types of hydrogen bonding interactions occurring in a polymer-penetrant system. Efforts should be devoted to the evaluation of entropy and energy of formation of the specific interactions that could be used to find trends to be extrapolated to the case of substances for which there is a lack of experimental characterization.

A key factor towards the attainment of increased predictive capability is to exploit the synergy between the different experimental techniques and the theoretical approaches, possibly combining the wealth of information delivered by vibrational spectroscopy, with gravimetry, dilatometry, EoS based modelling of sorption thermodynamics, molecular dynamics, quantum chemistry and quantum mechanics calculations. Important improvements are also needed for the prediction of sub-T_g relaxation behavior and the volumetric evolution of the material as a function of the histories of temperature, pressure and penetrant concentration, since polymer density in the mixture still remains an important parameter heavily affecting the reliability of sorption models for glassy polymers.

Worth of mention is the theory of Partial Solvation Parameters, a new type of predictive thermodynamic models, which combines elements from quantum mechanics, statistical thermodynamics and QSPR approaches and has the potential to remove some of the key limitations of the successful COSMO-type thermodynamic models. Its capacity to handle surface characterization of polymers / solids is one of its promising features of particular interest to the

Please cite this article in press as: G. Mensitieri, G. Scherillo, C. Panayiotou et al. Towards a predictive thermodynamic description of Fsorption processes in polymers: The synergy between theoretical EoS models and vibrational spectroscopy. Mater. Sci. Eng. R (2020), https://doi.org/10.1016/j.mser.2019.100525

Colloids and Surface Science Community. Much of its strength resides on the way hydrogen bonding is implemented in both concentrated as well as infinitely dilute systems.

Declaration of Competing Interest

None.

References

[1] E.A. Guggenheim, Mixtures, Oxford University Press, Oxford, 1952.
[2] P.J. Flory, Principles of Polymer Chemistry, Cornell University Press, Ithaca, NY, 1953.
[3] I.C. Sanchez, R.H. Lacombe, J. Phys. Chem. 80 (1976) 2352.
[4] R.H. Lacombe, I.C. Sanchez, J. Phys. Chem. 80 (1976) 2568.
[5] I.C. Sanchez, R.H. Lacombe, Macromolecules 11 (1978) 1145.
[6] C.G. Panayiotou, J. Phys. Chem. 92 (1988) 2960.
[7] M. Taimoori, C. Panayiotou, Fluid Phase Equilibr. 205 (2003) 249.
[8] C. Panayiotou, J. Chem. Thermodyn. 35 (2003) 349.
[9] C. Panayiotou, M. Pantoula, E. Stefanis, I. Tsivintzelis, I.G. Economou, Ind. Eng. Chem. Res. 43 (2004) 6592.
[10] E.E. Abdel-Hady, Polym. Degrad. Stabil. 80 (2003) 363.
[11] D. Kilburn, G. Dlubek, J. Pionteck, D. Bamford, M.A. Alam, Polymer 46 (2005) 869.
[12] H.S. Frank, W.-Y. Wen, Discuss. Faraday Soc. 24 (1957) 133.
[13] G.C. Pimentel, A.L. McClellan, The Hydrogen Bond, W.H. Freeman, San Francisco, CA, 1960.
[14] L.A. LaPlanche, H.B. Thompson, M.T. Rogers, J. Phys. Chem. 69 (5) (1965) 1482.
[15] S. Vinogradov, R. Linnell, Hydrogen Bonding, Van Nostrand Reinhold, New York, 1971.
[16] M.D. Joesten, L.J. Saad, Hydrogen Bonding, Marcel Dekker, New York, 1974.
[17] P.L. Huyskens, J. Am. Chem. Soc. 99 (1977) 2578.
[18] H. Walter, D. Brooks, D. Fisher (Eds.), Partitioning in Aqueous Two-Phase Systems, Academic Press, New York, 1985.
[19] K. Marsh, F. Kohler, J. Mol. Liquids 30 (1985) 13.
[20] H. Kleeberg, D. Klein, W.A.P. Luck, J. Phys. Chem. 91 (1987) 3200.
[21] M. Bourrel, R.S. Schechter (Eds.), Microemulsions and Related Systems, Marcel Dekker, New York, 1988.
[22] P. Hobza, R. Zahradnik, Intermolecular Complexes, Academia, Prague, Czech Republic, 1988.
[23] C. Reichardt, Solvent and Solvent Effects in Organic Chemistry, VCH Verlag GmbH, Weinheim, Germany, 1988.
[24] W. Burchard, S.B. Ross-Murphy (Eds.), Physical Networks, Polymers, and Gels, Elsevier Applied Science, London, 1990.
[25] M.M. Coleman, J.F. Graf, P.C. Painter, Specific Interactions and the Miscibility of Polymer Blends, Technomic, Lancaster, PA, 1991.
[26] G. Maes, J. Smets, J. Phys. Chem. 97 (1993) 1818.
[27] I.C. Sanchez, C. Panayiotou, in: S. Sandler (Ed.), Models for Thermodynamic and Phase Equilibria Calculations, Marcel Dekker, New York, 1994.
[28] W.E. Acree, Thermodynamic Properties of Nonelectrolyte Solutions, Academic Press, New York, 1984.
[29] J.M. Prausnitz, R.N. Lichtenthaler, E.G. de Azevedo, Molecular Thermodynamics of Fluid Phase Equilibria, 2nd ed., Prentice-Hall, New York, 1986.
[30] A. Heintz, Ber. Bunsenges. Phys. Chem. 89 (1985) 172.
[31] C. Panayiotou, J. Solut. Chem. 20 (1991) 97.
[32] C. Panayiotou, I.C. Sanchez, Macromolecules 24 (1991) 6231.
[33] S. Levine, J.W. Perram, in: A.K. Covington, P. Jones (Eds.), Hydrogen Bonded Solvent Systems, Taylor & Francis, London, 1968.
[34] W.A.P. Luck, Angew. Chem. 92 (1980) 29.
[35] B.A. Veytsman, J. Phys. Chem. 94 (1990) 8499.
[36] C. Panayiotou, I.C. Sanchez, J. Phys. Chem. 95 (1991) 10090.
[37] C. Panayiotou, in: K.S. Birdi (Ed.), Handbook of Surface and Colloid Chemistry, CRC Press, Boca Raton, FL, 2003.
[38] C. Panayiotou, in: K.S. Birdi (Ed.), Handbook of Surface and Colloid Chemistry, CRC Press, Boca Raton, FL, 2009.
[39] C. Panayiotou, I. Tsivintzelis, I.G. Economou, Ind. Eng. Chem. Res. 46 (2007) 2628.
[40] C. Panayiotou, Phys. Chem. Chem. Phys. 14 (2012) 3882.
[41] C. Panayiotou, J. Chem. Thermodynamics 51 (2012) 172.
[42] C. Panayiotou, J. Phys. Chem. B 116 (2012) 7302.
[43] C.G. Panayiotou, J. Chromatography A 1251 (2012) 194.
[44] C. Panayiotou, Polymer 54 (2013) 1621.
[45] W.G. Chapman, G. Jackson, K.E. Gubbins, Mol. Phys. 65 (1988) 1057.
[46] G. Jackson, W.G. Chapman, K.E. Gubbins, Mol. Phys. 65 (1988) 1.
[47] W.G. Chapman, K.E. Gubbins, G. Jackson, M. Radosz, Fluid Phase Equilibr. 52 (1989) 31.
[48] W.G. Chapman, K.E. Gubbins, G. Jackson, M. Radosz, Ind. Eng. Chem. Res. 29 (1990) 1709.
[49] S.H. Huang, M. Radosz, Ind. Eng. Chem. Res. 29 (1990) 2284.
[50] F. Doghieri, G.C. Sarti, Macromolecules 29 (1996) 7885.
[51] F. Doghieri, M. Quinzi, D.G. Rethwisch, G.C. Sarti, in: I. Pinnau, B.D. Freeman (Eds.), Advanced Materials for Membrane Separations, ACS Symposium ser. N. 876, 2004, pp. 74–90.
[52] G.C. Sarti, F. Doghieri, Chem. Eng. Sci. 19 (1998) 3435.
[53] C. Panayiotou, S. Mastrogeorgopoulos, V. Hatzimanikatis, J. Chem. Thermodynamics 110 (2017) 3.
[54] S. Mastrogeorgopoulos, V. Hatzimanikatis, C. Panayiotou, Ind. Eng. Chem. Res. 56 (38) (2017) 10900.
[55] C. Panayiotou, Polymer 136 (2018) 47.
[56] P.J. Flory, J. Chem. Phys. 9 (8) (1941) 660.
[57] M.L. Huggins, J. Chem. Phys. 9 (5) (1941) 440.
[58] K. Binder, Adv. Polym. Sci. 112 (1994) 181.
[59] L.D. Landau, E.M. Lifshitz, Statistical Physics, Pergamon, Oxford, 1958.
[60] H.E. Stanley, An Introduction to Phase Transitions and Critical Phenomena, Oxford University Press, Oxford, 1971.
[61] M.E. Fisher, Rev. Mod. Phys. 46 (1974) 597.
[62] D. Patterson, G. Delmas, Discuss. Faraday Soc. 49 (1970) 98.
[63] I. Prigogine, The Molecular Theory of Solutions, North Holland, Amsterdam, 1957.
[64] P.J. Flory, J. Am. Chem. Soc. 87 (1965) 1833.
[65] R. Simha, T. Somcynsky, Macromolecules 2 (1969) 342.
[66] R.K. Jain, R. Simha, Macromolecules 13 (1980) 1501.
[67] N.A. Smimova, A.I. Victorov, Fluid Phase Equilibr. 34 (1987) 235.
[68] K. von Konigslow, C.B. Park, R.B. Thompson, Phys. Rev. Appl. 8 (2017)044009.
[69] E. Neau, Fluid Phase Equilibr. 203 (2002) 133.
[70] K. von Konigslow, C.B. Park, R.B. Thompson, Soft Matter 14 (2018) 4603.
[71] K. von Konigslow, An Off-lattice Derivation and Thermodynamic Consistency Consideration for the Sanchez-Lacombe Equation of State Ph.D. Thesis, University of Waterloo, Waterloo, Ontario, Canada, 2017.
[72] C. Panayiotou, J.H. Vera, Can. J. Chem. Eng. 59 (1981) 501.
[73] C. Panayiotou, J.H. Vera, Polymer J. 14 (1982) 681.
[74] C. Panayiotou, Fluid Phase Equilibr. 237 (2005) 130.
[75] S. High, R.P. Danner, AIChE J. 36 (1990) 1625.
[76] S. You, S.J. Yoo, K.P. Yoo, C.S. Lee, J. Supercrit. Fluid 7 (1994) 251.
[77] M.S. Shin, K.P. Yoo, S.S. You, C.S. Lee, Int. J. Thermophys. 16 (1995) 723.
[78] D. Missopolinou, C. Panayiotou, J. Phys. Chem. A 102 (1998) 3574.
[79] D. Missopolinou, K. Ioannou, I. Prinos, C. Panayiotou, Z. Phys. Chem. 216 (2002) 905.
[80] R.B. Gupta, R.L. Brinkley, AIChE J. 44 (1998) 207.
[81] Q. Yan, H. Liu, Y. Hu, Fluid Phase Equilibr. 218 (2004) 157.
[82] G. Wilson, J. Am. Chem. Soc. 86 (1964) 127.
[83] W. Wang, J.H. Vera, Fluid Phase Equilibr. 85 (1993) 1.
[84] J.H. Vera, Fluid Phase Equilibr. 145 (1998) 217.
[85] T.L. Hill, An Introduction to Statistical Thermodynamics, Dover Publications, New York, 1986.
[86] A.J. Staverman, Rec. Trav. Chim. Pays-Bas. 69 (1950) 163.
[87] A. Fredenslund, R.L. Jones, J.M. Prausnitz, AIChE J. 21 (1975) 1086.
[88] A. Fredenslund, M.J. Sorensen, in: S. Sandler (Ed.), Models for Thermodynamic and Phase Equilibria Calculations, Marcel Dekker, New York, 1994.
[89] S. Kemeny, G. Balog, G. Radnai, J. Savinsky, G. Rezessy, Fluid Phase Equilibr. 54 (1990) 247.
[90] X. Li, D.J. Zhao, J. Chem. Phys. 117 (2002) 6803.
[91] E. Stefanis, I. Tsivintzelis, C. Panayiotou, Fluid Phase Equilibr. 240 (2006) 144.
[92] D. Missopolinou, I. Tsivintzelis, C. Panayiotou, Fluid Phase Equilibr. 238 (2005) 204.
[93] D. Missopolinou, I. Tsivintzelis, C. Panayiotou, Fluid Phase Equilibr. 245 (2006) 89.
[94] A. Grenner, I. Tsivintzelis, G.M. Kontogeorgis, I.G. Economou, C. Panayiotou, Ind. Eng. Chem. Res. 47 (2008) 5636.
[95] I. Tsivintzelis, T. Spyriouni, I.G. Economou, Fluid Phase Equilibr. 253 (2007) 19.
[96] I. Tsivintzelis, A. Grenner, I.G. Economou, G.M. Kontogeorgis, Ind. Eng. Chem. Res. 47 (2008) 5651.
[97] I. Tsivintzelis, I.G. Economou, G.M. Kontogeorgis, AIChE J. 55 (2009) 756.
[98] I. Tsivintzelis, I.G. Economou, G.M. Kontogeorgis, J. Phys. Chem. B 113 (2009) 6446.
[99] I. Tsivintzelis, G.M. Kontogeorgis, Fluid Phase Equilibr. 280 (2009) 100.
[100] C. Tsioptsias, I. Tsivintzelis, C. Panayiotou, Phys. Chem. Chem. Phys. 12 (2010) 4843.
[101] C. Panayiotou, I. Tsivintzelis, D. Aslanidou, V. Hatzimanikatis, J. Chem. Therm. 90 (2015) 294.
[102] C. Panayiotou, Ind. Eng. Chem. Res. 42 (2003) 1495.
[103] C. Panayiotou, Chem. Eng. Data 55 (2010) 5453.
[104] C. Panayiotou, Pure Appl. Chem. 83 (6) (2011) 1221.
[105] A. Klamt, F. Eckert, Fluid Phase Equilibr. 172 (2000) 43.
[106] A. Klamt, Ind. Eng. Chem. Res. 41 (2002) 2330.
[107] A. Klamt, G.J.P. Krooshof, R. Taylor, AIChE J. 48 (2002) 2332.
[108] A. Klamt, COSMO-RS, From Quantum Chemistry to Fluid Phase Thermodynamics and Drug Design, Elsevier, Amsterdam, 2004.
[109] S.-T. Lin, S.I. Sandler, Ind. Eng. Chem. Res. 41 (2002) 899.
[110] Z. Xue, T. Mu, J. Gmehling, Ind. Eng. Chem. Res. 51 (36) (2012) 11809.
[111] C.C. Pye, T. Ziegler, E. van Lenthe, J.N. Louwen, Can. J. Chem. 87 (7) (2009) 790.
[112] A. Klamt, V. Jonas, T. Burger, J.C.W. Lohrenz, J. Phys. Chem. 102 (26) (1998) 5074.
[113] C. Panayiotou, J.H. Vera, Fluid Phase Equilibr. 5 (1-2) (1980) 55.
[114] COSMObase Ver. C30_1401, COSMOlogic GmbH & Co., K.G., Leverkusen, Germany, 2014.
[115] G. Sadowski, Adv. Polym. Sci. 238 (2011) 329.
[116] S.H. Huang, M. Radosz, Ind. Eng. Chem. Res. 30 (1991) 1994.

Please cite this article in press as: G. Mensitieri, G. Scherillo, C. Panayiotou et al. Towards a predictive thermodynamic description of Fsorption processes in polymers: The synergy between theoretical EoS models and vibrational spectroscopy. Mater. Sci. Eng. R (2020), https://doi.org/10.1016/j.mser.2019.100525

[117] G.M. Kontogeorgis, G.K. Folas, Thermodynamic Models for Industrial Applications, John Wiley & Sons, Chichester, UK, 2010.
[118] M.S. Wertheim, J. Stat. Phys. 35 (1984) 19.
[119] M.S. Wertheim, J. Stat. Phys. 35 (1984) 35.
[120] M.S. Wertheim, J. Stat. Phys. 42 (1986) 459.
[121] M.S. Wertheim, J. Stat. Phys. 42 (1986) 477.
[122] M.S. Wertheim, J. Chem. Phys. 8 (1987) 7323.
[123] Y. Song, S.M. Lambert, J.M. Prausnitz, Macromolecules 27 (1994) 441.
[124] Y. Song, S.M. Lambert, J.M. Prausnitz, Ind. Eng. Chem. Res. 33 (1994) 1047.
[125] A. Gil Villegas, A. Galindo, P.J. Whitehead, S.J. Mills, G. Jackson, A.N. Burgess, J. Chem. Phys. 106 (1997) 4168.
[126] J. Chang, S.I. Sandler, Mol. Phys. 81 (1994) 745.
[127] T. Hino, J.M. Prausnitz, Fluid Phase Equilibr. 138 (1997) 105.
[128] F.J. Blas, L.F. Vega, Mol. Phys. 92 (1997) 135.
[129] Y.-H. Fu, S.I. Sandler, Ind. Eng. Chem. Res. 34 (1995) 1897.
[130] T. Kraska, K.E. Gubbins, Ind. Eng. Chem. Res. 35 (1996) 4727.
[131] T. Kraska, K.E. Gubbins, Ind. Eng. Chem. Res. 35 (1996) 4738.
[132] C. McCabe, A. Gil-Vilegas, G. Jackson, Chem. Phys. Lett. 303 (1999) 27.
[133] F.J. Blas, L.F. Vega, Ind. Eng. Chem. Res. 37 (1998) 360.
[134] J. Gross, G. Sadowski, Ind. Eng. Chem. Res. 40 (2001) 1244.
[135] N. von Solms, M.L. Michelsen, G.M. Kontogeorgis, Ind. Eng. Chem. Res. 42 (2003) 1098.
[136] A. Tihic, G.M. Kontogeorgis, N. von Solms, M.L. Michelsen, Fluid Phase Equilibr. 248 (2006) 29.
[137] G.M. Kontogeorgis, E. Voutsas, I. Yakoumis, D.P. Tassios, Ind. Eng. Chem. Res. 35 (1996) 4310.
[138] G.M. Kontogeorgis, I.V. Yakoumis, H. Meijer, E.M. Hendriks, T. Moorwood, Fluid Phase Equilibr. 158–160 (1999) 201.
[139] J. Wu, J.M. Prausnitz, Ind. Eng. Chem. Res. 37 (1998) 1634.
[140] E.M. Hendriks, J.M. Walsh, A.R.D. van Bergen, J. Stat. Phys. 87 (5/6) (1997) 1287.
[141] I.V. Yakoumis, G.M. Kontogeorgis, E.C. Voutsas, E.M. Hendriks, D.P. Tassios, Ind. Eng. Chem. Res. 37 (1998) 4175.
[142] M.L. Michelsen, E.M. Hendriks, Fluid Phase Equilibr. 180 (1–2) (2001) 165.
[143] M.L. Michelsen, Ind. Eng. Chem. Res. 43 (19) (2004) 6262.
[144] M.L. Michelsen, Ind. Eng. Chem. Res. 45 (25) (2006) 8449.
[145] S. Tamouza, J.-Ph. Passarello, P. Tobaly, J.-Ch. de Hemptinne, Fluid Phase Equilibr. 222–223 (2004) 67.
[146] S. Tamouza, J.-Ph. Passarello, P. Tobaly, J.-Ch. de Hemptinne, Fluid Phase Equilibr. 228–229 (2005) 409.
[147] T.X.N. Thi, S. Tamouza, P. Tobaly, J.-Ph. Passarello, J.-Ch. de Hemptinne, Fluid Phase Equilibr. 238 (2005) 254.
[148] F. Emami, A. Vahid, J.R. Elliott Jr, F. Feyzi, Ind. Eng. Chem. Res. 47 (2008) 8401.
[149] C. Le Thi, S. Tamouza, J.P. Passarello, P. Tobaly, J.-C. de Hemptinne, Ind. Eng. Chem. Res. 45 (2006) 6803.
[150] D.N. Huynh, M. Benamira, J.-Ph. Passarello, P. Tobaly, J.-Ch. de Hemptinne, Fluid Phase Equilibr. 254 (2007) 60.
[151] A. Tihic, G.M. Kontogeorgis, N. von Solms, M.L. Michelsen, L. Constantinou, Ind. Eng. Chem. Res. 47 (2008) 5092.
[152] A. Lymperiadis, C.S. Adjiman, A. Galindo, G. Jackson, J. Chem. Phys. 127 (2007) 234903.
[153] C.A. Lymperiadis, S. Adjiman, G. Jackson, A. Galindo, Fluid Phase Equilibr. 274 (2008) 85.
[154] J. Gross, G. Sadowski, Ind. Eng. Chem. Res. 41 (2002) 1084.
[155] F. Tumakaka, J. Gross, G. Sadowski, Fluid Phase Equilibr. 194 (197) (2002) 541.
[156] F. Tumakaka, G. Sadowski, Fluid Phase Equilibr. 217 (2004) 233.
[157] F. Tumakaka, J. Gross, G. Sadowski, Fluid Phase Equilibr. 228–229 (2005) 89.
[158] S.G. Sauer, W.G. Chapman, Ind. Eng. Chem. Res. 42 (2003) 5687.
[159] E.K. Karakatsani, T. Spyriouni, I.G. Economou, AIChE J. 51 (2005) 2328.
[160] E.K. Karakatsani, I.G. Economou, J. Phys. Chem. B 110 (2006) 9252.
[161] E.K. Karakatsani, G.M. Kontogeorgis, I.G. Economou, Ind. Eng. Chem. Res. 45 (17) (2006) 6063.
[162] J. Gross, J. Vrabec, AIChE J. 52 (2006) 1194.
[163] J. Gross, AIChE J. 51 (2005) 2556.
[164] M. Kleiner, J. Gross, AIChE J. 52 (2006) 1951.
[165] E.K. Karakatsani, I.G. Economou, Fluid Phase Equilibr. 261 (2007) 265.
[166] M. Kleiner, G. Sadowski, J. Phys. Chem. C 111 (2007) 15544.
[167] J. Gross, O. Spuhl, F. Tumakaka, G. Sadowski, Ind. Eng. Chem. Res. 42 (2003) 1266.
[168] R.M. Barrer, J.A. Barrie, J. Slater, J. Polym. Sci. 27 (1958) 177.
[169] A.S. Michaels, W.R. Vieth, J.A. Barrie, Appl. Phys. 34 (1963) 1.
[170] T. De Donder, P. van Rysselberghe, Thermodynamic Theory of Affinity, Stanford University Press, Menlo Park, 1936.
[171] A.J. Staverman, Rheol. Acta 5 (1966) 283.
[172] J.H. Gibbs, E.A. Di Marzio, J. Chem. Phys. 28 (1958) 373.
[173] G. Astarita, M.E. Paulaitis, R.G. Wissinger, J. Polym. Sci.: Polym. Phys. Ed. 27 (1989) 2105.
[174] R.G. Wissinger, M.E. Paulaitis, Ind. Eng. Chem. Res. 30 (1991) 842.
[175] R.M. Conforti, T.A. Barbari, P. Vimalchand, M.D. Donohue, Macromolecules 24 (1991) 3388.
[176] R.M. Conforti, T.A. Barbari, Macromolecules 26 (1993) 5209.
[177] M.G. De Angelis, F. Doghieri, G.C. Sarti, B.D. Freeman, Desalination 193 (2006) 82.
[178] G. Astarita, Thermodynamics. An Advanced Textbook for Chemical Engineers, Plenum Press, New York USA, 1989.
[179] S.S. Jordan, W.J. Koros, Macromolecules 28 (1995) 2228.
[180] D.S. Pope, G.K. Fleming, W.J. Koros, Macromolecules 23 (1990) 2988.
[181] M.G. De Angelis, T.C. Merkel, V.I. Bondar, B.D. Freeman, F. Doghieri, G.C. Sarti, J. Polym. Sci. Part B: Polym. Phys. 37 (1999) 3011.
[182] M. Giacinti Baschetti, F. Doghieri, G.C. Sarti, Ind. Eng. Chem. Res. 40 (2001) 3027.
[183] F. Doghieri, M. Canova, G.C. Sarti, in: B.D. Freeman, I. Pinnau (Eds.), Polymer Membranes for Gas and Vapor Separation, Am. Chem. Soc. Symp. Series 733, ACS, Whashington D.C., 1999, pp. 179.
[184] G. Scherillo, L. Sanguigno, M. Galizia, M. Lavorgna, P. Musto, G. Mensitieri, Fluid Phase Equilibr. 334 (2012) 166.
[185] K. Binder, B. Mognetti, W. Paul, P. Virnau, L. Yelash, Polymer Thermodynamics: Liquid Polymer-Containing Mixtures, in: Sabine Enders, Bernhard A. Wolf (Eds.), Advances in Polymer Science, 238, Springer Verlag, Berlin Heidelberg, 2011, pp. 329.
[186] I. Carmesin, K. Kremer, Macromolecules 21 (1988) 2819.
[187] H.P. Deutsch, K. Binder, J. Chem. Phys. 94 (1991) 2294.
[188] W. Paul, K. Binder, D.W. Heermann, K. Kremer, J. Phys. II 1 (1991) 37.
[189] W. Paul, J. Baschnagel, in: K. Binder (Ed.), Monte Carlo and Molecular Dynamics Simulations in Polymer Science, Oxford University Press, New York, 1995 p 307.
[190] B. Widom, J. Chem. Phys. 39 (1963) 2808.
[191] N. Metropolis, A.W. Rosenbluth, M.N. Rosenbluth, A.H. Teller, E. Teller, J. Chem. Phys. 21 (1953) 1087.
[192] G.C. Maitland, M. Rigby, E.B. Smith, W.A. Wakeham, Intermolecular Forces: Their Origin and Determination, Clarendon, Oxford, 1981.
[193] M. Heuchel, D. Fritsch, P.M. Budd, N.B. McKeown, D. Hofmann, J. Membrane Sci. 318 (2008) 84.
[194] A.A. Gusev, S. Arizzi, U.W. Suter, D.J. Moll, J. Chem. Phys. 99 (1993) 2221.
[195] A.A. Gusev, U.W. Suter, J. Chern. Phys. 99 (1993) 2228.
[196] W. Fang, L. Zhang, J. Jiang, Mol. Simul. 36 (2010) 992.
[197] W. Fang, L. Zhang, J. Jiang, J. Phys. Chem. C. 115 (2011) 14123.
[198] G. Kupgan, A.G. Demidov, C.M. Colina, J. Membrane Sci. 565 (2018) 95.
[199] S. Neyertz, D. Brown, Macromolecules 51 (2018) 7077.
[200] A. Kouskoumvekaki, N. von Solms, T. Lindvig, M.L. Michelsen, G.M. Kontogeorgis, Ind. Eng. Chem. Res. 43 (2004) 2830.
[201] S.M. Wiederhorn, R.J. Fields, S. Low, G.-W. Bahng, A. Wehrstedt, J. Hahn, Y. Tomota, T. Miyata, H. Lin, B.D. Freeman, S. Aihara, Y. Hagihara, T. Tagawa, in: H. Czichos, T. Saito, L. Smith (Eds.), Springer Handbook of Metrology and Testing, 2nd ed., Springer-Verlag, Berlin Heidelberg, 2011 chap. 7, sec. 7.6.9.
[202] M. Felder, G.S. Huvard, in: R. Fava (Ed.), Methods of Experimental Physics, Vol. 16C, Academic, New York, 1980 p. 315.
[203] C.C. McDowell, D.T. Coker, B.D. Freeman, Rev. Sci. Instrum. 69 (1998) 2510.
[204] B. Wong, Z. Zhang, Y.P. Handa, J. Polym. Sci. B 36 (1998) 2025.
[205] S. Areerat, E. Funami, Y. Hayata, D. Nakagawa, M. Ohshima, Polym. Eng. Sci. 44 (2004) 1915.
[206] Y. Wu, P. Akoto-Ampaw, M. Elbaccouch, M.L. Hurrey, S.L. Wallen, C.S. Grant, Langmuir 20 (2004) 3665.
[207] W.J. Koros, D.R. Paul, J. Polym. Sci., Pol. Phys. Ed. 14 (1976) 1903.
[208] G. Genduso, B.S. Ghanem, I. Pinnau, Membranes 9 (1) (2019) 10.
[209] E.B. Wilson, J.C. Decius, P.C. Cross, Molecular Vibrations, McGraw-Hill, New York, 1955.
[210] J.M. Chalmers, P.R. Griffiths (Eds.), Handbook of Vibrational Spectroscopy, Wiley, Chichester, U.K., 2002, pp. 1–149 Vol. 1, Introduction to the Theory and Practice of Vibrational Spectroscopy.
[211] J.M. Chalmers, P.R. Griffiths (Eds.), Handbook of Vibrational Spectroscopy,, Wiley, Chichester, U.K., 2002, pp. 2225–2336 Vol. 3, Quantitative Analysis.
[212] P.R. Griffiths, in: J.M. Chalmers, P.R. Griffiths (Eds.), Handbook of Vibrational Spectroscopy, Wiley, Chichester, U.K., 2002, pp. 2225.
[213] Y.A. Elabd, T.A. Barbari, AIChE J. 47 (2001) 1255.
[214] G.T. Fieldson, T.A. Barbari, Polymer 34 (1993) 1146.
[215] G.T. Fieldson, T.A. Barbari, AIChE J. 41 (1995) 795.
[216] N.J. Harrick, A.I. Carlson, Appl. Opt. 10 (1971) 19.
[217] E. Smith, G. Dent, Modern Raman Spectroscopy, John Wiley & Sons Ltd., Chichester, England, 2005.
[218] R.L. McCreery, in: J.M. Chalmers, P.R. Griffiths (Eds.), Handbook of Vibrational Spectroscopy, Wiley, Chichester, U.K., 2002, pp. 921.
[219] A.Y.C.N.A. Remizov, V.Ya. Povov, V.V. Lavrent'ev, Polymer Science U.S.S.R. (Vysokomol. soyed.) 24 (1982) 1853.
[220] H. Brandt, P. Rieger, Experimentelle Technik der Physik 32 (1984) 413.
[221] H. Brandt, Exp. Tech. Phys 33 (1985) 423.
[222] K. Hemmelmann, H. Brandt, Experimentelle Technik der Physik 37 (1989) 495.
[223] J.G. Van Alsten, Trends Polym. Sci. 3 (1995) 272.
[224] J. Crank, The Mathematics of Diffusion, 2nd ed., Clarendon Press, Oxford, 1975 chap. 4.
[225] Y.A. Elabd, J.M. Sloan, N.B. Tan, T.A. Barbari, Macromolecules 34 (2001) 6268.
[226] S.U. Hong, T.A. Barbari, J.M. Sloan, J. Polym. Sci.: Pol. Phys. Ed. 35 (1997) 1261.
[227] S.U. Hong, T.A. Barbari, J.M. Sloan, J. Polym. Sci.: Pol. Phys. Ed. 36 (1998) 337.
[228] S.U. Hong, T.A. Barbari, J. Polym. Sci.: Pol. Phys. Ed. 39 (2001) 908.
[229] P.Y. Furlan, Macromolecules 25 (1992) 6516.
[230] J.G. Van Alsten, J.C. Coburn, Macromolecules 27 (1994) 3746.
[231] C. Sammon, J. Yarwood, N. Everall, Polymer 41 (2000) 2521.
[232] E. Jabbari, N.A. Peppas, Macromolecules 26 (1993) 2175.
[233] J.G. Van Alsten, S.R. Lustig, B. Hsiao, Macromolecules 28 (1995) 3672.
[234] S.G. Kazarian, M.F. Vincent, F.V. Bright, C.L. Liotta, C.A. Eckert, J. Am. Chem. Soc. 118 (1996) 1729.
[235] S.G. Kazarian, N.H. Brantley, B.L. West, M.F. Vincent, C.A. Eckert, Appl. Spectrosc. 51 (1997) 491.

Please cite this article in press as: G. Mensitieri, G. Scherillo, C. Panayiotou et al. Towards a predictive thermodynamic description of Fsorption processes in polymers: The synergy between theoretical EoS models and vibrational spectroscopy. Mater. Sci. Eng. R (2020), https://doi.org/10.1016/j.mser.2019.100525

[236] S.G. Kazarian, Appl. Spectrosc. Rev. 32 (1997) 301.
[237] M.B. Flichy, S.G. Kazarian, C.J. Lawrence, B.J. Briscoe, J. Phys. Chem. B 106 (2002) 754.
[238] A.R.C. Duarte, L.E. Anderson, C.M.M. Duarte, S.G. Kazarian, J. Supercrit. Fluid 36 (2005) 160.
[239] S.G. Kazarian, N.H. Brantley, C.A. Eckert, Vib. Spectrosc. 19 (1999) 277.
[240] O.S. Fleming, K.L.A. Chan, S.G. Kazarian, Vib. Spectrosc. 35 (2004) 3.
[241] N.H. Brantley, S.G. Kazarian, C.A. Eckert, J. Appl. Polym. Sci. 77 (2000) 764.
[242] S.G. Kazarian, B.J. Briscoe, C.J. Lawrence, D. Coombs, G. Poulter, 6th Meeting on Supercritical Fluids: Chemistry and Materials, Nottingham, 1999, pp. 11.
[243] I. Pasquali, J.-M. Andanson, S.G. Kazarian, R. Bettini, J. Supercrit. Fluid 45 (2008) 384.
[244] A.A. Gabrienko, A.V. Ewing, A.M. Chibiryaev, A.M. Agafontsev, K.A. Dubkov, S. G. Kazarian, Phys. Chem. Chem. Phys. 18 (2016) 6465.
[245] O. Akin, F. Temelli, J. Supercrit. Fluid 60 (2011) 81.
[246] J.T. Culp, A.L. Goodman, D. Chirdon, S.G. Sankar, C. Matranga, J. Phys. Chem. C 114 (2010) 2184.
[247] T. Guadagno, S.G. Kazarian, J. Phys. Chem. B 108 (2004) 13995.
[248] A.V. Ewing, A.A. Gabrienko, S.V. Semikolenov, K.A. Dubkov, S.G. Kazarian, J. Phys. Chem. C 119 (2015) 431.
[249] R.T. Woodward, L.A. Stevens, R. Dawson, M. Vijayaraghavan, T. Hasell, I.P. Silverwood, A.V. Ewing, T. Ratvijitvech, J.D. Exley, S.Y. Chong, F. Blanc, D.J. Adams, S.G. Kazarian, C.E. Snape, T.C. Drage, A.I. Cooper, J. Am. Chem. Soc. 136 (2014) 9028.
[250] S.G. Kazarian, K.L.A. Chan, Appl. Spectrosc. 64 (2010) 135A.
[251] A.V. Ewing, S.G. Kazarian, J. Supercrit. Fluid 134 (2018) 88.
[252] S. Cotugno, D. Larobina, G. Mensitieri, P. Musto, G. Ragosta, Polymer 42 (2001) 6431.
[253] P. Musto, M. Galizia, P. La Manna, M. Pannico, G. Mensitieri, Front. Chem. 2 (2014)2.
[254] G. Mensitieri, G. Scherillo, P. La Manna, P. Musto, Membranes 9 (2019) 23.
[255] P. Musto, P. La Manna, M. Pannico, G. Mensitieri, N. Gargiulo, D. Caputo, J. Mol. Struct. 1166 (2018) 326.
[256] H. Behrens, N. Tamic, F. Holtz, Am. Mineral. 89 (2004) 301.
[257] M.G. Pastore Carbone, P. Musto, M. Pannico, A. Braeuer, G. Scherillo, G. Mensitieri, E. Di Maio, J. Phys. Chem. B 120 (2016) 9115.
[258] A.S. Braeuer, J. Supercrit. Fluid 134 (2018) 80.
[259] O.S. Fleming, F. Stepanek, S.G. Kazarian, Macromol. Chem. Phys. 206 (2005) 1077.
[260] A. de Nicola, A. Correa, G. Milano, P. La Manna, P. Musto, G. Mensitieri, G. Scherillo, J. Phys. Chem. B 121 (2017) 3162.
[261] P. Musto, P. La Manna, J.D. Moon, M. Galizia, B.D. Freeman, ACS Omega 3 (2018) 11592.
[262] Y. Maréchal, J. Mol. Struct. 648 (2003) 27.
[263] P. Musto, G. Ragosta, G. Mensitieri, M. Lavorgna, Macromolecules 40 (2007) 9614.
[264] M. Galizia, P. La Manna, M. Pannico, G. Mensitieri, P. Musto, Polymer 55 (2014) 1028.
[265] M. Pannico, P. La Manna, Front. Chem. 7 (2019) 275.
[266] L.K. DeNoyer, J.G. Dodd, in: J.M. Chalmers, P.R. Griffiths (Eds.), Handbook of Vibrational Spectroscopy,, Wiley, Chichester, U.K., 2002, pp. 2173.
[267] P. Musto, G. Mensitieri, M. Lavorgna, G. Scarinzi, G. Scherillo, J. Phys. Chem. B 116 (2012) 1209.
[268] I. Noda, Y. Ozaki, Two-dimensional Correlation Spectroscopy: Applications in Vibrational and Optical Spectroscopy, John Wiley and Sons, New York, 2004.
[269] Q. Jia, N.-N. Wang, Z.-W. Yu, Appl. Spectrosc. 63 (2009) 344.
[270] M. Galizia, P. La Manna, G. Mensitieri, M. Pannico, P. Musto, J. Mol. Struct. 1069 (2014) 290.
[271] P. Musto, M. Galizia, M. Pannico, G. Scherillo, G. Mensitieri, J. Phys. Chem. B 118 (2014) 7414.
[272] J.S. Yoon, H.W. Jung, M.N. Kim, E.S. Park, J. Appl. Polym. Sci. 77 (2000) 1716.
[273] M.J. Frisch, G.W. Trucks, H.B. Schlegel, G.E. Scuseria, M.A. Robb, J.R. Cheeseman, G. Scalmani, V. Barone, B. Mennucci, G.A. Petersson, et al., Gaussian 03, Gaussian Inc., Wallingford CT, 2004.
[274] S.F. Sousa, P.A. Fernandes, M.J. Ramos, J. Phys. Chem. A 111 (2007) 10439.
[275] R.E. Oakes, J.R. Beattie, B.W. Moss, S.E.J. Bell, J. Mol. Struc.-Theochem 626 (2003) 27.
[276] R.E. Oakes, J.R. Beattie, B.W. Moss, S.E.J. Bell, J. Mol. Struc.-Theochem 586 (2002) 91.
[277] I.J. Bruno, J.C. Cole, J.P.M. Lommerse, R.S. Rowland, R. Taylor, M.L. Verdonk, J. Comp.-Aid. Mol. Des. 11 (1997) 525.
[278] C.R. Groom, I.J. Bruno, M.P. Lightfoot, S.C. Ward, Acta Crystallogr. Sec. B 72 (2016) 171.
[279] G.M. Battle, F.H. Allen, J. Chem. Educ. 89 (2012) 38.
[280] M. Kamiya, T. Tsuneda, K. Hirao, J. Chem. Phys. 117 (2002) 6010.
[281] W. Kohn, Y. Meir, D.E. Makarov, Phys. Rev. Lett. 80 (1998) 4153.
[282] X. Wu, M.C. Vargas, S. Nayak, V. Lotrich, G. Scoles, J. Chem. Phys. 115 (2001) 8748.
[283] S. Kilic, S. Michalik, Y. Wang, J.K. Johnson, R.M. Enick, E.J. Beckman, Ind. Eng. Chem. Res. 42 (2003) 6415.
[284] S. Kilic, S. Michalik, Y. Wang, J.K. Johnson, R.M. Enick, E.J. Beckman, Macromolecules 40 (2007) 1332.
[285] J.R. Conder, C.L. Young, Physicochemical Measurements by Gas Chromatography, Wiley, New York, 1979.
[286] H.P. Schreiber, D.R. Lloyd, in: D.R. Lloyd, H.P. Schreiber, Ward T. C. (Eds.), ACS Symposium Series No. 391, American Chemical Society: Washington, DC, 1989 chap. 1.
[287] A. Sen, Inverse Gas Chromatography, Defence Scientific Information & Documentation Centre; Defence Research & Development Organisation, Ministry of Defence, UK, 2005.
[288] J. Guillet, Z.Y. Al-Saigh, Encyclopedia of Analytical Chemistry, Wiley, New York, 2006, pp. 1.
[289] C.L. Young, Chromatogr. Rev. 10 (1968) 129.
[290] D. Patterson, Y.B. Tewari, H.P. Schreiber, J.E. Guillet, Macromolecules 4 (1971) 356.
[291] P. Munk, Chem. Anal. 113 (1991) 151.
[292] J. Hildebrand, R.L. Scott, Regular Solutions, Prentice Hall, Englewood Cliffs, N. J., 1962.
[293] S. Abbott, H. Yamamoto, C.M. Hansen, Hansen Solubility Parameters in Practice, Complete With Software, Data and Examples 3rd Ed.-version 3.1.20 Hansen-Solubility.com, (2010) .
[294] G. DiPaola-Baranyi, J.E. Guillet, Macromolecules 11 (1978) 228.
[295] K. Ito, J.E. Guillet, Macromolecules 12 (1979) 1163.
[296] D. Lazidou, S. Mastrogeorgopoulos, C. Panayiotou, J. Mol. Liquids 277 (2019) 10.
[297] A. Niederquell, N. Wyttenbach, M. Kuentz, C. Panayiotou, Pharmaceutics 11 (2019) 17.
[298] R. Ho, J.Y.Y. Heng, KONA Powder Part J 30 (2013) 164.
[299] H. Balard, E. Brendlé, in: K.L. Mittal (Ed.), Acid–Base Interactions, Relevance to Adhesion Science and Technology, vol. 2, CRC Press, 2000 p. 299.
[300] A. Voelkel, Stud. Surf. Sci. Catal. 99 (1996) 465.
[301] F.M. Fowkes, Ind. Eng. Chem. Res. 56 (1964) 40.
[302] J. Schultz, L. Lavielle, C. Martin, J. Adhes. 23 (1987) 45.
[303] J. Schultz, L. Lavielle, ACS Symposium Ser. vol. 391, ACS Publications, 1989, pp. 185.
[304] G.M. Dorris, D.G. Gray, J. Colloid Interface Sci. 77 (1980) 353.
[305] J. Santos, M. Gil, A. Portugal, J. Guthrie, J. Cellulose 8 (2001) 217.
[306] S.K. Papadopoulou, C. Panayiotou, J. Chromatogr. A 1324 (2013) 207.
[307] M. Kawakami, S. Kagawa, Bull. Chem. Soc. Japan. 51 (1978) 75.
[308] Y. Yampolskii, N. Belov, Macromolecules 48 (2015) 6751.
[309] P. Zoller, P. Bolli, V. Pahud, H. Ackermann, Rev. Sci. Instrum. 47 (1976) 948.
[310] G. Scherillo, M. Petretta, M. Galizia, P. la Manna, P. Musto, G. Mensitieri, Front. Chem. 2 (2014)25.
[311] G. Sadowski, L. Mokrushina, W. Arlt, Fluid Phase Equilibr. 139 (1997) 391.
[312] A. Tihic, G.M. Kontogeorgis, N. von Solms, M.L. Michelsen, Fluid Phase Equilibr. 248 (2006) 29.
[313] M.A. Bashir, M. Al-haj Ali, V. Kanellopoulos, J. Seppälä, E. Kokko, S. Vijay, Macromol. React. Eng. 7 (2013) 193.
[314] A.F.M. Barton, Handbook of Solubility Parameters and Other Cohesion Parameters, CRC Press, Boca Raton, FL, 1983.
[315] C.M. Hansen, Hansen Solubility Parameters: A User's Handbook, CRC Press, Boca Raton, FL, 2000.
[316] J. Hildebrand, R.L. Scott, The Solubility of Nonelectrolytes, 3rd ed., Rheinhold, New York, 1950.
[317] M.J. Kamlet, R.W. Taft, J. Am. Chem. Soc. 98 (1976) 377.
[318] M.J. Kamlet, R.W. Taft, J. Am. Chem. Soc. 98 (1976) 2886.
[319] M.J. Kamlet, J.-L.M. Abboud, R.W. Taft, Progress in Physical Organic Chemistry, Wiley, New York, N.Y., 1981.
[320] R.W. Taft, M.J. Kamlet, M.H. Abraham, R.M. Doherty, J. Am. Chem. Soc. 107 (1985) 3105.
[321] M.J. Kamlet, R.M. Doherty, J.-L.M. Abboud, M.H. Abraham, R.W. Taft, Chemtech 16 (1986) 566.
[322] M.H. Abraham, Chem. Soc. Rev. 22 (1993) 73.
[323] M.H. Abraham, A. Ibrahim, A.M. Zissimos, J. Chromatogr. A 1037 (2004) 29.
[324] COSMObase Ver. C2.1 Rev. 01.06, COSMOlogic GmbH & Co., K.G., Leverkusen, Germany, 2006.
[325] N. Ulrich, S. Endo, T.N. Brown, N. Watanabe, G. Bronner, M.H. Abraham, K.-U. Goss, UFZ-LSER database v 3.2.1 [Internet], Helmholtz Centre for Environmental Research-UFZ, Leipzig, Germany, 2017 Available fromhttp://www.ufz.de/lserd(Accessed 23 April 2019).
[326] D. Lazidou, J. Teknetzi, D. Aslanidou, S.K. Papadopoulou, C. Panayiotou, J. Cult. Herit. 39 (2019) 1.
[327] C. Panayiotou, I. Zuburtikudis, V. Hatzimanikatis, Ind. Eng. Chem. Res. 58 (2019) 12787.
[328] C. Panayiotou, D. Aslanidou, Fluid Phase Equilibr. 406 (2015) 101.
[329] Y. Sato, M. Yurugi, K. Fujiwara, S. Takishima, H. Masuoka, Fluid Phase Equilibr. 125 (1996) 129.
[330] Y. Sato, K. Fujiwara, T. Takikawa, Sumarno, S. Takishima, H. Masuoka, Fluid Phase Equilibr. 162 (1999) 261.
[331] Y. Sato, T. Takikawa, A. Sorakubo, S. Takishima, H. Masuoka, Ind. Eng. Chem. Res. 39 (2000) 4813.
[332] D.L. Tomasko, H. Li, D. Liu, X. Han, M.J. Wingert, L.J. Lee, K.W. Koelling, Ind. Eng. Chem. Res. 42 (2003) 6431.
[333] P.D. Condo, I.C. Sanchez, C.G. Panayiotou, K.P. Johnston, Macromolecules 25 (1992) 6119-.
[334] E.A. Di Marzio, J.H. Gibbs, J. Polym. Sci. Part A 1 (1963) 1417.
[335] D. Liu, H. Li, M.S. Noon, D.L. Tomasko, Macromolecules 38 (2005) 4416.
[336] R.G. Wissinger, M.E. Paulatis, J. Polym. Sci. Part B: Polym. Phys. 25 (1987) 2497.
[337] D. Sanli, C. Erkey, J. Supercrit. Fluid 92 (2014) 264.
[338] A. Garg, E. Gulari, C.W. Manke, Macromolecules 27 (20) (1994) 5643.
[339] C. Wohlfarth, Vapour-Liquid Equilibrium Data of Binary Polymer Solutions; Physical Sciences Data 44, Elsevier, Amsterdam, The Netherlands, 1994.

Please cite this article in press as: G. Mensitieri, G. Scherillo, C. Panayiotou et al. Towards a predictive thermodynamic description of Fsorption processes in polymers: The synergy between theoretical EoS models and vibrational spectroscopy. Mater. Sci. Eng. R (2020), https://doi.org/10.1016/j.mser.2019.100525

[340] N. von Solms, I.A. Kouskoumvekaki, T. Lindvig, M.L. Michelsen, G.M. Kontogeorgis, Fluid Phase Equilibr. 222–223 (2004) 87.
[341] M. Goernert, G. Sadowski, J. Supercrit. Fluid 46 (2008) 218.
[342] P. Arce, M. Aznar, Fluid Phase Equilibr. 238 (2005) 242.
[343] D.Y. Peng, D.B. Robinson, Ind. Eng. Chem. Fund. 15 (1976) 59.
[344] Z. Chen, K. Cao, Z. Yao, Z. Huang, J. Supercrit. Fluid 49 (2009) 143.
[345] Y. Sako, A.H. Wu, J.M. Prausnitz, J. Appl. Polym. Sci. 38 (1989) 1839.
[346] Y. Sato, T. Takikawa, S. Takishima, H. Masuoka, J. Supercrit. Fluid 19 (2001) 187.
[347] J.A. Barker, D. Henderson, J. Chem. Phys. 47 (1967) 2856.
[348] J.A. Barker, D. Henderson, J. Chem. Phys. 47 (1967) 4714.
[349] E. Markocic, Z. Knez, J. Supercrit. Fluid 95 (2014) 635.
[350] T. Spyriouni, I.G. Economou, Polymer 46 (2005) 10772.
[351] I.A. Kouskoumvekaki, G.J.P. Krooshof, M.L. Michelsen, G.M. Kontogeorgis, Ind. Eng. Chem. Res. 43 (2004) 826.
[352] S.J. Suresh, J.R. Elliot Jr, Ind. Eng. Chem. Res. 31 (1992) 2783.
[353] O. Fukumoto, J. Polym. Sci. 22 (1956) 263.
[354] C. Giori, B.T. Hayes, J. Polym. Sci. Part A-1 8 (1970) 351.
[355] G. Wibawa, R. Hatano, Y. Sato, S. Takishima, H. Masuoka, J. Chem. Eng. Data 47 (2002) 1022.
[356] M. Herskowltz, M. Gottlleb, J. Chem. Eng. Data 30 (1985) 233.
[357] A.W. Andrews, K.W. Morcon, J. Chem. Thermodyn. 3 (1971) 519.
[358] H.V. Kehiaian, K. Sosnkowska-Kehiaian, R. Hryniewicz, J. Chim. Phys. Phys. Chim. Biol. 68 (1971) 929.
[359] H. Ohji, H.K. Tamura, J. Chem. Thermodyn. 35 (2003) 1591.
[360] A. De Torre, I. Velasco, S. Otin, C. Gutierrez Losa, J. Chem. Thermodyn. 12 (1989) 87.
[361] J.S. Rowlinson, B. Widom, Molecular Theory of Capillarity, Clarendon Press, Oxford, 1982.
[362] G. Scherillo, M.G. Pastore Carbone, M. Petretta, P. La Manna, C. Panayiotou, D. N. Bikiaris, P. Musto, G. Mensitieri, Polymer 97 (2016) 346.
[363] D.N. Bikiaris, G.Z. Papageorgiou, D.J. Giliopoulos, C.A. Stergiou, Macromol. Biosci. 8 (2008) 728.
[364] B. Bonavoglia, G. Storti, M. Morbidelli, Ind. Eng. Chem. Res. 45 (2006) 1183.
[365] I. Tsivintzelis, G.M. Kontogeorgis, Fluid Phase Equilibr. 280 (2009) 100.
[366] I. Tsivintzelis, C.G. Panayiotou, in: K.S. Birdi (Ed.), Handbook of Surface and Colloid Chemistry, fourth ed., CRC Press Taylor & Francis group, New York, 2015.
[367] M.G. Pastore Carbone, E. Di Maio, S. Iannace, G. Mensitieri, Polym. Test. 30 (3) (2011) 303.
[368] M.G. Pastore Carbone, E. Di Maio, G. Scherillo, G. Mensitieri, S. Iannace, J. Supercrit. Fluid 67 (2012) 131.
[369] K. Paduszyński, J. Chiyen, D. Ramjugernath, T.M. Letcher, U. Domańska, Fluid Phase Equilibr. 305 (2011) 43.
[370] A. Tsioptsias, I. Tsivintzelis, C. Panayiotou, Phys. Chem. Chem. Phys. 12 (2010) 4843.
[371] F. Doghieri, G.C. Sarti, J. Membrane Sci. 147 (1998) 73.
[372] S.S. Jordan, W.J. Koros, Macromolecules 28 (1995) 2228.
[373] M.G. De angelis, T.C. Merkel, V.I. Bondar, B.D. Freeman, F. Doghieri, G.C. Sarti, Macromolecules 35 (2002) 1276.
[374] G.C. Sarti, M.G. De Angelis, AIChE J. 58 (2012) 292.
[375] M. Galizia, M.G. De Angelis, G.C. Sarti, J. Membrane Sci. 405–406 (2012) 201.
[376] M. Minelli, S. Campagnoli, M.G. De Angelis, F. Doghieri, G.C. Sarti, Macromolecules 44 (12) (2011) 4852.
[377] E.S. Sanders, W.J. Koros, J. Pol. Sci., Pol. Phys. Ed. 24 (1986) 175.
[378] F. Grassia, M. Giacinti Baschetti, F. Doghieri, G.C. Sarti, in: I. Pinnau, B. Freeman (Eds.), NEW YORK, Oxford University Press, ACS Symposium Series, 552004.
[379] N. Muruganandam, D.R. Paul, J. Pol. Sci: Part. B: Polym. Phys. 25 (1987) 2315.
[380] E.M. Davis, M. Minelli, M.G. Baschetti, G.C. Sarti, Y.A. Elabd, Macromolecules 45 (2012) 7486.
[381] E.M. Davis, Y.A. Elabd, Ind. Eng. Chem. Res. 52 (2013) 12865.
[382] R.L. Scott, J. Phys. Chem. 62 (1958) 136.
[383] F. Doghieri, M.G. De Angelis, M.G. Baschetti, G.C. Sarti, Fluid Phase Equilibr. 241 (1) (2006) 300.
[384] Y. Song, T. Hino, S.M. Lambert, J.M. Prausnitz, Fluid Phase Equilibr. 117 (1996) 69.
[385] L. Liu, S.E. Kentish, Polymer 104 (2016) 149.
[386] G. Scherillo, M. Galizia, P. Musto, G. Mensitieri, Ind. Eng. Chem. Res. 52 (2013) 8674.
[387] J.F. Waters, W.R. Likavec, W.M. Ritchey, J. Appl. Polym. Sci. 53 (1994) 59.
[388] G. Marque, S. Neyertz, J. Verdu, V. Prunier, D. Brown, Macromolecules 41 (2008) 3349.
[389] R. Iwamoto, T. Matsuda, J. Polym. Sci. Part B: Polym. Phys. 43 (2005) 777.
[390] G. Scherillo, V. Loianno, D. Pierleoni, R. Esposito, A. Brasiello, M. Minelli, F. Doghieri, G. Mensitieri, J. Phys. Chem. B 122 (2018) 3015.
[391] D. Pierleoni, M. Minelli, G. Scherillo, G. Mensitieri, V. Loianno, F. Bonavolonta', F. Doghieri, J. Phys. Chem. B 121 (2017) 9969.
[392] I. Tsivintzelis, A.G. Angelopoulou, C. Panayiotou, Polymer 48 (2007) 5928.
[393] P.J. Flory, Proc. R. Soc. Lond. A 234 (1956) 60.
[394] C.G. Panayiotou, Polym. J. 18 (1986) 895.
[395] G. Mensiteri, G. Scherillo, in: L. Nicolais, A. Borzacchiello (Eds.), Wiley Encyclopedia of Composites, 2nd ed., John Wiley & Sons, Hoboken, NJ, 2012, pp. 804–829.
[396] J. Prinos, C. Panayiotou, Polymer 36 (1995) 1223.
[397] E.A. Di Marzio, A.J. Yang, J. Res. Inst. Stand. Technol. 102 (1997) 135.
[398] E.A. Di Marzio, Comput. Mater. Sci. 4 (1995) 317.
[399] J. Dudowicz, K.F. Freed, J.F. Douglas, J. Chem. Phys. 124 (2006)064901.
[400] H.-P. Wittmann, J. Chem. Phys. 95 (1991) 8449.
[401] J. Baschnagel, M. Wolfgardt, W. Paul, K. Binder, J. Res. Inst. Stand. Technol. 102 (1997) 159.
[402] M. Wolfgardt, J. Baschnagel, W. Paul, K. Binder, Phys. Rev. E 54 (1996) 1535.
[403] M. Mèzard, G. Parisi, J. Chem. Phys. 111 (1999) 1076.
[404] M. Mèzard, G. Parisi, Phys. Rev. Lett. 82 (1999) 747.
[405] M. Mèzard, G. Parisi, J. Phys. C 12 (2000) 6655.
[406] D.F. Baldwin, C.B. Park, N.P. Suh, Polym. Eng. Sci. 36 (1996) 1437.
[407] S. Siripurapu, J.M. DeSimone, S.A. Khan, R.J. Spontak, Adv. Mater. 16 (2004) 989.
[408] Z. Guo, A.C. Burley, K.W. Koelling, I. Kusaka, L.J. Lee, D.L. Tomasko, J. Appl. Polym. Sci. 125 (2012) 2170.
[409] M. Pintado-Sierra, L. Delgado, I. Aranaz, Á. Marcos-Fernández, H. Reinecke, A. Gallardo, D. Zeugolis, C. Elvira, J. Supercrit. Fluid 95 (2014) 273.
[410] D. Raps, N. Hossieny, C.B. Park, V. Altstädt, Polymer 56 (2015) 5.
[411] I. Tsivintzelis, C. Panayiotou, Macromol. Symp. 331–332 (2013) 109.
[412] I. Tsivintzelis, C. Panayiotou, in: S. Iannace, C.B. Park (Eds.), Biofoams: Science and Applications of Bio-Based Cellular Porous Materials, CRC Press, Boca Raton, London, New York, 2015.
[413] J.D. Gunton, J. Stat. Phys. 95 (1999) 903.
[414] R.G. Gabbard, The Development of a Homogeneous Nucleation Rate Model for the Thermoplastic Foams Based on a Molecular Partition Function and Fickian Diffusion PhD Thesis, New Jersey Institute of Technology, Department of Chemical Engineering, New Jersey, 2002.
[415] I. Kusaka, M. Talreja, D.L. Tomasko, AIChE J. 59 (8) (2013) 3042.
[416] J.W. Gibbs, The Scientific Papers of Willard Gibbs J., Volume One: Thermodynamics, Ox Bow, Woodbridge, CN, 1993, pp. 253.
[417] D.L. Tomasko, A. Burley, L. Feng, S.-K. Yeh, K. Miyazono, S. Nirmal-Kumar, I. Kusaka, K. Koelling, J. Supercrit. Fluid 47 (2009) 493.
[418] S.K. Goel, E.J. Beckman, Polym. Eng. Sci. 34 (1994) 1137.
[419] I. Tsivintzelis, G. Saccharidou, E. Pavlidou, C. Panayiotou, J. Supercrit. Fluid 110 (2016) 240.
[420] M. Pantoula, C. Panayiotou, J. Supercrit. Fluid 37 (2005) 254.
[421] R. Reid, J.M. Prausnitz, B.E. Poling, The Properties of Gases and Liquids, 4th edition, McGraw-Hill international editions, Singapore, 1988.
[422] P.J. Flory, J. Rehner Jr, J. Chem. Phys. 11 (1943) 521.
[423] P.J. Flory, J. Chem. Phys. 18 (1950) 108.
[424] C. Panayiotou, I.C. Sanchez, Polymer 33 (1992) 5090.
[425] T.M. Birshtein, V.A. Pryamitsin, Macromolecules 24 (7) (1991) 1554.
[426] C.G. Panayiotou, Can. J. Chem. Eng. 62 (1984) 578.
[427] M.M. Prange, H.H. Hooper, J.M. Prausnitz, AIChE J. 35 (1989) 803.
[428] J. Shim, K.P. Johnston, AIChE J. 35 (1989) 1097.
[429] A.K. Lele, M.V. Badiger, M.M. Hirve, R.A. Mashelkar, Chem. Eng. Sci. 50 (1995) 3535.
[430] M. Marchetti, S. Prager, E.L. Cussler, Macromolecules 23 (1990) 3445.

Pellegrino Musto earned the Laurea of Doctor in Chemistry at the University Federico II, Naples, Italy and the Ph.D. in Polymer Technology and Materials Engineering at the University of Loughborough, England. He is currently Director of Research at the Institute of Polymers, Composites and Biomaterials of the Italian National Research Council. (IPCB-CNR) where he leads the Molecular Spectroscopy Lab (MSL). He has been, from September 1987 to September 1989, Research Associate at the Department of Polymer Science and Engineering, University of Massachusetts, Amherst, MA, USA, with Profs. W.J. MacKnight and Frank E. Karasz. The main research interests include: Science and Technology of Polymers. Infrared spectroscopy (FTIR, FT-NIR, IR micro-spectroscopy). Raman and SERS Spectroscopy. Raman imaging for biomedical applications. Molecular-mechanics and quantum-chemistry based normal coordinate analysis. Diffusion properties of polymer systems. Photo-oxidative and thermo-oxidative stability of polymers. Dr Musto has published more than 150 papers in refereed media, two books, numerous book chapters, is co-author of one patent and is Editor in Chief of the journal Frontiers in Chemistry, Polymer Chemistry Section.

Please cite this article in press as: G. Mensitieri, G. Scherillo, C. Panayiotou et al. Towards a predictive thermodynamic description of Fsorption processes in polymers: The synergy between theoretical EoS models and vibrational spectroscopy. Mater. Sci. Eng. R (2020), https://doi.org/10.1016/j.mser.2019.100525